GRAVITY GRADIENT STABILIZATION SYSTEM for the

APPLICATIONS TECHNOLOGY SATELLITE

DOCUMENT NO. 65SD4381
20 JULY 1965

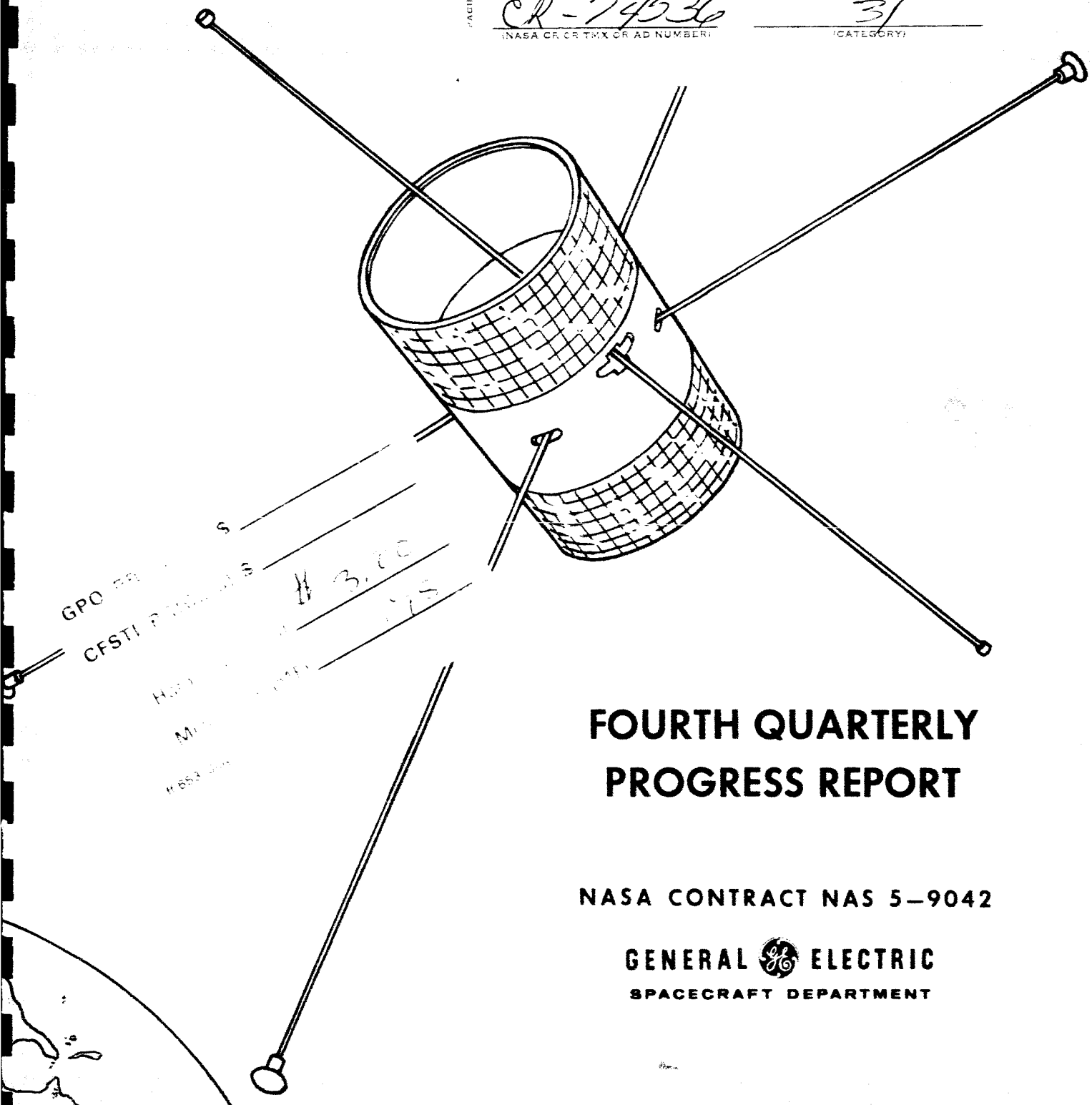

FOURTH QUARTERLY PROGRESS REPORT

NASA CONTRACT NAS 5–9042

GENERAL ELECTRIC
SPACECRAFT DEPARTMENT

DOCUMENT NO. 65SD4381
20 July 1965

GRAVITY GRADIENT STABILIZATION SYSTEM FOR THE APPLICATIONS TECHNOLOGY SATELLITE

FOURTH QUARTERLY PROGRESS REPORT

1 April through 30 June, 1965

CONTRACT NO. NAS 5-9042

for the
NATIONAL AERONAUTICS AND SPACE ADMINISTRATION

WENDELL SUNDERLIN
ATS TECHNICAL OFFICER

APPROVED BY _____

R. J. Katucki, Manager
Passive Attitude Control Programs

GENERAL ELECTRIC
SPACECRAFT DEPARTMENT
A Department of the Missile and Space Division
Valley Forge Space Technology Center
P. O. Box 8555 • Philadelphia, Penna. 19101

TABLE OF CONTENTS

Section			Page
1	INTRODUCTION		1-1
	1.1	Purpose	1-1
	1.2	Program Contract Scope	1-1
2	SYSTEMS ANALYSIS AND INTEGRATION		2-1
	2.1	Event Summary	2-1
	2.2	ATS Mathematical Model	2-2
	2.3	Attitude Determination Program	2-2
		2.3.1 Input Data Block	2-2
		2.3.2 Diagnostic Data Block	2-4
		2.3.3 Output Diagnostic Data	2-4
		2.3.4 Compute Orbit Block	2-4
		2.3.5 Compute Decision Block	2-4
		2.3.6 Compute Attitude Block	2-4
		2.3.7 Output Attitude Data	2-5
	2.4	Orbit Test Plan	2-5
		2.4.1 Launch Constraints	2-5
		2.4.2 Orbit Test Sequence	2-7
	2.5	Flight Evaluation Plan	2-7
	2.6	Analytical Studies and Results	2-13
		2.6.1 ATS-A Capture Analysis	2-13
		2.6.2 Inversion Studies	2-24
		2.6.3 Hysteresis Damper Studies	2-24
	2.7	Boom Thermal Bending Analysis	2-47
		2.7.1 ATS Mathematical Model Equations	2-47
		2.7.2 Numerical Evaluation of Shell Equation	2-57
		2.7.3 Preliminary Thermal Bending Tests	2-58
	2.8	Test Requirements and Performance	2-58
		2.8.1 Micrometeorite Testing	2-58
		2.8.2 Qualification of Primary Boom and Damper Boom Subsystems	2-58
		2.8.3 Qualification of Combination Passive Damper	2-59
		2.8.4 Solar Vacuum Test Requirements	2-59
		2.8.5 Aerospace Ground Equipment	2-60

TABLE OF CONTENTS (Continued)

Section			Page
3	BOOM SUBSYSTEM		3-1
	3.1	Deployment	3-1
		3.1.1 Primary Boom Extension Speed	3-1
		3.1.2 Boom Extension and Scissoring Drive Motors Preliminary Test Plan	3-1
		3.1.3 O-Ring Seal Evaluation, Boom Drive	3-1
	3.2	Structure and Materials	3-2
		3.2.1 Lubrication	3-2
		3.2.2 Silver Plated Tarnish Studies	3-2
	3.3	Power Requirements	3-3
	3.4	Spacecraft Interface	3-4
	3.5	Primary Boom Assembly	3-4
		3.5.1 Transmission Assembly	3-5
		3.5.2 Erection Unit	3-5
	3.6	Damper Boom	3-5
		3.6.1 Design Changes	3-5
		3.6.2 Cable Cutter Assembly	3-5
	3.7	Boom Subsystem Test Equipment	3-5
		3.7.1 Test Tank	3-5
		3.7.2 Test Trolley	3-17
	3.8	Summary of Test Results	3-17
	3.9	Hardware Status	3-18
		3.9.1 Mock-Up	3-18
		3.9.2 Thermal Model	3-18
		3.9.3 Dynamic Model	3-18
		3.9.4 Engineering Unit No. 1	3-18
	3.10	RF Experiment	3-18
4	COMBINATION PASSIVE DAMPER		4-1
	4.1	Introduction	4-1
		4.1.1 Summary of Major Events During Reporting Period	4-1
		4.1.2 CPD Specification Status	4-2

TABLE OF CONTENTS (Continued)

Section			Page
	4.2	Design Development Effort	4-2
		4.2.1 General	4-2
		4.2.2 CPD Package	4-3
		4.2.3 Testing	4-9
		4.2.4 Solenoid	4-10
		4.2.5 Eddy Current Damper	4-11
		4.2.6 Passive Hysteresis Damper	4-14
		4.2.7 Damper Boom Angle Indicator	4-17
		4.2.8 Dynamic Model	4-20
		4.2.9 Thermal Model	4-21
	4.3	Test Equipment	4-21
		4.3.1 Low Order Force Fixture (LOFF)	4-21
		4.3.2 Dipole Measurement Fixture	4-22
		4.3.3 Advanced Damping Test Fixture	4-22
		4.3.4 Test Console	4-22
5	ATTITUDE SENSOR SUBSYSTEM		5-1
	5.1	Subsystem Description	5-1
	5.2	TV Camera Subsystem (TVCS)	5-1
		5.2.1 Subcontract Activities	5-1
		5.2.2 Design Activities	5-2
		5.2.3 Earth Simulation Tests	5-6
	5.3	Power Control Unit	5-6
		5.3.1 Mechancial Design	5-6
		5.3.2 Electrical Design	5-7
	5.4	Solar Aspect Sensor	5-11
		5.4.1 Detector - Electronics Interface Investigation	5-11
		5.4.2 Subcontract Activities	5-14
6	QUALITY CONTROL		6-1
	6.1	Quality Control Engineering	6-1
		6.1.1 TV Camera Subsystem	6-1
		6.1.2 Boom Subsystem	6-1
		6.1.3 Solar Aspect Sensor	6-1
		6.1.4 Combination Passive Damper	6-2

TABLE OF CONTENTS (Continued)

Section			Page
	6.1.5	Power Control Unit	6-2
	6.1.6	Parts Program	6-2
	6.1.7	General	6-2
6.2	Test Equipment Engineering		6-3
	6.2.1	Solar Aspect Sensor	6-3
	6.2.2	Combination Passive Damper	6-3
	6.2.3	Power Control Unit	6-3
	6.2.4	TV Camera Subsystem	6-3
	6.2.5	Boom Subsystem	6-3
	6.2.6	General	6-4
6.3	Inspection and Test		6-4
	6.3.1	Solar Aspect Sensor	6-4
	6.3.2	Parts Program	6-4
	6.3.3	TV Camera Subsystem	6-4
	6.3.4	Power Control Unit	6-5
	6.3.5	Combination Passive Damper	6-5
	6.3.6	Boom Subsystem	6-6
	6.3.7	General	6-6
6.4	Materials and Processes		6-6
	6.4.1	Solar Aspect Sensor	6-6
	6.4.2	Boom Subsystem	6-6
	6.4.3	TV Camera Subsystem	6-7
	6.4.4	Combination Passive Damper	6-7
7	MANUFACTURING		7-1
8	RELIABILITY, AND PARTS AND STANDARDS		8-1
8.1	Reliability		8-1
	8.1.1	Solar Aspect Sensor	8-1
	8.1.2	Passive Hysteresis Damper	8-6
	8.1.3	TV Camera	8-14
	8.1.4	Power Control Unit	8-14
8.2	Parts and Standards		8-15
	8.2.1	Introduction	8-15
	8.2.2	Parts, Drawings and Parts Lists	8-15

TABLE OF CONTENTS (Continued)

Section			Page
	8.2.3	Parts Qualification	8-18
	8.2.4	Degradation Analysis	8-24
9	NEW TECHNOLOGIES		9-1
10	GLOSSARY		10-1
Appendix A			A-1

LIST OF ILLUSTRATIONS

Figure		Page
2-1	Attitude Determination Program Modular Blocks	2-3
2-2	Shadow Time Prediction	2-6
2-3	ATS Information System	2-10
2-4	Information System Schedule	2-11
2-5	In-house Information Flow	2-12
2-6	Weekly In-house Schedule	2-12
2-7	ATS Capture, Run No. 1	2-16
2-8	ATS Capture, Run No. 2	2-17
2-9	ATS Capture, Run No. 3	2-18
2-10	ATS Capture, Run No. 4	2-19
2-11	ATS Capture, Run No. 5	2-20
2-12	ATS Capture, Run No. 6	2-21
2-13	ATS Capture, Run No. 7	2-22
2-14	ATS Capture, Run No. 8	2-23
2-15	ATS-A Performance Following Initial Capture, Worst Case Condition (Run 9)	2-24
2-16	ATS-A Performance Following Initial Capture, Nominal Condition (Run 10)	2-25
2-17	ATS-A With Constant Saturation Torque Hysteresis Damper Time To Damp To Various Earth Pointing Errors as a Function of Hysteresis Saturation Torque	2-28
2-18	ATS-D with Constant Saturation Torque Hysteresis Damper Time to Damp To Various Earth-Pointing Errors as a Function of Hysteresis Saturation Torque	2-29
2-19	ATS-A Damping Performance	2-31
2-20	ATS-D Damping Performance	2-32
2-21	ATS-A Damping Performance	2-33
2-22	ATS-A Damping Performance	2-34
2-23	ATS-D Damping Performance	2-35
2-24	ATS-D Damping Performance	2-36
2-25	Typical Bow-Tie Configuration for one quadrant	2-37
2-26	Time to settle to 2.8 from an initial 5^{o} pitch error as a function of T_{SAT} for ATS-A	2-39
2-27	Time to settle to 4^{o} from the Standard Transient as a function of slope 1 for ATS-A	2-40
2-28	Maximum Earth-pointing error at 200 hours as a function of γ_1 for ATS-A	2-41
2-29	Response of ATS-A Vehicle with a "Bow-Tie" Hysteresis Damper to the Standard Transient	2-43
2-30	ATS-A Damping Characteristics	2-44

LIST OF ILLUSTRATIONS (Continued)

Figure		Page
2-31	Response of ATS-D vehicle with a "Bow-tie" Hysteresis Damper to the Standard Transient	2-45
2-32	Effects of Parameter Tolerances of Bow-tie Hysteresis Damper upon Damping Performance	2-46
2-33	ATS-A Damping Performance with torsion wire spring constant reduced by indicated percentage	2-48
2-34	ATS-A Damping Performance with Torsion wire spring constant saturated at $\gamma = \gamma_A$	2-49
3-1	Details of the O-Ring Seal	3-3
3-2	End-On View of Transmission Assembly	3-6
3-3	Scissoring Mechanism, Transmission Assembly	3-7
3-4	Transmission Assembly, Top Plate and Clutch Driven Gears Removed	3-8
3-5	Sealed Drive Major Subassemblies	3-9
3-6	Sealed Drive Assembly	3-10
3-7	Primary Boom, Upper View	3-11
3-8	Primary Boom, Bottom View	3-12
3-9	Primary Boom, Tip Mass Assembly	3-13
3-10	Damper Boom Assembly	3-14
3-11	Test Trolley	3-15
3-12	Test Track	3-16
3-13	RF Experiment Details, ATS Primary Boom Assembly GE Dwg SK56152-115	3-20
4-1	CPD Package	4-5
4-2	Results of Force vs Travel Test for Solenoid to the R4606 Component Specification	4-12
4-3a	Passive Hysteresis Damper Engineering Unit No. 1	4-17
4-3b	Passive Hysteresis Damper Engineering Unit No. 1 (Cover Removed)	4-17
4-4	Angle Indicator Layout	4-19
4-5	Typical bit Circuit for the Angle Indicator	4-20
5-1	GE/HAC Electrical Interface (GE Dwg 47E207151)	5-3
5-2	Nomogram of Vent Hole	5-4
5-3	Earth Simulation Test Pictures	5-6
5-4	PCU Mock-up	5-7
5-5	Motor Field Driver Schematic	5-10
5-6	Typical Cell Characteristics	5-14
8-1	Solar Aspect Sensor Reliability Block Diagram	8-3

LIST OF TABLES

Table		Page
2-1	ATS Preliminary Flight Evaluation Plan Outline	2-8
2-2	Capture Results, ATS-A	2-15
4-1	Status of CPD Specifications	4-3
4-2	Angle Indicator Detector Data	4-21
8-1	Summary of SAS Reliability Analysis	8-1
8-2	Functional Failure Effects Analysis	8-4
8-3	Possible Failure and Degradation Effects for SAS	8-5
8-4	Demonstrated Reliability at Various Confidence Levels	8-13
8-5	Group A - Parts Requiring Qualification	8-19
8-6	Group B - Parts for Tear-Down and Analysis	8-20

ABSTRACT

Preliminary documentation was completed for the "ATS Data Processing System Design" and the "Flight Evaluation Plan" during the quarter. Summaries of both documents are included in the section on Analysis and Integration. Studies that were completed since April include: capture analysis for the ATS-A vehicle; results of inversion studies for both thruster and flywheel inversion; and hysteresis damper studies for both constant and variable saturation torque damping, the so called "bow-tie" concept. By direction at the end of the quarter, all analytical and design efforts were discontinued on the variable torque hysteresis damping concept. The values of hysteresis damping torques recommended by GE are nominally 175 dyne-cm for the ATS-A and 50 dyne-cm for the ATS-D/E.

Engineering analysis for the ATS Mathematical Model has been completed, except for incorporation of the rod thermal bending module.

The status of the design and fabrication of the Boom Subsystem is given in Section 3. An evaluation of the O-ring seal used in the boom drive assembly and results of lubrication tests are reported. The results are presented for the first three weeks of silver plated tarnishing tests. The object of the test is to measure the degradation of the rod absorptivity due to exposure to ambient environment. A series of photographs illustrate the developmental models of the transmission assembly, TV tip targets and test fixtures which were fabricated and initially tested at deHavilland.

A report is included showing the results of the tests run on the development and engineering units of the boom assembly.

The emphasis changed during the reporting period from conceptual layouts and engineering development tests of the Combination Passive Damper to the preparation of the detailed design drawings that are required for fabrication and assembly of the engineering units, thermal model and dynamic model. An explanation of the CPD functions is presented with the aid of the top assembly drawing (Figure 4-1). This drawing combines the CPD package with the baseplate and shows the damper boom attachment. Testing activity in support of the CPD design included impact cushion tests, of the caging when the damper is uncaged; corrosion tests of CPD materials to the humidity conditions of the applicable specification (SVS-7314); and evaluation of the force vs. travel characteristics of the damper clutch solenoid.

The dynamic model and Engineering Unit No. 1 of the Passive Hysteresis Damper were received from TRW Inc. during June. Testing has been initiated on these units.

The latest design of the damper boom angle indicator is included in the report, together with the layout drawing (Figure 4-6). An in-house design review was conducted at GE

on June 30th to review the design and the adequacy of the angle indicator concept. Reliability information was presented at the meeting on the performance of the phototransistors to be used in the angle indicator. Similar phototransistors have been operated successfully in Gemini ground checkout equipment, and the same family of photo devices have been operated in orbit, aboard an NRL satellite, for over 15,000 hours without a failure.

The TV camera has been designated as the Lear-Siegler Model 0431F, a modification of Model 0431C, which has been flown successfully on at least two ECHO launches.

An attempt was made to obtain photographs of the TV monitor to show the terminator on a three-foot model globe with the use of actual sunlight as the illumination source. Two photographs are included of the earth simulation tests. These initial results were not satisfactory; however, other tests of this type are planned during the next quarter.

Vending requirements for the TV camera were established, to prevent corona. Supporting analysis is included.

An illustration of the wooden modkup is shown of the Power Control Unit that was fabricated during the reporting period. The mechanical layout of the PCU was completely redesigned to reduce the weight from an estimated 18 pounds to 10.75 pounds. Seven PCU functions were eliminated as a result of the weight reduction. A listing of the present PCU functions is given.

An analysis of the Solar Aspect Sensor detector-electronics interface that was performed during the quarter is presented in this report.

A detailed report of Quality Control activities is given. These activities are divided into four areas that include: engineering, test, in-house and subcontractor surveillance, and materials and processes investigations in support of the ATS development.

Reliability analyses were completed for the Solar Aspect Sensor and the Passive Hysteresis Damper. A summary of Parts and Standards activities is included, together with the most significant items of progress. A computer program is provided which will be used as a basis for predicting degradation of parts under power aging. The program and its advantages are also reported as a new technology in Section 9.

SECTION 1

INTRODUCTION

1.1 PURPOSE

This report documents the technical progress made during the period from April 1, 1965 to June 30, 1965, toward the design and development of Gravity Gradient Stabilization Systems for the Applications Technology Satellites.

1.2 PROGRAM CONTRACT SCOPE

Under Contract NAS 5-9042, the Spacecraft Department of the General Electric Company has been contracted to provide gravity gradient stabilization systems for three Applications Technology Satellites: one to be orbited at 6000 nautical miles (ATS-A), and two to be orbited at synchronous altitude (ATS-D and ATS-E). Each system will consist of primary booms, damper boom, damper, attitude sensors and the power conditioning unit. In addition to the flight systems, GE will provide a thermal model, a dynamic model, engineering unit and two prototype units. GE will also supply two sets of aerospace ground equipment.

2. SYSTEMS ANALYSIS AND INTEGRATION

2.1 EVENT SUMMARY

Events having a significant bearing on the course and direction of ATS systems analysis efforts during the past quarter are summarized as follows:

14 April 1965: GE status presentation to Mr. Dan Mazur, NASA/GSFC, including a summary of negotiated systems work packages and plan of attack for each.

16 April 1965: Received HAC's "Shadow Time Prediction Nomogram". Based on pursuant studies, only two launch periods in 1967 will meet all known launch constraints: (1) 3/10/67 to 3/27/67 or (2) 9/10/67 to 9/25/67 (See paragraph 2.4).

20 April 1965: Finalized version of negotiated work statement.

21 April 1965: ATS Trajectory Meeting at Lewis Research Center. The decision was made to yaw the Agena 90 degrees relative to the orbit plane prior to separation of the ATS gravity gradient spacecraft. Tolerances on this maneuver plus separation rate tolerances and orbit tolerances were obtained. The decision to deploy the stabilization booms by ground telemetry command was confirmed. (See paragraph 2.6.1 for ATS-A Capture Analysis).

13 May 1965: Meeting at NASA/GSFC to review progress and establish definitive ground rules for the subliming rocket inversion maneuver. (See paragraph 2.6.2).

May - June 1965: Concerted systems analysis efforts by NASA/GSFC and GE/SD to arrive at a mutually acceptable and realistic design specification for the Passive Hysteresis Damper (PHD). "Bow-tie" and constant torque profiles were analyzed and optimized relative to performance data for the Eddy Current Damper (ECD). An "optimum" bow-tie specification was presented unofficially to TRW, Inc. on 8 June 1965. Characteristic performance of this damper (relative to "optimum" values for constant-torque profiles and eddy-current damping) is presented in paragraph 2.6.3. Implementation problems associated with the bow-tie approach are complicated by the inherent negative magnetic spring characteristic.

25 June 1965: Joint meeting of NASA/GSFC, GE/SD and TRW at TRW to review results and recommendations of TRW's systems analysis group relative to optimum PHD performance. GSFC and GE results were accepted as valid.

1 July 1965: Received direction from NASA/GSFC to utilize GE's recommended constant saturation torque values of 175 dyne-cm for ATS-A and 50 dyne-cm for ATS-D. The work on "bow-tie" configuration is to be halted due to implementation and schedule problems.

2.2 ATS MATHEMATICAL MODEL

The engineering analysis for the ATS Math Model is complete except for incorporation of equations for the rod thermal bending module. This should be completed by mid-August. However, the formal documentation will require about two months due to the length and complexity of material involved. Target date for delivery to NASA/GSFC has been established as 15 October. Programming and checkout will continue beyond that date with delivery of the final report and listing by the end of December. Work has commenced on a Math Model Acceptance Specification. Equations utilized to account for rod thermal bending are discussed in paragraph 2.7.

2.3 ATTITUDE DETERMINATION PROGRAM

The basic engineering analysis of ATS attitude measurements and measurement errors is essentially complete. Documentation of the solar aspect sensor/antenna polarization measurement system analysis is all that remains. Emphasis during the forthcoming quarter will shift to heavier use of the computer as a design tool. Two investigative-type programs are being developed: (1) Simulation program for producing theoretical sensor data, (2) Data processing investigation program. These two programs will be used in conjunction to investigate techniques for data correction and smoothing and will utilize basic procedures to be incorporated in the Attitude Determination Program.

An ATS Data Processing System Preliminary Design Specification has been completed and forwarded to NASA/GSFC for review and comment. A meeting to negotiate agreement on the contents of the document (as well as the ATS Preliminary Flight Evaluation Plan - paragraph 2.5) is planned for the latter part of July. A summary of the Data Processing System Preliminary Design Specification is given in the following paragraphs.

The Attitude Determination Program (ADP) has been developed sufficiently to be described by the modular blocks shown in Figure 2-1. Continuing data processing and reduction studies will be performed on each block for the program specification yet to be written. It should not be construed that the program will not undergo configuration changes as a result of these developmental studies; however, this present configuration represents concisely all the data processing functions that must be performed as stipulated by the ATS data handling requirements.

2.3.1 INPUT DATA BLOCK

All data to be processed by the ADP will be read by the Input Data block, both quick-look data from teletype and long term data from tape. The raw data to be utilized in the program will be selected here and functionalized, i.e., converted to engineering units. The Input Data block will then output the selected data either for diagnostic data processing or for attitude determination.

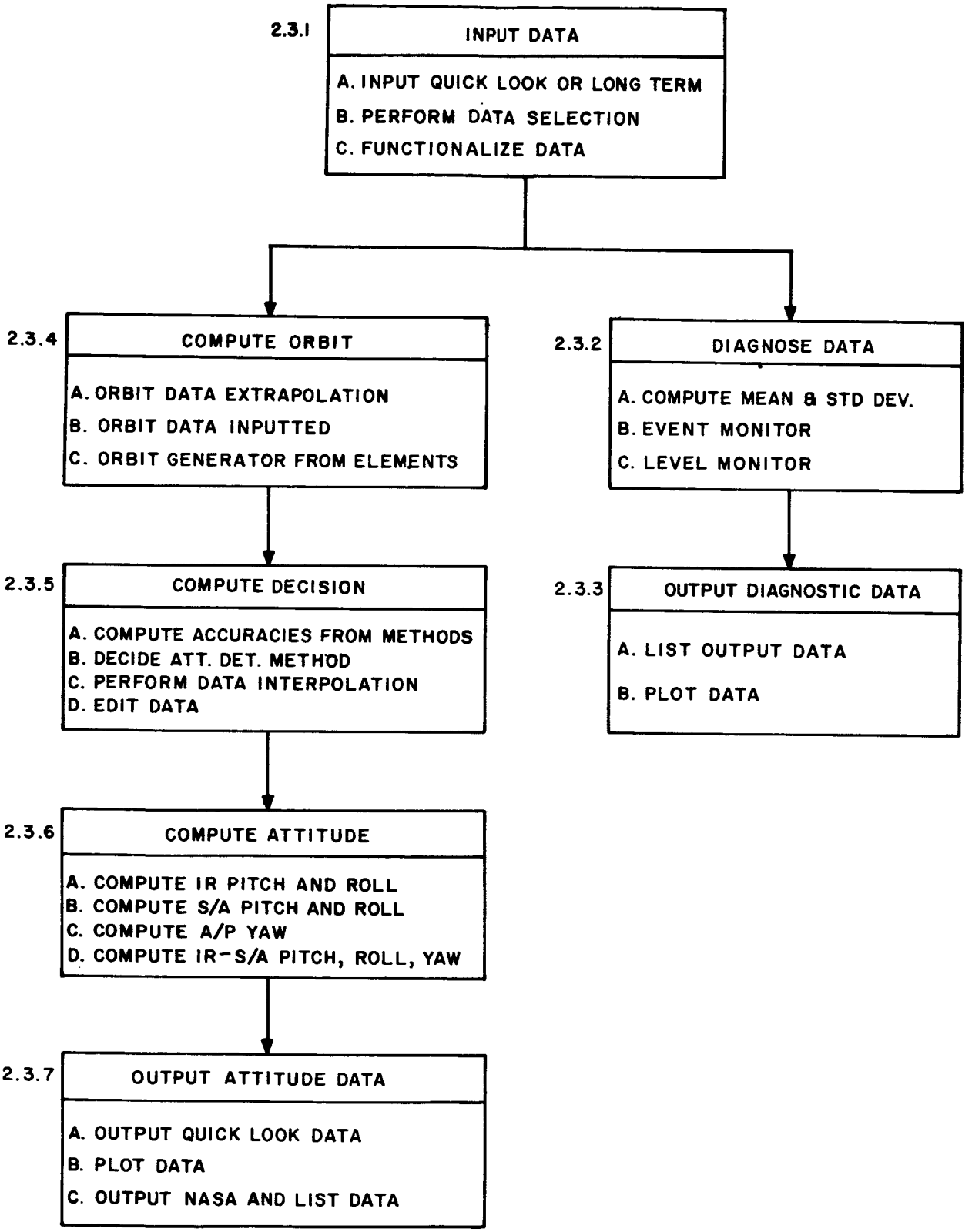

Figure 2-1. Attitude Determination Program Modular Blocks

2.3.2 DIAGNOSTIC DATA BLOCK

In this function block the data will be scrutinized or analyzed for performance evaluation of the gravity gradient subsystem. Event data and command data will be monitored for changes in significant occurrences in events and commands, level changes of interest for steady state functions will be monitored; means and standard deviations for the telemetry functions will be computed for a comprehensive yet concise history of the subsystem operation.

2.3.3 OUTPUT DIAGNOSTIC DATA

All diagnostic data, whether volumetrically reduced by diagnostic monitoring or required at its original sampling rate, will be outputted in a listed form or plotted. Primary usage of these output data will be for in-house subsystem data evaluations.

2.3.4 COMPUTE ORBIT BLOCK

The orbit block will compute the vehicle orbital parameters required for attitude determination. As presently envisioned, it will handle either orbital elements or will have the capability to read in the time-dependent latitude and longitude available from the NASA/WMSAD output.

2.3.5 COMPUTE DECISION BLOCK

The Compute Decision block will:

1. Compute the errors for the different means of determining attitude.
2. Make decision as to which attitude determination method is to be used or apply weighting technique for combinations of methods.
3. Interpolate all data to within an allowed time coincidence band.
4. Edit or filter the data as required before computation of attitude.

2.3.6 COMPUTE ATTITUDE BLOCK

This function block will compute the satellite attitude using all the previously processed data. Submodules will be available for each sensor-paired combinations required for the calculation. This block will use basically IR data, Solar Aspect data, and Antenna Polarization data or any combination dependent on data availability from "no data available" (from any one sensing scheme) to redundant Antenna Polarization data from several station sources. The basic philosophy will be to use all available data to compute attitude.

2.3.7 OUTPUT ATTITUDE DATA

The Output Attitude Data block formats all data for outputting and writes the data on the proper media for presentation to customers. Outputting of data includes the teletype output of Quick Look data and the BCD data written on magnetic tape for transmission to NASA. In-house customers of data will receive, along with the NASA output, printed listings of all parameters required to evaluate the satellite attitude. These parameters are intermediate outputs of each module described in the functional flow for attitude determination.

2.4 ORBIT TEST PLAN

2.4.1 LAUNCH CONSTRAINTS

The ATS Gravity Gradient Orbit Test Plan (reference GE's First and Third Quarterly Reports) calls for an initial 27-day period of continuous sunlight following orbit injection. The purpose of this requirement is to isolate the possible spacecraft attitude perturbations due to gravity gradient boom "thermal twang" phenomena at eclipse entry and exit. This effect can range from negligible to severe depending upon the phase relationship of the excitation dynamics of the individual booms. If the booms are dynamically identical, the effect of "thermal twang" will produce in-phase motion of all booms and result in a simple center-of-mass translation transient with negligible effect on spacecraft attitude dynamics. However, if the booms are not dynamically identical (a more probable situation), the effect of "thermal twang" will be to induce individual boom motion which tends to creep out-of-phase with respect to motions of the other booms. This could lead to a significant transfer of rotational energy to the spacecraft central body and produce an appreciable effect on spacecraft attitude dynamics. To insure the opportunity for an initial evaluation of spacecraft performance, free of the complexities of possible boom dynamics perturbations, the initial period of continuous sunlight is required. An exact 27-day period is not required but it is felt that at least 3 to 4 weeks is necessary to obtain the required performance data.

If the initial period of continuous sunlight is to be accomplished, however, the associated launch constraints must be compatible with the additional (and primary) constraints associated with the requirement that the sun vector be no more than 25 degrees out of the orbit plane for the entire useful life of the spacecraft. (This latter constraint is a design condition for the HAC solar power supply). The HAC "Shadow Time Prediction Nomagram", p. 2-7, HAC Quarterly Progress Report No. 2, facilitates a relatively quick tradeoff on these conditions.

Three curves are shown in Figure 2-2. All are plotted versus launch date. Periods of continuous sunlight have been maximized subject to the constraint that $\delta' \leq 25$ degrees for greater than 15 months. (δ' = solar incidence angle relative to orbit plane). The first curve gives the length of time that $\delta' \leq 25$ degrees; the second curve gives initial conditions on the HAC nomogram); the third curve gives the maximum days

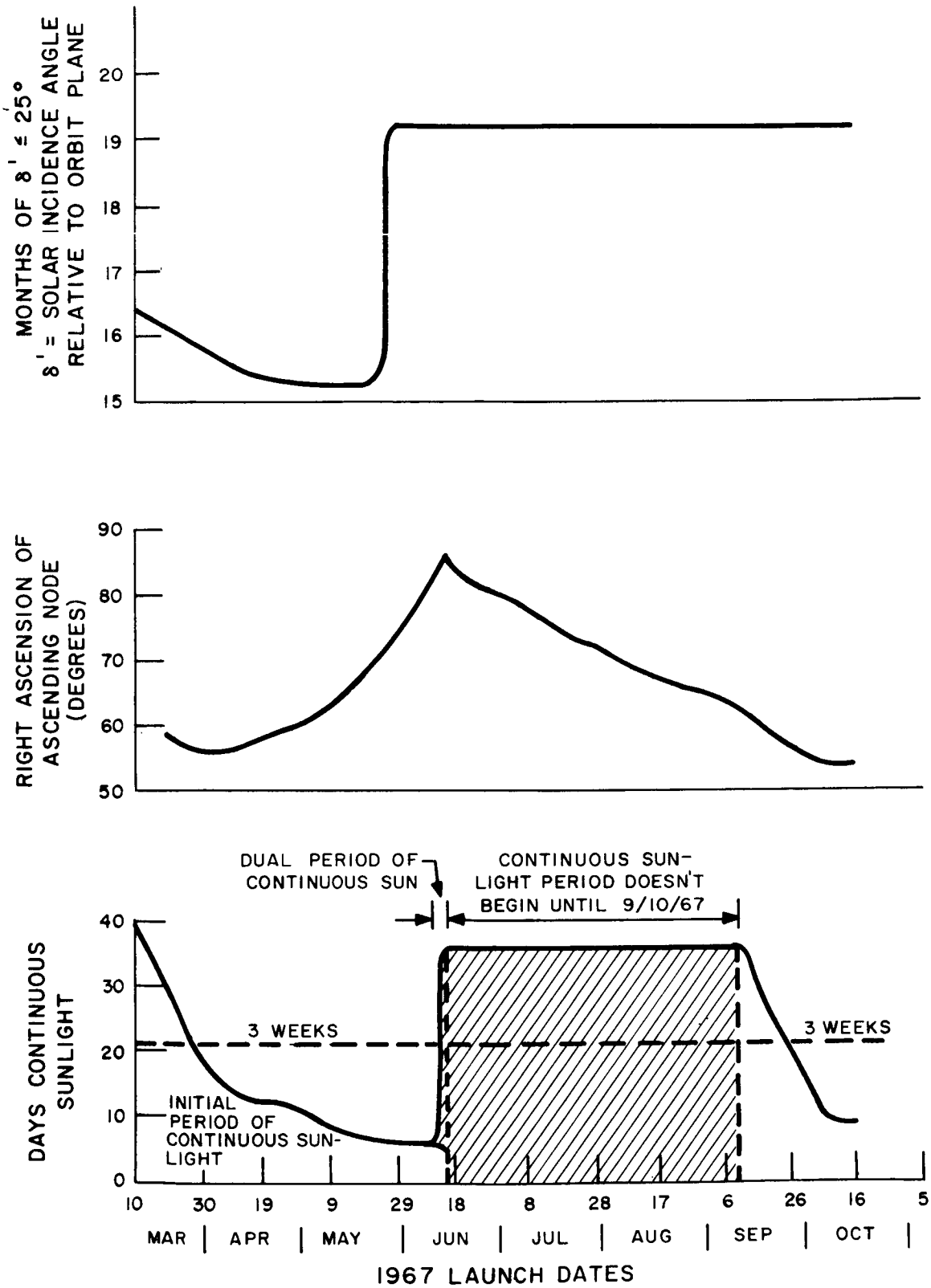

Figure 2-2. Shadow Time Prediction

continuous sunlight. It quickly becomes apparent that there are only two periods during 1967 where all conditions are satisfied:

1. 3/10/67 to 3/27/67
2. 9/10/67 to 9/25/67

The first period provides better than 16 months of $\delta' \leq 25$ degrees and the second period provides better than 19 months.

Current Launch planning does not fall within the above dates. If the present schedule is adhered to, an alternative but less desirable course of action is manifested by the shaded area on the third curve. Launch on any date past June 14, 1967 (up until September 10 date) will provide a 36-day period of continuous sunlight beginning September 10. Launch during this period (6/14/67 - 9/10/67) will produce an acceptable orbit based on solar incidence angle constraints but immediately places the satellite in a discontinuous sunlight region. The separation of "thermal twang" effects will have to wait until September 10 and an undesirable uncertainty in the early phase of flight data evaluation is introduced.

2.4.2 ORBIT TEST SEQUENCE

The sequence of planned orbital tests, as summarized in GE's Third Quarterly Progress Report and modified in GE's Tenth and Eleventh Monthly Progress Reports, is currently unchanged.

2.5 FLIGHT EVALUATION PLAN

The following is a summary of the ATS Preliminary Flight Evaluation Plan forwarded, for comment and review, to NASA/GSFC on July 9th.

The ATS Flight Evaluation Plan establishes a framework within which the flight analysis effort will be applied in order 1) to derive and provide objective vehicle performance information, and 2) to provide an evaluation of the ATS gravity experiment through a well-planned, thorough analysis of flight data. The plan is outlined in Table 2-1.

A general description of the flight evaluation plan was published in the Third Quarterly Report - paragraph 2.1.4.2 (covering Section 2 of Table 2-1). This description also includes a discussion of the ATS operational organization, for both on-orbit operations, and for post-flight analysis activity.

Measurement system definition (Section 3 of Table 2-1) includes a listing and description of all information to be used as input in the overall flight evaluation effort. Areas covered include: 1) data to be obtained from the vehicle during flight, through both PCM telemetry and television picture transmission; 2) antenna polarization data, to

TABLE 2-1. ATS PRELIMINARY FLIGHT EVALUATION PLAN OUTLINE

1.0 Introduction

2.0 General description

3.0 Measurement system
- 3.1 Vehicle telemetry system
- 3.2 Vehicle television system
- 3.3 Antenna Polarization
- 3.4 Orbit information
- 3.5 Supplementary information

4.0 Information system
- 4.1 Long term data - external
- 4.2 Long term date - at GE/SD
- 4.3 Quick-look data
- 4.4 Operational system
- 4.5 Schedules

5.0 Data reduction and processing
- 5.1 Data reduction computer programs
- 5.2 Long-term data
- 5.3 Quick-look data
- 5.4 GE/SD data system checkout
- 5.5 GE/SD computer facility
- 5.6 Television data

6.0 Flight analysis and evaluation
- 6.1 Approach
- 6.2 Task areas

7.0 Reporting
- 7.1 Preliminary reports
- 7.2 Weekly data package
- 7.3 Final report
- 7.4 Program summary report
- 7.5 Quarterly progress report (contribution)

be obtained from the respective tracking stations; and 3) orbit data to be obtained from NASA/GSFC. In each case, definition of particular items included rate of obtaining information, and form in which such information will be received (analog, binary, etc., and °F, °C, volts, amps, etc.).

The ATS information system is described in the Flight Evaluation Plan (Section 4 of Table 2-1) as the means of facilitating transfer of measurement data, other information, and necessary operational communications in conjunction with orbital flight. Information flow channels between the ATS vehicle and GE/SD, through the tracking station network and NASA/GSFC, are covered (Figures 2-3 and 2-4), with data formats and flow schedules listed. The in-house flow of ATS data is also illustrated in Figures 2-5 and 2-6. Channels available for operational use are also mentioned.

The data reduction and processing activities to be employed in ATS flight analysis efforts are described (Section 5 of Table 2-1). These activities will be centered around two major computer programs:

1. Attitude determination program
2. ATS math model program

to be operated on the large scale computer facility at GE/SD. Block diagram outlines of both programs, and a brief description of the GE-635 computer facility to be employed, are included. In addition to these automated activities, manual extraction and reduction of gravity gradient X-boom and vehicle attitude data (from television pictures) is covered.

The flight analysis/evaluation portion of the Flight Evaluation Plan (Section 6 of Table 2-1) describes the approach to be used in analyzing and evaluating input information, and defines the various specific tasks to be accomplished through flight analysis in meeting the objectives of the ATS program. Areas included in the description of the approach to analysis are:

1. Operational assurance evaluation
2. Systems capability analysis

Each area is defined in its applicability to the various specific task areas to be covered in the ATS program. Specific task areas are listed in three categories:

1. Vehicle dynamic performance evaluation — to cover attitude performance of the vehicle, and specific subsystem contributions to such performance.
2. Systems diagnostic evaluation — to cover system and subsystem "health" and operational status.
3. Flight analysis system evaluation — to cover planning and techniques employed in the evaluation effort.

Definition and format of the various flight evaluation reports to be issued are covered in Section 7 of Table 2-1. The preliminary, quick-look, weekly, final, and program summary reports, and contributions to the program quarterly reports, are discussed

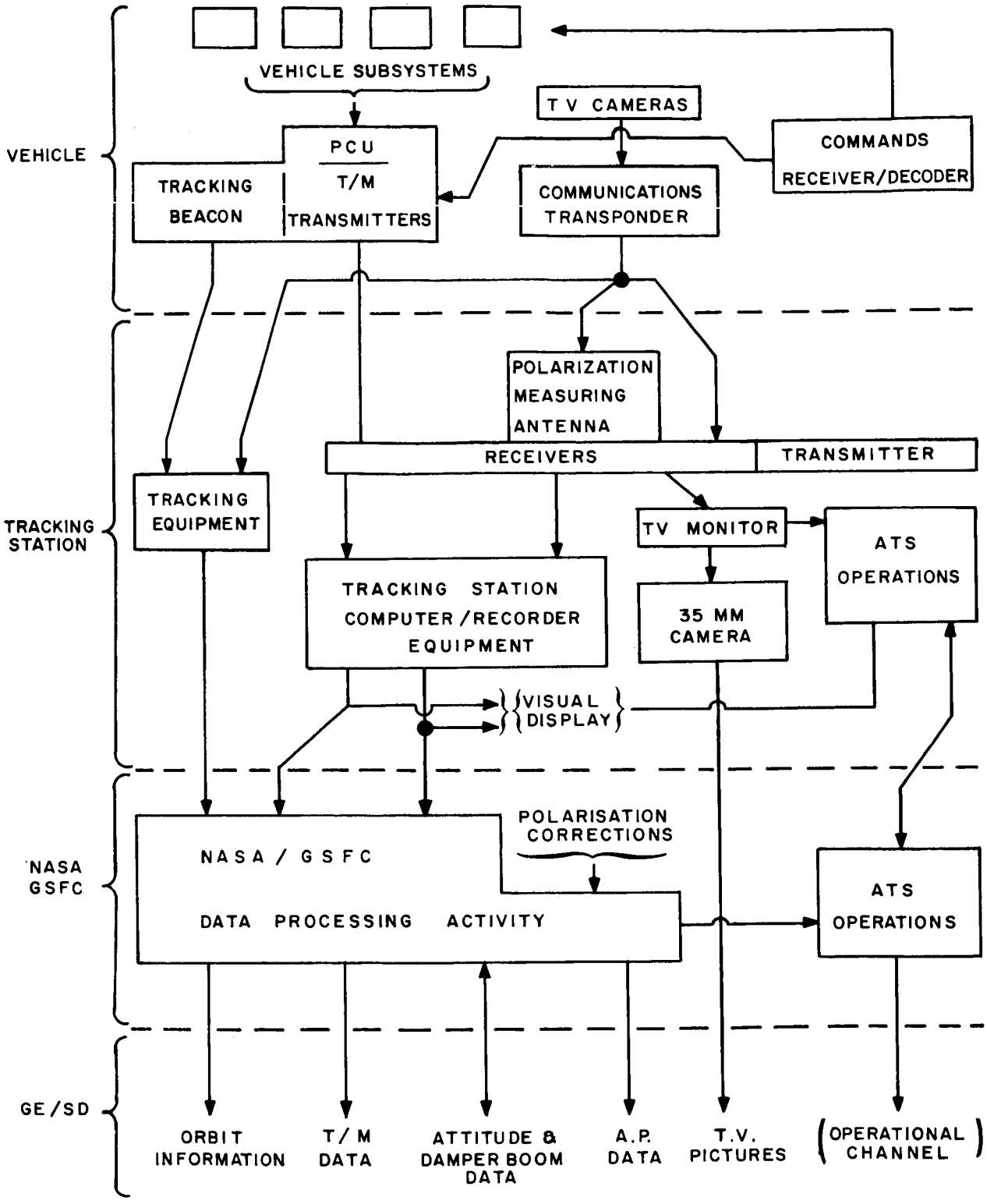

Figure 2-3. ATS Information System

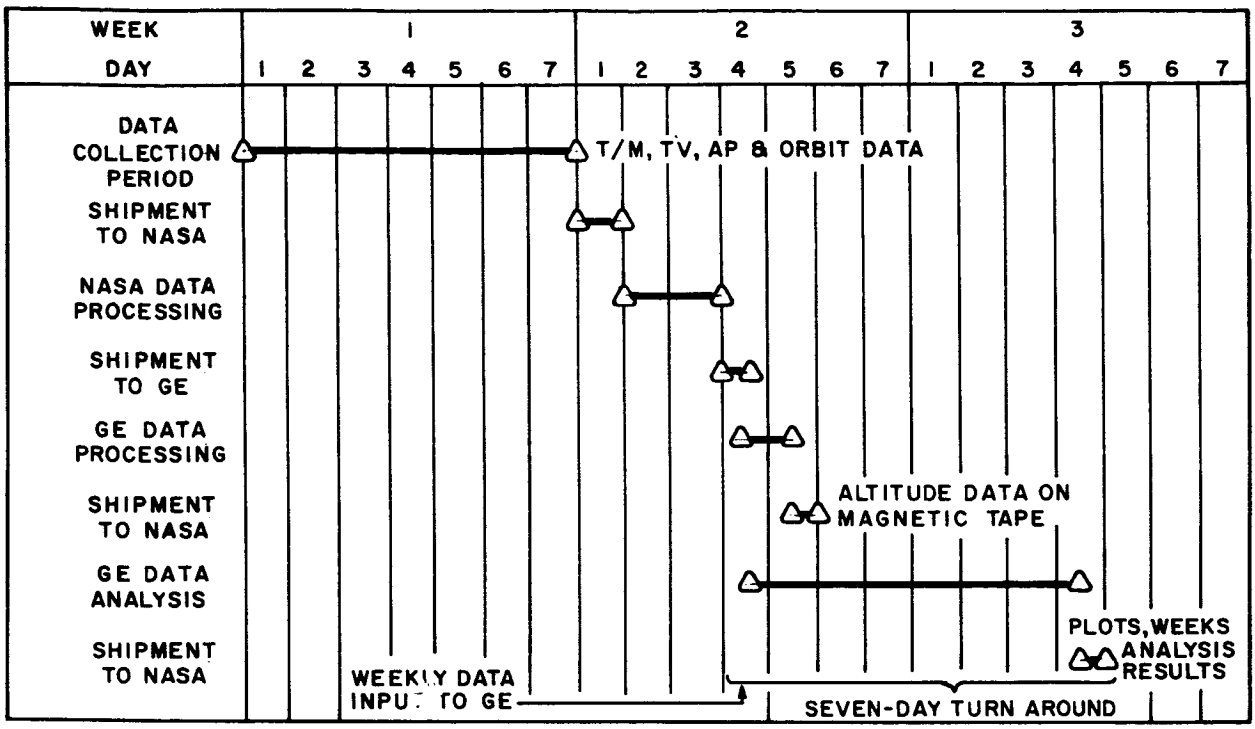

Figure 2-4. Information System Schedule

in detail, along with typical report outlines, as needed. Also, output data packages such as quick-look, weekly, and other are defined as to content and format.

A preliminary version of this plan has been completed, and distributed for comment. The rough draft will be updated and revised in accordance with comments received. Areas and topics of particular interest, insofar as revision and up-dating are concerned, include:

1. IR Earth Sensor — present status; actual field of view for both medium and synchronous altitude application; focal length of sensor optics.
2. Antenna Polarization — further definition of technique; reference system to be used; application of necessary corrections; availability - quick look and long term.
3. Orbit Information — world map calculation technique; verification of parameters to be made available; accuracies available.
4. Input Data Formats — telemetry (will a quality factor be available?); antenna polarization data; world map data.
5. Output Data Formats — quick look (teletype) output; weekly data package (magnetic tapes, plots).
6. Scheduling Considerations — delivery time allotments; turn-around times; teletype capabilities.

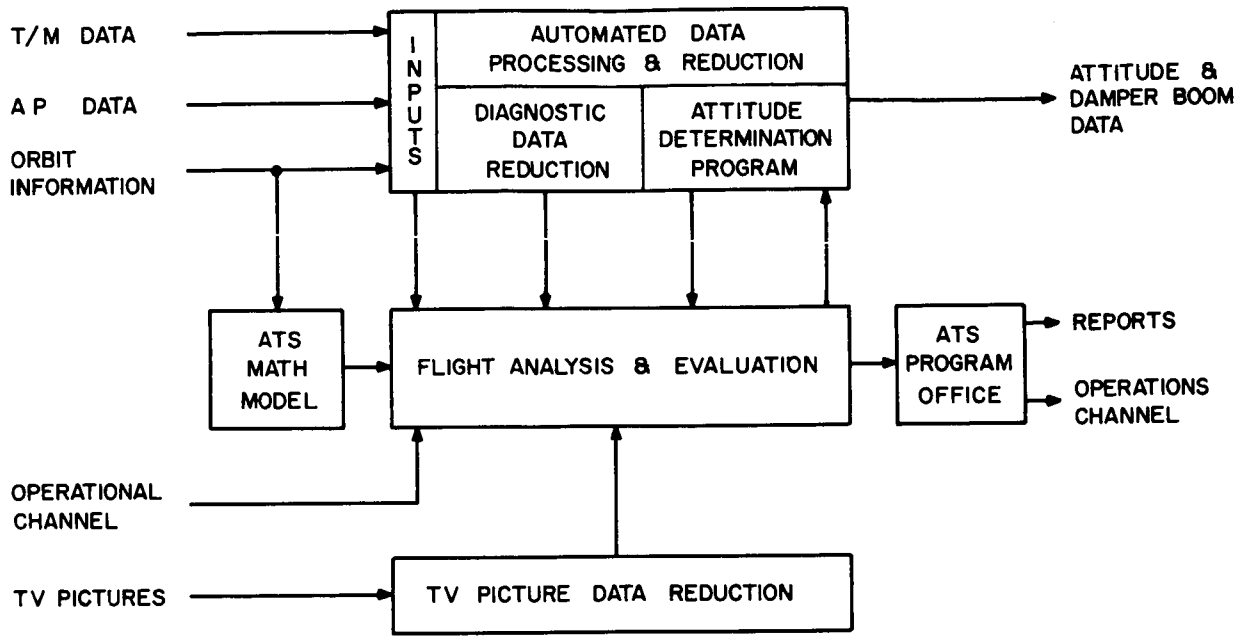

Figure 2-5. In-house Information Flow

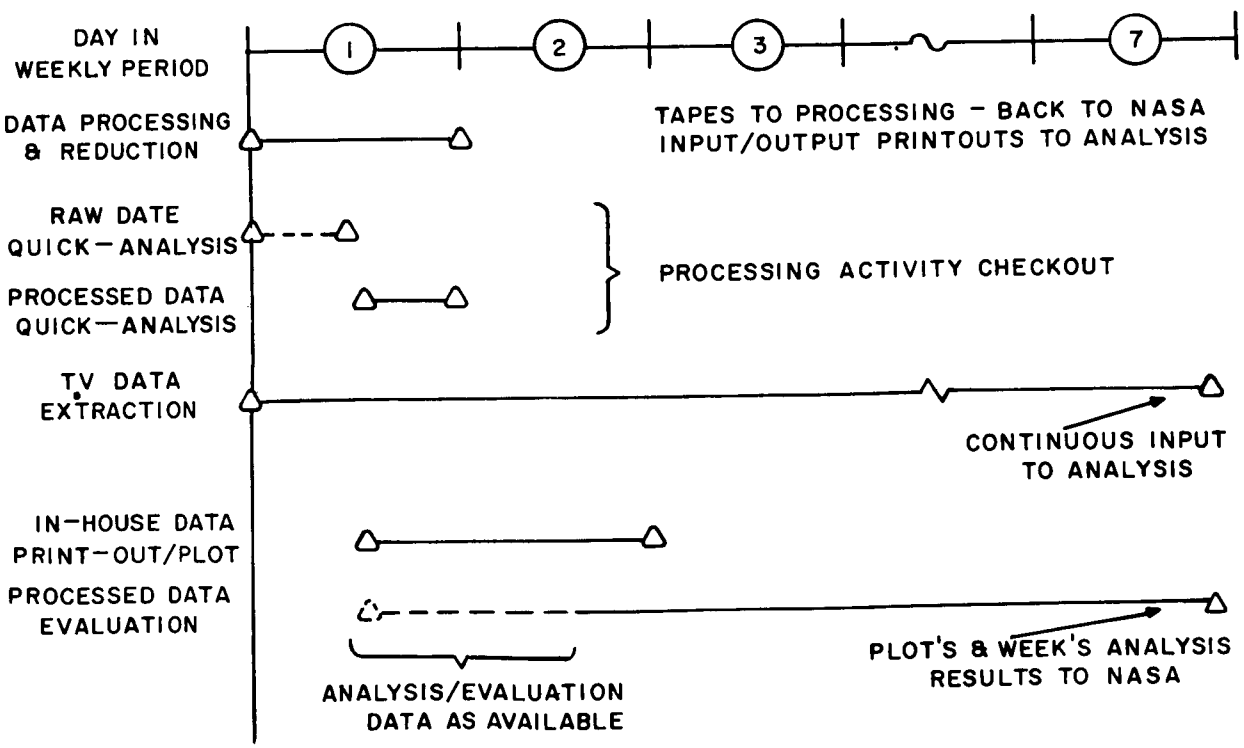

Figure 2-6. Weekly In-house Schedule

2.6 ANALYTICAL STUDIES AND RESULTS

2.6.1 ATS-A CAPTURE ANALYSIS

The decision to yaw the Agena through 90 degrees prior to ATS-A spacecraft separation (ATS Trajectory Meeting, Lewis Research Center, 21 April 1965), has eliminated the necessity for an initial Agena attitude and rate bias to insure upright capture. The incorporation of a delay time between Agena second burn cut-off (A2CO) and spacecraft separation (to account for possible "burping" of the Agena) has also eliminated the necessity for a delay time between spacecraft separation and initial deployment of the X-booms.

Updated capture studies have been completed and are based on the following sequence of events:

1. Spacecraft separation
2. 3-second delay time (max.)
3. X-Boom deployment to full-extension length of 132.3 feet at 19 degrees half-angle
4. Immediate scissoring of X-booms to nominal 25 degree half-angle
5. 2-day delay time prior to deployment of damper boom (tentative)
6. Deployment of damper booms
7. Uncaging of damper.

Initial conditions used in capture studies are as follows. If initial rates or moments of inertia exceed the values indicated, results of the capture analysis will require modification.

Initial Moments of Inertia

Pitch: 47.94 slug-ft^2 (max.)

Roll: 54.60 slug-ft^2

Initial Body - Axis Rates (3σ conditions)

Pitch: ±0.40 deg/sec

Roll: ±1 deg/sec

Yaw: ±1 deg/sec

Initial rates are based on discussions at the ATS Trajectory Meeting on 21 April 1965 and include contributions from both the Agena and the spring separation system. Initial moment of inertia values were obtained from Hughes Aircraft Company on 16 April 1965.

Capture studies included the effects of initial position errors (± 1 degree in pitch and roll and ± 5 degrees in yaw), worst case tolerances on boom lengths, and a variety of boom extension rates. For the stated maximums on initial rates and moments of inertia, upright capture is achieved for all extension rates down to 0.80 ft/sec. Based on these studies, the specification on X-boom extension rates has been revised downward to relieve the previously encountered problem of boom dynamic loading during boom extension and retraction maneuvers. Current specifications call for an extension rate of no less than 0.90 ft/sec and no greater than 1.50 ft/sec.

2.6.1.1 Computer Runs

Two series of capture runs were made to determine performance under a variety of conditions. Their characteristics are listed in Table 2-2. The first series of eight runs includes a range of conditions from worst-case to nominal. Plots of these eight runs are shown in Figures 2-7 through 2-14.

Worst case conditions are used in Runs 2 and 3. They are defined to be:

1. Maximum negative initial pitch angle and pitch rate, and maximum values of roll and yaw attitudes and rates. The roll and yaw polarities have been assigned to maximize body rates about the X_1 and Z_1 axis in Run 2 and the X_1 and Y_1 axis in Run 3. The nominal vehicle state is with zero angular errors, zero roll and yaw rates, and positive pitch rate equal to orbital rate. These conditions represent the maximum departure from nominal conditions.
2. Minimum rod extension rate. This provides the minimum rate of moment of inertia growth.
3. One rod in both rod pairs two feet short. This provides the minimum values of final moments of inertia.

Run 1 employs maximum positive initial angles and rates, minimum rod extension rate, and nominal rod length. Run 4 represents the worst-case conditions except that initial pitch angle and rate are positive. Runs 5 and 8 use the worst-case conditions of Run 3, except that the rod extension rate is the nominal value in Run 5 and the maximum value in Run 8. Run 6 is an attempt to define an arbitrary set of nominal conditions. Initial angles and rates are one-half those of the worst-case conditions in Run 3. Nominal values are used for rod extension rate and extended rod length. Run 7 repeats Run 6, except that the rod extension rate is the maximum value.

Right-side up capture is achieved in each of the first eight runs. As expected, the maximum pitch and roll angles occur in the worst-case runs. Also, the vehicle is spinning in yaw because of the initial yaw rate.

The second series of seven runs employed worst-case conditions and rod extension rates below the present specified minimum value of 1.5 ft/sec. No plots were made

TABLE 2-2. CAPTURE RESULTS, ATS-A

Run	Initial Angles (deg)			Initial Rates (deg/sec)			Rod Extension Rates (ft/sec)	Rod Length* (ft)
	θ_P	θ_R	θ_Y	θ_P	θ_R	θ_Y		
1	1	1	5	.4	1	1	1.5	132.34
2	-1	1	5	-.4	1	1	1.5	130.34
3	-1	1	-5	-.4	1	1	1.5	130.34
4	1	-1	5	.4	1	1	1.5	130.34
5	-1	1	-5	-.4	1	1	2	130.34
6	- .5	.5	-2.5	-.2	.5	.5	2	132.34
7	- .5	.5	-2.5	-.2	.5	.5	3	132.34
8	-1	1	-5	-.4	1	1	3	130.34
9	-1	1	-5	-.4	1	1	1.2	130.34
10	-1	1	-5	-.4	1	1	1.0	130.34
11	-1	1	-5	-.4	1	1	0.75	130.34
12	-1	1	-5	-.4	1	1	0.50	130.34
13	-1	1	-5	-.4	1	1	0.80	130.34
14	-1	1	-5	-.4	1	1	0.85	130.34
15	-1	1	-5	-.4	1	1	0.90	130.34

*Only one rod in each rod pair can be two feet short. The number listed is the length of the shorter rod in both rod pairs. The other rod length is the nominal value of 132.34 feet.

of the second set of runs since these runs were made to determine an absolute minimum value of rod extension rate that will allow right-side up capture. The vehicle tumbled when the rod extension rate was reduced to 0.75 ft/sec or less. The minimum value for right-side up capture is 0.80 ft/sec.

To determine the vehicle performance after the damper is uncaged, the final values of angles and rates from two capture runs were used as initial conditions for GAPS IV computer runs. (GAPS IV is the original GAPS III program written in FORTRAN IV.) This was done for one of the worst-case conditions runs (Run 2) and the nominal-conditions run (Run 8). Plots of these runs are shown in Figures 2-15 and 2-16. The 19° X-rod half-angle was also used in these runs to duplicate actual orbit conditions

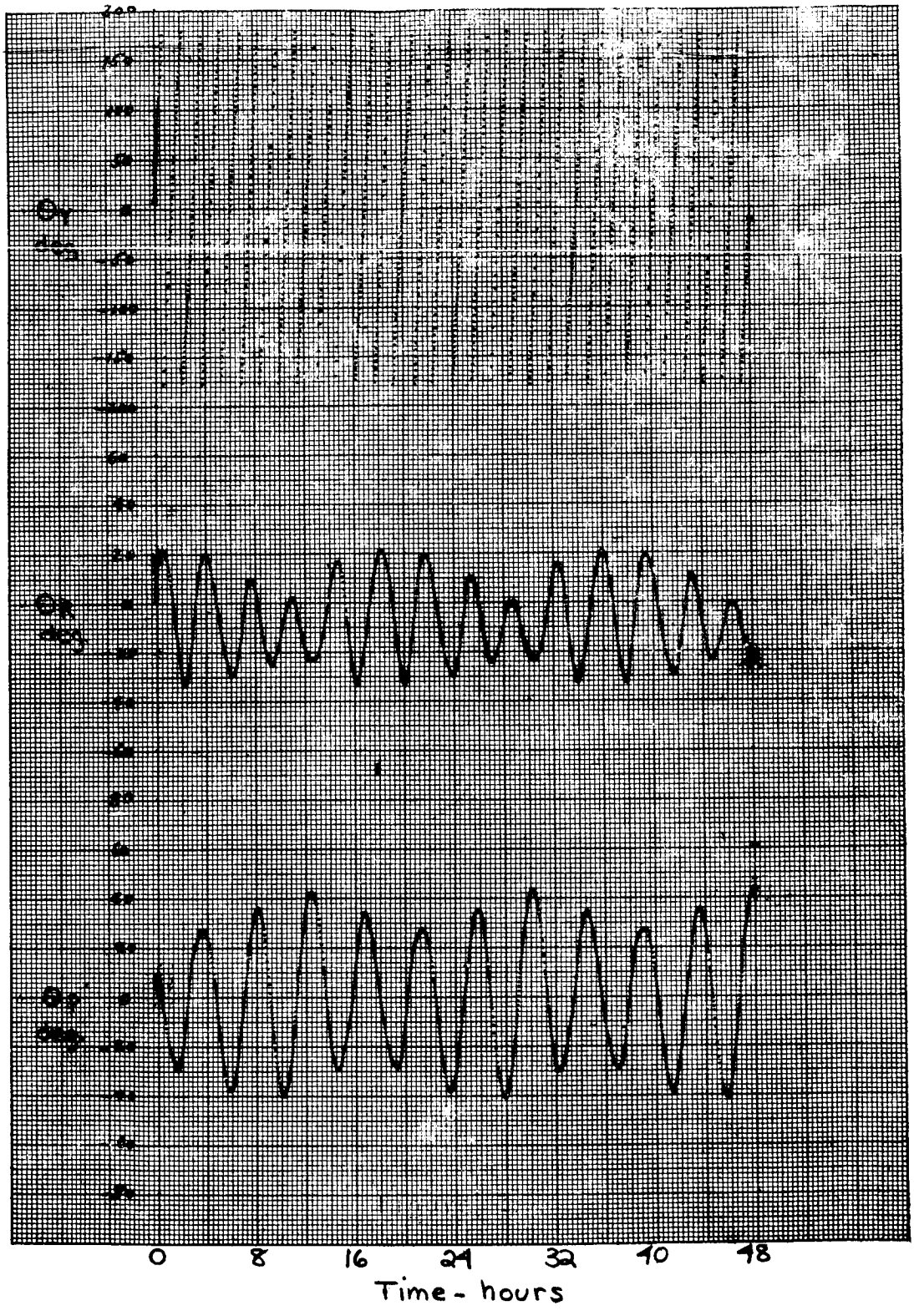

Figure 2-7. ATS Capture, Run No. 1

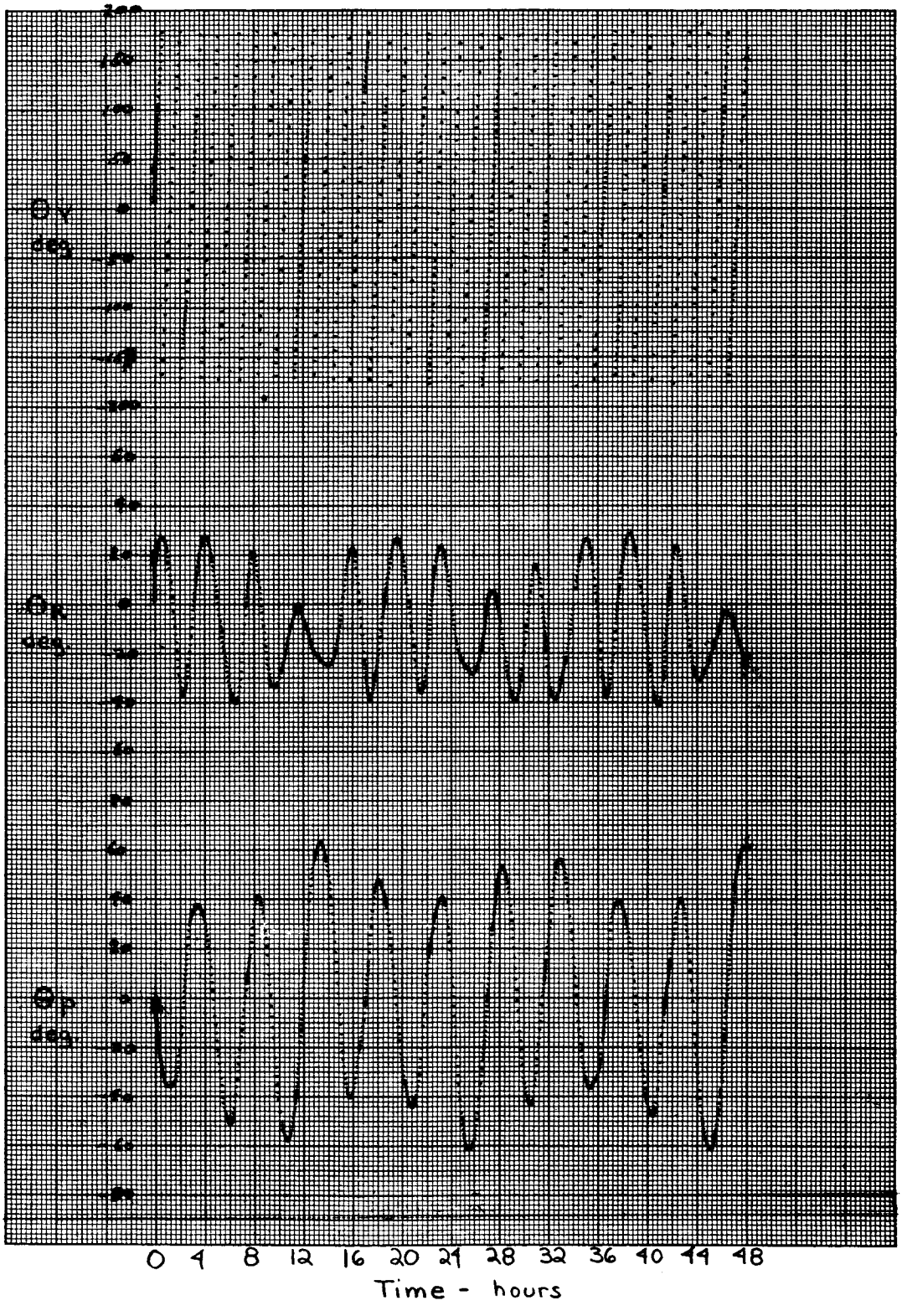

Figure 2-8. ATS Capture, Run No. 2

4669

FIG-3

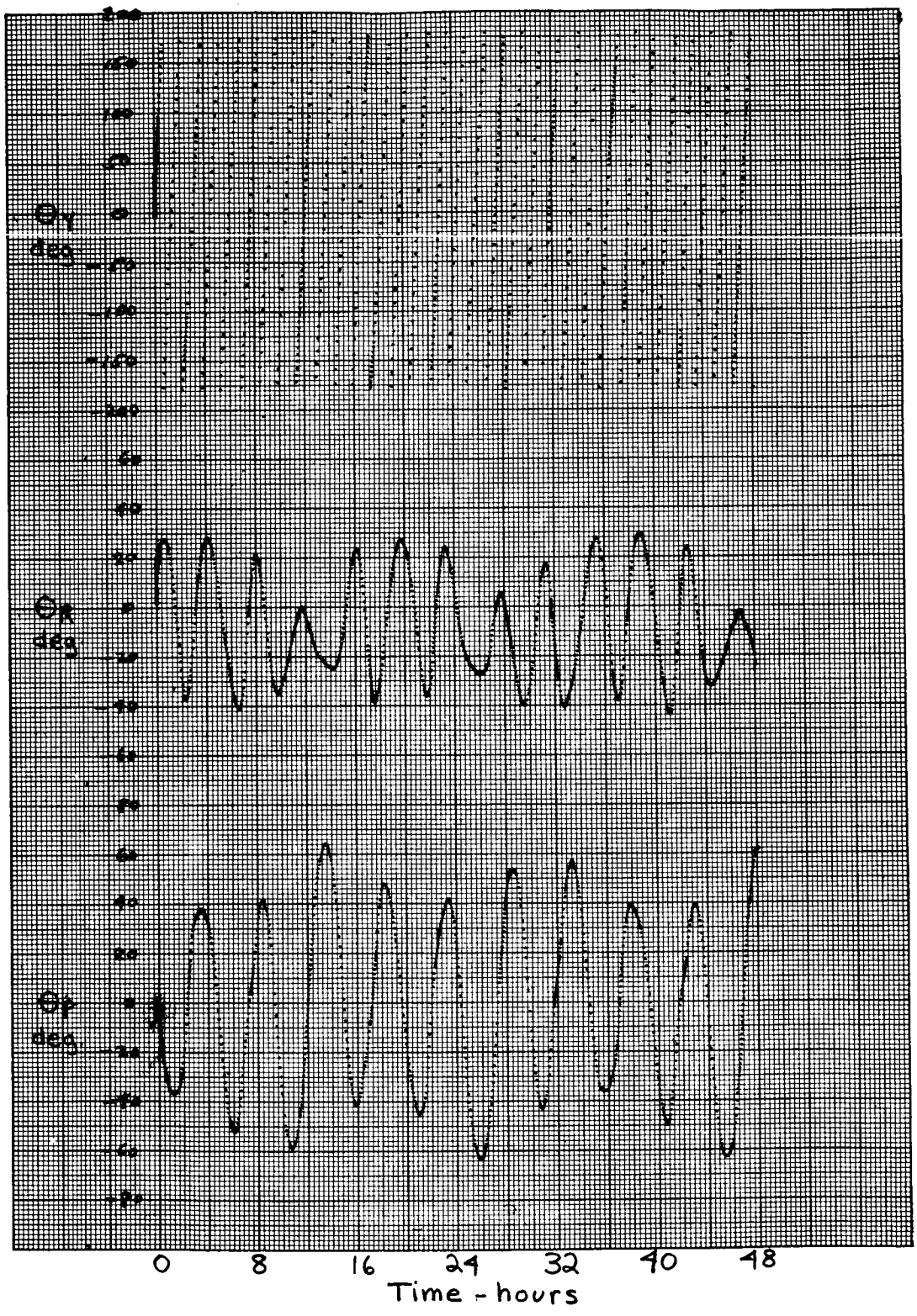

Figure 2-9. ATS Capture, Run No. 3

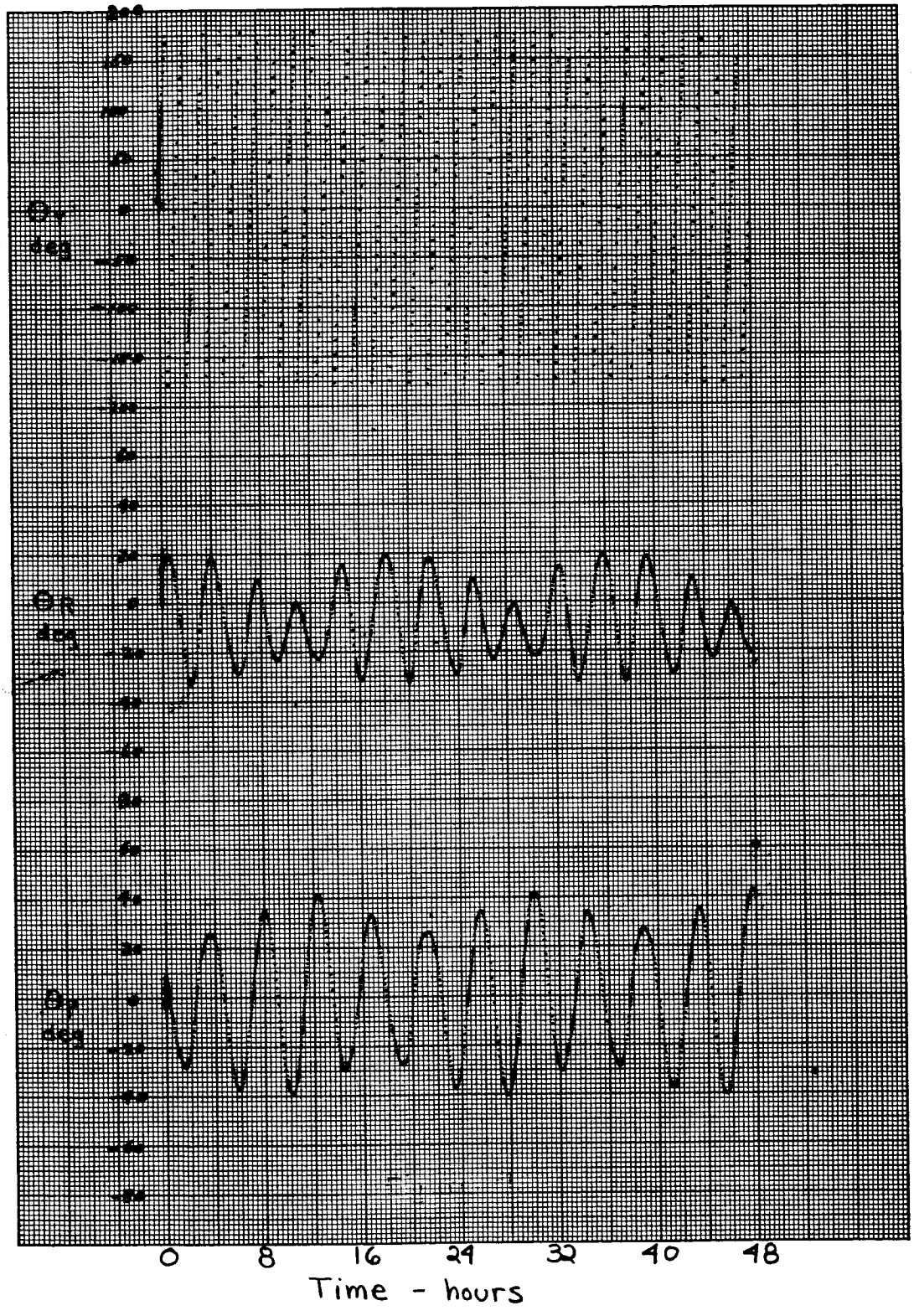

Figure 2-10. ATS Capture, Run No. 4

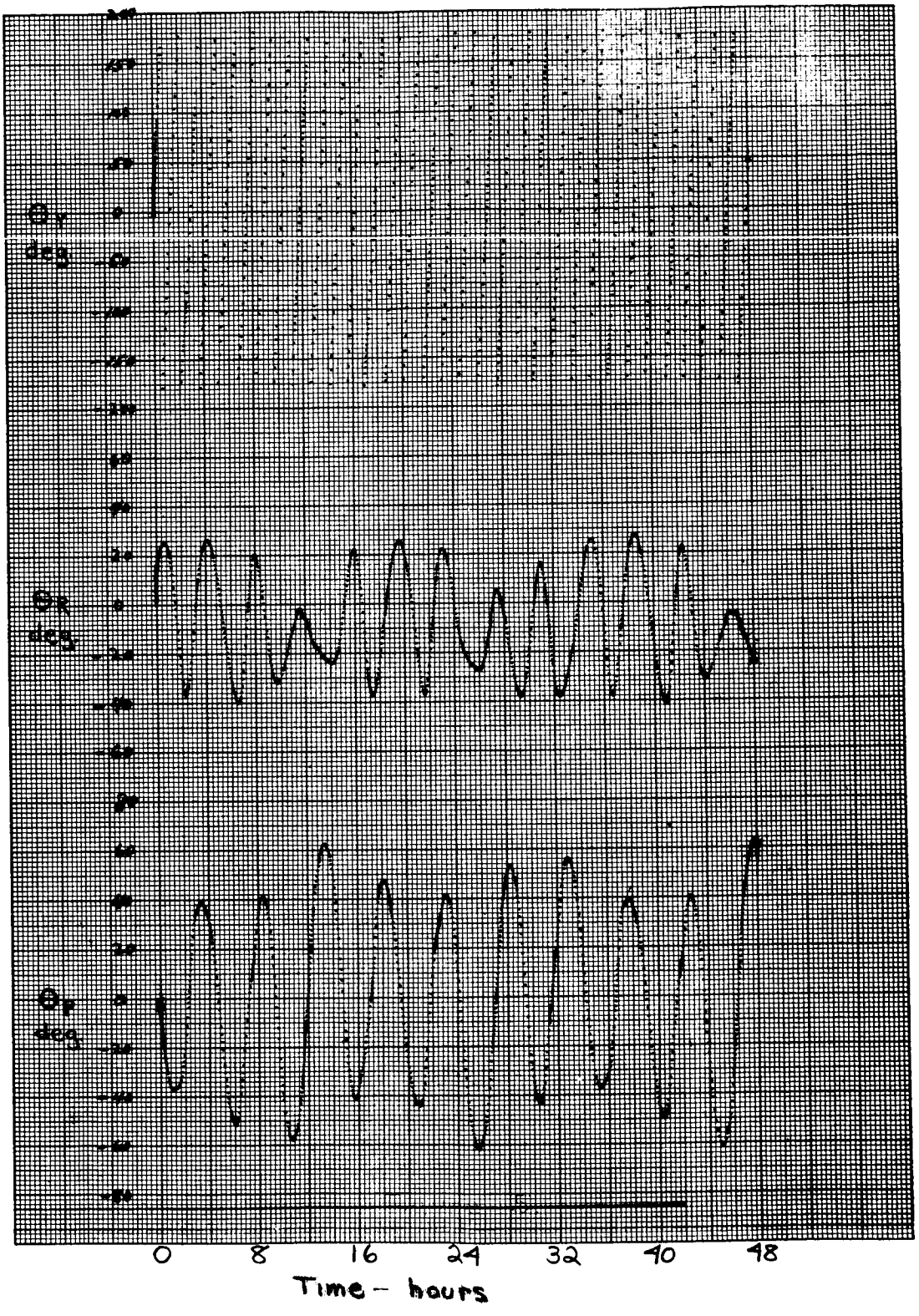

Figure 2-11. ATS Capture, Run No. 5

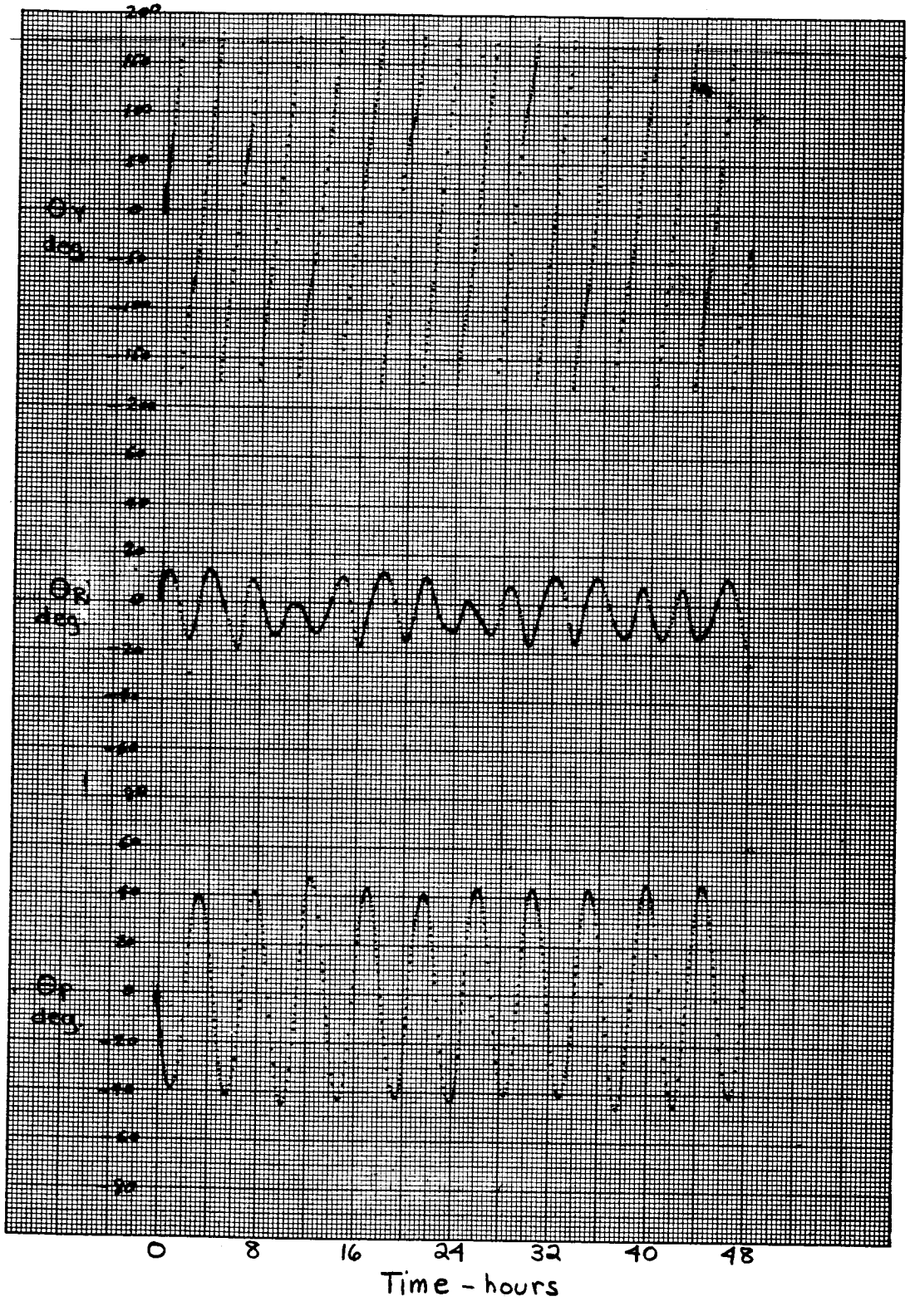

Figure 2-12. ATS Capture, Run No. 6

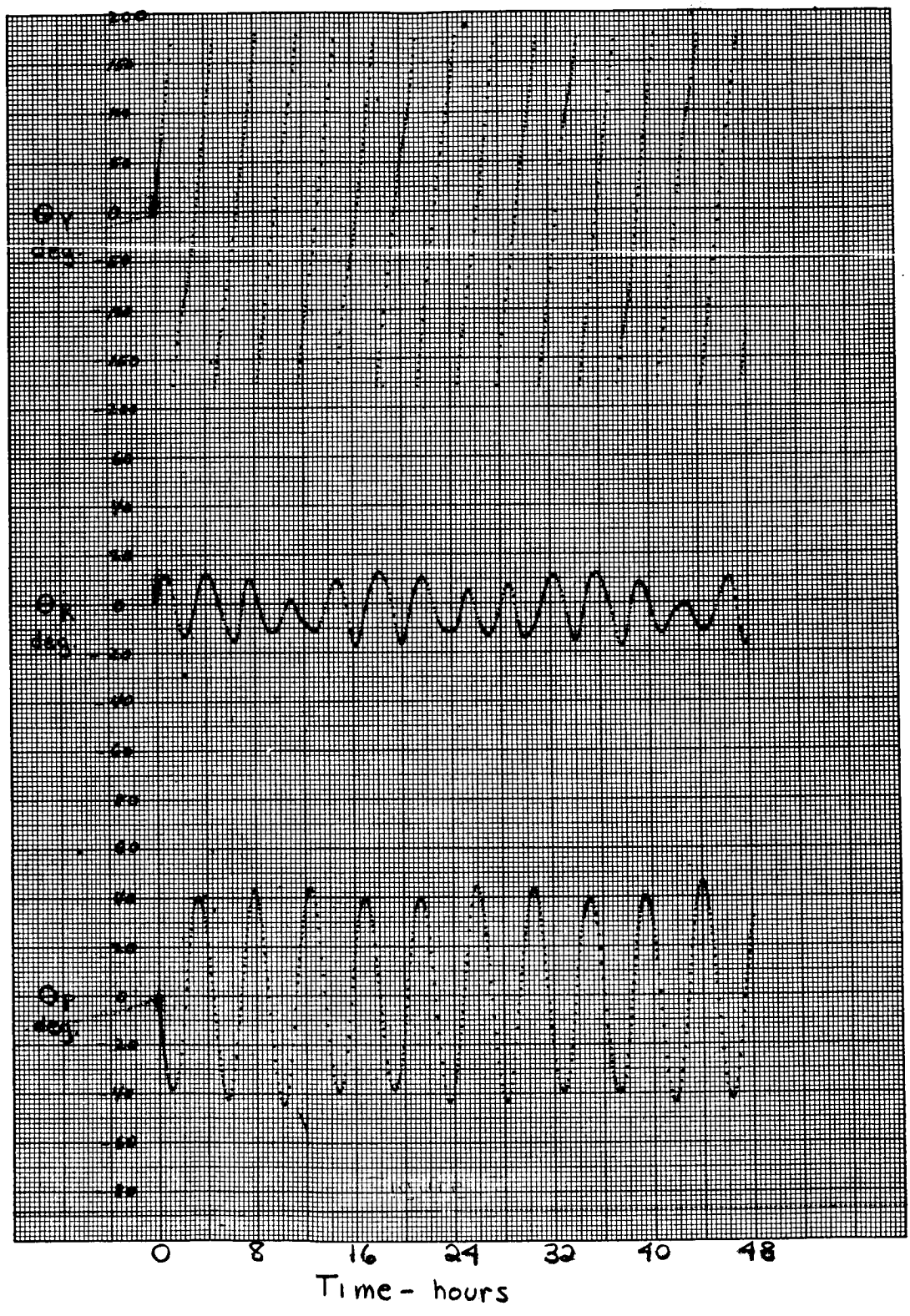

Figure 2-13. ATS Capture, Run No. 7

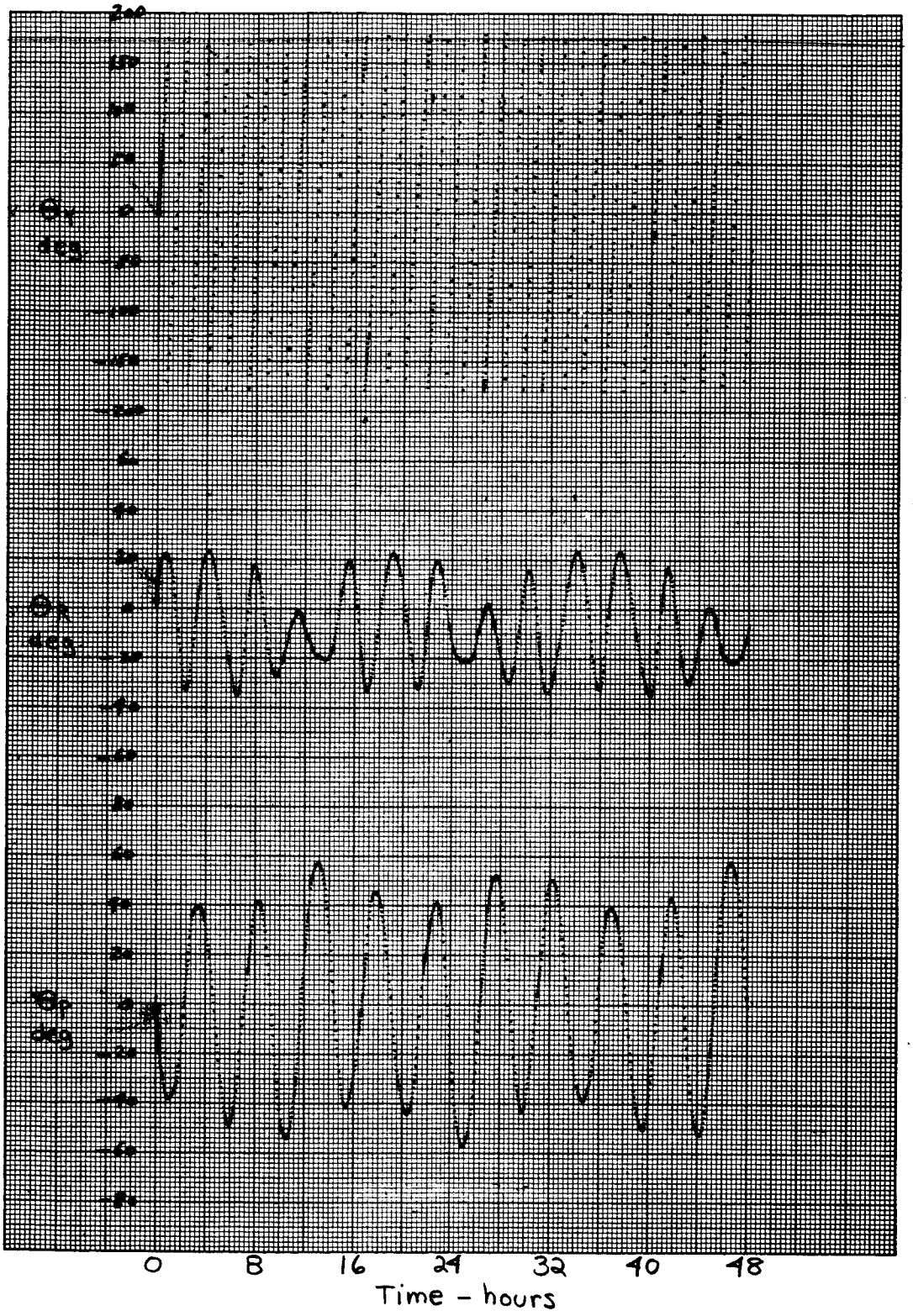

Figure 2-14. ATS Capture, Run No. 8

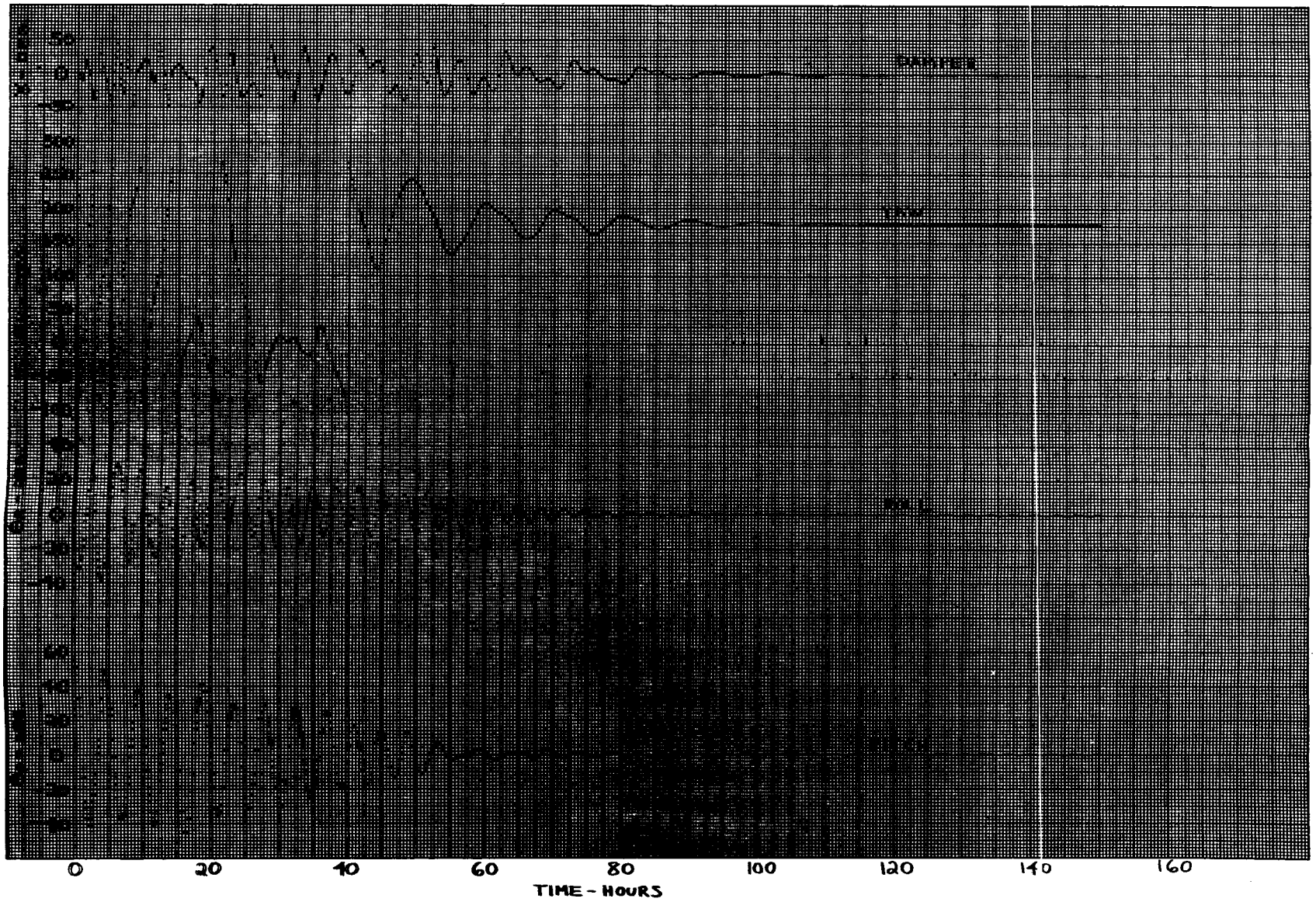

Figure 2-15. ATS-A Performance Following Initial Capture, Worst Case Condition (Run 9)

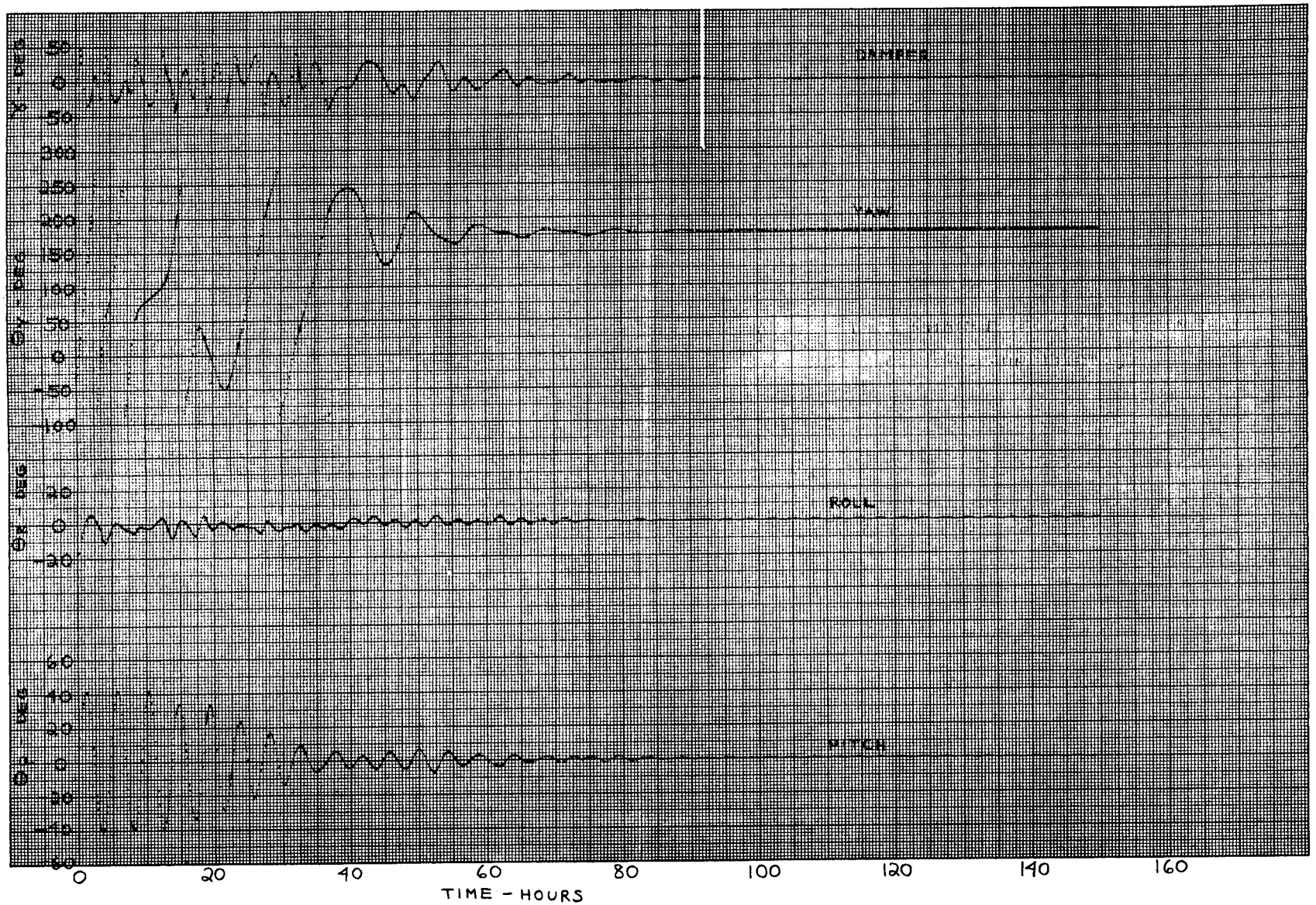

Figure 2-16. ATS-A Performance Following Initial Capture, Nominal-Condition (Run 10)

as presently planned. This reduced the vehicle damping. In both runs, using the eddy current damper, steady-state conditions were not reached after 150 hours in orbit. This is not apparent on the plots because of the large scale used to accommodate the initial transient. For this reason, it is recommended that the X-rod half-angle be changed from 19° to the nominal value of 25° immediately after completing rod extension.

2.6.2 INVERSION STUDIES

Studies are progressing for both thruster inversion and flywheel inversion. The flywheel inversion study is near completion and hardware implementation requirements are being defined. The thruster inversion studies were expanded to include consideration of coast-phase maneuvers and utilization of data from the solar aspect sensor. Ground rules for thruster inversion studies were established on 13 May 1965 (at NASA/GSFC) based on partial results of coast-phase and inversion energy studies at GE. Established ground rules are as follows:

1. Nominal torque level for the HAC subliming rockets will be increased to 13 x 10^{-4} ft-lbs.
2. A maximum of four hours will be allowed for total inversion time (from initial thrust on to counter thrust off).
3. A coast-phase maneuver will be utilized to minimize the energy input into the system. (Nominally, the inversion thruster will be on for an initial period of about 45 minutes; the system will then coast through the 90 degree point to a symmetrical point on the other side of 90 degrees; at this point the counter-thrust will be applied for a nominal period of about 45 minutes).
4. A ten-minute rise and decay time (± 2 1/2 minutes) will be assumed for all thrusters.
5. Minimum torque level approximately 6.75 x 10^{-4} ft-lbs; maximum torque level approximately 19 x 10^{-4} ft-lbs. (for purposes of study).
6. Basic maneuver will be accomplished on the basis of pre-determined time commands; attitude estimates (based on SAS data) will be utilized for real-time back-up data and to improve on predetermined time estimates if warranted.

2.6.3 HYSTERESIS DAMPER STUDIES

2.6.3.1 Constant Saturation Torque Damping

2.6.3.1.1 Discussion

In a hysteresis damped system utilizing a damper with a constant value of hysteresis saturation torque, T_{SAT} the optimum hysteresis value is selected based upon two

factors. First, sufficient damping must be provided to minimize the time required to reduce the vehicle pointing error to a level where the vehicle can perform its mission. Second, T_{SAT} must be high enough to limit the damper boom motion to the ±45° between the mechanical stops. Steady-state pointing accuracy is virtually independent of T_{SAT}, and is not a factor in determining its value.

Figures 2-17 and 2-18 show the time required to settle to various levels of earth-pointing error as a function of T_{SAT} for the ATS-A and ATS-D vehicles respectively. These curves are based upon data obtained from a series of GAPS IV computer runs. The conditions used in these runs are:

		ATS-A	ATS-D
1.	Vehicle initial attitude (deg.)		
	Pitch	-35.9	-35.9
	Roll	8.1	8.1
	Yaw	180.5	180.5
	Damper Boom	0	0
2.	Vehicle initial attitude rates $\left(\frac{\text{deg}}{\text{sec}}\right)$		
	Pitch	.0175	-.00467
	Roll	.01408	-.00376
	Yaw	.005993	.0016
	Damper Boom	0	0
3.	Orbit Eccentricity	.01	0
4.	Magnetic Dipole Along Roll Axis (pole-cm)	1000	1000
5.	Solar Effects	None	None

The vehicle initial conditions listed in 2-17 and 2-18 above define a standard transient which has been used throughout this study to provide meaningful comparisons of data. This standard transient was taken from an ATS-A capture study run (Figures 2-7 through 2-16). The vehicle rates were scaled down for use with ATS-D.

Immediately evident in Figures 2-17 and 2-18 is the amount of scattering of the data. There are several reasons for this. Initially the vehicle is spinning in yaw. In some runs the vehicle steady-state yaw angle is 0°, in other runs it is 180°. This difference in rotating through half a revolution will materially affect settling times. Another factor that contributes to the data scatter in Figures 2-17 and 2-18 is the use of arbitrary levels of earth-pointing errors. For example, consider the following hypothetical case. At 150 hours, two runs yield the following data:

T_{SAT}	θ_E
150	4.9
175	5.1

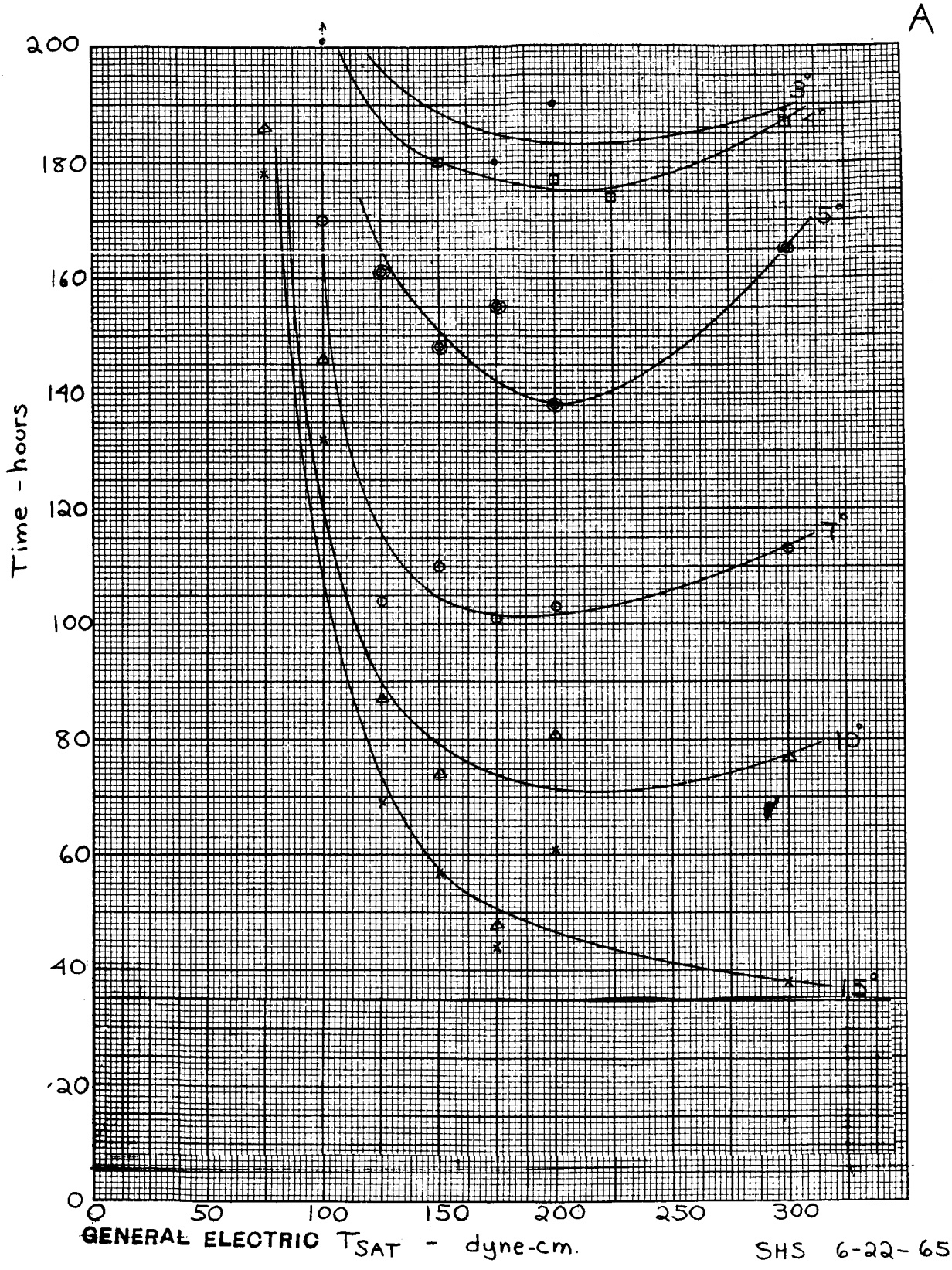

Figure 2-17. ATS-A with Constant Saturation Torque Hysteresis Damper Time to Damp to Various Earth Pointing Errors as a Function of Hysteresis Saturation Torque

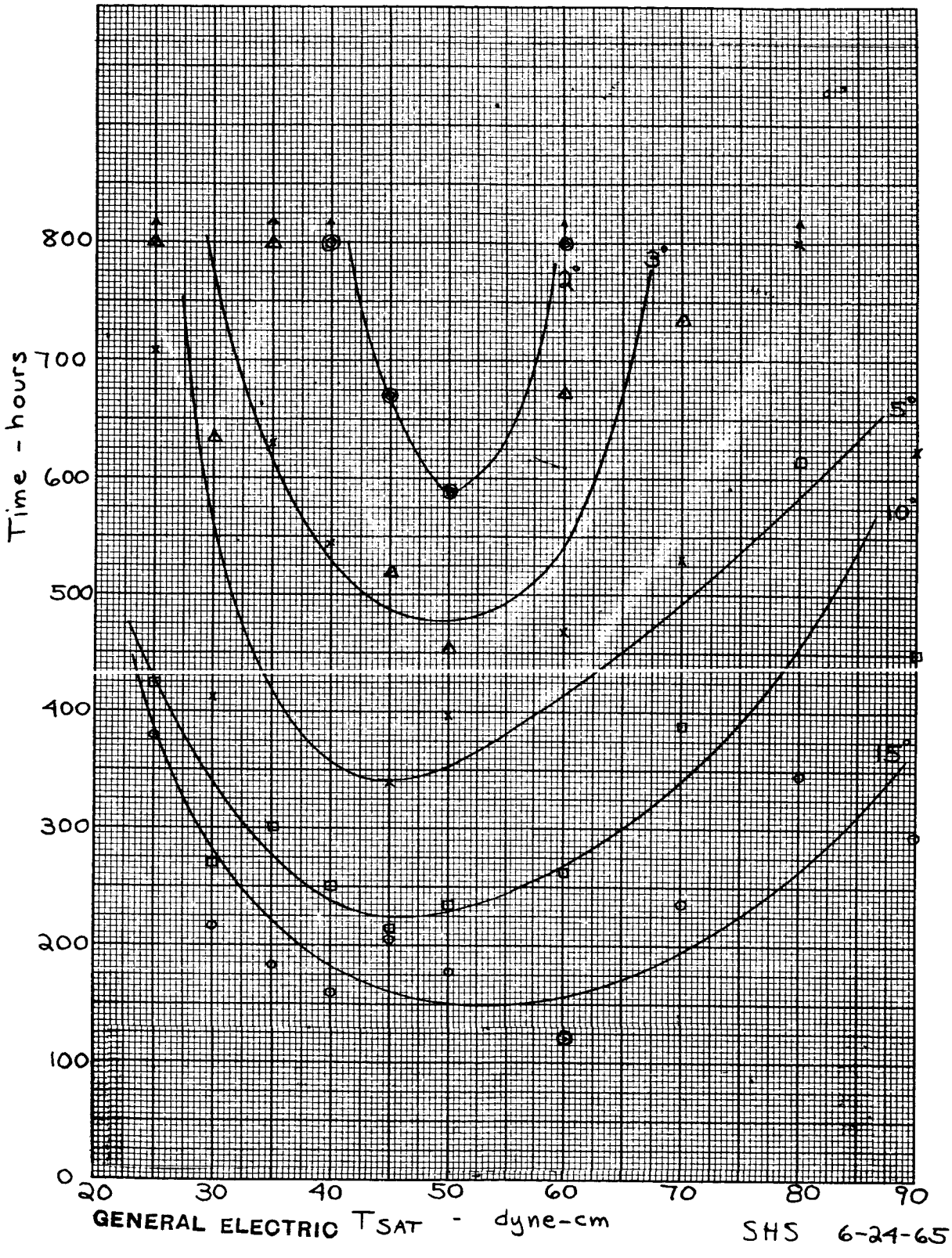

Figure 2-18. ATS-D with Constant Saturation Torque Hysteresis Damper Time to Damp to Various Earth-Pointing errors as a Function of Hysteresis Saturation Torque

The first run has already settled to 5°. The second has not, and may not reach 5° or less for another 30 or 40 hours. This yields scattered data points although it is apparent that these two runs are very similar.

Despite the data scatter there are obvious trends to be seen. Based upon these data the following nominal values of T_{SAT} were chosen to minimize damping time to low values of pointing error.

ATS-A	ATS-D
175 dyne-cm	50 dyne-cm

These values were checked with additional GAPS IV runs with solar effects included. For ATS-A, three 600-hour runs were made with T_{SAT} = 150,173 and 200 dyne-cm. For ATS-D, three 2250 - hour runs were made with T_{SAT} = 40, 50 and 60 dyne-cm. The resulting damping characteristics are plotted in Figures 2-19 and 2-20. Scattering of the data is not present in these curves because settling times to arbitrary values of error are not used. The curves shown are the envelopes of the earth-pointing error oscillations. Figures 2-19 and 2-20 show similar damping performance for all the values of T_{SAT} used for each vehicle. As time increases, the effect of the value of T_{SAT} on damping performance decreases. All the values used provide satisfactory damping performance, and this was used to select the tolerances of T_{SAT} to ±25 for ATS-A and ±10 for ATS-D. These tolerances are not necessarily absolute limits but they include the range of values checked with computer runs. If it becomes desirable to widen these tolerances, it may be possible to do so. However, it would first be necessary to check the new values of T_{SAT} with additional computer runs.

Figures 2-21 through 2-24 show the performance with the nominal values of T_{SAT} for both ATS-A and ATS-D. The 30-hour gap in the ATS-A curves between 190 and 220 hours was necessary to provide a convenient large scale plot for both transient and steady-state conditions.

2.6.3.1.2 Conclusions:

The recommended values of hysteresis damper saturation torque are:

ATS-A 175 ± 25 dyne-cm

ATS-D 50 ± 10 dyne-cm.

The primary effect of variations in the value of saturation torque is to change the damping time. Steady-state pointing error is virtually unaffected.

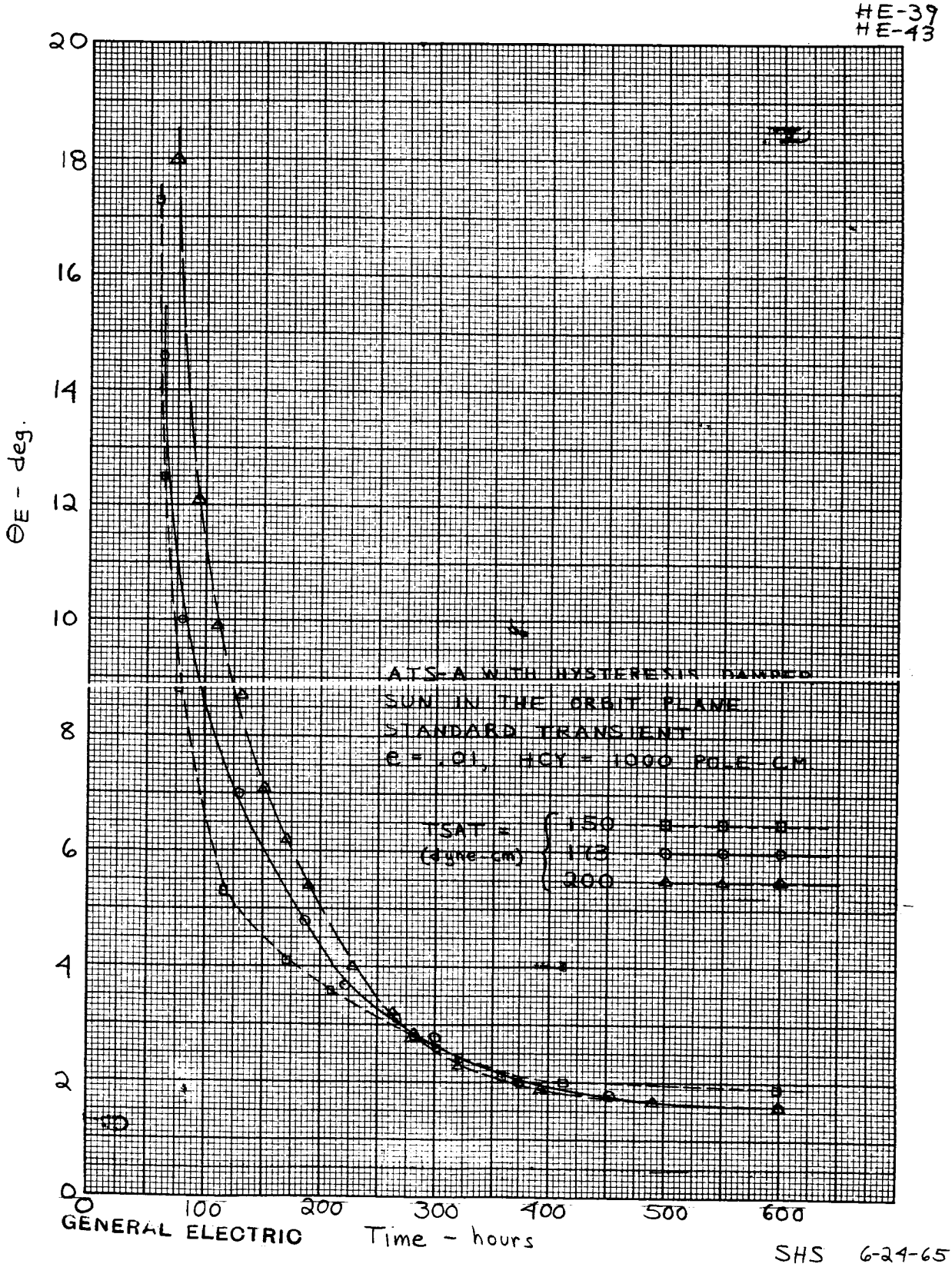

Figure 2-19. ATS-A Damping Performance

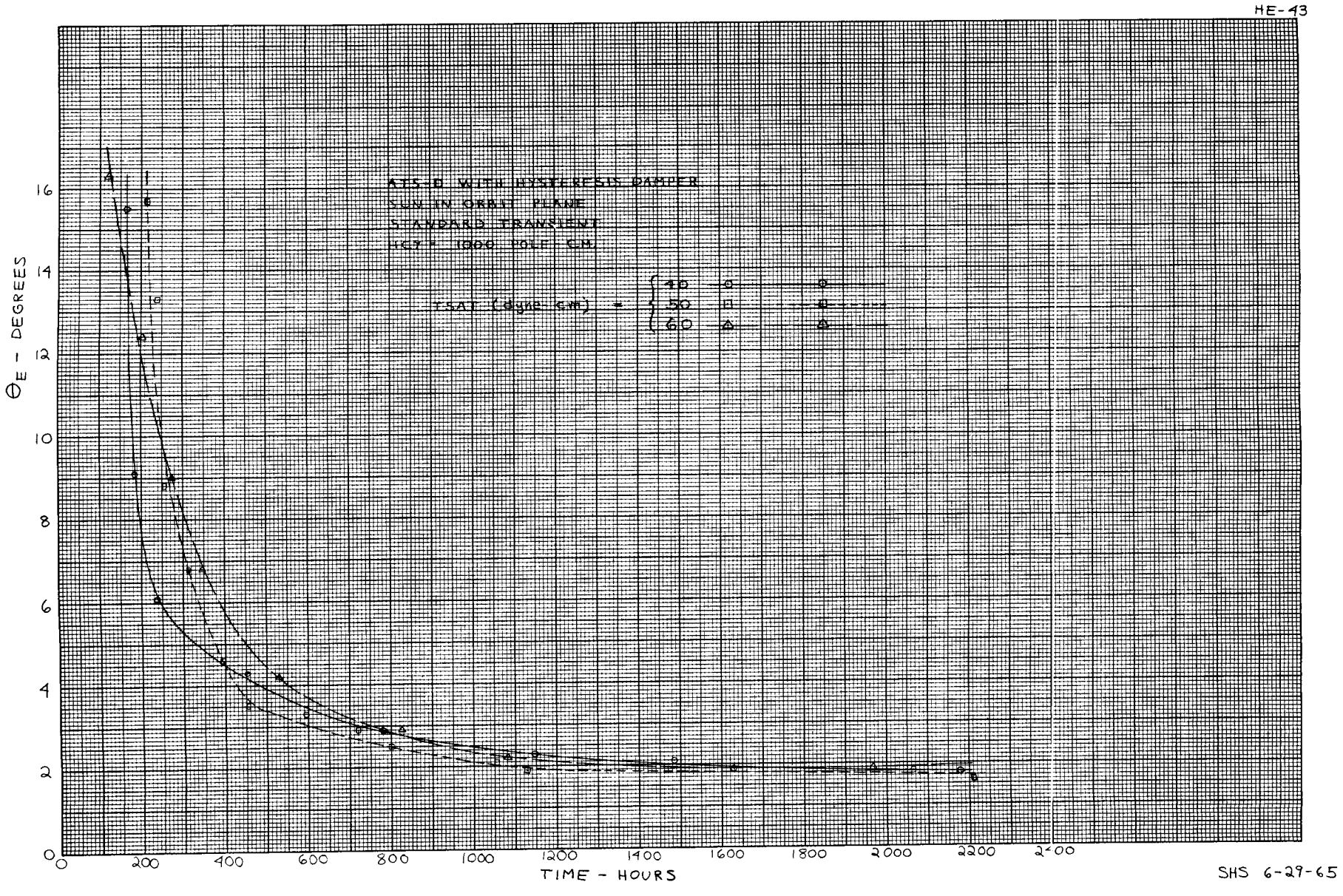

Figure 2-20. ATS-D Damping Performance

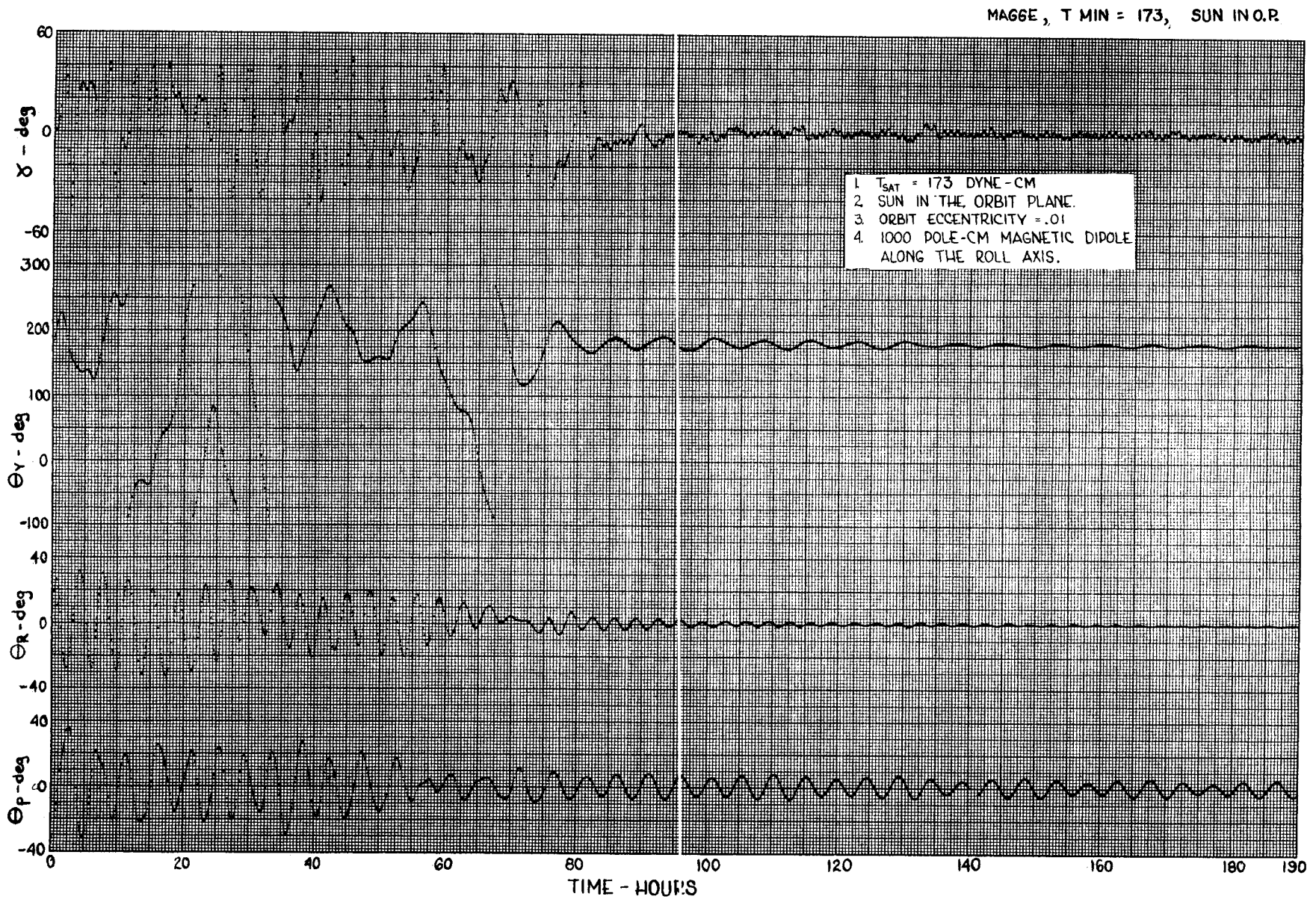

Figure 2-21. ATS-A Damping Performance

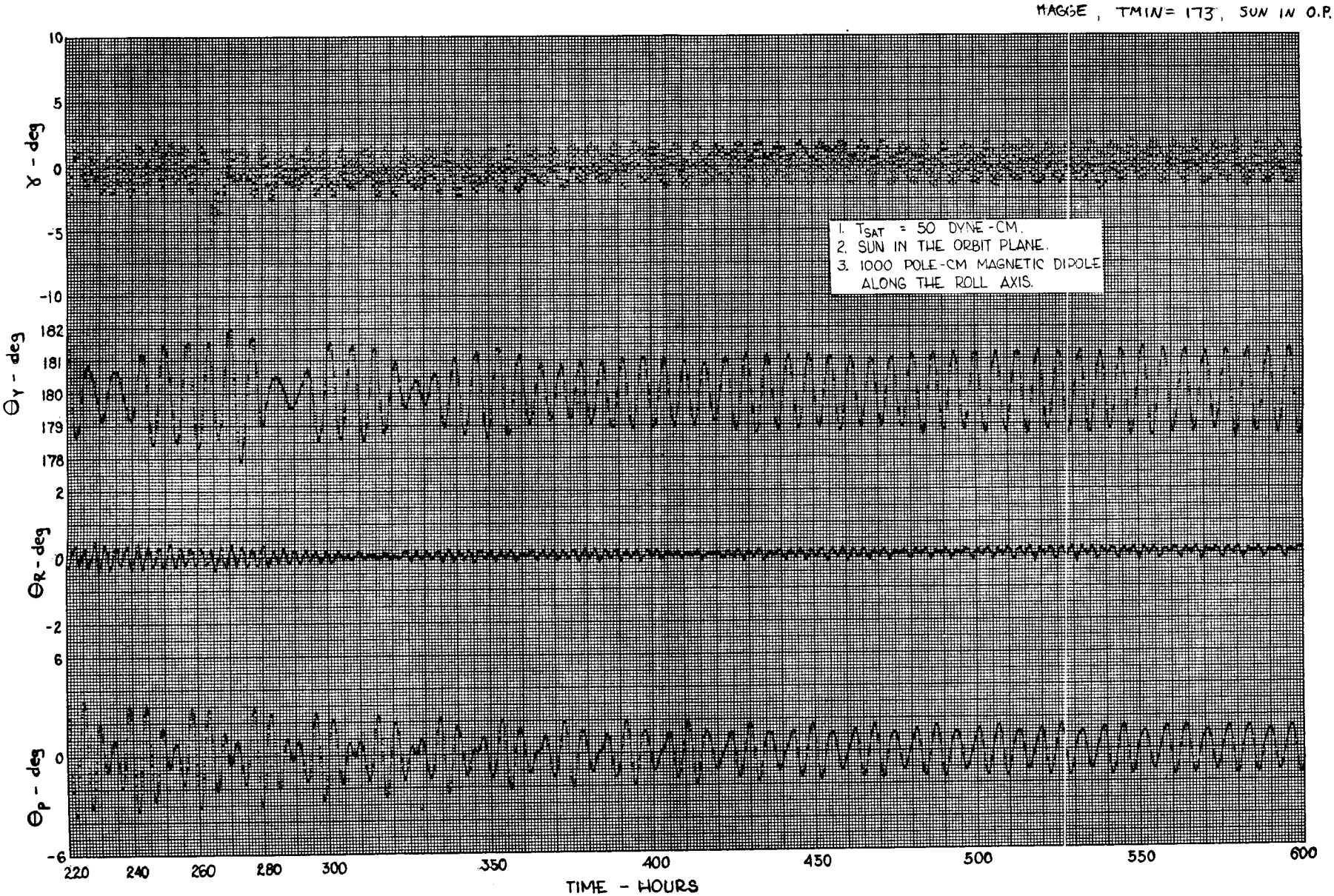

Figure 2-22. ATS-A Damping Performance

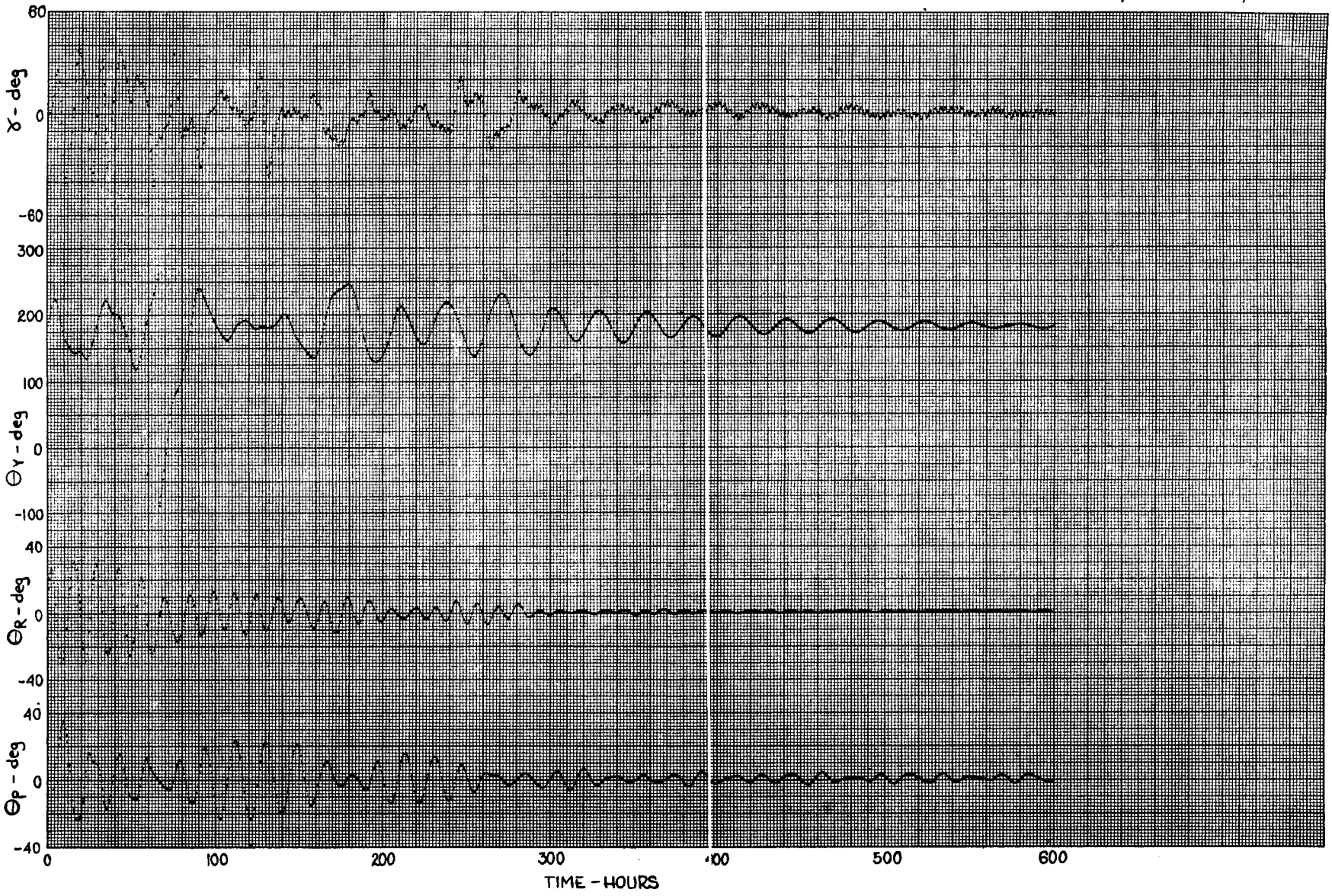

Figure 2-23. ATS-D Damping Performance

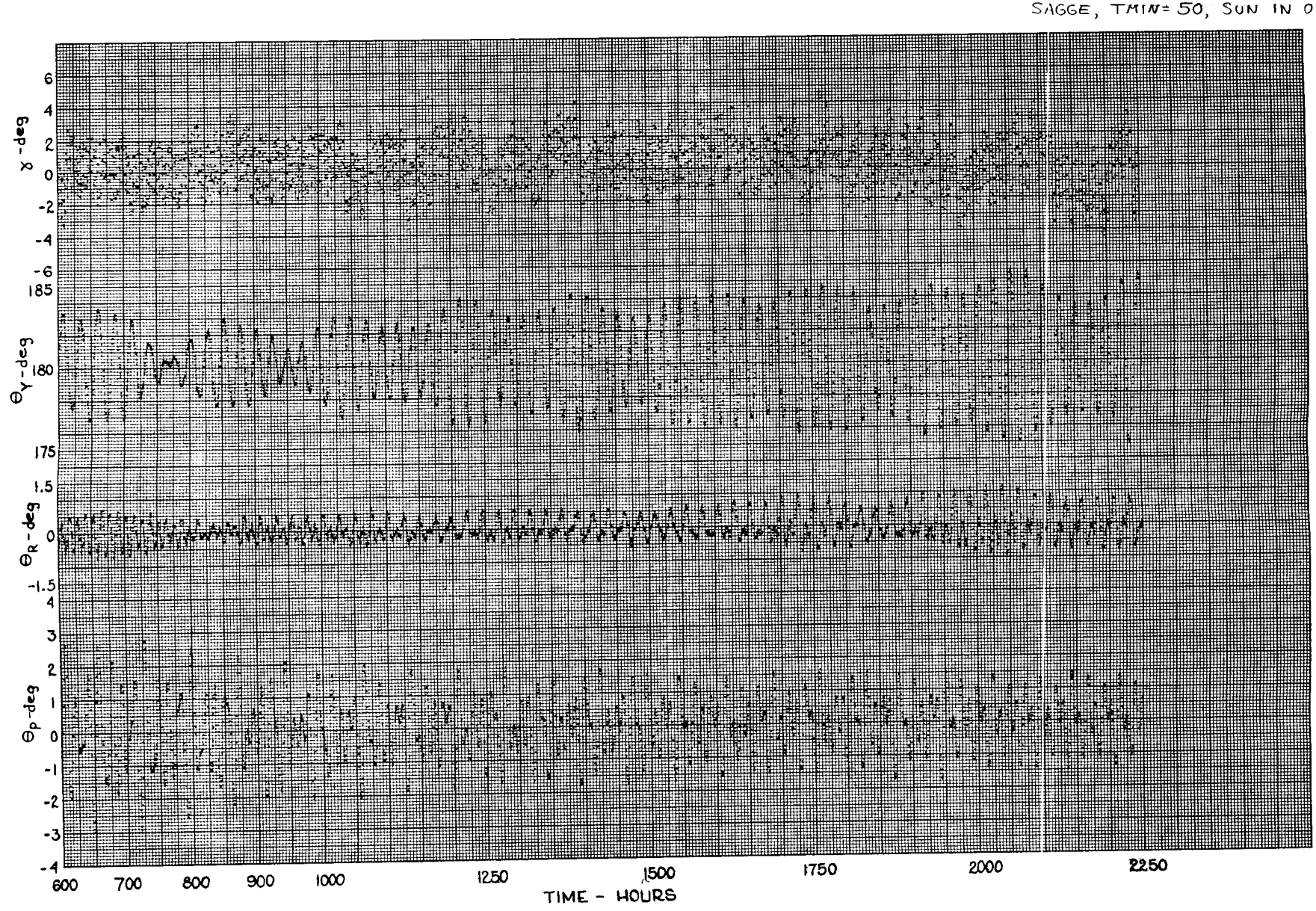

Figure 2-24. ATS-D Damping Performance

2.6.3.2 Variable Saturation Torque Damping

2.6.3.2.1 Introduction

The present hysteresis damper employs a constant value of hystersis saturation torque, T_{SAT}. The value of T_{SAT} represents a compromise between good damping of large and small disturbances. If T_{SAT} is high there is good damping of large transients, and the damper boom motion is not excessive. However, when the disturbance errors are small the damper boom motion is too limited to provide good damping. Conversely, low values of T_{SAT} provide good damping for small disturbances. However, damping in the presence of large disturbances is completely inadequate, and damper boom motion is excessive. In an attempt to improve hysteresis damper performance, a damper was designed in which T_{SAT} is a function of damper boom angular rotation, γ. This has been called the "bow-tie" concept. At present no further work is being done on this design. All of this work was done for ATS-A. The recommended parameters were scaled down for use in ATS-D, and one run was made to obtain ATS-D performance.

2.6.3.2.2 Discussion

To improve hysteresis damper performance, it is necessary to provide low values of T_{SAT} for small vehicle disturbances, and large values for large disturbances.

This is accomplished by making T_{SAT} a function of γ. The model used is shown in Figure 2-25 for the first quadrant. The other three quadrants are similar.

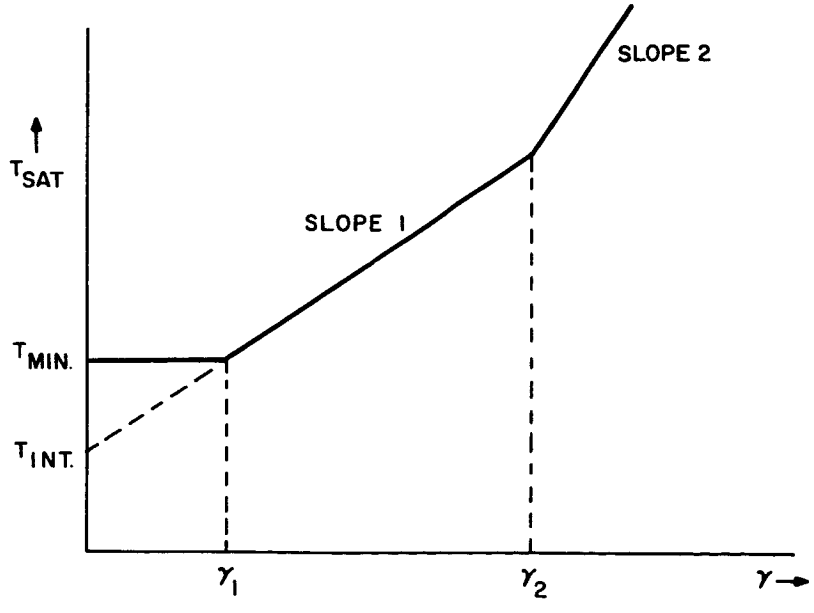

Figure 2-25. Typical "Bow-Tie" Configuration for One Quadrant

To determine T_{MIN} a series of computer runs was made for a 5^{o} pitch displacement, and constant values of T_{SAT}. The time to damp to 2.8^{o} earth-pointing error as a function of T_{SAT} are shown in Figure 2-26. From this data T_{MIN} was chosen to be 20 dyne-cm.

γ_1 was originally set at the value of the steady-state damper boom oscillation amplitude from the above runs. This was $\gamma_1 = 4$ degrees.

Using $T_{MIN} = 20$ dyne-cm and $\gamma_1 = 4$ degrees, a series of runs was made with values of SLOPE 1 from 15 to 35 dyne-cm/deg. Initial conditions were a large transient taken from an ATS-A capture run. This transient, often called the standard transient, has been used in many computer runs to permit meaningful comparisons of data. Its values are:

	Attitude (deg)	Attitude Rate $\left(\frac{\text{deg}}{\text{sec}}\right)$
Pitch	-35.9	-0.0175
Roll	8.1	-0.01408
Yaw	180.5	0.005993
Damper Boom	0	0

Initial conditions also include 0.01 orbit eccentricity, and a 1000 pole-cm magnetic dipole along the vehicle roll axis.

Figure 2-27 shows the time to damp to an earth-pointing error of 4^{o} for various values of SLOPE 1. From Figure 2-27 SLOPE 1 was chosen to be 20 dyne-cm/deg.

Another series of runs was made to confirm the value of γ_1. Using $T_{MIN} = 20$ dyne-cm and SLOPE 1 = 20 dyne-cm/deg values of γ_1 from 1-10 degrees were used. Initial conditions were the standard transient. Figure 2-28 is a plot of the earth-pointing error at 200 hours as a function of γ_1. There is some data scatter beyond $\gamma_1 = 5^{o}$ but a trend is evident. γ_1 was chosen to be 5^{o}.

This set of parameters provided relatively good damping for moderate and small disturbances. To improve large disturbance damping SLOPE 2 was set at 30 dyne-cm/deg and γ_2 at 15^{o}. No additional runs were made to confirm these values. They were based upon the data already obtained combined with engineering judgment.

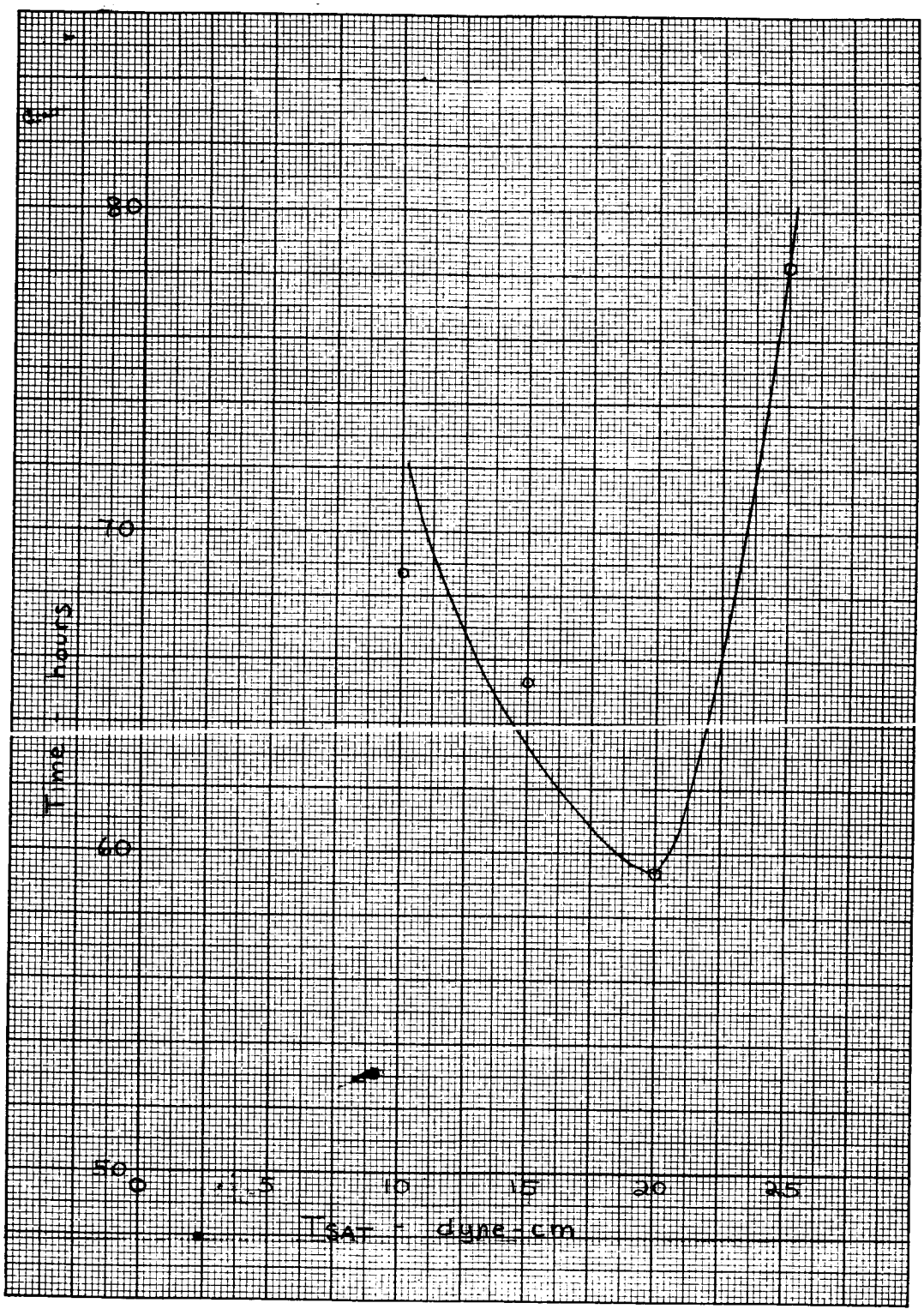

SHS 7-2-65

Figure 2-26. Time to Settle to 2.8^{o} from an Initial 5^{o} Pitch Error as a Function of T_{SAT} for ATS-A

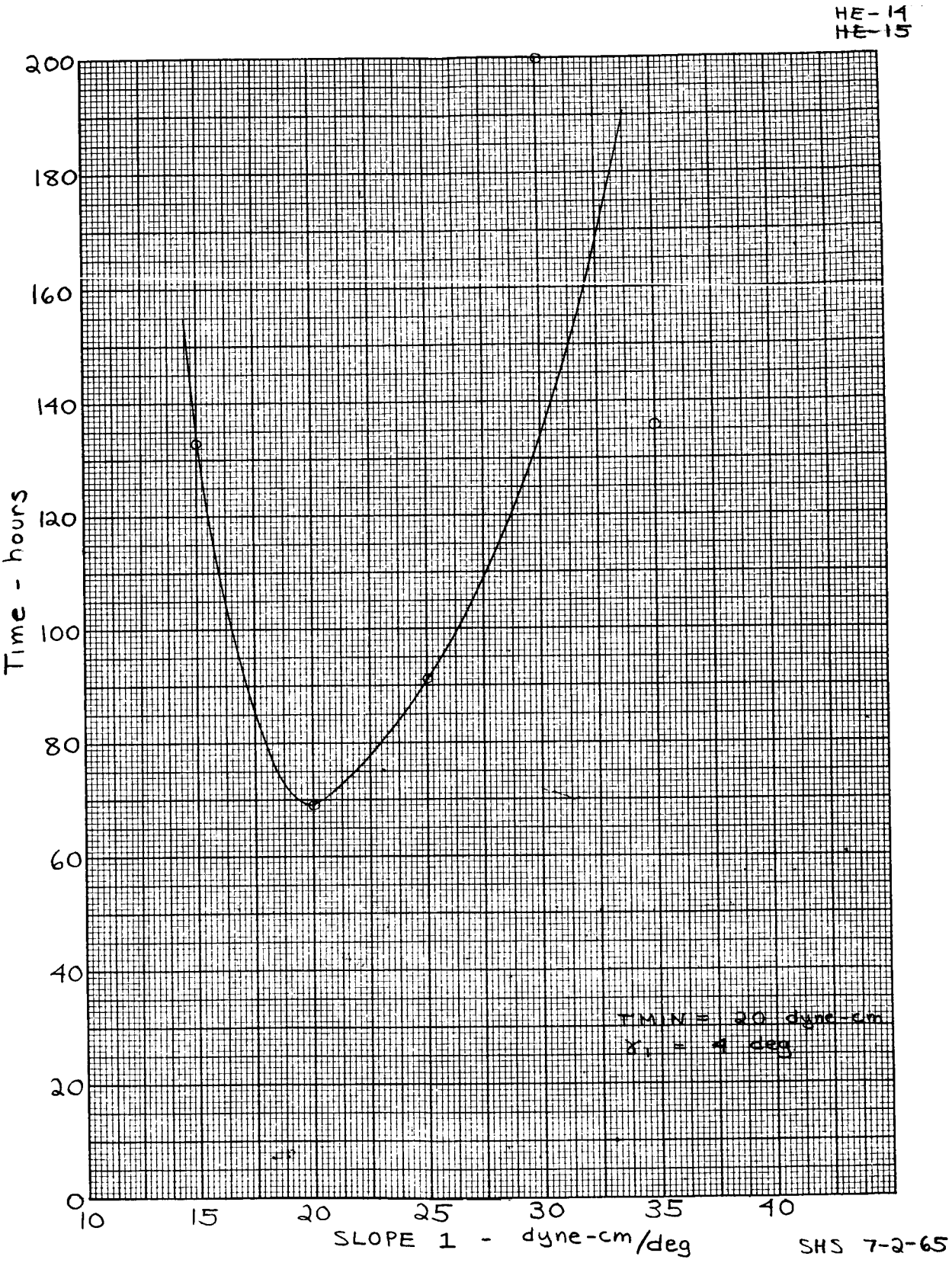

Figure 2-27. Time to Settle to 4^{o} from the Standard Transient as a Function of Slope 1 for ATS-A

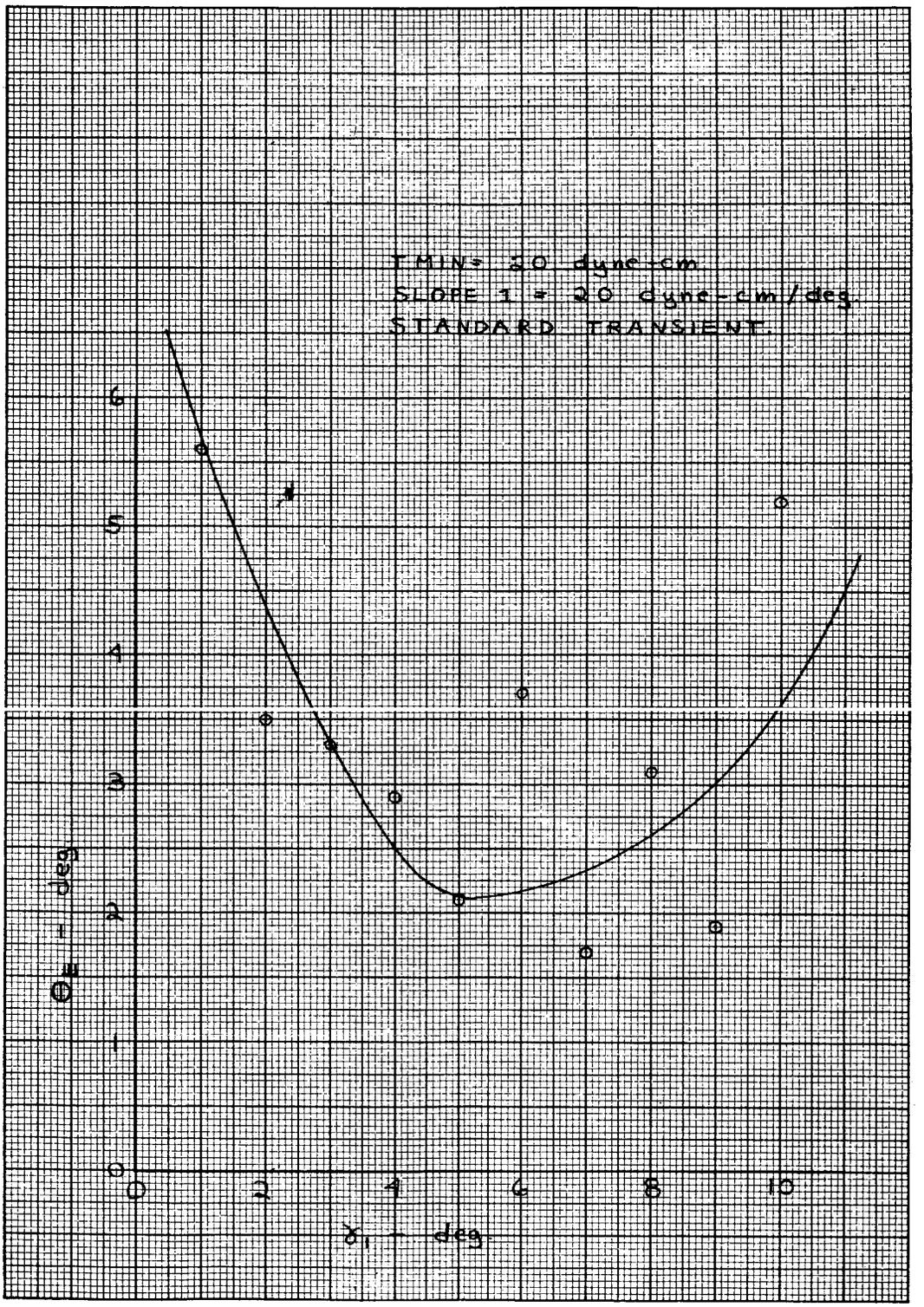

SHS 7-2-65

Figure 2-28. Maximum Earth-pointing Error at 200 Hours as a Function of γ_1 for ATS-A

The recommended set of parameters and tolerances are listed below:

T_{MIN}	20 ±5	dyne-cm
γ_1	5 ±1	deg
γ_2	15 ±2	deg
SLOPE 1	20 ±5	dyne-cm/deg
SLOPE 2	30 ±5	dyne-cm/deg

Figure 2-29 is a plot of the system response to the standard transient using the nominal hysteresis damper parameters, and including solar effects. Figure 2-30 shows its damping performance compared to the performance of: (1) the present hysteresis damper in ATS-A in which T_{SAT} is constant at 175 dyne-cm, and (2) the present eddy current damper.

The parameters for the ATS-D bow-tie hysteresis damper can be scaled from the ATS-A values. The scale factor is:

$$\frac{\left[I_D \omega_o^2\right]_{ATS\text{-}A}}{\left[I_D \omega_o^2\right]_{ATS\text{-}D}} = 6.00$$

where

I_D = damper moment of inertia

ω_o = orbital rate

T_{MIN}, SLOPE 1 and SLOPE 2 in ATS-A must be divided by 6.00 to obtain the equivalent values for ATS-D. γ_1 and γ_2 remain unchanged.

One computer run was made of the nominal ATS-D bow-tie hysteresis damper. This is plotted in Figure 2-31. Initial conditions included the standard transient with the rates scaled for synchronous altitude. Solar effects and orbit eccentricity were not included. This was the only ATS-D run made.

Several runs were made to determine the effects of the parameter tolerances. Figure 2-32 is a comparison of damping performance of the nominal hysteresis torque characteristic and the upper and lower boundary characteristics. The upper boundary is defined as the T_{SAT} - γ curve in which T_{MIN}, SLOPE 1 and SLOPE 2 are at their upper limits. The lower boundary is defined in a corresponding manner.

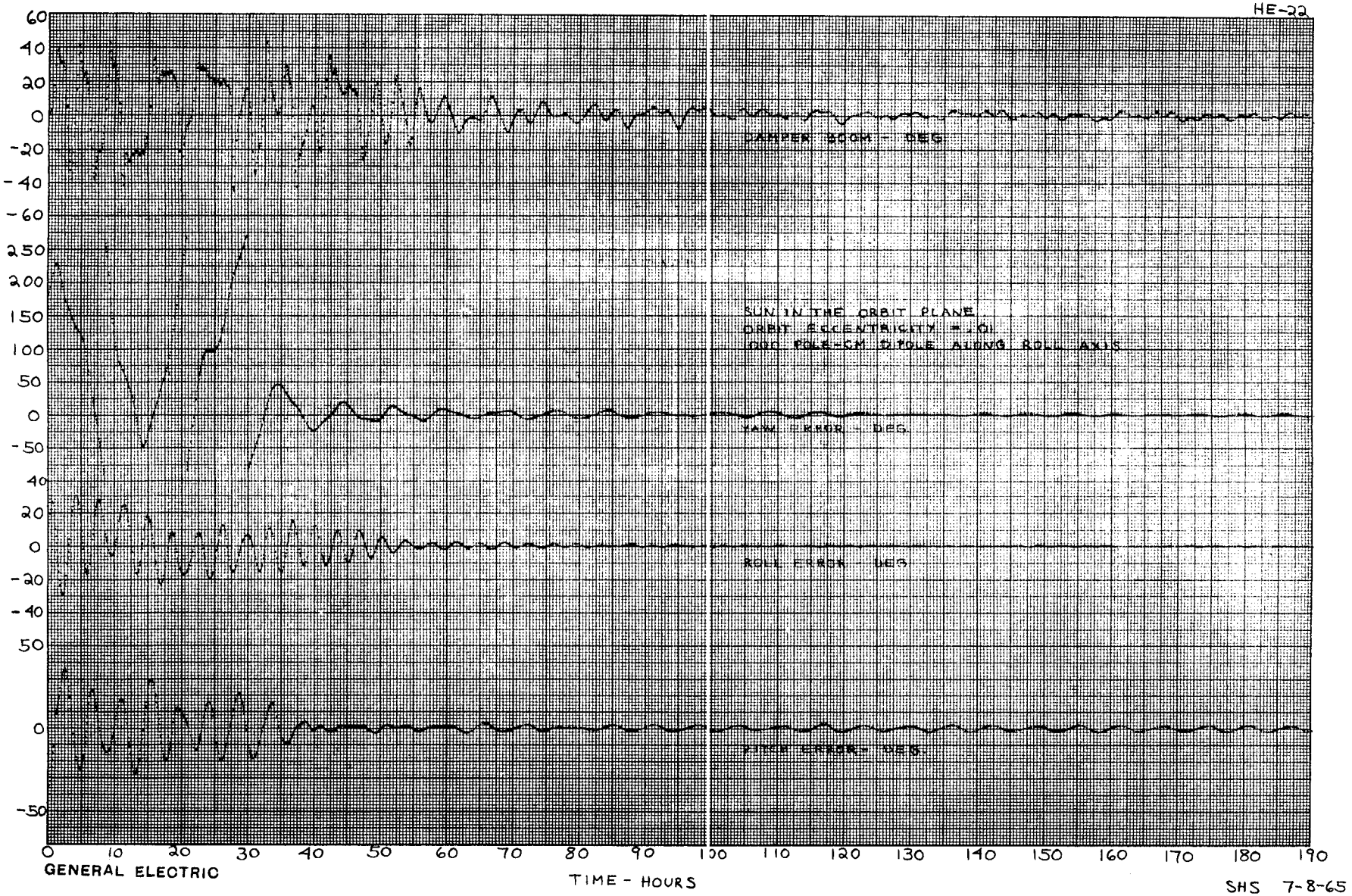

Figure 2-29. Response of ATS-A Vehicle with a "Bow-Tie" Hysteresis Damper to the Standard Transient

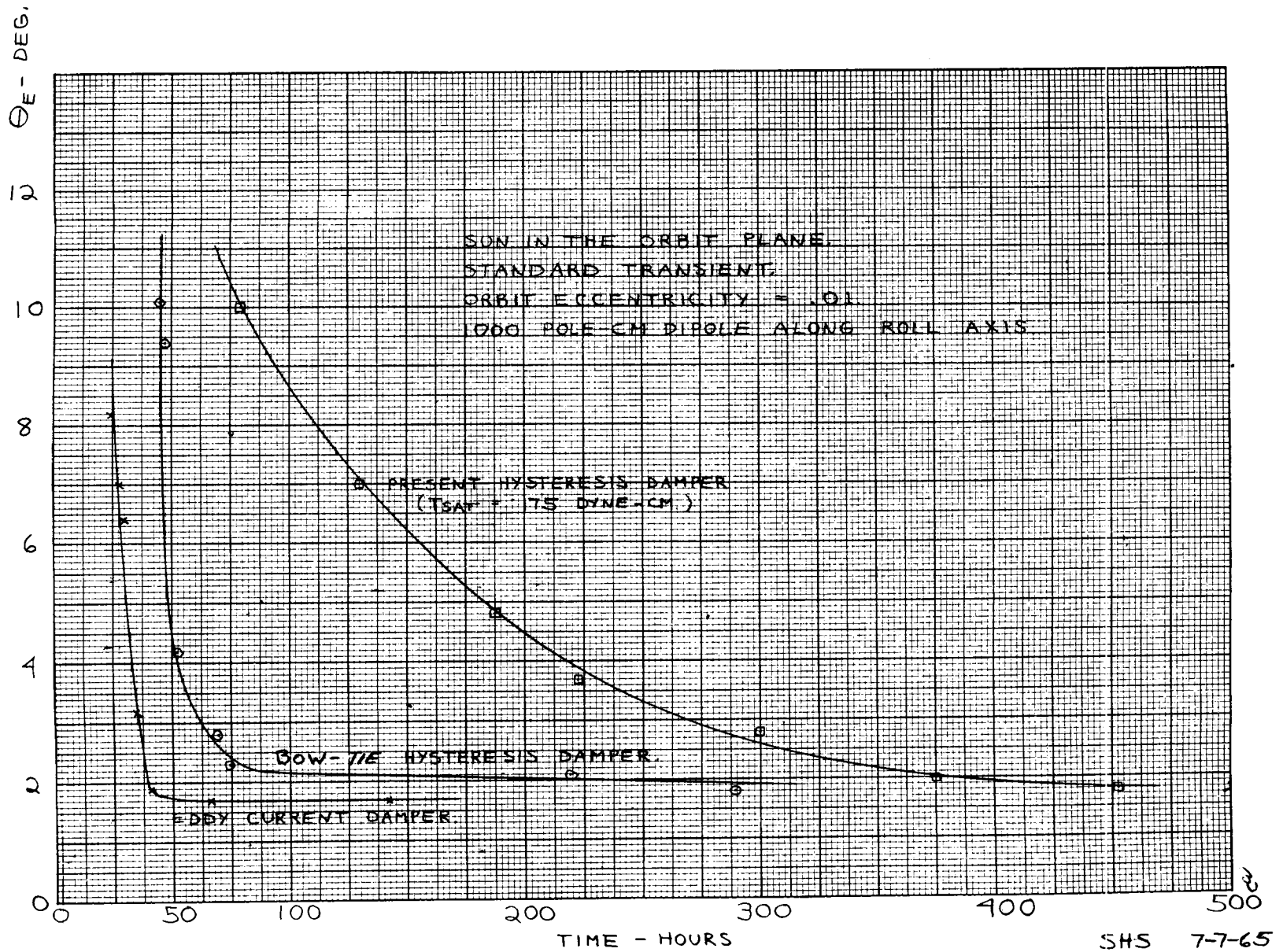

Figure 2-30. ATS-A Damping Characteristics

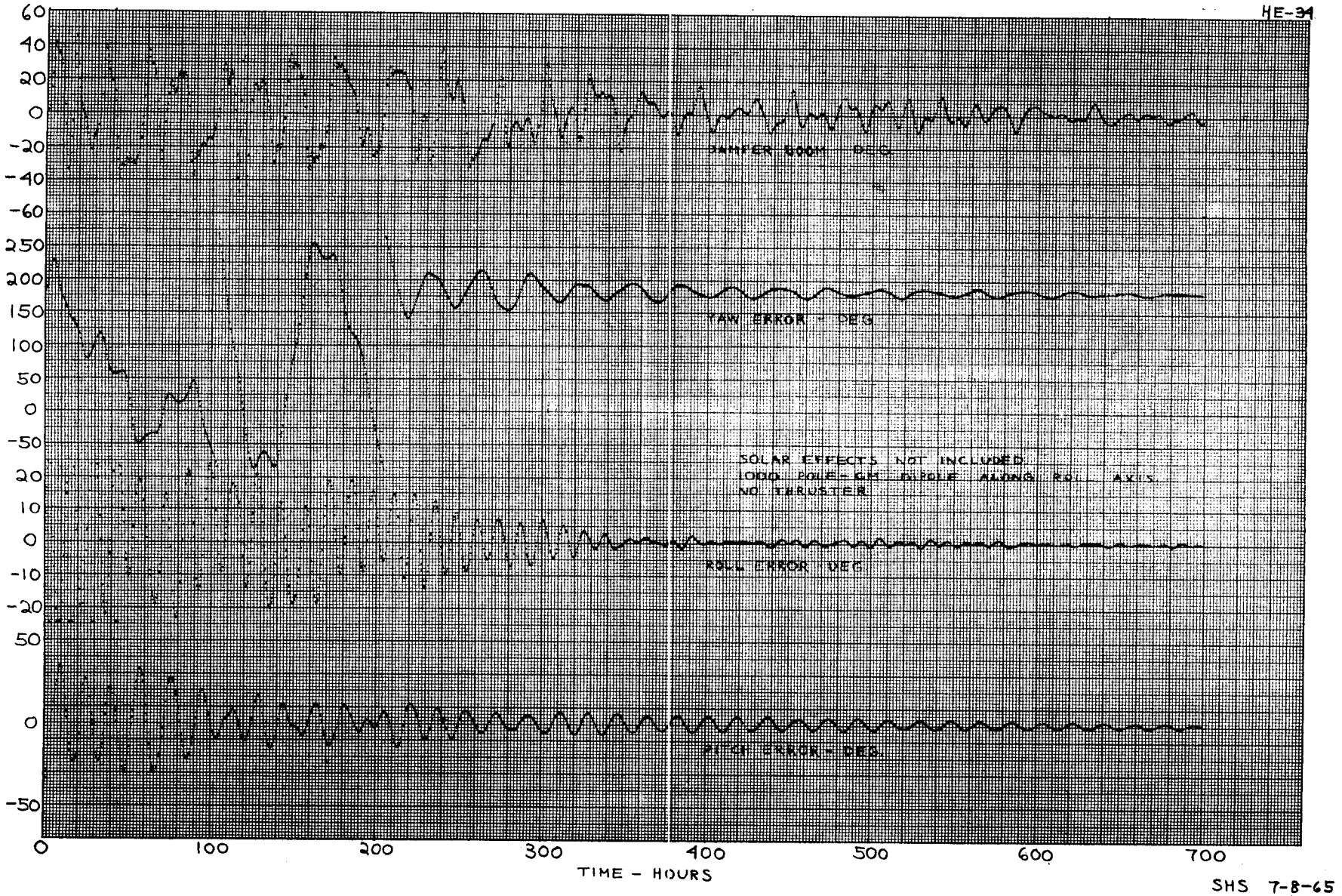

Figure 2-31. Response of ATS-D Vehicle with a "Bow-Tie" Hysteresis Damper to the Standard Transient

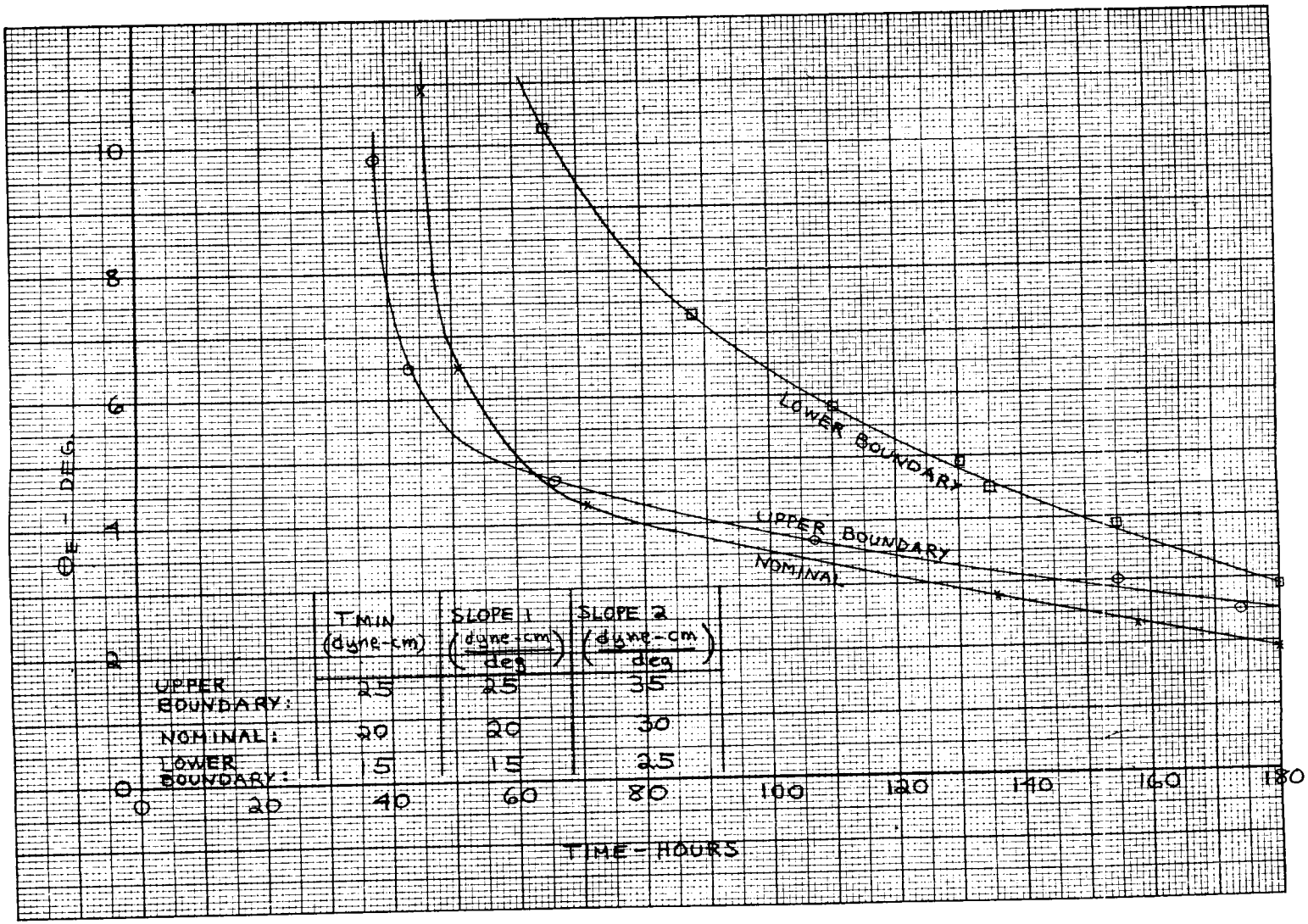

Figure 2-32. Effects of Parameter Tolerances of Bow-tie Hysteresis Damper Upon Damping Performance

To obtain the required bow-tie shape, hysteresis torque characteristic requires that the amount of magnetic material in the damper magnetic field be a function of γ. This introduces a magnetically caused torque on the damper boom. The effect of this torque is to oppose the torque caused by the torsion wire. At this time the size of this magnetic torque is not known. However, several preliminary series of runs were made to determine how this magnetic spring effect might affect performance. These runs are best summarized in Figures 2-33 and 2-34. In Figure 2-33 the torsion wire spring constant, KL, is assumed to be reduced by a fixed percentage over the entire range of γ. In Figure 2-34 KL is assumed to reach a saturation value at various values of γ. These runs used the standard transient, .01 orbit eccentricity. 1000 pole-cm dipole along the roll axis, and no solar effects. Figure 2-33 shows that when KL is reduced more than 40% damping performance rapidly deteriorates. In Figure 2-34 damping performance is well below nominal for $\gamma_A = 20^o$ or less. If the magnetic spring effect approaches either of these conditions, compensation will be required to provide satisfactory damping.

2.6.3.2.3 Conclusions

The bow-tie hysteresis damper provides substantially better damping performance than the present hysteresis damper which uses a constant hysteresis saturation torque. This improvement in damper performance is obtained only if the magnetic spring effect inherent to the bow-tie damper is compensated or is insignificant compared to the torsion wire spring constant. Steady-state pointing accuracy is unaffected.

The eddy current damper provides better damping performance than either hysteresis damper. Their performances are compared in Figure 2-30.

2.7 BOOM THERMAL BENDING ANALYSIS

2.7.1 ATS MATHEMATICAL MODEL EQUATIONS

The equations provided for incorporation into the ATS Mathematical Model are developed in the following paragraphs. The magnitude of the constant coefficients for the equations will be specified at the conclusion of current efforts in shell analysis and thermal testing.

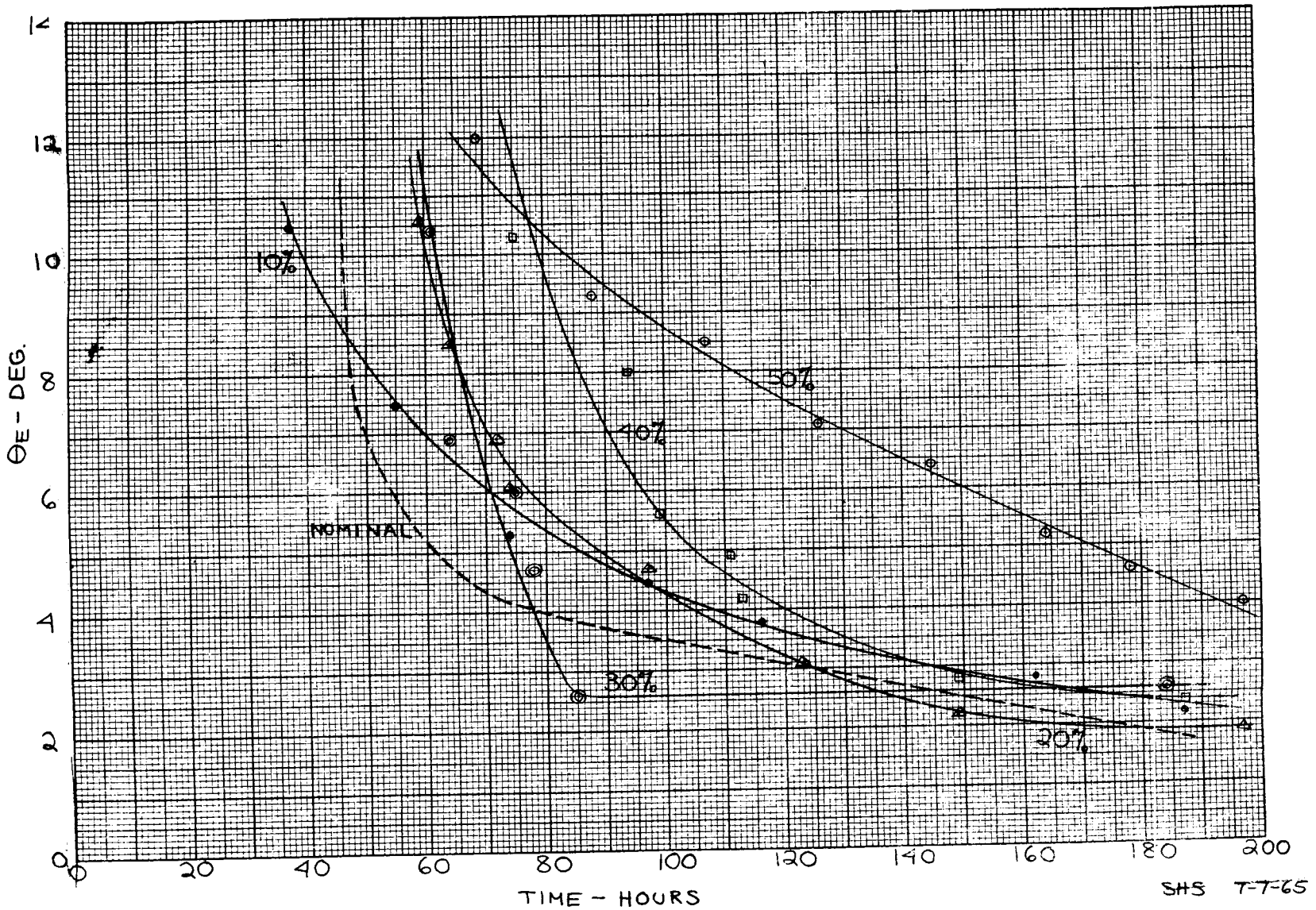

Figure 2-33. ATS-A Damping Performance with Torsion Wire Spring Constant Reduced by Indicated Percentage

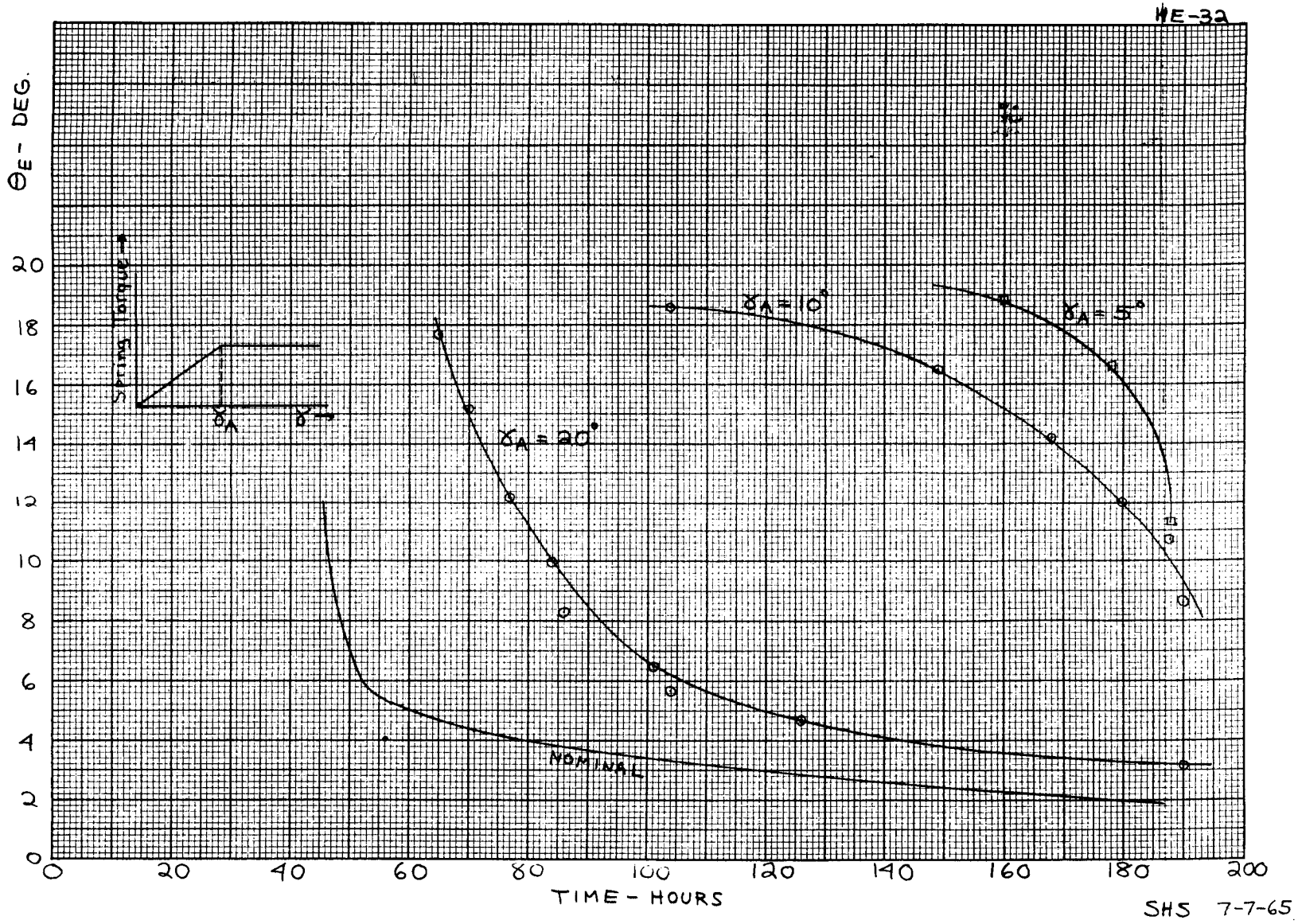

Figure 2-34. ATS-A Damping Performance with Torsion Wire Spring Constant Saturated at $\gamma = \gamma_A$

2.7.1.1 Sign Convention

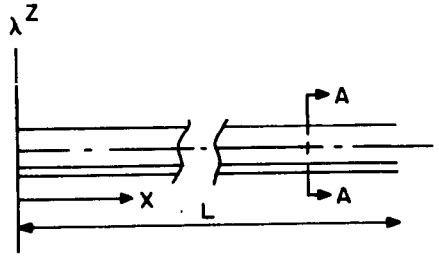

Section A-A:

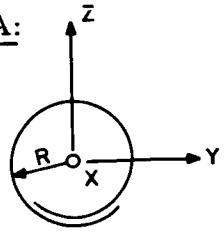

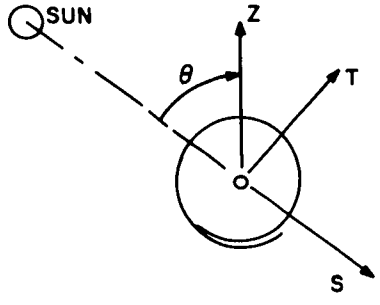

Positive Rod Seam Twist Sees Seam Rotating In Clockwise Direction When Viewed From Built-in End of Rod.

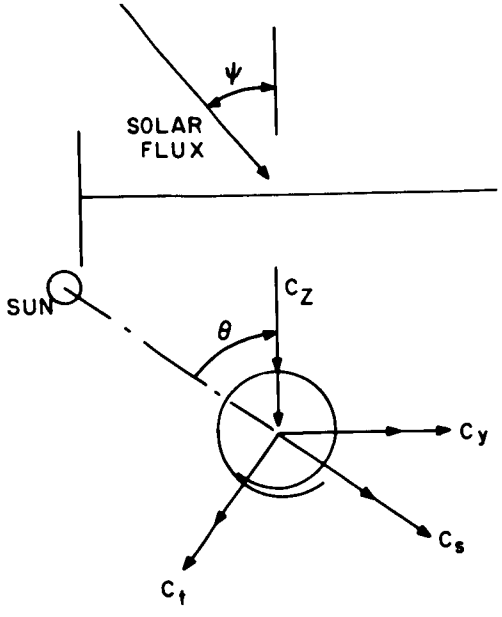

C_y chosen positive when it produces positive z deflection when integrated from 0 to x

C_z chosen positive when it produces positive y deflection when integrated from 0 to x

C_t chosen positive when it produces positive s deflection when integrated from 0 to x

C_s chosen positive when it produces positive t deflection when integrated from 0 to x

2.7.1.2 Beam Curvature at Steady-State in Zero g Field

$C(\psi, \theta, F, \alpha_o, \epsilon, k, t, r, h, \alpha_e, S)$

ψ = $\sphericalangle$ of incidence of solar flux rector on rod

θ = $\sphericalangle$ between sun-rod plane and rod overlap

F = solar flux

α_a = absorptance coefficent

ϵ = emittance coefficient

k = thermal conductivity

t = thickness of rod material

r = radius of rod

h = specific heat coefficient

α_e = coefficient of thermal expansion

s = circumferential length of rod

ψ is a constant along the length of the rod if:

$$\psi + \varphi_s \approx \psi$$

where

ψ_s is the local rod slope departure from the nominal chosen to define ψ.

θ is a variable along the length of the rod. Dependent upon rod-satelite-sun orentation and fabrication.

F is a constant along rod in full sunlight.

α & ϵ will vary on the rod surface dependant upon manufacturing and handling.

α_e, k & c are probably constant dependent upon the manufacturing control of alloying constituents.

s, r & t will vary in rod dependent upon manufacture.

Assume nominal values are adequate for the definition of ψ, F, α, ϵ, k, c, α_e, r & t. Then the remaining variable θ must still be considered. Review of work to date indicates that an assumption of constant curvature along length of rod should introduce an error of no more than 10% in inplane bending of the rod. However, out-of-plane bending is not well defined and the error can not be evaluated.

$$\therefore (C_t)_x = C_t$$

$$(C_s)_x = C_s\,(\theta(X))$$

The slope of any point x along the rod is:

$$\varphi_x = \int_0^x C\,dx + \Delta\varphi \quad (\psi, F \text{ etc.})$$

$\Delta\varphi$ is a term (as yet unproven) to account for shearing type deformation in the rod. From an analysis, all variables can be considered constant except the θ term (seam twist).

$$\therefore (\theta_t)_x = C_t \int_0^x dx + \Delta\varphi_t \qquad (\Delta\varphi_t)_x = \Delta\varphi_t\,(\theta(x))$$

$$(\theta_s)_x = \int_0^x C_s\,dx + \Delta\varphi s \qquad (\Delta\varphi_s)_x = \Delta\varphi_s\,(\theta(x))$$

Rod deflection is obtained as:

$$\delta_x = \int_0^x \theta\,dx = \int_0^x \int_0^x C\,dx\,dx + \int_0^x \Delta\varphi\,\epsilon\,dx$$

$$(\delta_s)_x = C_t \int_0^x \int_0^x dx\,dx + \int_0^x \Delta\varphi_s\,dx$$

$$(\delta_s)_x = \int_0^x \int_0^x C\,s\,dx\,dx + \int_0^x \Delta\varphi_s\,dx$$

Assume θ a periodic function as

$$\theta = \frac{\alpha\pi n}{L}\,x + a\,,$$

where

N is the number of twist cycles in rod

L is the length of the rod

a_1 is the angle between sun-rod plane and rod z axis of x = 0

Principal rod curvatures produced by the temperature distribution can be represented as:

$$C_y = A_1 \sin(\theta + a_2)$$

$$C_z = A_2 \cos(\theta + a_{2'})$$

where

A_1 and A_2 are curvature amplitudes a_2 and a_2 are phase angles. From prior work $a_2 \approx a_2$, (Doc. 64SD4368) and

$$C_y = A_1 \sin(\theta + a_2)$$

$$C_z = A_2 \cos(\theta + a_2)$$

The principal rod curvatures are transformed into sun-rod plane coordinates by:

$$C_s = C_y \sin\theta + C_z \cos\theta$$

$$C_t = C_y \cos\theta\ C_z \sin\theta$$

or

$$C_s = A_1 \sin(\theta + a_2)\sin\theta + A_2 \cos(\theta + a_2)\cos\theta$$

$$C_t = -A_1 \sin(\theta + a_2)\cos\theta + A_2 \cos(\theta + a_2)\sin\theta$$

Taking advantageof trigonometric identities, C_s and C_t can be brought to the form:

$$C_s = \frac{1}{2}\left[\left(A_2 - A_1\right)\cos\ (2\theta + a_2) + \left(A_1 + A_2\right)\cos a_2\right]$$

$$C_t = \frac{1}{2}\left[\left(A_2 - A_1\right)\sin (2\theta + a_2) + \left(A_1 + A_2\right)\sin a_2\right]$$

Substituting for θ i.e., then

$$\theta = \frac{2\pi N}{L}x + a_1 = \eta x + a_1$$

$$C_s = \frac{1}{2}\left[\left(A_2 - A_1\right)\cos\left(2\eta x + 2a_1 + a_2\right) + \left(A_1 + A_2\right)\cos a_2\right]$$

$$C_t = \frac{1}{2}\left[\left(A_2 - A_1\right)\sin\left(2\eta x + 2a_1 + a_2\right) + \left(A_1 + A_2\right)\sin a_2\right]$$

The beam slope is obtained as:

$$\varphi = \int C dx + \Delta\varphi\left(\theta(x)\right)$$

$$\varphi_s = \frac{1}{2}\left(A_2 - A_1\right)\int\cos\left(2\eta x + 2a_1 + a_2\right)dx + \frac{1}{2}\left(A_1 + A_2\right)\cos a_2 \int dx$$

$$+ \Delta\theta_s\left(\theta(x)\right).$$

$$\varphi_t = \frac{1}{2}\left(A_2 - A_1\right)\int\sin\left(2\eta x + 2a_1 + a_2\right)dx + \frac{1}{2}\left(A_1 + A_2\right)\sin a_2 \int dx$$

$$+ \Delta\varphi\epsilon\left(\theta(x)\right)$$

Performing the integration yields:

$$\varphi_s = \left(\frac{A_2 - A_1}{4\eta}\right)\sin\left(2\eta X + 2a_1 + a_2\right) + \left(\frac{A_1 + A_2}{2}\right)\cos a_2\ x$$

$$+ \Delta\varphi s\left(\theta(x)\right) + \varphi so.$$

$$\varphi_t = -\left(\frac{A_2 - A_1}{4\eta}\right)\cos\left(2\eta x + 2a_1 + a_2\right)\left(\frac{A_1 + A_2}{2}\right)(\sin a_2)\ x$$

$$+ \Delta\varphi t\left(\theta(x)\right) + \varphi_{to}.$$

It is assumed that the form of $\Delta\varphi$ (θ (x)) is the same as for C

$$\therefore \Delta\varphi_s = \frac{1}{2}\left[\left(A_4 - A_3\right) \cos\left(2\eta x + 2a_1 + a_3\right) + \left(A_3 + A_4\right)\cos a_3\right]$$

$$\Delta\varphi_t = \frac{1}{2}\left[\left(A_4 - A_3\right) \sin\left(2\eta x + 2a_1 + a_3\right) + \left(A_3 + A_4\right)\sin a_2\right]$$

Beam deflection is obtained as

$$\delta_t = \int \varphi \, sdx$$

$$\delta_s = \int \varphi \, tdx$$

$$\delta_\epsilon = -\frac{A_2 - A_1}{8\eta^2} \cos\left(2\eta x + 2a_1 + a_2\right) + \frac{A_1 + A_2}{4}\left(\cos a_2\right) x^2$$

$$+\frac{A_4 - A_3}{4\eta} \sin\left(2\eta x + 2a_1 + a_3\right) + \frac{A_3 + A_4}{2}\left(\cos a_3\right) x$$

$$+\varphi_{so} x + \delta_{to}.$$

$$\delta_s = -\frac{A_2 - A_1}{8\eta^2} \sin\left(2\eta x + 2a_1 + 0_2\right) + \frac{A_1 + A_2}{4}\left(\sin a_2\right) x^2$$

$$-\frac{A_4 - A_3}{4\eta} \cos\left(2\eta x + 2a_1 + a_3\right) + \frac{A_3 + A_4}{2}\left(\sin a_3\right) x$$

$$+\varphi_{to} x + \delta_{so}$$

The amplitudes A_1, A_2, A_3 & A_4, as well as the phase angles, are determined from temperature distributions which are based on flux, rod optical properties, physical properties, and geometry. It is assumed that these properties will be known for each rod before flight. It is further assumed that the twist rate η of the seam will also be determined before flight.

Phase angles a_1, a_2, a_3 are of course dependent upon sun position at X=O. As such, they are dependent upon rod/satellite/sun orientation. Consider then the form:

$$a_1 = a_{1v} + a_{1F}$$

$$a_2 = a_{2v} + a_{2F}$$

$$a_3 = a_{3v} + a_{3F}$$

where subscripts

v = variable component

F = fixed component

The fixed components will be obtained considering the sun position to be on the +z rod axis at X=O. Thus, a_{1F}=O and θ = O.

For the condition of a reverse tube overlay, the Cy curvature will have the wrong sign, and the amplitude A_1 must have its sign changed.

From the preceding it is seen

$$a_1 = a_{1v}$$

and

$$a_2 = a_1 + a_{2F}$$

$$a_3 = a_1 + a_{3F}$$

$$\delta_t = -\frac{A_2 - A_1}{8\eta^2} \cos\left(2\eta x + a_{2F} + 3a_1\right) + \frac{A_1 + A_2}{4}\left(\cos(a_{2F} + a_1)\right) X^2$$

$$+ \frac{A_4 - A_3}{4\eta} \sin\left(2\eta x + a_{3F} + 3a_1\right) + \frac{A_3 + A_4}{2}\left(\cos\left(a_{3F} + a_1\right)\right) X$$

$$+ \varphi_{s_o} x + \delta_{to}.$$

and

$$\delta_s = -\frac{A_2-A_1}{8\eta^2}\sin(2\eta x+a_{2F}+3a_1) + \frac{A_1+A_2}{4}\left(\sin(a_{2F}+a_1)\right)X^2$$

$$-\frac{A_4-A_3}{4\eta}\cos(2\eta x+a_{3F}+3a_1) + \frac{A_3+A_4}{2}\left(\sin(a_{3F}+a_1)\right)X$$

$$+ \varphi_{to}\,x + \delta_{so}\,.$$

Rewriting:

$$\delta_t = \beta_1\cos(2\eta x+a_{2F}+3a_1) + \beta_2\sin(2\eta x+a_{3F}+3a_1)$$

$$+ \beta_3\left(\left(\cos(a_{2F}+a_1)\right)X^2 + \left(\beta_4\left(\cos(a_{3F}+a_1)\right) + \varphi_{so}\right)X + \delta_{to}\,.\right.$$

$$\delta_s = \beta_1\sin(2\eta+a_{2F}+3a_1) - \beta_2\cos(2\eta x+a_{3F}+3a_1)$$

$$+ \beta_3\left(\sin(a_{2F}+a_1)\right)X^2 + \left(\beta_4(\sin(a_{3F}+a_1) + \varphi_{to}\right)X + \delta_{so}\,.$$

where

$$\beta_1 = -\frac{A_2-A_1}{8\eta^2} \qquad \beta_4 = \frac{A_3+A_4}{2}$$

$$\beta_2 = \frac{A_4-A_3}{4\eta}$$

$$\beta_3 = \frac{A_1+A_2}{4}$$

2.7.2 NUMERICAL EVALUATION OF SHELL EQUATIONS

The difficulty in numerical evaluation of the shell equations was traced to an inconsistency in assumptions with regard to the small roots of the characteristic equation being equal to zero. With this knowledge, the solution was rewritten and is currently being reprogrammed for solution on the IBM 7094 Computer.

2.7.3 PRELIMINARY THERMAL BENDING TESTS

A series of preliminary thermal tests on a bare BeCu rod samples demonstrated that the method of attaching thermocouples has a strong perturbing effect on test results. An effort is underway to establish an optimum method of instrumenting the rods and establishing a well defined procedure of thermal testing.

2.8 TEST REQUIREMENTS AND PERFORMANCE

An ATS system test meeting was held at NASA/GSFC on April 6th. Test personnel from the Hughes Aircraft Company presented the general test philosophy they intend to employ for qualification and acceptance testing at the system level. HAC described their planned test facilities, equipment they intend to use and handling fixtures. Requirements for co-contractor inputs to the system test documentation was discussed.

2.8.1 MICROMETEORITE TESTING

Preparations were made to perform the micrometeorite testing of rod samples. These tests will be conducted to measure the effect of simulated micrometeorites on the thermal radiative and mechanical properties of bare and silver plated beryllium-copper gravity gradient rods. Calibration tests were run to determine particle velocity, size, and count that will be used for the tests. In addition, a stripable coating was evaluated which protects the target from carbonaceous matter that result from the explosive during the calibration firings.

2.8.2 QUALIFICATION OF PRIMARY BOOM AND DAMPER BOOM SUBSYSTEMS

The tip masses are the only difference between the ATS-A and ATS-D/E configurations of the Primary and Damper Boom subsystems. The difference in tip masses could cause different responses internal to the assembly during vibration testing. In order to insure that each configuration is qualified prior to flight, the following plan will be followed based upon considerations for the technical, economical, and schedule aspects of the ATS Program.

1. The Prototype No. 1 component will be the ATS-D configuration and will be tested to the component environments of SVS-7316.
2. The Engineering No. 1 component will be ATS-A configuration and will be tested to the environments called out in SVS-7316.
3. Both tests will be monitored by Quality Control and all data will be recorded for the Integrated Test Program Board (ITPB) review.
4. If both the Prototype and Engineering components successfully pass the environments of SVS-7316 as evidenced by a formal review of the ITPB, both the ATS-A and ATS-D configurations would then be considered qualified.

The following differences exist between the ATS-A and ATS-D/E damper designs:

1. The weight of the damper boom that is supported by the damper shaft is different for the ATS-A and ATS-D/E configuration.
2. The torsion wire for the hysteresis damper is different for the ATS-A and ATS-D/E designs.
3. The magnets for the eddy current damper are different for the ATS-A and ATS-D/E designs. (Magnetization level only)

The differences between the ATS-A and ATS-D/E designs could cause different responses internal to the damper assembly during vibration testing. Therefore, qualification testing of one design would not qualify both designs. In selecting which design should become Prototype No. 1 the following factors were considered.

The present schedule favors the ATS-A design because the engineering testing of this design is expected to be complete by November 1965. The engineering testing of the ATS-D/E design should be complete by January 1966.

There will be two Engineering units, ATS-A and ATS-D/E.

The following plan will be followed based upon the aforementioned considerations and other technical, economical, and schedule aspects of the ATS Program.

1. Prototype No. 1component will be the ATS-A configuration and will be tested to the component environments of SVS-7314.
2. Engineering No. 2 component will be the ATS-D/E configuration and will be tested to the component environments of SVS-7314.
3. Both tests will be monitored by Quality Control and all data will be recorded for ITPB review.
4. If both the Prototype and Engineering components successfully pass the environments of SVS-7314 as evidenced by a formal review of the ITPB, both the ATS-A and ATS-D/E configurations would then be considered qualified.

2.8.4 SOLAR VACUUM TEST REQUIREMENTS

The solar aspect sensor, TV camera and damper boom/damper will be exposed to solar radiation during the ATS mission; therefore, these components will undergo solar vacuum cycle testing during the engineering evaluation test phase. The IR earth sensor will be excluded from this testing because the IR sensor is Government furnished. The objectives of the solar vacuum cycling tests are:

1. To insure that the component will pass the system solar vacuum cycling test at HAC and obtain some confidence of successful operation in orbit

2. To insure that the component will pass the thermal vacuum component qualification test

3. To ascertain any degrading of the components as a result of exposure to solar vacuum

4. To ascertain thermal gradient occurring on the components as a result of the simulated space environment.

Details of the solar vacuum cycling test were published in a GE internal document, PIR 4730-098, dated May 28, 1965. The IR earth sensor will also be exposed to solar radiation during the mission, but it is not scheduled for solar vacuum testing because it is Government furnished.

Work progressed on schedule toward implementation of the solar vacuum engineering evaluation tests. The carbon arc solar simulator was received, and the design and drafting were completed for modifications to the 5 by 6-foot test chamber. Consideration has been given to the performance of qualification testing of the solar aspect sensor in the same facility.

2.8.5 AEROSPACE GROUND EQUIPMENT

The following list comprises the AGE that will be utilized in subsystem testing at GE and field tests at HAC.

1. Solar Aspect Sensor Stimulator - This equipment will be used to stimulate each solar aspect detector during subsystem functional tests.

2. TV Monitor - The video monitor will be used to establish overall performance of each TV camera in the ATS system.

3. Targets and Illuminator - This equipment will provide a means to evaluate the television operation by using a resolution chart with a known illumination.

4. ATS Test Console - This is a two-bay console which houses the monitor panels, distribution panels, command simulator, and readout equipment.

5. IR Sensor Stimulator - This equipment will be GFE and will be used to stimulate each IR sensor during a functional test.

6. Damper Simulator - This equipment will be used to simulate the electrical load for all commands and telemetry channels of the Damper.

7. Squib Firing Enclosure and Squib Simulator - This is a metal enclosure to house and ignite live squibs. Provisions will be made to simulate the squibs and tests could be run to ascertain the voltage and current characteristics during a firing test.

8. Harnesses and Breakout Boxes - The harnesses will be used to interconnect the components during subsystem tests and connect the AGE with the Power Control Unit and any telemetry outputs from the components. The breakout boxes will be used during any troubleshooting operations.

SECTION 3

BOOM SUBSYSTEM

3.1 DEPLOYMENT

3.1.1 PRIMARY BOOM EXTENSION SPEED

Normal extension speed of the primary booms will be reduced by a factor of approximately 2:1 because of boom structural limitations. The speed reduction was implemented by a gear change within the sealed drive unit. deHavilland was directed to make the change, and appropriate changes were made to the applicable specifications. The change has no effect on emergency extension speed, but it will have the secondary benefit of reducing the emergency scissoring rate by approximately 2:1.

3.1.2 BOOM EXTENSION AND SCISSORING DRIVE MOTORS PRELIMINARY TEST PLAN

Each Primary Gravity Gradient Boom System contains two motors: one extends and retracts the booms, while the other controls their angular relationship, or scissoring. A clutching mechanism is provided to enable either motor to perform the function of the other in the event of a motor failure. These motors, manufactured by Globe Industries, are dc, shunt wound, size 10 units. Both basic motors are identical. The armature and field windings are the same in both units. The field and armature leads are brought out separately in each unit to simplify reversing. The boom drive motor has an integral brake, which locks its shaft when power is removed. The brake releasing electromagnet winding is in parallel with the extension motor field. The scissoring motor has a 3382:1 reduction gearhead, rather than a brake.

To ensure the adequacy of thermal design, life, output torque and speed, and to verify compatibility of these motors with the drive electronics being designed at GE, a series of engineering tests is planned.

The proposed tests will include measurements of motor temperature as a function of input power, baseplate temperature, output speed and torque. The tests will also include a determination of permissible duty cycle and a teardown inspection.

3.1.3 O-RING SEAL EVALUATION, BOOM DRIVE

The boom erection drive is hermetically sealed and pressurized to one-half atmosphere. The output shaft has a double seal. The inner seal is a flexible metal bellows and the outer seal is a rotating gland seal, that uses an O-ring as the sealing member. While the inside of the bellows is common with the sealed drive housing, and therefore at

one-half atmosphere, the small volume between the seals will essentially remain at atmospheric pressure until launch (the effects of environmental pressure cycling are considered negligible). After launch, the pressure across the O-ring seal, will slowly drop from 14.7 psia to the vehicle internal pressure, i.e., 10^{-4} to 10^{-6} Torr. This should have no adverse effect on the two ball bearings between the seals, since they are dry film lubricated (Duroid retainer on 440C-SS) and, therefore, relatively non-pressure-dependent. Since the metal bellows is welded in place and is theoretically impermeable, it will provide the primary seal for the drive assembly output shaft.

The O-ring will be called upon to perform the major sealing function only in the event of bellows leakage. If minor leakage due to minute welding imperfections or material flaws occurs, the Δp across the seal will be low and sealing will result from the static radial compression of the O-ring (due to the mounting groove dimensions). With increasing leakage rates, the Δp would increase and better sealing would result, due to the axial compression of the O-ring, which translates into greater radial compression.

The ring that is used is a Parker 2-10, molded of duPont Viton "A" fluoro-elastomer. The details of its installation and use are given in Figure 3-1. The particulars of the deHavilland design of this item have recently been the subject of a detailed evaluation by GE to preclude a compromise in the reliability of the drive train.

It was concluded that the Viton O-ring seal, used as a backup on the boom extension drive represents good practice in design and materials applications; they are not expected to be a source of drive train malfunction.

3.2 STRUCTURE AND MATERIALS

3.2.1 LUBRICATION

Lubrication tests have been completed with the testing of Cindol 2309. Previous tests indicated that G-300 grease (silicon oil base), and Beacon 325 grease (diester oil base) were satisfactory for the hermetically sealed transmission unit, over the required temperature range. Shell APL grease (petroleum oil base) was entirely too stiff and was not suitable. It has been decided that the optimum lubricant selection for the sealed drive unit is the G-300 grease based on its proven compatibility with motor bearings and back-up it offers in the event of loss of pressure. Engineering tests of the boom system will provide final checkout of the suitability of the lubricant.

3.2.2 SILVER PLATED TARNISH STUDIES

A meeting was held on May 27th at GE with representatives from the NASA/GSFC Materials Research and Development group and the ATS Project primarily to discuss the means for precluding critical degradation of the silver plated surface of the booms.

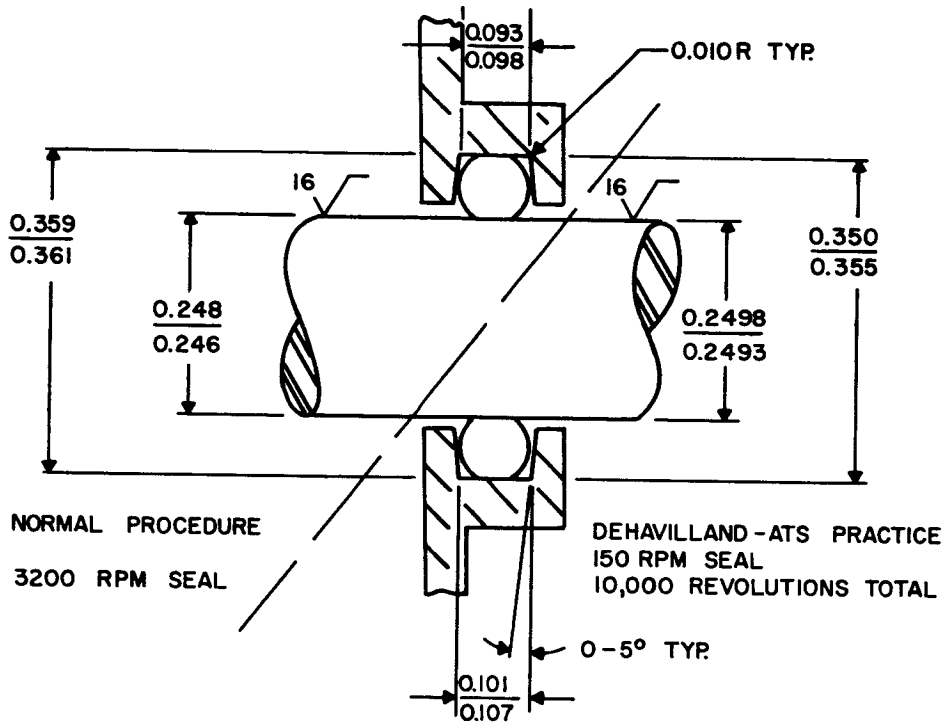

Figure 3-1. Details of the O-Ring Seal

GE gave NASA/GSFC a schedule of time, environment, temperature history of the silver plate from initial manufacture until launch. NASA discussed the specifics of the silver-plate problem gained from their research and development on the topic.

A silver-plate tarnishing study (test) was begun at GE to investigate the degradation of the silver plated surface of the booms. Four specimens of rod were exposed in the test, two at ambient without protection and two protected in a plastic envelope. The alpha of all four specimens was in the range of 0.07. After one week the alpha of the unprotected specimens was measured at 0.111 and approximately 0.18 at the end of three weeks. The two protected specimens demonstrated an alpha of 0.09 after three weeks exposure. These tarnish tests are scheduled to continue indefinitely.

3.3 POWER REQUIREMENTS

The characteristics of the Boom Subsystem squibs are:

- Bolt Cutter Part No. - deHavilland Drawing No. 5325-L4
- Bolt Cutter Specification - deHavilland No. DHC-SP-SG.58
- Squib Part No. - Hercules Powder Co. No. CC91. (This is an improved design of the No. CC63 primer qualified on another GE Program)

- No. of Bridge Wires/Squib - 1
- No. of Squibs/Bolt Cutter - 2 (mutually redundant)
- Maximum No-Fire Conditions* - 1 amp/1 watt for five minutes
- Minimum All-Fire Current* - 3 amps
- Recommended Firing Current* - 5 amps
- Recommended Minimum Firing Pulse Width - 50 ms.

*Values given are per bridge wire; therefore, per squib.

3.4 SPACECRAFT INTERFACE

In response to a HAC request, the primary boom package design was reviewed with regard to mounting on only three bolt hole locations. It was determined that, with a heavier gauge material in the component skin, the package could sustain the loads imposed by such a mounting. It was also determined that 1/4-inch diameter bolts would be required. This information was relayed to NASA/GSFC at a meeting held at GE on May 6, 1965. A detailed interface requirements drawing was prepared as a result of this meeting and delivered to NASA/GSFC on May 14, 1965.

GE is currently evaluating the feasibility of a request by HAC to move both the interface connector and the RF experiment connector, as well as a request to change the alignment mirror location. The outline drawing is being revised in response to a HAC request to indicate boom traverse envelopes, rather than required vehicle cutouts as presently shown.

GE and deHavilland worked out the mechanical details of the thermal boot recommended by HAC. It is planned to insert the thermal boot on the primary boom package at the boom clearance slots provided in the spacecraft. Details of the thermal boot were incorporated into the primary boom interface drawing which was one of the drawings corrected at the NASA/HAC/GE interface meeting on May 19th.

3.5 PRIMARY BOOM ASSEMBLY

The following changes have been made to the primary boom assembly:

1. Primary boom length was decreased from 150 feet to 134 feet for ATS-A and to 123 feet for ATS-D/E
2. Primary boom tip mass weights were reduced from 10 pounds to 8 pounds on the ATS-D/E
3. Erection rate of the primary booms has been established at a maximum speed of 1.5 feet/second and a minimum speed of 0.9 feet/second.

3.5.1 TRANSMISSION ASSEMBLY

Figures 3-2 through 3-4 show various views of the deHavilland Engineering model of the transmission assembly. The labels on each of the illustrations point out the functional components. Figure 3-5 is an exploded view of the bellows sealed drive assembly. The drive assembly is shown in Figure 3-6.

3.5.2 ERECTION UNIT

The top and bottom views of the primary boom erection unit are shown in Figures 3-7 and 3-8, respectively; the cover plate is removed. Figure 3-9 shows a tip mass assembly attached to a primary boom as the rod emerges from an erection unit.

3.6 DAMPER BOOM

Figure 3-10 shows an exploded view of the parts of the damper boom assembly. This assembly was attached to the test trolley shown in Figure 3-11, and the damper boom was deployed by extending the trolley along the test track shown in Figure 3-12.

3.6.1 DESIGN CHANGES

The following changes have been made to the damper boom assembly:

1. Tip mass weight for ATS-D and ATS-E was reduced from 7.14 pounds to 4.0 pounds.
2. Tip mass weight for ATS-A was reduced from 1.9 pounds to 1.6 pounds.

3.6.2 CABLE CUTTER ASSEMBLY

A decision was made on the squib selection in the Conax cutter for the damper boom. Two squibs will be used each having a single bridgewire. The bridgewires will be connected to the power supply on separate circuits and will be fired simultaneously. The charge to be used will be Hercules CC91.

3.7 BOOM SUBSYSTEM TEST EQUIPMENT

3.7.1 TEST TANK

The test tank to be used at deHavilland for boom straightness measurements was completed and tested for leaks. The adjustable platform which will be used for mounting erection units to the tank, was designed and is in the process of manufacture. A portion of the test tank is shown on the right of Figure 3-12.

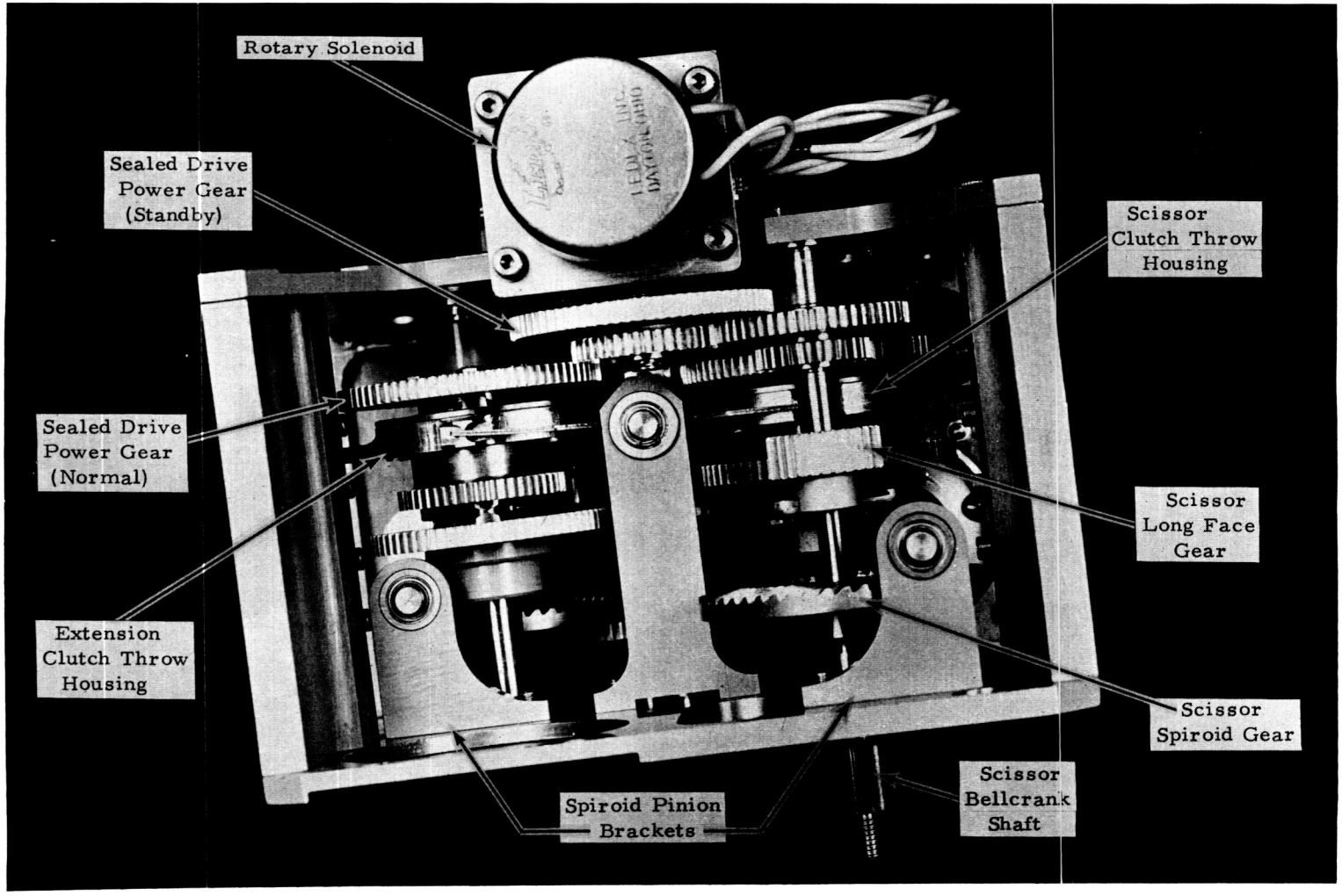

Figure 3-2. End-on View of Transmission Assembly

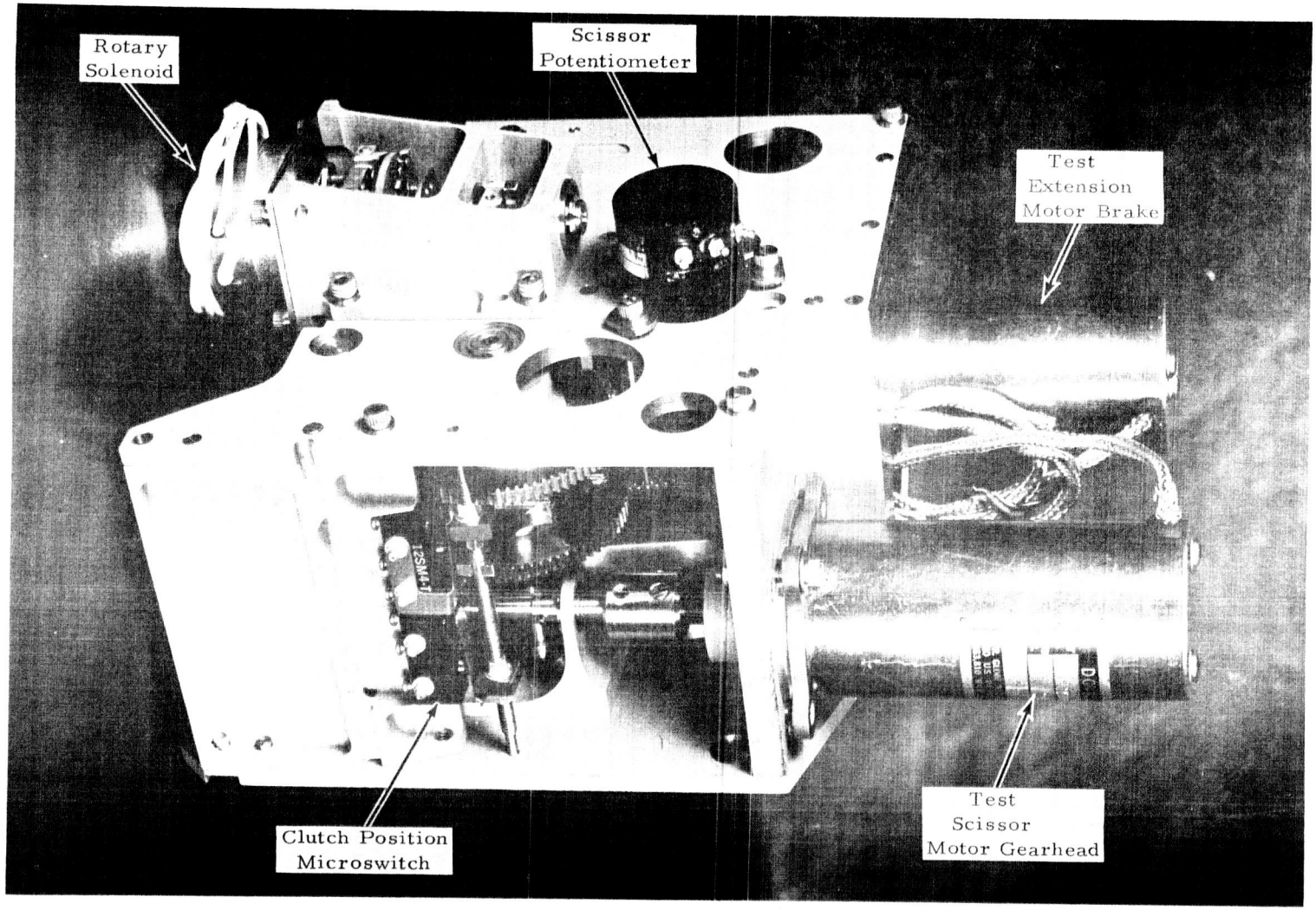

Figure 3-3. Scissoring Mechanism, Transmission Assembly

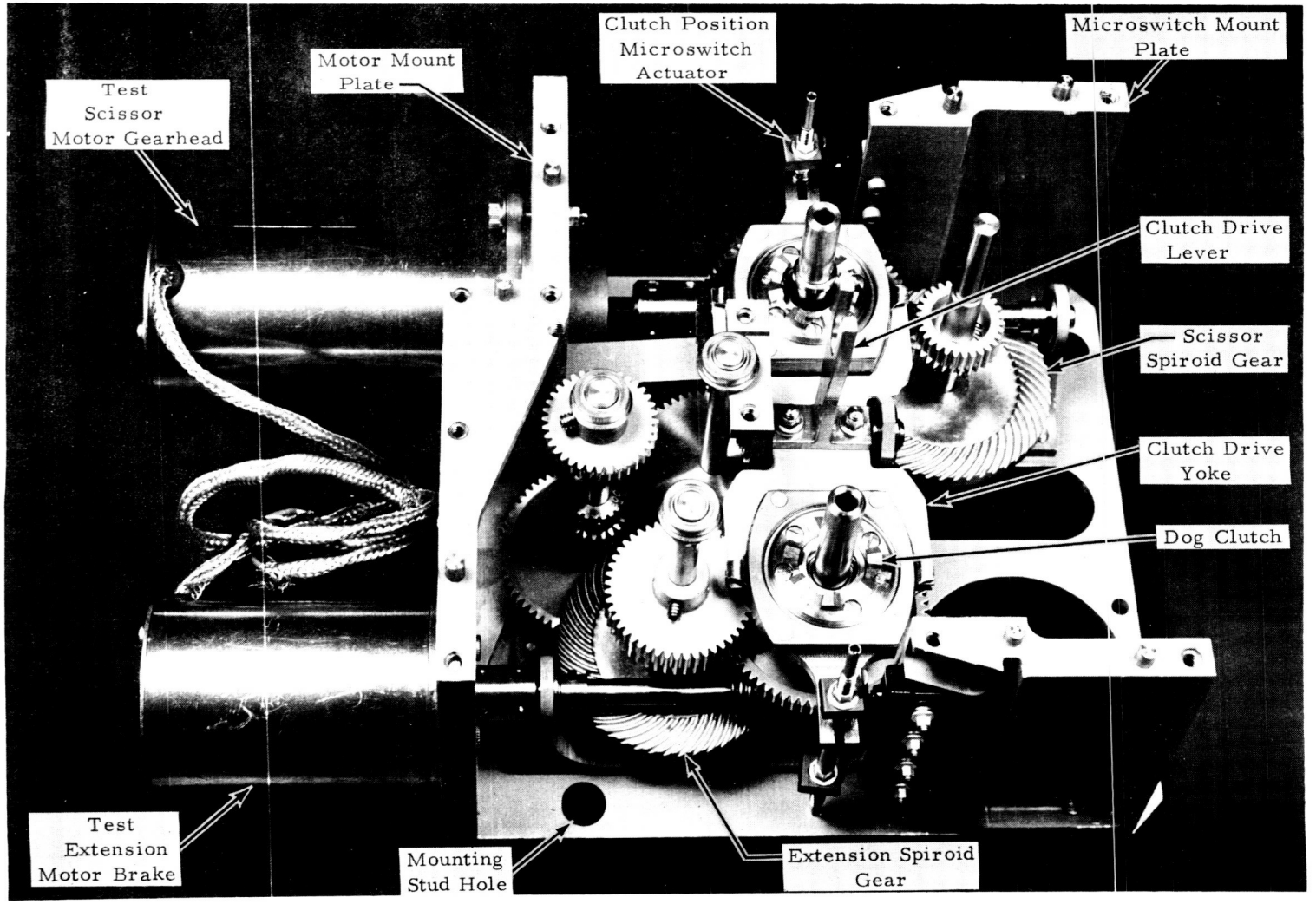

Figure 3-4. Transmission Assembly, Top Plate and Clutch Driven Gears Removed

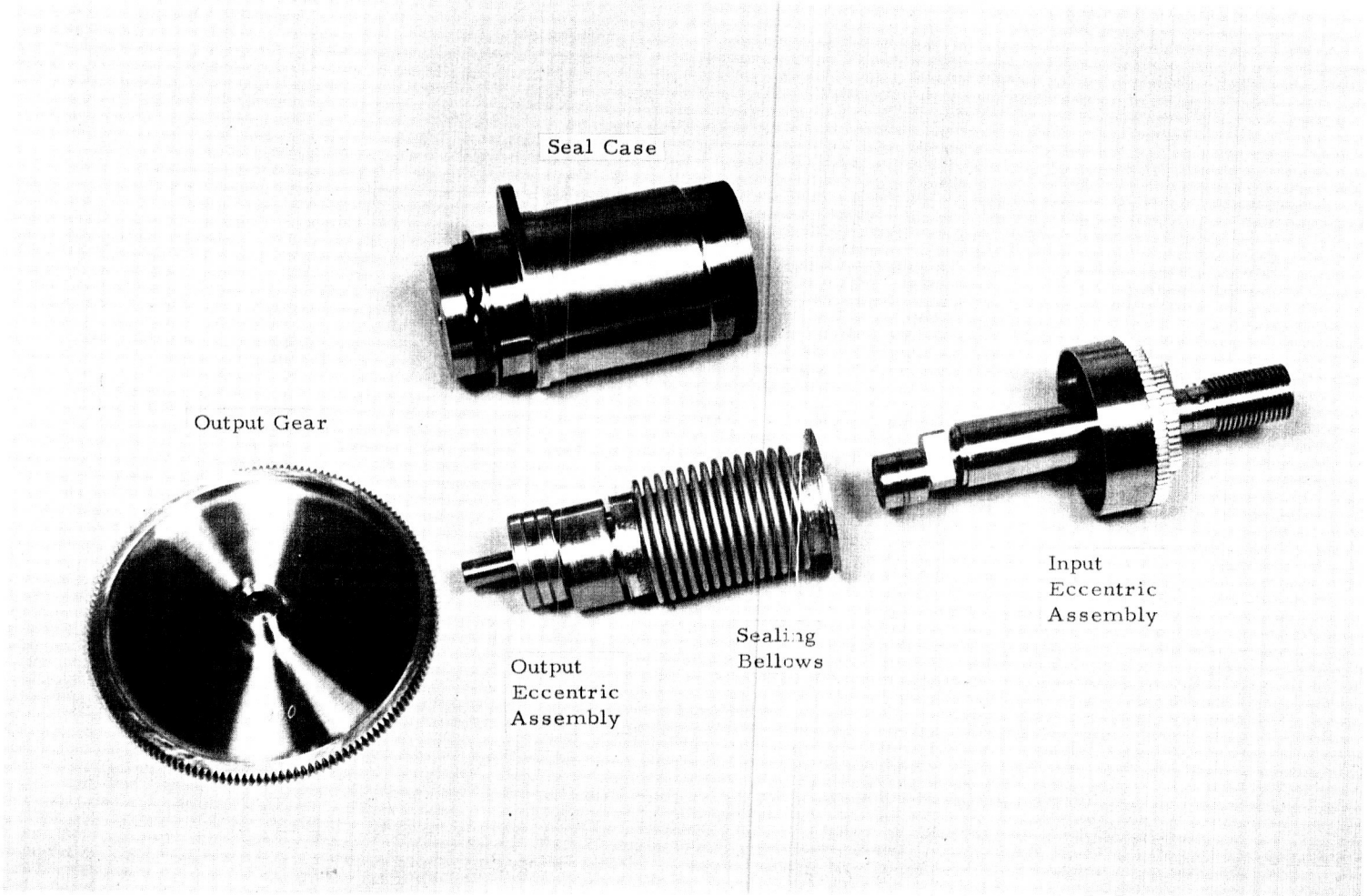

Figure 3-5. Sealed Drive Major Subassemblies

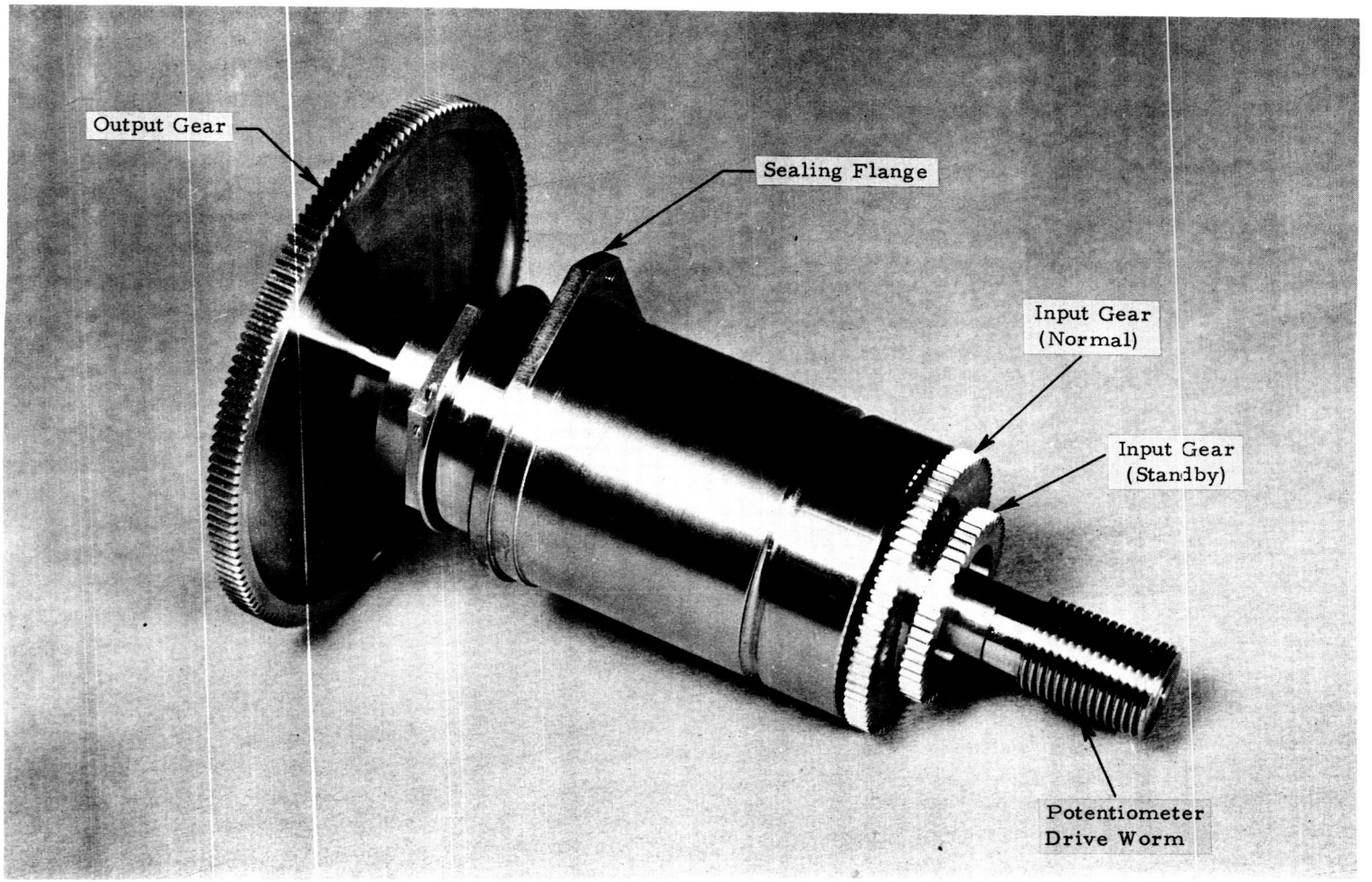

Figure 3-6. Sealed Drive Assembly

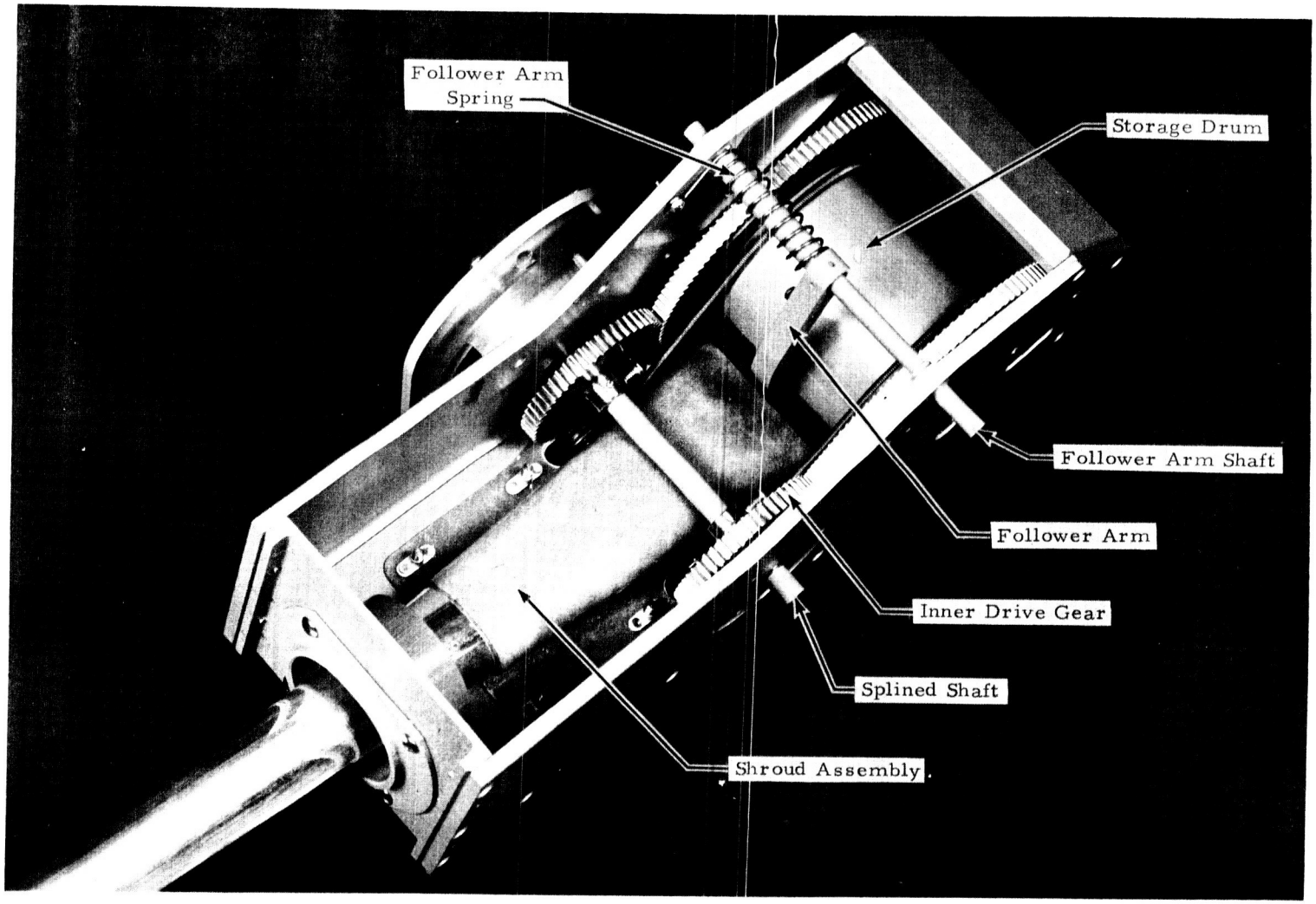

Figure 3-7. Primary Boom, Upper View

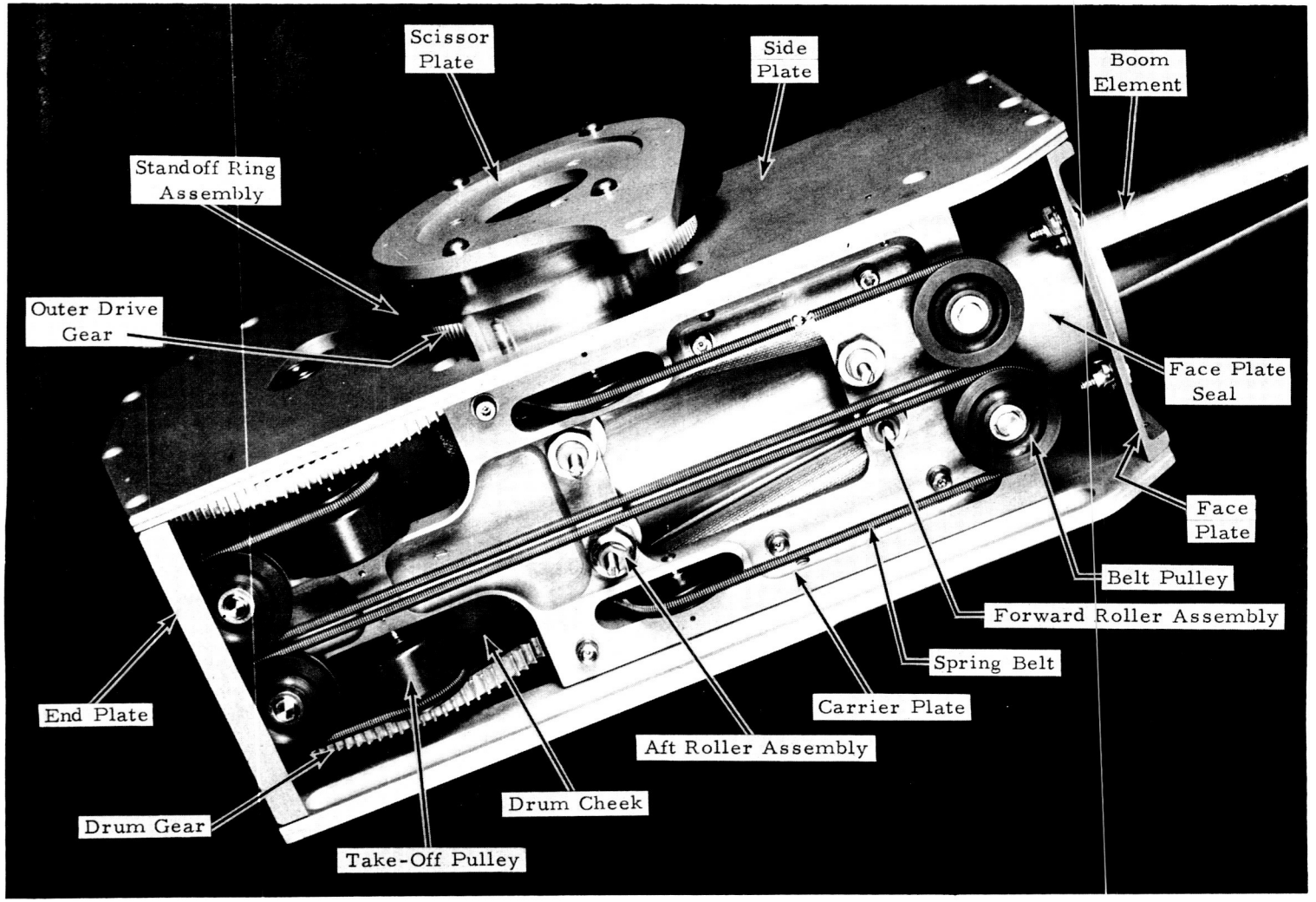

Figure 3-8. Primary Boom, Bottom View

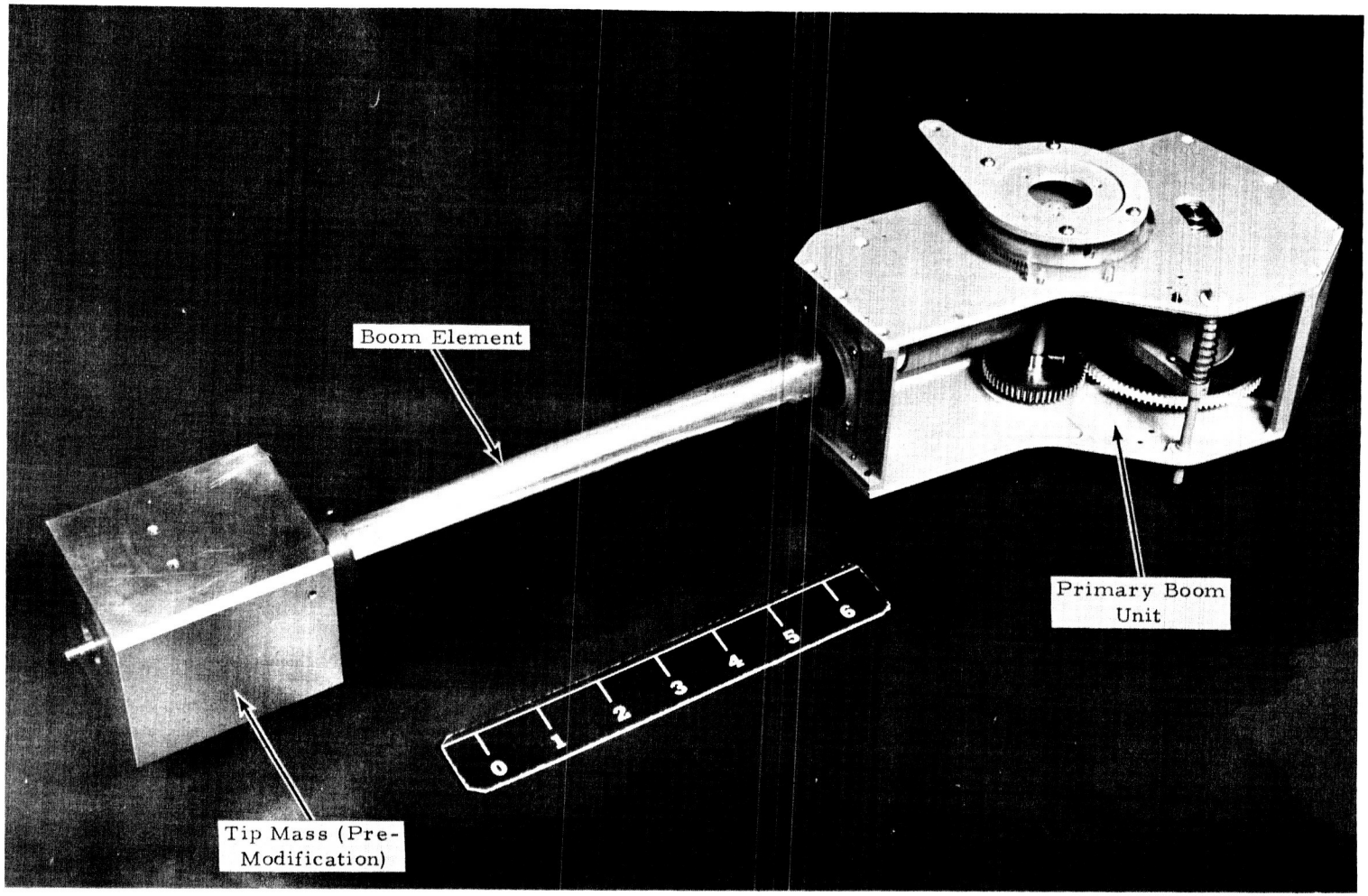

Figure 3-9. Primary Boom, Tip Mass Assembly

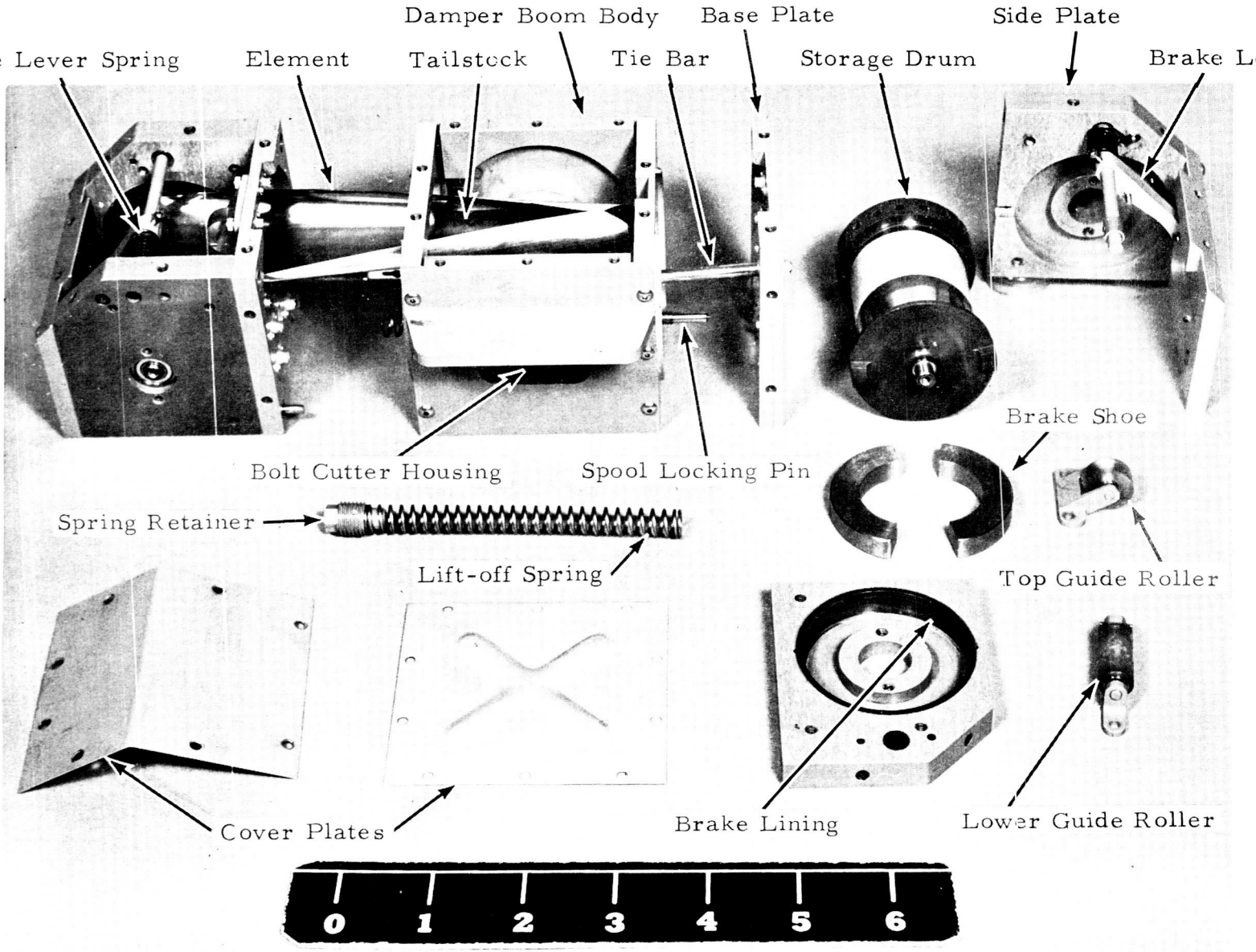

Figure 3-10. Damper Boom Assembly

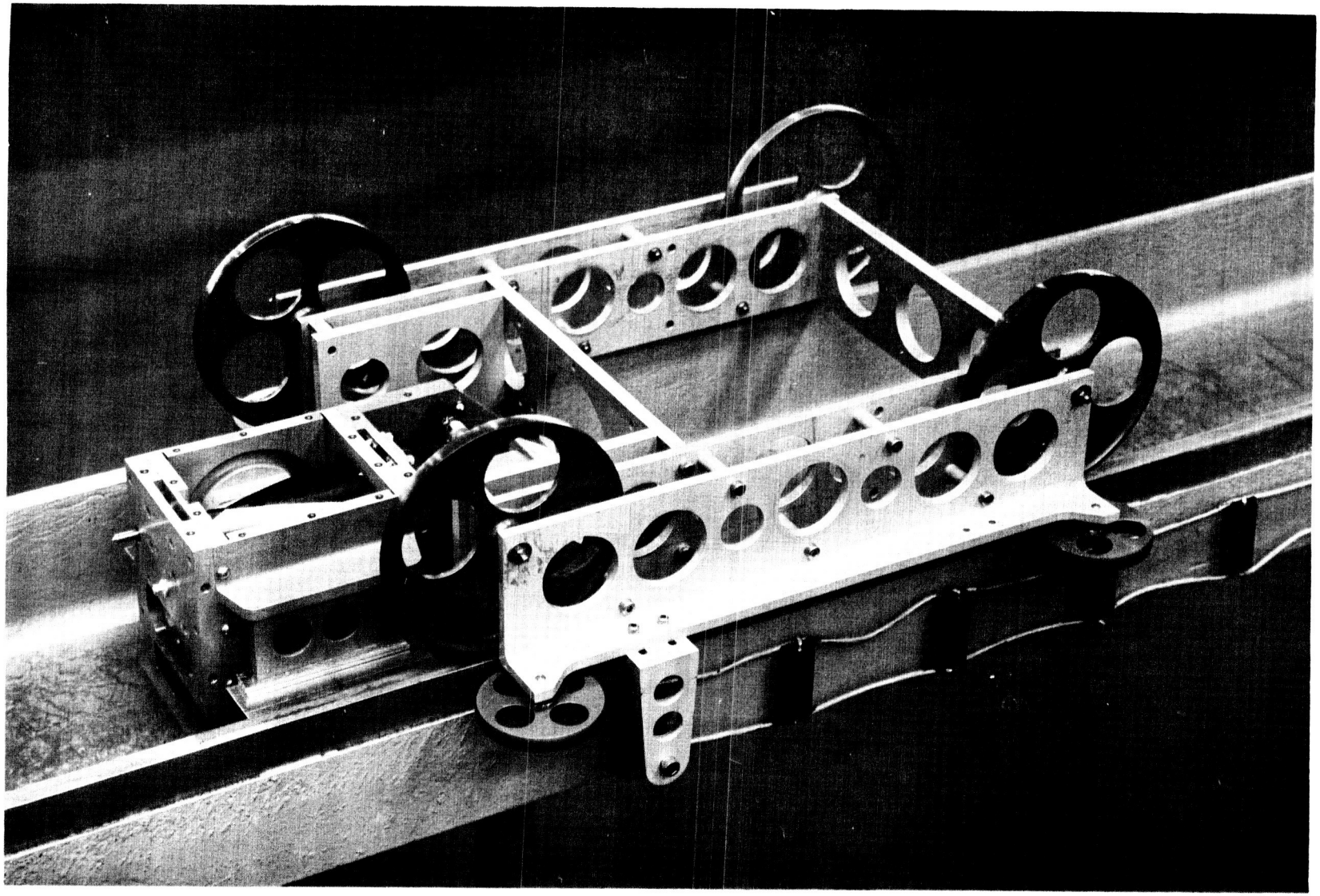

Figure 3-11. Test Trolly

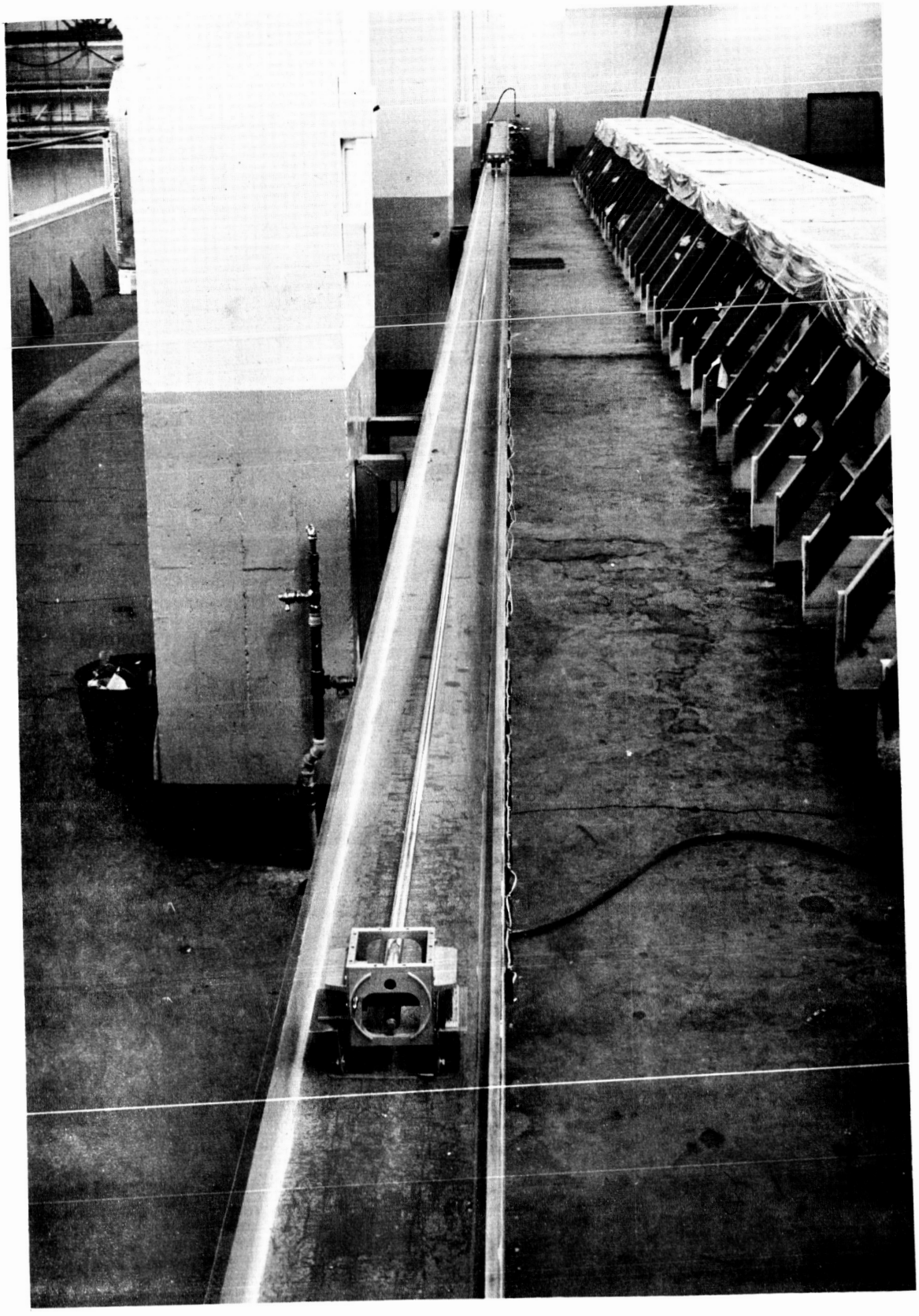

Figure 3-12. Test Track

3.7.2 TEST TROLLEY

Developmental models of the test trolley were completed and have been used for the damper boom deployment tests. See Figure 3-11 GE test trollies are in house at GE Spacecraft Department. The test track to be used at GE is currently being assembled.

3.8 SUMMARY OF TEST RESULTS

The tip mass for the deHavilland Engineering Unit of the damper boom was designed to keep the center of gravity close to the tip mass/center body interface in order to reduce the affect of launch vibration loads. As a consequence, initial test deployments in a normally long environment caused local boom damage on simulated lift off due to the gravity torque applied by the cg displacement from the tip mass/test trolley pivot point. To preserve the system integrity under vibration, the tip mass cg was retained in the design position and test balance weights were added to balance the system statically about the pivot point in the vertical plane. The increase in effective tip mass resulting from the counter balance weight is not detrimental to development tests because the total mass to be accelerated/decelerated is made unrealisitc by the presence of the test trolley. Hence, tests remain valid providing the total increase in effective mass is compensated for during analysis of the velocity/time profiles.

Deployment tests subsequent to counter-balancing occasioned a slight modification to the lift-off spring in order to further reduce lift-off rotation. Further deployment resulted in minor modifications to the centrifugal brake. Velocity/time strip chart recordings were taken and an average deployment velocity of 1.5 feet/second was measured over six runs.

It is recommended that all ground tests that are conducted on the damper boom should be performed only with counter balance weights attached. The proper weight will be supplied with each unit.

The centrifugal brake was later evaluated to determine whether the problem lies in the design of the brake or in the assembly procedure. The damper boom brake shoe was changed from tungsten to nickel-plated copper, as a result of this evaluation, in order to allow higher extension speeds.

Initial development deployment tests were conducted using a single deHavilland engineering model primary boom erection unit. This test was performed with a test drive motor connected to the erection unit input shaft. Erection rate was one foot/second and was accomplished on the deHavilland test track. Repeated extension and retractions were accomplished up to a maximum of 35 feet and with tip weights up to 8 pounds. Both the erection unit and boom performed as required. Based on the demonstrated compatibility with the primary erection unit, the test trolleys used in the test were accepted by Quality Control representatives from GE and delivered to GE in June.

The GE Engineering Unit of the primary boom assembly was functionally checked. Scissoring and emergency extension functioned successfully. However, normal mode extension resulted in a higher power drain by the extension motor than had been anticipated. The unit is currently being re-adjusted to eliminate friction and the test track will be modified to preclude artifically induced drag.

A preliminary Development Test Plan for Engineering Unit No. 1 was documented in a recently issued PIR. The plan is the initial version toward final detailed instructions which will be used by technicians as directions when performing the developmental test at GE.

3.9 HARDWARE STATUS

3.9.1 MOCK-UP

The mockup unit of the Boom Subsystem was completed by deHavilland. The unit was accepted for GE by a Quality Control representative. Delivery to GE was made in June. The mockup boom system is now in-house at GE. This mockup will have to undergo retrofit at GE to incorporate the connector position changes requested by HAC when resolved.

3.9.2 THERMAL MODEL

The thermal model is 95% complete. A temporary hold on this model took place during resolution of the connector position change.

It was decided that this model would be delivered with the connector in its current location. Delivery is expected during the week ending July 23rd.

3.9.3 DYNAMIC MODEL

The dynamic model is 85% complete. However, delivery will be held pending resolution of the connector position change.

3.9.4 ENGINEERING UNIT NO. 1

The engineering units (1a) of both the damper boom and the primary boom assembly are complete and are undergoing functional checks at deHavilland prior to delivery to GE. Further delineation is provided in the Development Test Section.

3.10 RF EXPERIMENT

Discussions were held with Dr. Stone of NASA/GSFC pertaining to the RF Experiment. The RF connector was defined and proposed location on the primary boom housing was

shown on the HAC interface drawing. However, it is understood that HAC requested a change to the RF experiment interface, which is currently under consideration. At the request of NASA/GSFC, GE prepared a drawing that shows the details of the RF experiment pickup and cable routing through the primary boom packages. The drawing was turned over to NASA/GSFC during ehri visit to GE on May 27th.

Figure 3-13 is a presentation of this drawing. It is understood that HAC desires a change from the RF connector location shown. The effect on RF cable rooting and scissor functioning is presently being evaluated.

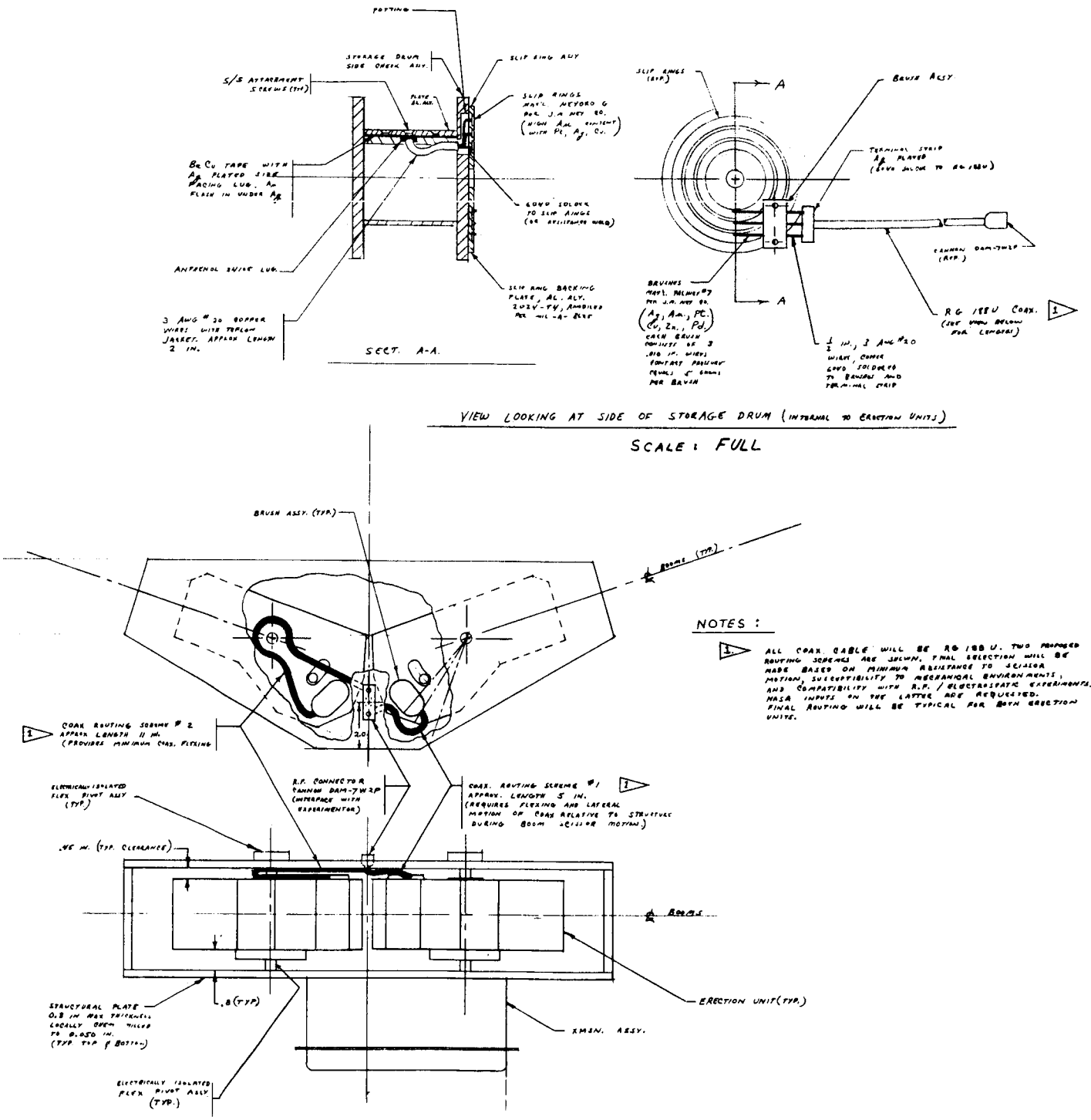

Figure 3-13. RF Experiment Details, ATS Primary Boom Assembly (GE DWG SK56152-115)

SECTION 4.

COMBINATION PASSIVE DAMPER

4.1 INTRODUCTION

4.1.1. SUMMARY OF MAJOR EVENTS DURING REPORTING PERIOD

2 April 1965	Final negotiations were held with TRW Inc. (formerly Space Technology Labs) relative to the passive hysteresis damper (PHD) contract.
5 April 1965	Agreement on the CPD caging mechanism design concept was reached with NASA.
8 April 1965	TRW Inc. was authorized by GE to proceed on the damper design by TWX.
14 April 1965	A design summary presentation on the overall CPD design concept was made to NASA management personnel at GE.
22 April 1965	First indication of performance problems with the "constant torque" hysteresis damper as a result of preliminary systems analysis at GE.
27-29 April 1965	GE personnel visited TRW Inc. and Hughes Aircraft Co. (HAC) to discuss mutual interface and engineering problems on the PHD and the CPD/vehicle interfaces respectively. A Quality Control Survey was made of the TRW Inc. facility during the visit.
5 May 1965	The first Design Review of the PHD was held at GE with presentations made by personnel from TRW Inc.
12 May 1965	Problems in the Quality Control System of a potential vendor for the solenoids required re-evaluation of other vendors and subsequent award of the job to another company.
19 May 1965	An informal interface meeting was held at GE with HAC and NASA personnel at which HAC prints were "marked up" to conform with GE component requirements.
26 May 1965	GE and TRW Inc. personnel attended a meeting at NASA to discuss the variable torque requirement to produce optimum hysteresis damper performance. Methods of developing and incorporating a

26 May 1965 (Continued)	"bow tie" disc into the prototype damper with no schedule slippage and minimum costs were discussed. TRW Inc was asked to submit cost and schedule estimates.
7 June 1965	Final Design Review of the PHD was held at TRW Inc. The deletion of the caging mechanism simplifies the PHD design and reduces the weight of the damper. The "bow tie" torque requirements were also discussed.
15 June 1965	GE received an overall cost estimate from TRW Inc. which traded off various cost reductions in the PHD effort against the potential costs to perform a feasibility study of the "bow tie" torque requirement.
16 June 1965	Adverse vendor information relative to the utilization of solar cells as sensors in the damper boom angle indicator application resulted in a re-evaluation and the decision to search for a more suitable detector. Phototransistors are the most likely candidates for this application.
17 June 1965	First "bow tie" test performed at GE-SD on a test fixture which utilized magnets furnished by TRW Inc.
23 June 1965	TRW Inc. completed tests on PHD Engineering Unit No. 1.
25 June 1965	GE Systems Analysis personnel visited TRW Inc. to discuss unofficial TRW Inc. systems analysis efforts which had disagreed with the analysis performed at GE. The discussions revealed that an error had been made in the TRW Inc. computer programming and that there was, in fact, agreement between the two analytical efforts.

4.1.2 CPD SPECIFICATION STATUS

Table 4-1 lists the status of the specifications directly applicable to the CPD.

4.2 DESIGN DEVELOPMENT EFFORT

4.2.1 GENERAL

The emphasis has changed, during this reporting period, from conceptual layouts and engineering development tests to the preparation of the detailed design drawings required for fabrication and assembly of the engineering units, the thermal model and dynamic model. It is the plan that qualification and flight units will be built from

TABLE 4-1. STATUS OF CPD SPECIFICATIONS

Specification Title	Specification No.	Status
Combination Passive Damper	SVS-7314	Issued on June 4, 1965
Passive Hysteresis Damper	SVS-7331	Issued on March 5, 1965
Angle Detector	SVS-7315	This specification is no longer applicable because the angle indicator is being developed by GE-SD. Its requirements are now included in the CPD Specification (SVS-7314).
Solenoid	R4612	Engineering development hardware was purchased to previously issued piece-part drawing R4606. The many ensuing changes in the requirement made it desirable to establish a new drawing number (R4612) to preclude any possible use of the wrong part.
Electroexplosive Pressure Cartridge and Cable Cutter	SVS-5292	Issued on May 10, 1965
Pyrolytic Graphite Simple and Complex Shapes	171A4211	Issued on Oct. 24, 1964. Revised to reflect ATS requirements on Jan. 22, 1965.

drawings which will be identical or very similar to the documentation for the engineering units. To this end, all drawings released have been accorded the same treatment as is given to drawings for prime equipment insofar as supporting technology and manufacturability analysis. In the paragraphs below, the design status of each of the elements of the damper are summarized.

4.2.2 CPD PACKAGE

The following description is for the design from which the Engineering Models will be built. The detail drawings are essentially complete and released for procurement and manufacture. Assembly drawings are partially completed and released. The design is shown in Figure 4-1. The circled numbers in their description correspond to the numbers indicating parts in Figure 4-1.

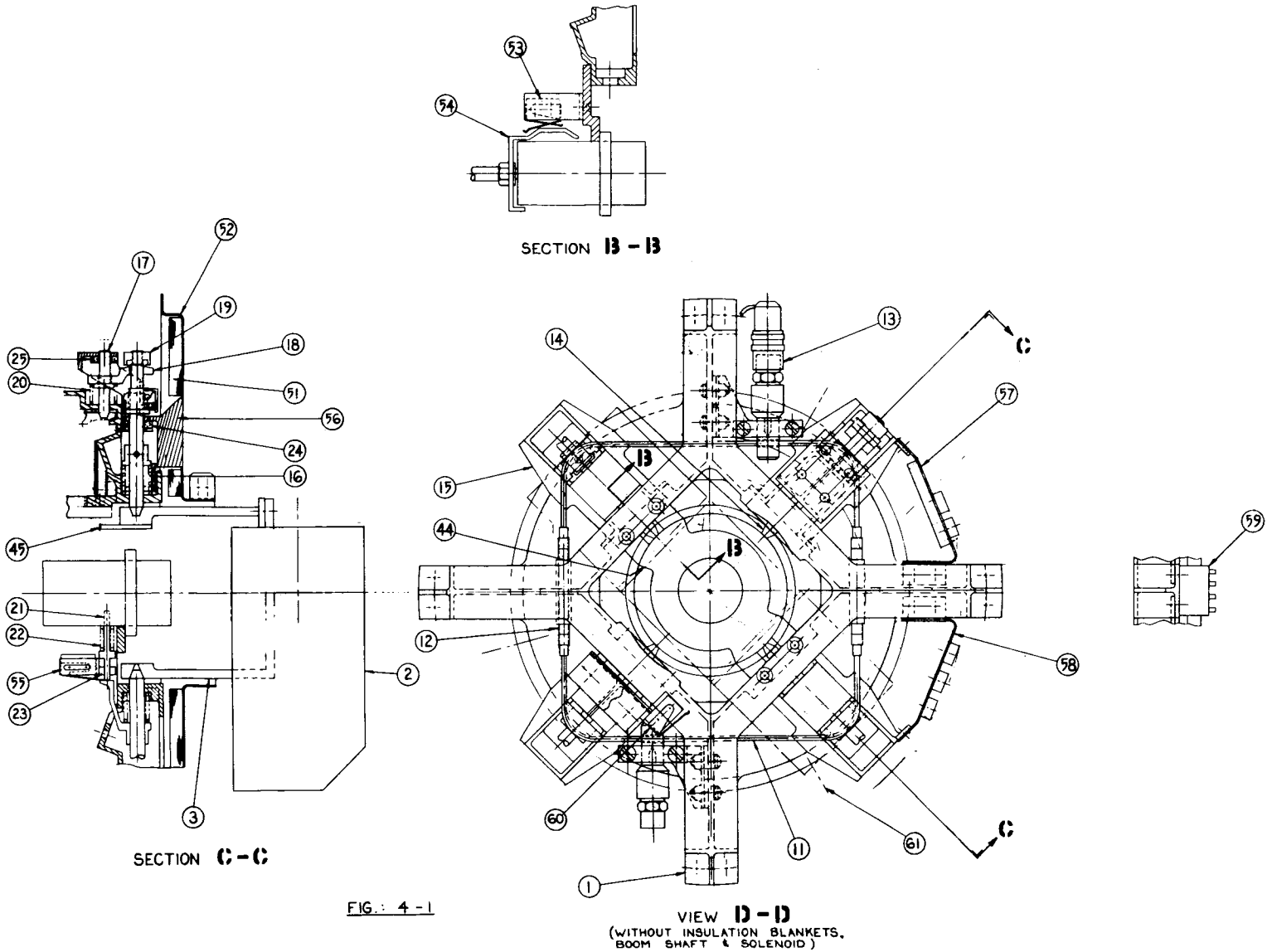

Figure 4-1. CPD Package (Sheet 1 of 3)

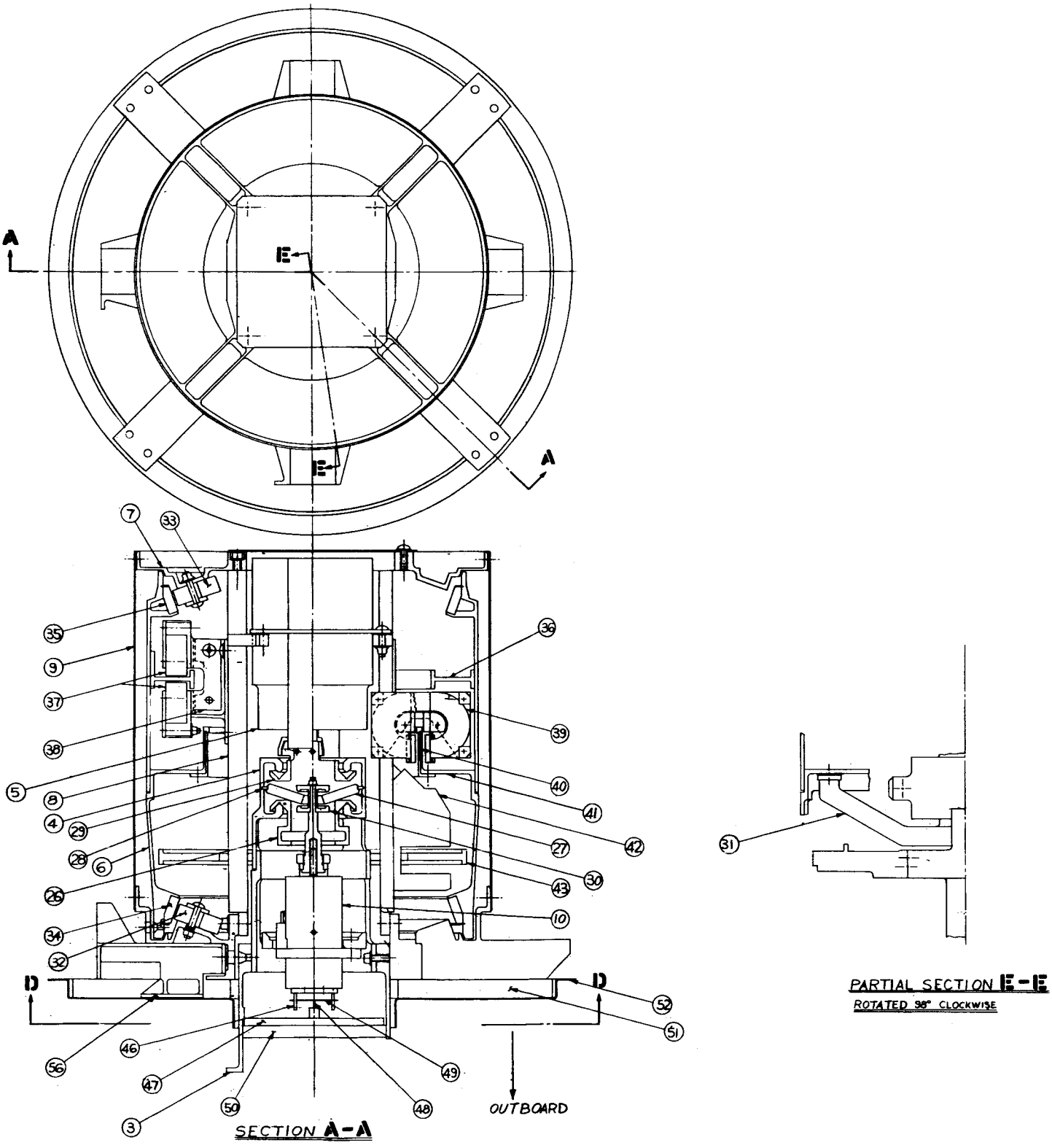

Figure 4-1. CPD Package (Sheet 2 of 3)

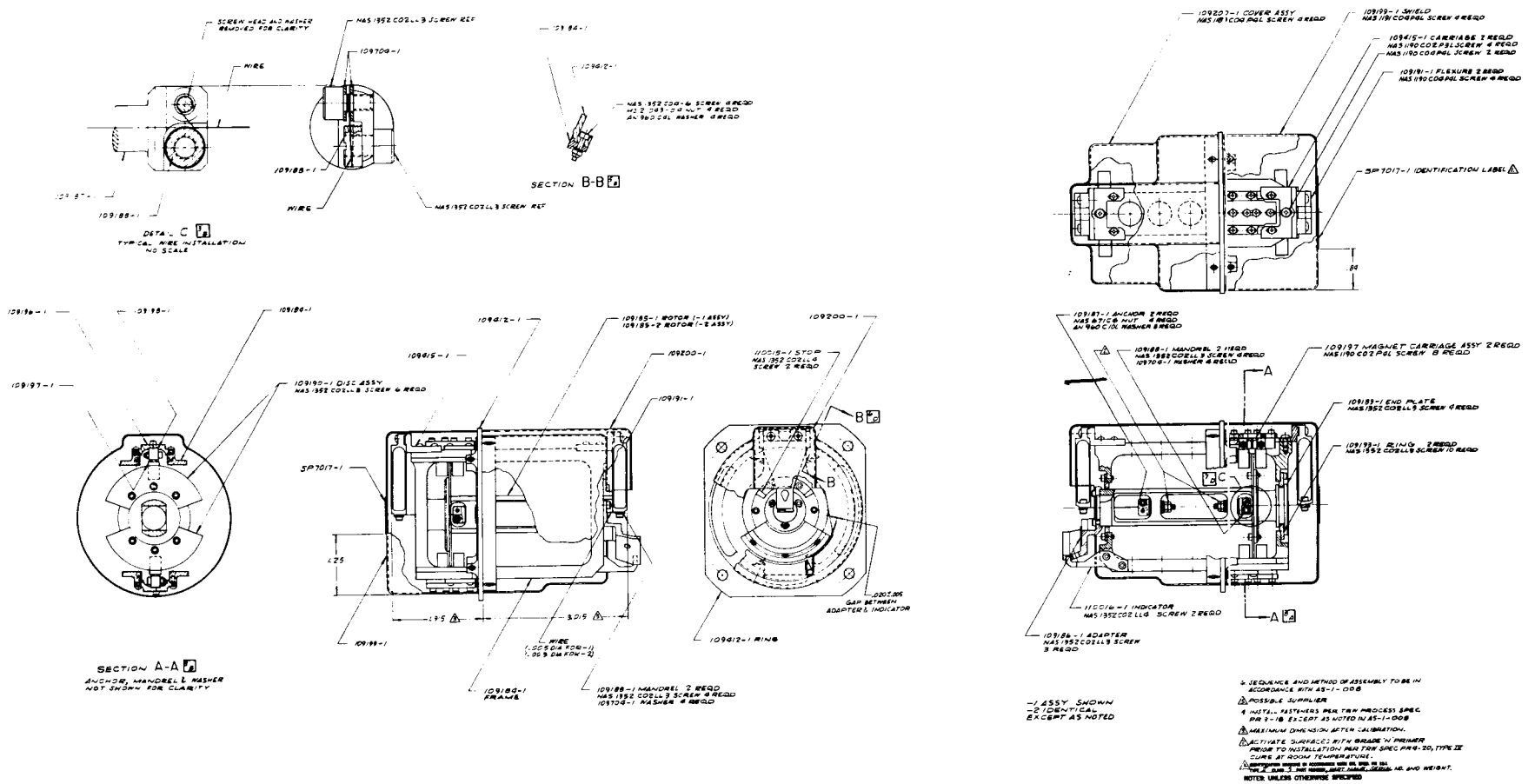

Figure 4-1. Passive Hysteresis Damper Details (Sheet 3 of 3)

The package has been integrated into the Hughes Aircraft Company structure and is attached to it at the inboard face of the four projecting beams of the base plate (1). The damper boom package (2), by de Havilland, is attached at the outboard end of the boom shaft (3). In operation, the damper booms rotate ±45° from a null position, and about the axis of the damper package.

There are four main parts to the CPD Package:

1. The boom shaft (3), which connects the booms to the clutch housing (4).
2. The hysteresis damper (5), procured from TRW Inc., which is connected to the booms in one position of the clutch (Figure 4-1, Sheet 3).
3. The eddy current damper rotor (6), which is connected to the boom in the other position of the clutch.
4. The structure, which consists principally of the base plate (1), the inboard plate (7) at the inboard end of the damper, the two posts 8 connecting the inboard and base plates internally, and the cover 9, connecting the inboard and base plates externally.

At launch the boom shaft (3), the eddy current rotor (6), and the core of the solenoid 10 (used to shift the clutch) are all caged to the structure. They are supported on pins which are held in the caged position by the 0.125 inch diameter cable (11). The cable is tensioned by the turnbuckles (12). To uncage, the cable is cut by a pyrotechnic fired guillotine (13) and/or its diametrically opposite redundant mate. The cable is roved through saddles on the main caging pins (14). The pins have tapered points where they enter tapered holes in the boom shaft (3). The cable, when tensioned, holds the pins snugly in the tapered holes. The pins pass through a hole in the base plate (1) and another hole in the pin bracket (15) (with clearances of 0.004 inch to 0.008-inch diameter). A 49-pound spring (16) retracts the pin when the cable is cut.

The eddy current rotor is caged by a pin (17) which also has a tapered point that seats in a tapered hole in the rotor. This pin also passes through a hole in the baseplate and another hole in the bracket (with clearances of 0.004 to 0.008-inch diameter). The pin is engaged by a fork (18), loaded by a nut (19) on the end of the main caging pin. When the cable is cut and the main caging pin retracts, it allows the eddy current pin to be retracted by the 25-pound spring (20). It was agreed that GE-SD should proceed with this caging arrangement at a meeting at NASA/GSFC on 5 April, 1965. The core of the solenoid is caged by pin (21) held in engagement by a foot on a sleeve of one of the main caging pins. When the main caging pin retracts it allows a 10-pound spring (22) to disengage the solenoid pin. The pin is straight and fits in the solenoid and in the guide (23) (with 0.005-inch to 0.008-inch diametral clearance). Pin (61) is provided for individual manual caging of the eddy-current rotor during handling and testing of the hysteresis damper. This feature is required because the diamagnetic

suspension will not support the eddy-current damper in the earth's gravitational field. Buna—S rubber cushions (24) and (25) are provided to absorb the energy of the main and eddy-current caging pins, at release and thus to prevent distortion of the bracket (15), particularly under repeated operation during testing.

The loads generated by launch vibration in the boom package and in the boom shaft and clutch are transferred to the baseplate by the main caging pins. The launch loads from the eddy-current rotor are carried to the baseplate by the eddy-current caging pins. The loads in the posts and the parts attached to them are either carried directly into the baseplate or to the top plate. The loads in the top plate, plus the loads from the mass of the top plate itself and the parts attached to it, are carried by the cover, along with the loads due to the mass of the cover, into the baseplate. The baseplate is designed for adequate strength and rigidity to take these loads into the HAC structure.

In normal operation, the boom shaft structure is designed to have a nominal radial clearance of 0.1 inch between it and the baseplate. Within the CPD, the boom shaft structure connects to the clutch housing (4). This clutch housing has two circular vee clutch faces. These faces mate with matching vee-groove clutch plates. The eddy-current clutch plate (26) is shown in the engaged position in Figure 4-1. It is held in contact by the coned diaphragm (27). The reaction of the force that holds the clutch faces in engagement is taken by the pivot ring (28). When the clutch is shifted the diaphragm pivots about this ring, over center, and "flips through" in the opposite direction, to force the hysteresis clutch plate (29) into engagement with the other vee face of the clutch housing. The diaphragm is pushed over center by the actuator spool (30), which is moved by the solenoid (1). The solenoid is further discussed in paragraph 4.2.4. The positioning and size of the solenoid and diaphragm are such that the actuator does not touch the diaphragm during damping operation. Also, the dimensioning and locations of the clutch faces are such that the disengaged faces do not contact during damping operation. The two clutch plates are held in position by the suspension systems of either the hysteresis or eddy-current damper. Thus, when the clutch is shifted, the clutch housing and everything attached to it (including the damper booms) must move axially a distance equal to the clearance between the disengaged clutch faces. This distance is about 0.14 inch. In the caged position the clutch is engaged in the eddy-current mode. The booms move outboard, about 0.14 inch, when shifted to the hysteresis mode.

The hysteresis clutch plate (29) is attached to the hysteresis damper (5) by screws. This damper is discussed under paragraph 4.2.6. The damper is attached to posts (8) by bolts through oversized holes and with shims. This method will allow proper alignment of the clutch faces and the boom shaft when engaged.

The eddy-current damper rotor (6) is attached to the eddy-current clutch plate (26) by arm (31). The arm is attached to the rotor by bolts in oversized holes and shims

to allow proper alignment as in the case of the hysteresis damper. The rotor is supported by 10 magnets (32) attached to the baseplate and by 10 magnets (33) attached to the inboard plate. Each set of suspension magnets will be mounted, poles facing out, in a flat cone of total included angle of about 140° apex. The magnets support the rotor by the diamagnetic repulsion of the pyrolytic graphite rings (34) and (35) set in each end of the rotor. The angular arrangement of the magnets is such that the largest force is supplied in the radial direction, which is the direction of greatest loads. The axial component resulting from the angle of the cone produces sufficient axial force to support the imposed loads in that direction. There is a nominal clearance of 0.050 inch between the graphite and the magnet face. The ends of the rotor are shaped such that they fit, with clearance, corresponding surfaces on the baseplate and inboard plate to form stops. These stops prevent the magnets and the pyrolytic graphite rings from contacting in the event that transient forces experienced are greater than the design operating loads. No physical damage will occur when the stops are engaged.

The aluminum eddy-current damping ring (36) is bolted to the rotor. Two sets of magnets (37) are bolted to brackets (38) on the posts (8) through oversized holes to allow alignment with the damping ring. The eddy-current damping is created by the magnetic flux of the two sets of two magnets each that cause electrical currents to flow in the aluminum ring. The interaction of the flux resulting from the current flow in the aluminum and the flux of the magnets produces the damping force and consequently the torque. The faces of the magnets are spaced approximately 0.050 inch away from the aluminum surface.

Torsional restraint for the eddy-current damper is provided by an arrangement of magnets (39) and a thin crescent of magnetic material (40) mounted on a cylindrical extension of a flange (41) of the eddy-current rotor. The wider portion of the thin crescent has a greater attraction for the magnets producing the torque that returns the rotor to the null corresponding to this wider portion. There are two sets of torsional restraint magnet arrangements disposed symmetrically about the centerline of the damper. This arrangement tends to balance loads induced on the diamagnetic suspension. The magnets are bolted through oversized holes, to a face on bracket (38) to allow the 0.25-inch gap between the pole piece to be centered on the magnetic material (40).

Two angle indicator heads (42) are located diametrically opposite each other and attached to the posts (8). The angle indicator disc (43) is attached to the boom shaft (3). The angle indicator is described more fully under paragraph 4.2.7.

Faces (44) on the solenoid support bracket form one side of the rotational hard stop for the damper booms. Arms (45) which are part of the boom shaft will contact the faces at about ±45° from the damper null position.

The fixed portion of the soft stop, which provides an increased spring rate of 1000 dyne cm/deg in the range of 40° to 45°, consists of two pins (46) mounted on the outboard

end of the solenoid (10). The rotating part is attached to a spider (47) in the boom shaft. A torsion wire (48), about 0.8 inch long and attached to the center of the spider, has a crossbar (49) attached to its inboard end. In operation, when the damper booms turn about 40° off the null position, the crossbar will contact the pins and produce the required restraining torque of about 1000 dyne cm/degree for the medium altitude dampers, and 250 dyne cm/degree for the synchronous altitude dampers.

The spider (47) also supports an insulation pad (50) consisting of aluminized mylar. An insulation blanket (51), 13 inches in diameter, is located on the outboard face of the baseplate (1). The blanket consists of 30 layers of aluminized mylar. It is attached, at its outboard face, to an aluminum sheet (52), which is flanged to fasten it to the HAC insulation blanket. The aluminum sheet is attached, through plastic spacers, to the baseplate. The outboard face of the aluminum sheet and other parts on the outboard end of the damper will either be polished and given a thin alodine coating or it will be coated with a thermal control paint, depending on the results of a thermal analysis. The remainder of the damper will be thermally black, both outside and inside, to provide thermal control. Black on the inside of the damper will also be of benefit in reducing light reflection for operation of the angle indicator. The space between the aluminized sheets and the face of the baseplate will be used to run electrical wiring.

Two switches (60) are mounted on a clip on the outboard face of the baseplate to indicate when the damper booms have extended. Two additional switches (53) are mounted to a clip on the solenoid support bracket (44) and activated by a ramp (54) on the solenoid core. They indicate, by the position of the solenoid plunger, whether the damper is in the hystersis or eddy-current mode. Another switch (55) is mounted on a clip on the solenoid caging pin guide, to sense when a caging pin has been retracted, thus indicating that uncaging has been effected.

A foundation (56) is provided to accommodate the catcher bracket furnished with the damper boom package. The catcher restrains the electrical connector which is ejected, to allow the booms to turn freely, at the same time the booms are extended. The electrical connector for the wires from the catcher fits in bracket (57). The wires from the uncaging guillotine (13) also go to a connector in bracket (57). HAC will connect directly to the second guillotine. All the other wires will go to connectors in bracket (58). An electronic module (59) is mounted on the inboard face of the baseplate beam between the two connector brackets. The purpose of this module is to provide common tie points for various circuits and to mount electronic components required for telemetry and temperature sensing circuits.

4.2.3 TESTING

4.2.3.1 Impact Cushions

Tests were run on Buna-S rubber cushions to be used to absorb the caging pin energy when the damper is uncaged. The cushions will prevent the pin bracket plates from

yielding particularly under repeated operations during testing. The tests are reported in PIR 4371-0063. Load vs. compression tests and a 300-cycle impact test were run. The load corresponding to the required design energy of 12-inch pounds is about 220 pounds from the load vs. compression curve. The bracket is adequate to take this load. The cushion satisfactorily withstood the 300-cycle test. The cushion is considered satisfactory for flight and also for repeated testing on the ground.

4.2.3.2 Corrosion Tests

Corrosion tests were run under the humidity conditions required by the damper specification (SVS-7314). Anodized 6061 aluminum alloy against magnesium with a Dow 9 coating and no zinc chromate or other paint showed no evidence of corrosion. A test of molybdenum against beryllium copper did show signs of corrosion. The corrosion products are being analyzed. The seriousness of this condition can be evaluated better when the results of the analysis are known.

4.2.4 SOLENOID

Two solenoids were obtained from the G. W. Lisk Co. which conformed to R4606 with the exception of the force vs. travel requirement. These solenoids are to be used to provide design information relative to force vs. travel characteristics which could be obtained from the required solenoid size. Calculations indicated the design to be marginal. The test data obtained from the solenoids indicated, as shown in Figure 4-2, that this design could not fill the required force vs. travel requirement.

During May the input voltage specified was changed from -24 ±2.5 vdc (because of required PCU weight reduction) to approximately -22.3 to -30 vdc. The maximum allowable current was permitted to increase, the temperature range shifted slightly and the mechanical configuration changed slightly. Since solenoids were delivered to Component Specification R4606, it was decided to issue a new specification, R4612 for the required solenoid design. New quotations were obtained from solenoid vendors and the contract for the manufacturing and testing of the solenoids was awarded to Koontz-Wagner. They were low bidder, they have an excellent quality control organization and their preliminary data indicated that all requirements of R4612 could be met.

A meeting was held at Koontz-Wagner on June 3rd to discuss the details of the design and testing of the solenoid. Koontz-Wagner immediately began design and construction of a development model which will be used to obtain engineering data before construction is started on the engineering unit. Preliminary test data obtained on the development model late in June, indicated that the design was marginal, but that the specified requirements could be met. Tests on engineering unit No. 1 are expected to begin in early July with delivery of the unit to GE by mid-July. Functional testing will be done at GE before the solenoid is installed into the CPD engineering unit No. 1.

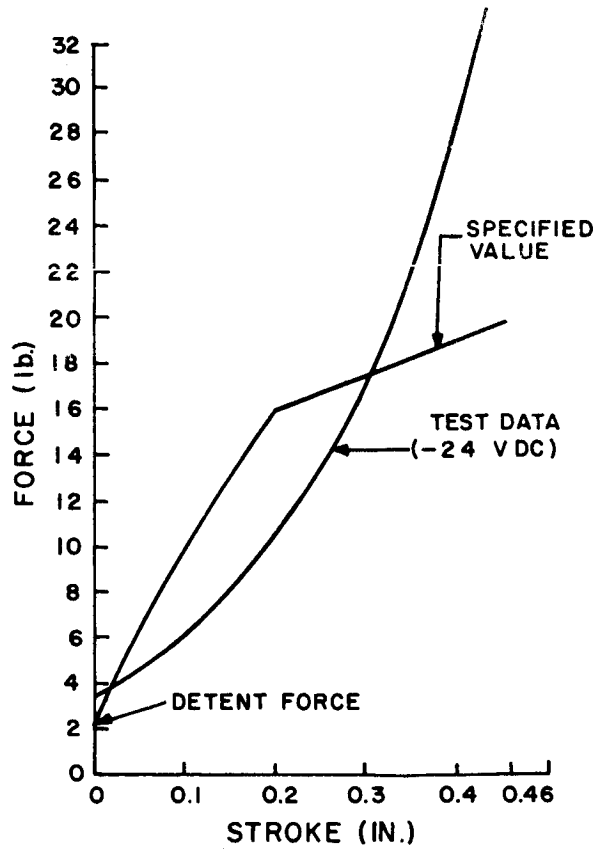

Figure 4-2. Results of Force vs. Travel Test for Solenoid to the R4606 Component Specification

The solenoids obtained from the G. W. Lisk Co. are presently being used in the hysteresis damper mode changing tests at TRW Inc. They will also be used to run Bellville Washer spring endurance/life tests. The input voltage will be increased to obtain the required force vs.travel requirements during these tests. The voltage will be approximately 35 vdc for tests at room temperature.

4.2.5 EDDY-CURRENT DAMPER

4.2.5.1 Eddy-Current Damping

Early in April, Analysis of system performance showed that the eddy-current damping coefficient should be changed from 2.63×10^4 dyne-cm-sec/deg to 1.58×10^4 dyne-cm-sec/deg for the medium altitude flight, and 0.9867×10^4 dyne-cm-sec/deg for the synchronous altitude flights.

The lower damping specification permitted the use of a damper disc material with lower electrical conductivity than copper, and the copper disc was replaced by aluminum alloy 1100-0, with a weight saving of about one pound. Use of a smaller damping magnet was also considered. Tests showed that the same magnet will be required for the medium altitude units, but that a smaller magnet may be used at synchronous altitude, with a weight saving of about 1/4 pound per CPD.

4.2.5.2 Magnetic Torsional Restraint Design

A decision was made to specify the material for the torsional restraint pattern as Eastman Sound Recording Tape, Type A303, rather than 304 stainless steel foil. Satisfactory torque vs. angle characteristics had been obtained experimentally using each material. The choice was based on a comparison of the hysteresis and lateral force characteristics of the two materials. The stainless steel exhibited lower (better) hysteresis characteristics than the sound tape, but produced prohibitively high lateral force loads on the diamagnetic suspension. The hysteresis torques in the Eastman sound tape are within the acceptable limits, and the undesirable lateral forces are less than half those produced by the stainless steel.

A materials investigation is in progress to seek a material with still better hysteresis and lateral force characteristics. This investigation is discussed in the following paragraph.

4.2.5.3 Magnetic Torsional Restraint Investigation

As indicated above, it has been decided to investigate various promising magnetic materials in an attempt to obtain lower hysteresis loss in the ECD torsional restraint system without compromising other performance parameters. Eight new materials have been tested during this reporting period. These include paramagnetic and feebly magnetic metallic materials (such as Hastelloy F, 65-30 CuNi, 10-8 MnNi, and 17-7 PH) antiferromagnetic compounds (including $MnCl_2 \cdot 4H_2O$ and MnO) and plastic materials with a magnetic filler (including PR1422 polymer and iron powder dispersed in epoxy resin). Of the materials listed, all exhibited lower hysteresis loss than either 302 stainless steel or A303 sound tape, except the 10-8 Mn-Ni steel. Hastelloy F exhibited almost immeasureable hysteresis loss but the torsional restraint varies excessively with temperature and lateral force is relatively high. PR1422 polymer was found to have unacceptable outgassing characteristics and 65-30 CuNi exhibited high lateral force. Testing of antiferromagnetic compounds was discontinued due to the difficulties forseen in adapting this type of material to the design. Of the two remaining materials, 17-7PH and the epoxy/iron dispersion, both are superior in performance to 302 stainless steel and A303 sound tape from the standpoint of lower hysteresis loss and lower lateral force output. With these two materials the hysteresis loss is roughly halved, whereas an order of magnitude reduction is being sought.

The iron dispersion in epoxy resin represents but one of a general category of mixtures of this type which can be formulated, thus offering extensive flexibility since specimen thickness, proportions of epoxy and filler material and the filler material itself can all be varied over a relatively broad range. The investigation of this type of material will continue during the next quarter in an effort to identify a torsional restraint material with significantly lower hysteresis loss than the material currently being used for the engineering model CPD.

4.2.5.4 Diamagnetic Suspension

A report was completed on the analytical design of diamagnetic suspensions, and is included as Appendix A. The analysis therein predicts the behavior of the CPD shaft under the influence of the worst combination of external cocking torques, radial forces, axial forces, and internal lateral force loads. The performance criterion employed is the amount of clearance remaining between the rotor and stator at their closest point of proximity, for a given set of design parameters and a given set of loads. A positive value calculated for clearance implies successful performance for the suspension for the given conditions.

In Figures 12 through 24 of Appendix A, values of the rotor clearance are plotted against the critical design parameter: lateral force load gradient. It may be seen from these curves that the external loads will be supported with positive clearance, provided the lateral force gradient produced by the magnetic torsional restraint does not exceed some critical value. This critical value depends upon the number of suspension magnets in each ring, the nominal air gap setting for these magnets, and upon certain dimensions in the CPD design.

The curves in Appendix A were used to evaluate the effects on the suspension caused by a revision of the specified external loads resulting from systems analysis in April. The revised loads are as follows:

Load	Units	Old Spec	New Spec
Cocking Torque	dyne-cm	±2500	±1200
Radial Force	dyne	±100	±10
Axial Force	dyne	±50	±10

Figure 16 of Appendix A indicates that 8 magnets per ring set at a 0.050 inch air gap will support these loads for a lateral force gradient of less than about 11 dynes per mil (i.e., per 0.001 inch displacement of the rotor). However, as the expected lateral force gradient, using Eastman sound tape for the torsional restraint, is 10 dynes per mil, it was decided to use 10 magnets per ring, to provide some safety factor. In the CPD design the 10 suspension magnets are not uniformly spaced. In the direction of the lateral force, the suspension magnets are spaced at 30 degrees between centers, the equivalent of 12 magnets per ring. The expected performance, therefore, is better represented by Figure 13, which assumes 12 equally spaced magnets per ring. This curve shows satisfactory performance for lateral force gradients up to 16 dynes per mil, which gives an adequate margin of safety over the expected load of 10 dynes per mil. Thus, the non-uniform spacing of the suspension magnets gives additional safety margin without additional weight penalty.

4.2.6 PASSIVE HYSTERESIS DAMPER

4.2.6.1 TRW Inc. Design Activities

Final negotiations with TRW Inc. (formerly Space Technology Laboratories) were completed and the specification and work statement were revised to reflect the design changes and working agreements. TRW Inc. has submitted the various software for final approval. Tentative approval had been granted on most software items prior to final testing and delivery of the first hardware.

During April GE personnel visited TRW Inc. to resolve any apparent design and/or testing problems. Particular points discussed were the caging device design and the magnetic circuit and shielding design. The caging device has since been eliminated from the damper because vibration tests on both the development model, using ATS-A and ATS D/E suspension configurations, and on the Engineering Unit No. 1 have indicated that it was not necessary. Questions on the ordnance device were answered by a series of test firings at GE which proved the device to be satisfactory if properly applied. The shielding problems were resolved when GE measured the field within the hysteresis damper envelope on the CPD Dipole Simulator. The field was found to be an order of magnitude lower than previously anticipated. The change was due partly to relocation of the hysteresis damping disc and to the relocation of the damping, suspension and torsional restraint magnets in the eddy-current damper. Weight savings of approximately one pound were realized because of the elimination of the caging and some of the shielding. Two design reviews were held during the quarter. During the first review the basic conceptual design and supporting analyses were presented, along with detailed discussion of the assembly and adjustment procedures, performance test plans, development test plans and reliability analyses. No serious problems were found in the TRW Inc. design.

The second design review was held after development model testing and testing of engineering unit No. 1 had begun. During this review TRW Inc. presented all data from the testing as well as final drafts of all required analyses, test plans and procedures, and miscellaneous software items.

During this meeting TRW Inc. was given the requirements for the optimized or "Bow-Tie" hysteresis damping torque requirement. TRW Inc. and GE are to investigate the design feasibility of such a damping configuration and pool the results of these investigations by Mid-July so that basic program direction can be given concerning the final design configuration. The progress of the work on the "Bow-Tie" development is summarized in the section following. TRW Inc. was given redirection on the testing program for Engineering Unit No. 1 and prototype No. 1 to maintain the program schedule and costs while taking on additional tasks. TRW Inc. has submitted costs to GE which were based on the above directions.

The Dynamic Model was delivered to GE on June 6th, two weeks ahead of schedule. Engineering Unit No. 1 was delivered on June 25th, (Shipped from TRW Inc. on June 23rd) one day behind schedule. This unit is shown in Figure 4-3a and 4-3b. The Dynamic Model was sized (weight and center of gravity) by calculations. The weight and CG measurements taken on the Engineering Unit No. 1 indicate the Dynamic model to be overweight by 0.16 pound and the CG to be off by about 0.25 inch. The model will be reworked at GESD to conform to the actual damper. Testing of Engineering Unit No. 1 at TRW Inc. indicated that the unit met all specified requirements. This unit will undergo a basic functional test at GE before it is installed into the CPD Engineering Unit No. 1.

TRW Inc. has completed the qualification tests on the wire to be used in the dampers. Preliminary results indicate that 100 "missions" had been completed on each of 5 samples with no apparent degradation of the wire. In addition to these tests on the suspension system (wires), TRW Inc. has set up and run 100 mode changes on the development model without any apparent degradation to the unit. These tests were performed by using a solenoid and a Bellville washer spring with the same characteristics that will be used in the CPD, (the solenoid, and washer and fixture were supplied to TRW Inc. by GE). Additional tests will be performed during the next quarter to accumulate more reliability data.

4.2.6.2 "Bow-Tie" Development

System analysis which was conducted at GE of the performance of the spacecraft when being stabilized by the hysteresis damper indicated that an excessively long time would be required to damp out vehicle oscillations. In the mathematical model of the damper, the hysteresis damping was a constant regardless of angular position of the damper boom with respect to the vehicle and, of course, regardless of the relative velocities. Further analysis revealed that more nearly optimized damping could be achieved if the damping were low when the damper boom was near the null and larger when angular relationship was large. The plot of damping torque versus angular position resulting in a figure which resembled a bow-tie.

GE has initiated the effort on the bow-tie development by setting up test equipment in which the performance of various damping discs and magnetic circuit configurations can be evaluated. As a starting point, it was decided to test the existing TRW Inc. magnetic configuration to provide correlation data. TRW Inc. delivered the necessary components to GE and testing was started. Several other materials have also been checked but no conclusive results have been obtained from these tests to date.

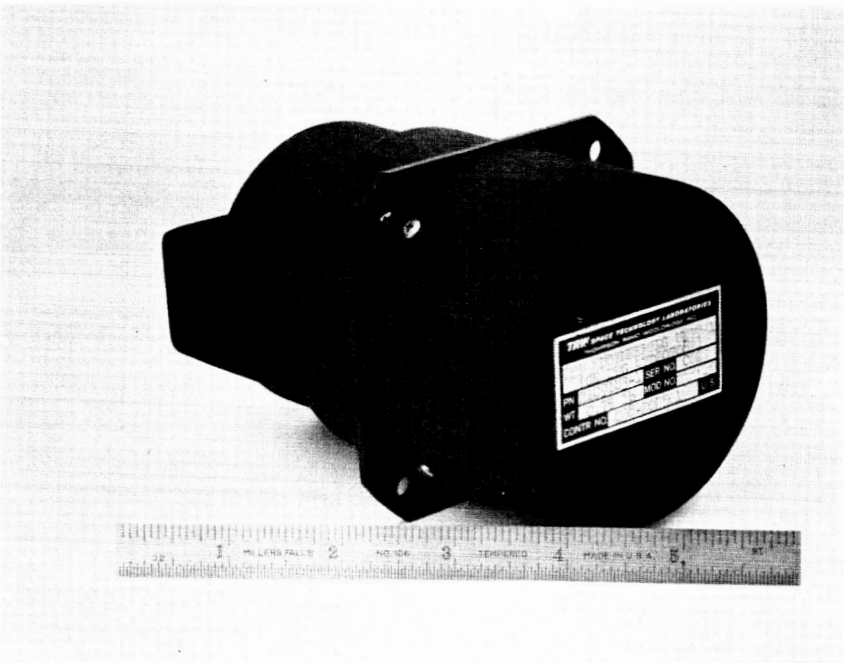

Figure 4-3a. Passive Hysteresis Damper Engineering Unit No. 1

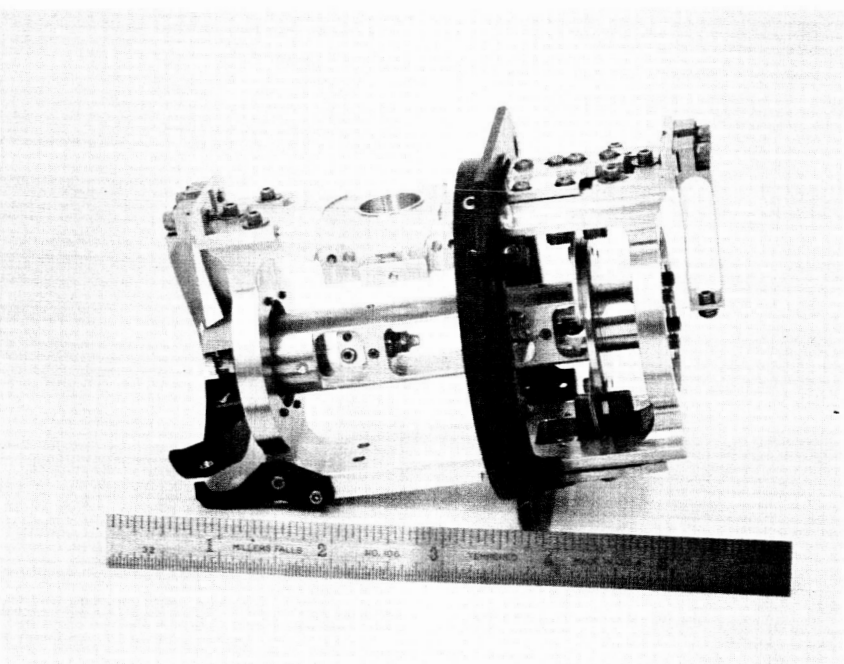

Figure 4-3b. Passive Hysteresis Damper Engineering Unit No. 1 (Cover Removed)

4.2.7 DAMPER BOOM ANGLE INDICATOR

4.2.7.1 Design Description

Figure 4-4 shows the general arrangement of the angle indicator sensing head and reflects the change in the light source location from that described in the Eleventh Monthly Progress Report. This change allows for a lighter weight and a more efficient design. Each sensing head is now a complete unit in itself, i.e., the light source, fiber optics assembly and all electronics for one head are integral in one package; no electrical or mechanical interconnections are required between the heads. No point-to-point wiring is required within the CPD because there is a connector mounted directly on the sensing head.

The double filament lamp (1) is potted into the lamp housing (2) which contains a lens set (3) for focusing the light onto a circular fiber optics pipe (4). The fiber optics are potted into a shell (5) which is separable from the head assembly. The single fiber optics pipe is divided into five equal diameter pipes (6). These pipes project the light onto a second set of lenses (7) which, in turn, focus the light through the coded disc (8) onto the detectors (9). The detectors are phototransistors. The use of phototransistors represents a change as compared to the decision to use solar cells as reported in the Eleventh Monthly Progress Report and is described in paragraph 4.2.7.3. The detectors and lamps are wired directly to the electronics module (10). All components are mounted to the head (11) which makes an integral package. The simple electronic circuit required for each phototransistor to supply one bit of data is shown in Figure 4-5. There are five of these circuits for each angle indicator head.

4.2.7.2 Position Sensing Accuracy

The position sensing accuracy of the angle indicator has been changed as follows: ±1° for angles from 0° to 4°, ±1.5° for angles from 4° to 20° and ± (10% +0.5°) from 20° to 45°. This accuracy was formerly ±1° from angles 0° to 10° and ±10% from 10° to 45°. This change was necessary because the disc itself is capable of only the original set of tolerances and the detector, due to its physical size, subtends an angle of 1°. Then, if it is assumed that initially it requires only 25% detector exposure to reach signal level, this would introduce an error which gives the accuracy stated above. If 50% detector exposure is required to reach signal level, the accuracy would be as before. This may in fact happen as the system degrades over the mission life; however, there is no practical way of predetermining when this degradation has taken place. It should be noted that this increase in error was based on using solar cells but it seems reasonable to expect a similar condition to exist with any detector that subtends a finite angular width unless the detector can be made to "fire" at exactly the same exposure under any changing environment and under systems degradation with mission life. When the evaluation of the engineering unit is complete, a more detailed approach to the error analysis will be possible. The greater sensitivity of the phototransistors should be helpful.

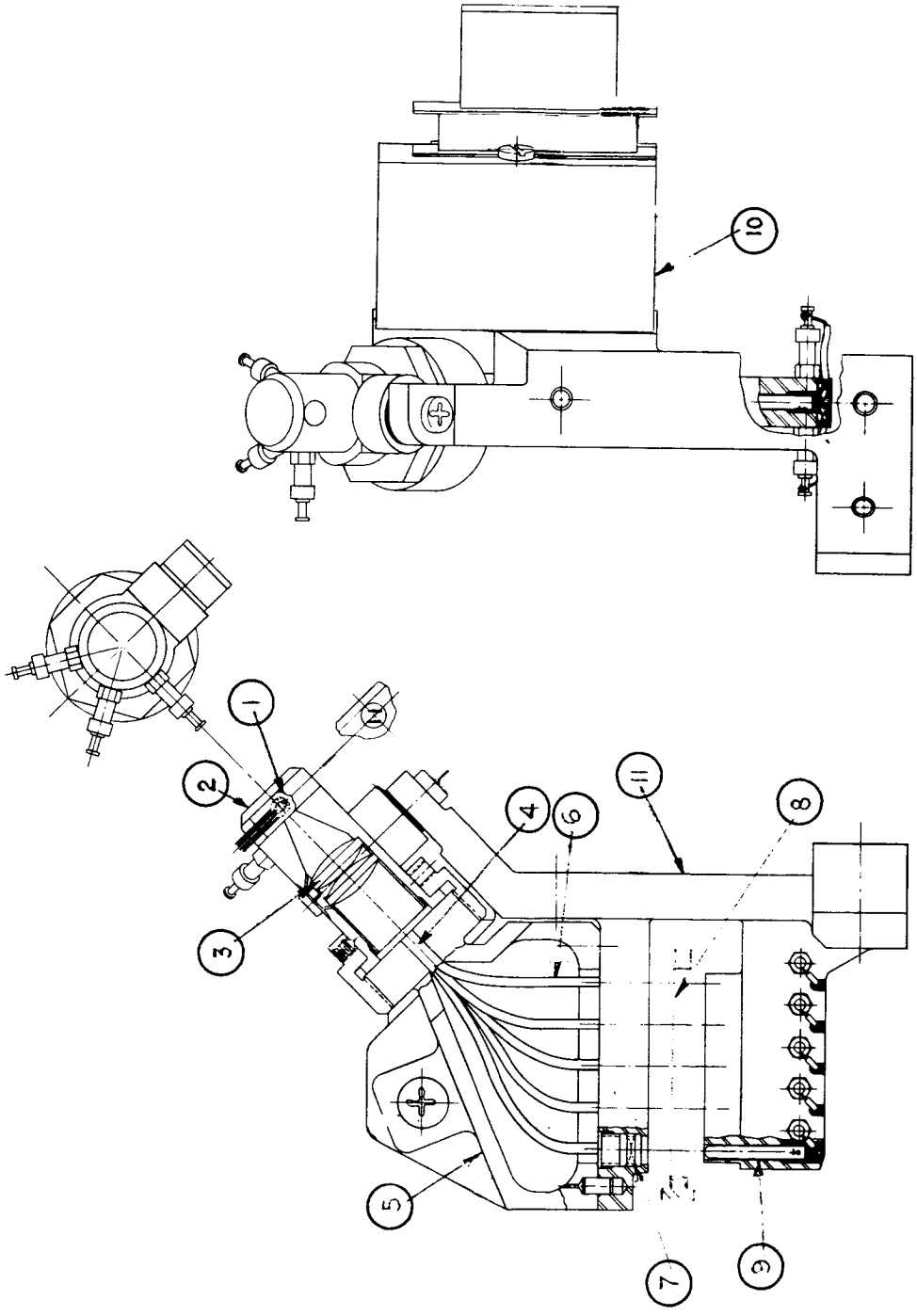

Figure 4-4. Angle Indicator Layout

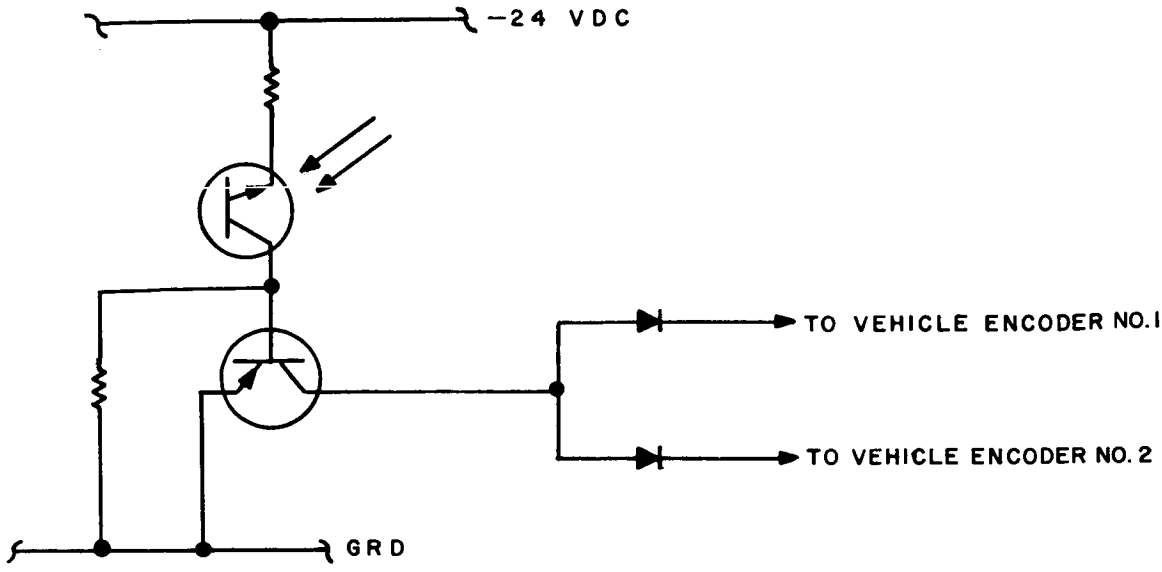

Figure 4-5. Typical Bit Circuit for the Angle Indicator

4.2.7.3 Detector Selection

Texas Instrument phototransistors type LS 443 (selected for low leakage currents) have been selected to replace the solar cells. Initially the phototransistor was investigated and put aside because of the lack of test data and field data; the reliability data showed reason for concern to use the device in the circuit then proposed which was to have the output go directly to the encoders without amplification. The failures described in this initial data were based on the light current falling below a level which was then intolerable. With the present circuits, lower light currents can be handled due to increased design margins. Also, the reliability information and the test reports presently available indicate that these devices are acceptable using the present design. For these reasons, it was initially felt that a different type detector should be investigated in parallel with the phototransistor investigations. Solar cells seemed to offer the best choice because of the large usage of these devices on space vehicles. Initial designs were based on information available for power cells and also vendor information. This information proved unsatisfactory when designing cells for use as low-level light sensors. It became evident that the type cell required was non-standard and would have to be developed and tailored to the specific needs of the system. The major problems encountered with the solar cells has been in the ratio of signal-to-noise. With the low level illumination available, the signal level is so low as to require extensive amplification which would result in increased weight and complexity of circuits. The narrow

anticipated margin of 5:1 between minimum light current (signal) to maximum leakage (noise) is so small as to reduce confidence in performance. The margin anticipated with the phototransistors is 200:1. Both of these ratios are worst case with allowance for temperature variations and degradation due to indication and light decrease due to life. It would be possible to increase the light current by using an individual lamp for each cell, but this is not feasible because the method would consume too much power and would be less reliable than the present scheme. Other light sources were investigated (neon and galium arsenide) but proved fruitless. Table 4-2 gives a comparison between the two detectors.

TABLE 4-2. ANGLE INDICATOR DETECTOR DATA

	Solar Cell	Photo Transistor
Max. Output at Min. Illumination	10 μa (est.)	400 μa (est.)
Output with 3-year estimated degradation	5 μa (est.)	200 μa (est.)
Leakage (Max.)	1 μa	1 μa
Margin (signal-to-noise)	5:1	200:1
Stages Amplification	4	1
Piece Parts/Head	100 (est.)	35
Weight	2 oz/head (est.)	1 oz/head (est.)
Availability	None	Stock Item
Performance Information Available	Must be Evaluated	Parameters

4.2.8 DYNAMIC MODEL

The dynamic model which is to be used for vehicle systems tests is to be designed to serve two basic purposes:

1. Use by HAC in their ATS systems vibration test
2. Use as a design adjunct by GE as follows:
   a. Provide data on dynamic integrity of the CPD by in-house testing in advance of such testing on Engineering Unit No. 1
   b. Data on CPD - Boom interface dynamic environment
   c. Data on Vehicle - CPD interface dynamic environment as the result of HAC tests.

To this end, the Dynamic Model will incorporate all parts from the engineering unit design which have a significant effect upon the dynamic response of the CPD. The parts to be used will be made from issued drawings in the same fashion as the engineering units. All parts will be inspected during manufacturing for dimensional accuracy. The mounting interface will remain exactly as designed for the engineering units. Cable connectors will also be located at the proper position to permit HAC to attach the electrical cables at the proper point.

Where new drawings are required, the simplest possible configurations will be utilized consistent with the intended use of this model. The information for all such new drawings has been generated and designing effort is scheduled to start early in July.

4.2.9 THERMAL MODEL

Engineering design has been completed and drawings have been issued for the CPD Thermal Model. The design objective in the Thermal Model was to obtain a simulation of the CPD heat transfer characteristics suitable for the overall ATS thermal testing, using modifications to the CPD design which would minimize the engineering and manufacturing costs, consistent with the intended use of the equipment.

The mounting interfaces with both the Boom Subsystem and the HAC vehicle were kept identical in the Thermal Model to the engineering units to ensure a good simulation of conductive heat transfer. In addition, the external parts of the CPD, which transfer thermal energy by radiation, will be identical to those of the engineering units.

Internally, the energy dissipated by the CPD in the normal orbital condition will be simulated by two resistors, which are mounted in the same thermal location as the two angle indicator heads (lamps and electronics modules) in the engineering units. The remaining internal elements of the CPD are thermally simulated by simple blocks of aluminum, designed with the same thermal inertias and transfer characteristics as the elements which they replace.

4.3 TEST EQUIPMENT

4.3.1 LOW ORDER FORCE FIXTURE (LOFF)

There has been no change in the status of the first Low Order Force Fixture (LOFF), and it has been in continuous use throughout this quarter for engineering development tests.

LOFF No. 2 has been completely assembled, tested, and calibrated. Data obtained, using a "standard" magnet and a sample of pyrolytic graphite, indicate that data obtained on LOFF No. 1 and LOFF No. 2 agree within the required accuracy ($\pm 1\%$) of the system. CPD and hysteresis damper adapting fixtures for performing LOFF tests will be designed and built during July.

4.3.2 DIPOLE MEASUREMENT FIXTURE

There is no change in status in the Dipole Fixture Helmholtz coils. The hysteresis damper Dipole Fixtures were designed and are presently in manufacturing. Dipole testing of this damper will begin in early July. CPD fixtures for Dipole testing are to be designed and manufactured in mid-July.

4.3.3 ADVANCED DAMPING TEST FIXTURE

The Advanced Damping Test Fixture (ADTF) has been completely assembled, including the structure, air bearing, torque measuring system, tachometer, and torquer electronics. Calibration runs have been completed in the eddy-current test modes, and the ADTF has been used to obtain engineering design data for the CPD eddy-current damper. Hysteresis damping tests will begin in mid-July on Engineering Unit No. 1 Hysteresis Damper. The adapting fixtures for this damper are presently being designed. The damping fixture design for the CPD will follow upon completion of these fixtures.

The change in basic concept of angle indicator design from an analog device to a digital device has necessitated a change in system test mechanization. The angle indicator which is included in the CPD was to be used during the damping tests to indicate the angle of the rotor. Since an analog signal is required for the X-Y plotter, the use of a ten-turn potentiometer driven from the rate table is being investigated.

4.3.4 TEST CONSOLE

The design of the instruments console for testing the CPD has been completed and is presently being assembled. Completion and checkout is scheduled for late July.

SECTION 5

ATTITUDE SENSOR SUBSYSTEM

5.1 SUBSYSTEM DESCRIPTION

The present electrical configuration of the ATS Gravity Gradient Stabilization System is shown in Figure 5-1. The principal change since the publication of the Third Quarterly Report is the complete redefinition of the Power Control Unit. The interconnections of most of the other components were affected by the PCU redesign and by better definition of their individual requirements. For example, the telemetry outputs of the angle indicator of the Combination Passive Damper now interface directly with the two Hughes Aircraft Company telemetry encoders rather than with the GE Power Control Unit. Better definition of the TV Camera lens and shutter has resulted in the establishment of a separate direct electrical cable between the TV-Camera control unit and the sun protection shutter mechanism. The implementation and connections of the Damper Boom squib and Eddy Current Damper squibs have also been revised.

Since the ATS Gravity Gradient System Electrical Block diagram is updated and published monthly in the GE Interface Reports, the latest electrical configuration can be obtained during the interim between the publication of Quarterly Progress Reports by consulting the Monthly Interface documents.

5.2 TV CAMERA SUBSYSTEM (TVCS)

5.2.1 SUBCONTRACT ACTIVITIES

A purchase order for ten operating TV Camera Subsystems and five non-operating models was placed with the Electronic Instrumentation Division of Lear Siegler, Incorporated on 23 April 1965. The contract specifies that the subsystems will meet all of the requirements of the TVCS Work Statement 9744-WS-001-C and the Component Specification, SVS-7310-C with the exception of paragraph 3.5.4.4, which specifies that the vendor shall out-gas and purge all operating TVCS units prior to shipment. Subsequent discussions with LSI/EID have resulted in two revisions of these documents, the major details of which are discussed in the following sections.

The prime contractor for the TV Camera Subsystem has in turn subcontracted the ruggedized vidicon to the Radio Corporation of America and the lens and shutter combination to the Wollensak Division of the Minnesota Mining and Manufacturing Company. Lear Siegler has designated the camera subsystem as LSI/EID Model 0431F, a modification of their missileborne Model 0431C Camera, which has flown successfully on at least two ECHO launches as early as 1962.

5.2.2 DESIGN ACTIVITIES

5.2.2.1 Calculation of Vent Hole Diameter

The TV camera and control units will be provided with a vent hole to allow the air inside the units to escape during launch. The ultimate pressure in the units will correspond to the near vacuum of its surroundings in the ATS orbits. One-hundred minutes after launching, the internal pressure must have fallen to a pressure too low to support corona. This pressure will be determined by tests on the engineering model but the present estimate is that $5X\ 10^{-5}$ mm Hg is sufficiently low.

In order for the internal pressure to fall to the assumed safe level, the diameter of the vent hole must be sufficient to allow the internal gases to be released to the outside. If the internal gases were simply air, a small hole would be adequate. However, there will be outgassing of the piece parts that constitute the camera system and this outgassing will occur at a slow rate, thereby prolonging the time needed for the pressure to drop to the desired level. The diameter of the vent hole is consequently determined by the desired level of internal pressure, the rate of outgassing, and the exposed surface area of the parts that contribute to outgassing. A nomogram, from which the size of vent opening can be determined if the quantities mentioned above are known, is shown in Figure 5-2.

At the present time, these quantities are estimated as follows.

	Camera	Control
Interior Surface Area, cm^2	750	1750
Outgassing Rate, mm liters/sec cm^2	$5x10^{-7}$	$5x10^{-7}$
Pressure, mm Hg	$5x10^{-5}$	$5x10^{-5}$
Vent Hole Size, cm^2	0.6	1.25

The values are arrived at as follows.

Internal area of camera cylinder = $a_1 = 20 \times 6\pi = 377\ cm^2$

Internal area of camera parts = $a_2 = a_1 = 377\ cm^2$

Total internal area of camera = $a_t = a_1 + a_2 = 750\ cm^2$

Internal area of control = $a_3 = (2x17x12) + (2x8x17) + (2x8x12) = 408+272+192=872 cm^2$

Internal area of control parts = $a_4 = a_3$

Total internal area of control $a_c = 1750\ cm^2$

Outgassing Rate, a_1 and $a_3 = 2 \times 10^{-7}$ mm liters/sec cm^2

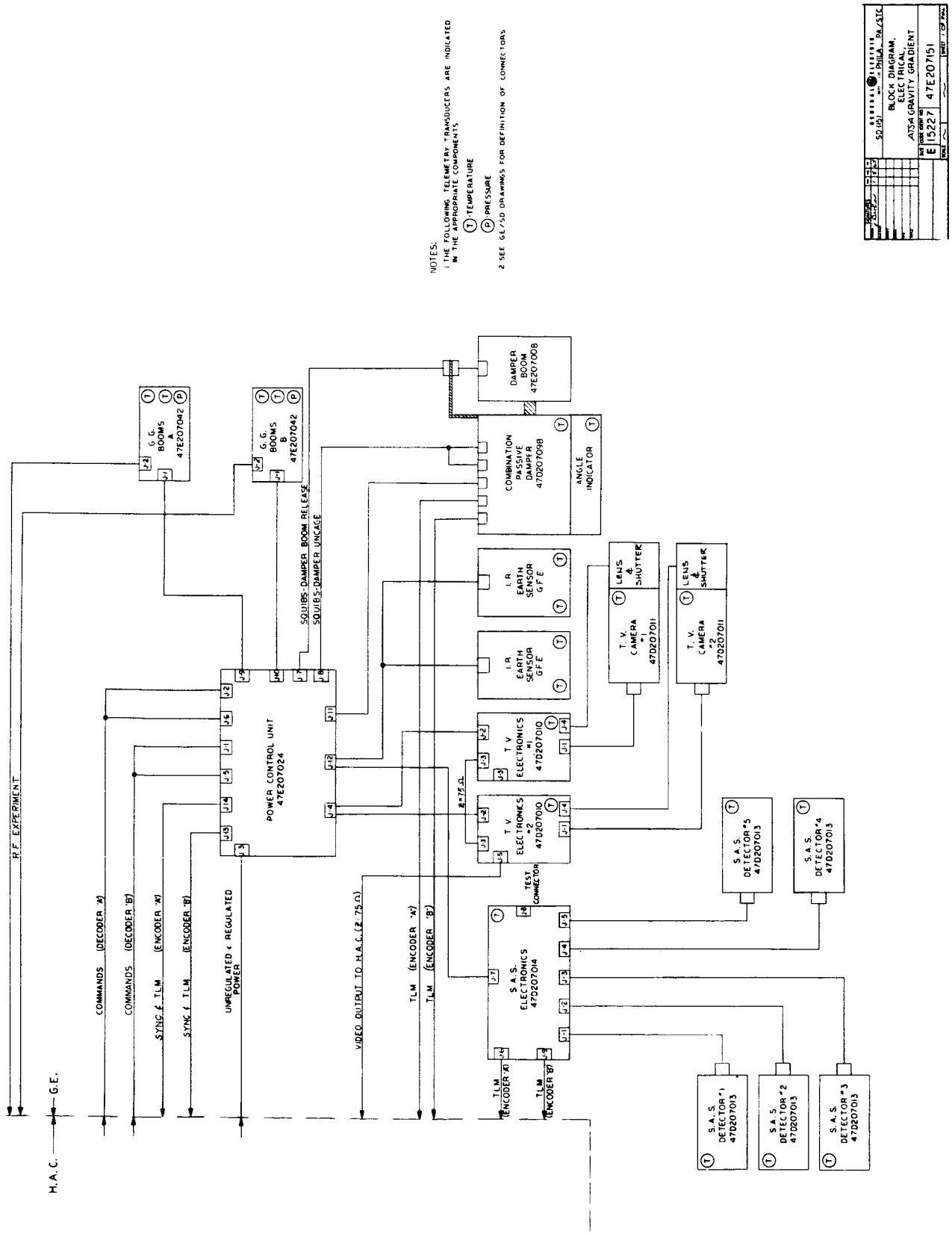

Figure 5-1. GE/HAC Electrical Interface (GE Dwg. 47E207151)

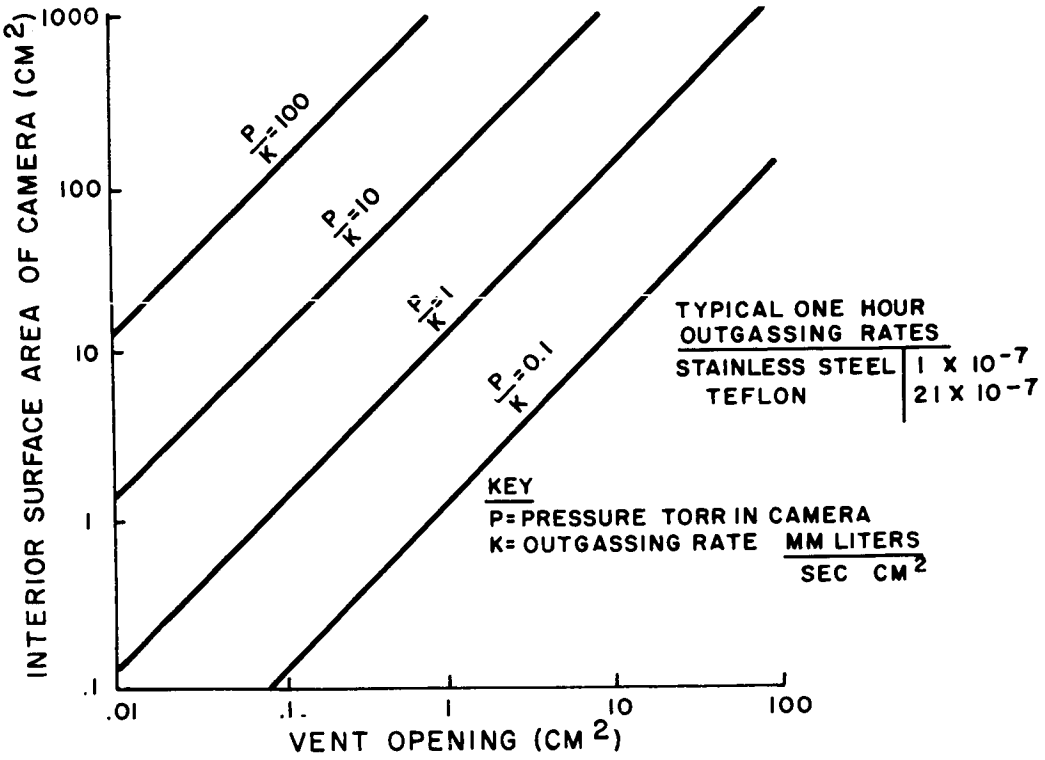

Figure 5-2. Nomogram of Vent Hole

Outgassing Rate, a_2 and a_4 = 8×10^{-7} mm liters/sec cm^2

Outgassing Rate, a_c and a_t = 5×10^{-7} mm liters/sec cm^2

With the estimated pressure of 5×10^{-5} mm Hg, the value of P/K for both units is 100. From the nomogram, the required vent areas for camera and control at P/K = 100 and ordinates of 750 and 1750 cm^2 are approximately 0.6 and 1.25 cm^2 respectively. These correspond to diameters of 0.344 and 0.496 inch respectively, leading to standard sizes of 3/8 and 1/2 inch diameter. However, due to space limitations on the rear of the Camera, the total venting area required will be obtained by using four or five holes tapped for No. 10-32 screws.

5.2.2.2 Bandwidth Limitations

As discussed in section 2.4.2.1.1 of the Third Quarterly Report, the 8 mc/s video output available from the standard camera electronics will be limited to 3.5 mc/s by a low pass filter. One result of this artificial limitation of the video bandwidth is that the 1 mil reticle graduations originally specified for the vidicon retina would be very poorly reproduced. Consequently, the graduation line width was respecified to be 3 mils, which results in the index marks being approximately equal to the space between marks.

Tests were conducted at LSI/EID to determine if the video lines of both TV Cameras on ATS-A could be permanently electrically connected in order to eliminate the video relay in the Power Control Unit. It was determined that this connection can be made as long as the signal grounds of the two TV systems are at the same potential and there is no desire to operate the two cameras simultaneously. The interconnection will be made at the 8 mc/s video points allowing the utilization of one 3.5 mc/s low pass filter by both cameras. The 8 mc/s video output connection also will permit better testing of the true resolution capability of the camera systems.

5.2.2.3 Mounting Provisions

It was established that the mounting arrangement for the TV Camera will consist of two D-brackets, one at each end of the cylindrical case. This configuration will permit a three point mounting interface in a plane parallel to the longitudinal, the z - axis of the camera. Rotational adjustment may be accomplished by loosening the clamp screws in the D-brackets. The mounting provisions for both the camera unit and control unit are shown in the 12th Monthly Interface Report.

The new vibration levels specified by NASA/GSFC during this quarter can be satisfactorily encountered with the two bracket mounting arrangement described above.

5.2.3 EARTH SIMULATION TESTS

An attempt was made to obtain photographs of the TV monitor which would show the terminator on a three-foot scale model globe, using actual sunlight as the illumination source. The results were unsatisfactory, however, due to haze and ground reflections.

Further tests were performed indoors using both incandescent and xenon-light sources and a 60-inch parabolic mirror as the collimating device. Two of the pictures obtained with a Polaroid camera are shown in Figure 5-3. Since these photographs are more satisfactory, additional pictures will be taken using a 35 mm camera, so that the accuracy and repeatability of the film reading process may be determined.

5.3 POWER CONTROL UNIT

A photograph of the wooden mockup of the Power Control Unit is shown in Figure 5-4. It may be noted that the fourteen electrical connectors occur in six distinct rows which result from the direct incorporation of the connectors as part of the six printed circuit boards internal to the unit.

5.3.1 MECHANICAL DESIGN

The mechanical layout of the Power Control Unit was completely redesigned this quarter in order to reduce the weight from an estimated 18 pounds to 10.75 pounds or less. At present all drawings have been released for production of the engineering, thermal and

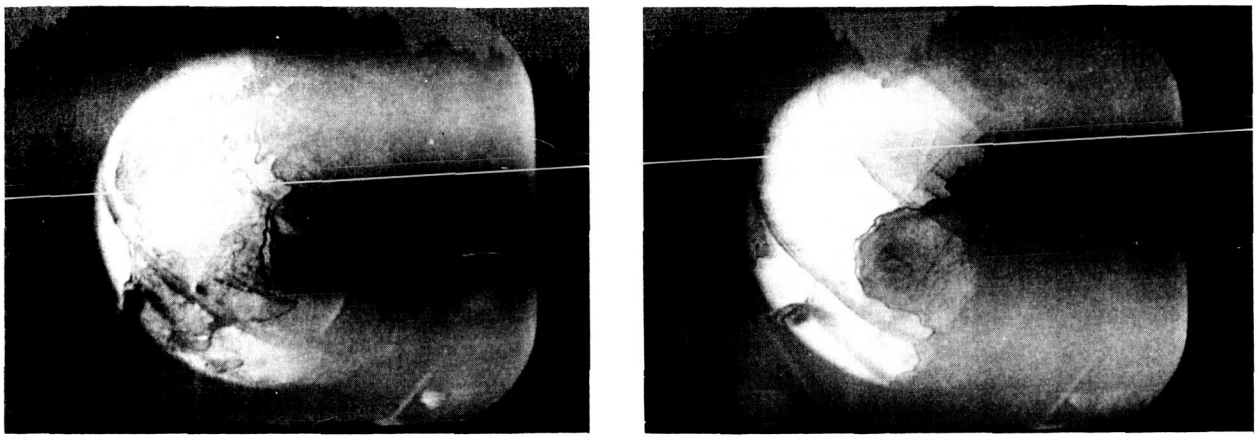

Figure 5-3. Earth Simulation Test Pictures

structural models. The printed circuit boards have been received from the vendor, Melpar Company, and approximately 85% of the required modules have been potted and post-pot tested.

Both stress and thermal analyses have been performed on the new PCU design. In order to be conservative, the entire box will be filled with foam after the completion of all electrical tests to hold the printed circuit loads rigid during the vibration and acceleration environments.

5.3.2 ELECTRICAL DESIGN

The electrical design of the PCU was considerably simplified in order to reduce the weight to the goal established by NASA/GSFC. The functions eliminated from the PCU were:

- Motor Speed Control
- Separation Timer and Automatic Boom Stops
- Boom Motor Current Sensors and AC Power Supply
- Video Relay and Automatic Alternator
- Bridge Resistors for Temperature Detectors

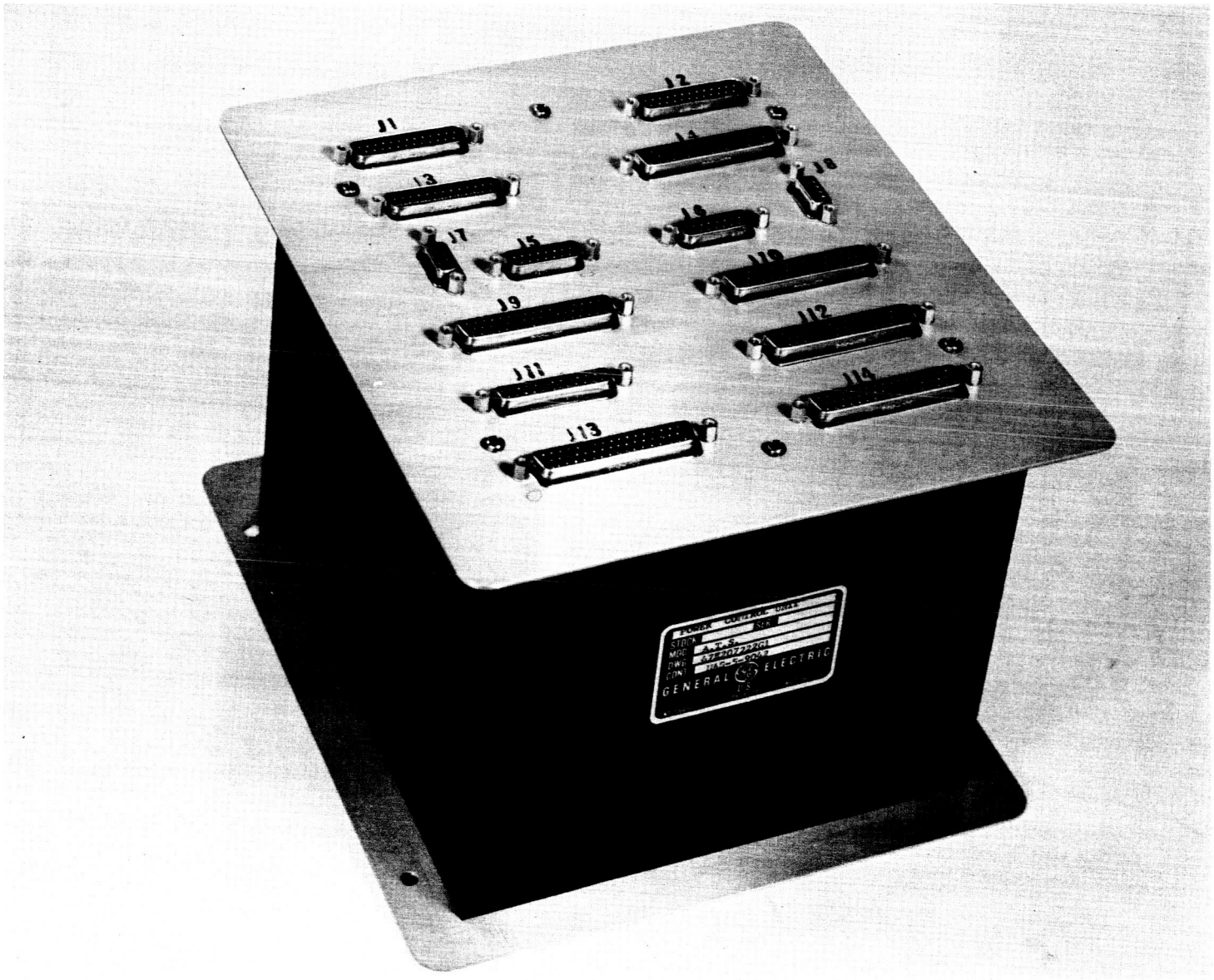

Figure 5-4. PCU Mockup

- Pulsed Power Regulator for Damper Solenoid
- Minus Six Volt Regulated Power Supply

The remaining functions of the Power Control Unit are:

1. Power Switching to:
   - TV Camera subsystem
   - Solar aspect sensor and angle indicator
   - IR earth sensor
   - Angle indicator redundant lamps
   - Extension and scissor motors.
2. Squib firing to:
   - Damper booms
   - Eddy current damper and damper boom shaft
3. Solenoid switching to:
   - Damper clutch
   - Primary boom assembly A clutch
   - Primary boom assembly B clutch.
4. Telemetry synchronization pulse to SAS.
5. Emergency power reset.
6. Ground return distribution.
7. Telemetry analog signal paralleling.
8. Event channel Digital to Analog networks.
9. Digital monitor paralleling and isolation.
10. Power supply for damper angle indicator lamps.
11. Telemetry reference voltage power supply.
12. Telemetry voltage monitors.

The design and support efforts for the report period were concentrated in the following areas:

- Detailed analysis of circuits to determine the design margins.
- Redesign of the motor field driver circuit to meet function requirements.
- Support of the mechanical packaging design effort.
- Redrafting of the component specification.
- Reworking of the component breadboard and the Engineering Test Rack.
- Testing of the module assemblies to be used in the Engineering Unit.

5.3.2.1 Circuit Analysis

Calculations on the basic circuits used in the Power Control Unit were performed in order to establish that they will perform satisfactorily when subjected to parameter degradations dictated by the temperature environment, and the radiation and life requirements of SVS-7325-C ("Standard Parts, Materials and Processes, Use of"). In addition, design margins on the gain and leakage currents of semiconductors were determined. As a result of these analyses, a few resistor values will be changed in the prototype unit to increase the design margins.

5.3.2.2 Motor Field Driver

The schematic of the Motor Field Driver is shown in Figure 5-5.

It is a transistorized bipolar switch which is a modification of the previous design in that it eliminates a series diode in the power switch path and thus reduces the saturation voltage across the field winding to bring it within the limits required by the primary boom motors. The resistor values of R1 and R3 are tailored to either the extension or the scissoring motor since the former presents a lower impedance with its parallel brake winding.

5.3.2.3 Support Activities

The major portion of the engineering activity this quarter was directed toward specification writing, test planning and testing, reconstruction of the breadboard and test rack, checking of drawings, and the general activities required to produce a developmental piece of hardware and prepare for its testing.

Since the breadboard rework required considerable time to incorporate major design requirements changes, breadboard testing on a component level has been restricted. However, individual circuit testing and analysis have verified adequate design margins. Further confidence in the design will be established by the extensive testing of the engineering model, to be performed during the next reporting quarter.

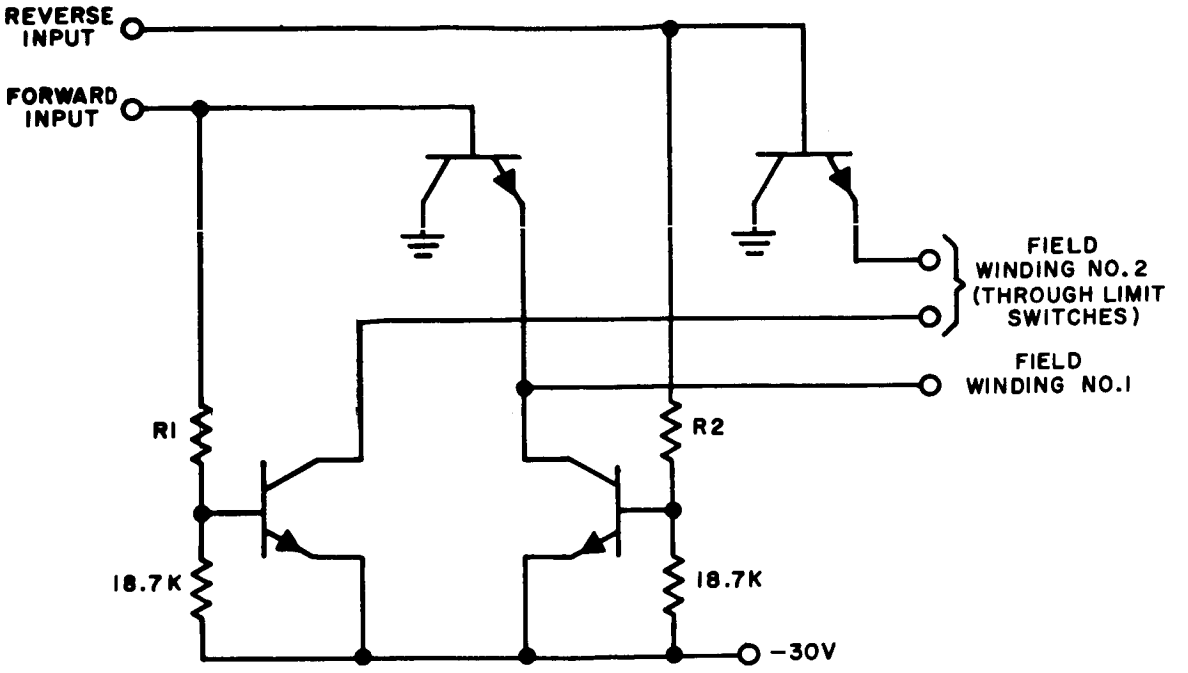

Figure 5-5. Motor Field Driver Schematic

5.4 SOLAR ASPECT SENSOR

5.4.1 DETECTOR - ELECTRONICS INTERFACE INVESTIGATION

The accuracy of the Solar Aspect Sensor is determined by the accuracy of the transition edges. The transition edges are those points where the current through the AGC amplifier matches the current through the 16-bit amplifiers. The slope of the analog output of the bit cells, however, is only 15 μa/degree at the edge of the field of view, so that the sensor is extremely sensitive to small variations in input current.

Therefore, it is necessary that the input characteristics of the amplifiers are closely matched and that the solar cells are able to develop the necessary voltage range at a constant current output throughout the temperature range. Tests were performed to measure both the amplifiers and the solar cells.

The amplifiers were tested by measuring the voltage across a constant current source. This voltage varied from 40 mv to 48 mv for the 16-bit amplifiers and from 52 mv to 60 mv for the 5 AGC amplifiers at a current of 50 μa. The detector cells, therefore, have to develop 40 mv to 60 mv across the amplifier at essentially constant current output.

Available solar cells were measured at 85^{o}C which is the highest temperature expected. The measurements showed that the cell characteristics degraded at the high temperature

such that the variation in the amplifiers caused a mismatch of bit-cell output to AGC-cell output of 5-10 μa at the edge of the field of view.

The ideal performance of a solar cell can be characterized by the following equivalent circuit.

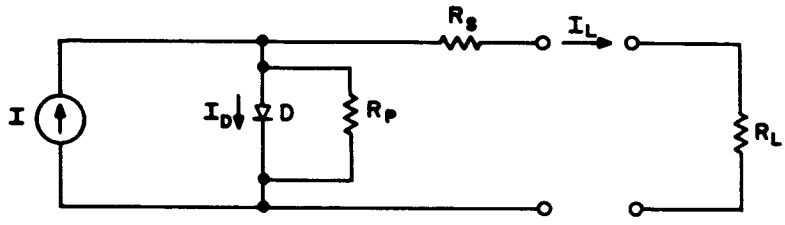

where I is a current generator

D is an ideal diode

R_P is the leakage across the diode

R_S is a negligible series resistance

The current into a load R_L is then (R_S is negligible)

$$I_L = I_{sc} - I_D$$

where I_{sc} is the short-circuit current of the solar cell. The performance of the cell is then established once the saturation current of the diode, I_s, and the value of R_P are known, since I_{sc} is a function of the incident light and

$$I_D = I_S \left(e^{\frac{9v}{kT}} - 1 \right) + \frac{V}{R_P} .$$

The performance of the semiconductor diode, therefore, becomes the limiting factor in the performance of the cell at high temperatures.

$$I_S \approx K \; e^{-Wg/kT}$$

where K = Constant

Wg = Energy gap of silicon = 1.1 ev

k = Boltsmann's constant = 8.6×10^{-5} e v/deg

T = Absolute temperature

Therefore:

$$\frac{I_{S\ 85^oC}}{I_{S\ 25^oC}} \approx 10^3$$

at 50 mv then,

$$I_{D\ 25^oC} = 6.1\ I_{S\ 25^oC} + \frac{0.050}{R_P}$$

$$I_{D\ 85^oC} = 4.2 \times 10^3\ I_{S\ 25^oC} + \frac{0.050}{R_P}$$

The saturation-current density is

$$j_s = \frac{q\ D_p\ p_m}{L_p} + \frac{q\ D_n n_p}{L_n}$$

where q = electronic change = 1.6×10^{-19} coulombs

D_p = diffusion constant for holes = 6.5 cm^2/sec

D_n = diffusion constant for electrons = 31 cm^2/sec

L_p = diffusion length for holes = 0.06 cm

L_n = diffusion length for electrons = 0.1 cm

p_n = minority hole concentration

n_p = minority electron concentration

$n_n = \sigma_n / q\ \mu_n$, $P_p = \sigma_p / q\ \mu_p$

$$p_n = \frac{n_i^2}{n_n}$$

$$n_p = \frac{P_i^2}{P_p},\ n_i = P_i = \frac{\sigma_i}{q\ (\mu_n + \mu_p)}$$

n_i = intrinsic electron concentration

P_i = intrinsic hole concentration

σ_n = conductivity of the n-region = 1 $(\text{ohm-cm})^{-1}$

σ_p = conductivity of the p-region = 0.1 $(\text{ohm-cm})^{-1}$

μp = mobility of holes = 250 $cm^2/V\text{-sec}$

μn = mobility of electrons = 1200 $cm^2/V\text{-sec}$

σ_i = Intrinsic conductivity = $(63,600)^{-1}$

Then

$$j_s = \frac{1.6\times10^{-19} \times 6.5 \times 8.8 \times 10^5}{.06}$$

$$+ \frac{1.6 \times 10^{-19} \times 31 \times 1.8 \times 10^6}{0.1}$$

$$= 1.0 \times 10^{-10} \text{ amp/cm}^2$$

The junction area is 0.228 cm x 2.21 cm = 0.506 cm^2

Therefore,

$$I_S \approx 5 \times 10^{-11} \text{ amp}$$

for typical doping levels.

Figure 5-6 shows the diode characteristic and the solar cell V-I curve assuming very leaky surfaces (R_p = 31K). Also shown is a typical cell characteristic as measured.

To resolve the discrepancy between the predicted and actual behavior of the solar cells the following is planned: Verification of the manufacturing process which is not available at present, more refined measurement of typical solar cells, verification of the equivalent circuit.

5.4.2 SUBCONTRACT ACTIVITIES

A summary of the present status of the subcontract to the Adcole Corporation for the Solar Aspect Sensor is as follows:

The engineering model electronics unit is complete and has successfully passed all functional, temperature, and environmental tests to qualification levels.

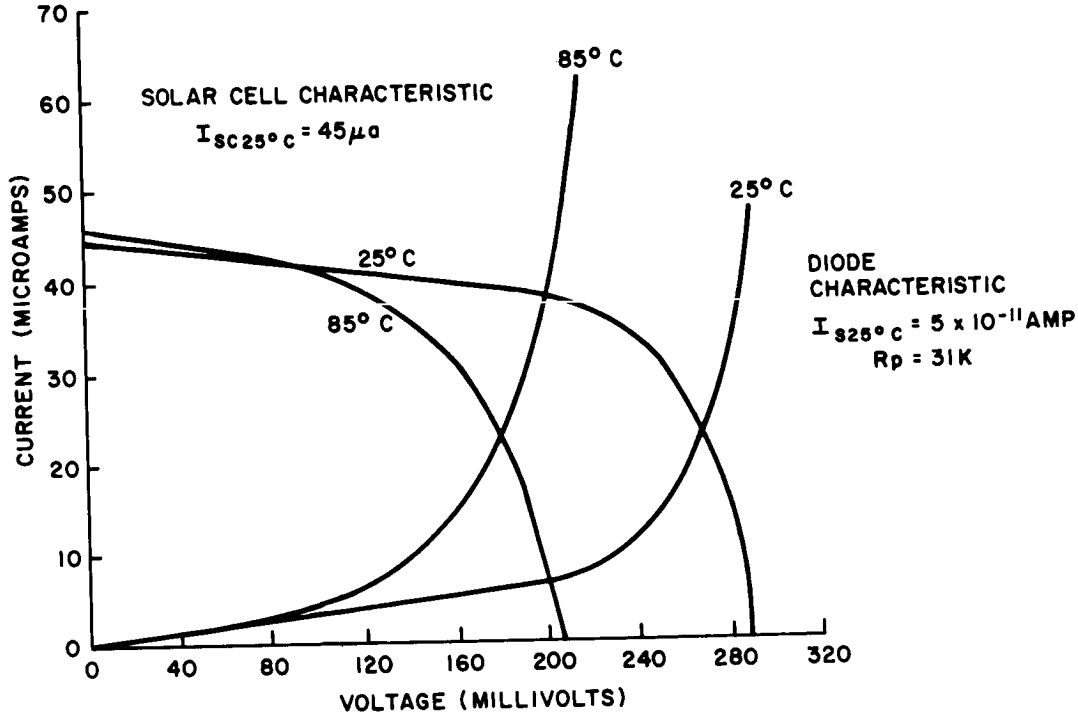

Figure 5-6. Typical Cell Characteristics

One pre-engineering model detector unit was assembled using solar cells which meet their specifications at room temperature but not at the high temperature limit of 85°C. Vibration tests on this unit resulted in no visual degradation but electrical tests were inconclusive due to improper alignment of test equipment during pre-vibration calibration testing.

All mechanical parts for the five detectors have been received at Adcole. Solar cell assemblies are being manufactured by Hoffman.

The test equipment is complete and final check-out is in progress.

The wooden mockup has been received at GE. The dynamic and thermal models are on schedule.

SECTION 6

QUALITY CONTROL

6.1 QUALITY CONTROL ENGINEERING

6.1.1 TV CAMERA SUBSYSTEM

The quality control requirements of NPC 200-3 and Standing Instruction 217,260 were discussed in detail with Lear Sigler, Inc. (the TV camera subcontractor) during negotiations held at General Electric. The requirements were reviewed item by item with their QC representative and complete documented agreement was reached.

A test requirements document was prepared to define the test equipment that will be required for testing the TVCS at GE.

The camera and control units are to be vented just before launch to decrease the external pressure to a value below the corona critical range by the time the TVCS is first turned on in orbit. Current plans for venting and testing for corona are documented in PIR 4323-FM-098, "Testing and Prevention of Corona in the ATS Television Camera Subsystem."

A rough draft of the QC test plan for the TV-Camera was circulated to cognizant personnel for their Comments.

6.1.2 BOOM SUBSYSTEM

The rough draft of the component test plan was generated. The plans include components for the development, prototype, and flight units.

Damper boom interface tooling was reviewed with Manufacturing and Engineering representatives and accepted by QC Engineering.

6.1.3 SOLAR ASPECT SENSOR

Detailed quality requirements for the wood mockup, thermal model, and dynamic model were generated.

The Adcole Corporation Inspection/Test Instruction for the SAS Engineering Unit was prepared by their Quality Assurance Manager and forwarded to GE for review. Their test equipment was reviewed in detail by Quality Control Engineering.

Adcole has taken action on items previously found discrepant on a GE vendor survey and presently meets the requirements of NPC 200-3.

The SAS functional test plan is approximately 80% complete. The plan describes those tests that will be performed at GE.

6.1.4 COMBINATION PASSIVE DAMPER

The TRW Inc. proposal for fabrication of the Passive Hysteresis Damper (PHD) was reviewed and negotiated for compliance to QC requirements. A document, "Exceptions to NASA Quality Publication NPC 200-2," was generated between TRW Inc. and GE and forms an integral part of the contract.

A document defining the in-house inspection activity pertaining to the CPD Engineering Units was issued as PIR 4323-FM-088.

The CPD Quality Control Plan was issued.

The design review on the PHD held at TRW Inc. was attended by the Quality Control Engineer; the results are summarized in a Trip Report, No. 4323-FM-033.

A decision was reached between GE and the Defense Contract Administration Service Office representative to delegate Material Review Board activities to TRW Inc. for any item of the Passive Hysteresis Damper not directly affected by GE source control drawings or specifications.

6.1.5 POWER CONTROL UNIT

A test requirement document (TR 11012) for the test cables and fixtures was issued.

6.1.6 PARTS PROGRAM

The solenoid specification for the CPD and the transformer specification for the SAS were reviewed and quality control requirements incorporated.

PIR 4323-FM-060 was issued defining the color code system to be used to identify piece parts for Engineering, Prototype or Flight according to SVS 7325 and applicable parts specifications.

Basic ground rules were established for incorporating quality control requirements into the parts specifications for ATS.

The basic parts qualification program was established and the plan was documented.

6.1.7 GENERAL

A complete review of the GE exceptions to NPC 200-2 was held with the NASA Quality Assurance Representative. The result was "Exhibit B" of the NAS 5-9042 contract.

The Magnetic Test Facility was partially evaluated and indications thus far indicate dipole testing appears feasible at this GE facility. A gross check of a SAS transformer was made.

Major ATS vendors were contacted to determine the effect on cost and schedule of making NPC 200-4 (requirements of hand soldering) part of the contract. Additional cost and schedule slippage could be expected although some of these vendors are implementing the document on their own with no extra cost to GE.

6.2 TEST EQUIPMENT ENGINEERING

6.2.1 SOLAR ASPECT SENSOR

The functional electrical test console is approximately 80% fabricated. The solar simulator fabrication is also about 80% complete. Test cables have been completed. The two-axis table and associated fixtures are about 70% complete and must be installed and checked out. Fabrication of the alignment fixture was started. The vibration and acceleration fixtures are complete.

6.2.2 COMBINATION PASSIVE DAMPER

The vibration and acceleration fixtures are being fabricated as well as the thermal vacuum fixture. The LOFF and ATDF are operational. The thermal control box for the LOFF and ATDF is about 70% complete for the basic engineering design. Inspection gages and fixtures for the CPD detail parts have been started. Design of the angle detector test fixtures is started.

6.2.3 POWER CONTROL UNIT

Engineering test consoles are available for testing the modules and the PCU box. Modifications are presently being made. The temperature and thermal-vacuum test cables are being fabricated.

The vibration and acceleration fixtures are being fabricated in addition to the T-V feedthrough.

6.2.4 TV CAMERA SUBSYSTEM

Design has begun on the console and fixtures.

6.2.5 BOOM SUBSYSTEM

A facility to house the 150-foot test track is being set up. The track sections have been fabricated and are ready for assembly. One section will require modification to accept the "cable catcher."

Holding fixtures for the primary and secondary booms have been designed and fabrication was started.

The acceleration fixture has been designed for testing at an outside laboratory because the capability to test does not exist in-house. Compatability with vendor equipment was verified.

The test dolly to be used for boom deployment tests has been completed at deHavilland and accepted by GE.

Fabrication of the electrical console is approximately 80% complete but it will require some modifications based on latest definition.

The scissor calibration interface was resolved at deHavilland and test equipment design effort is starting.

6.2.6 GENERAL

Schedules for all pieces of test equipment are being maintained.

6.3 INSPECTION AND TEST

6.3.1 SOLAR ASPECT SENSOR

Trips were made by vendor surveillance personnel to perform a vendor capability survey and follow up on the corrective actions with Adcole Corporation. In addition, the specific quality requirements of the Purchase Order were discussed with their Quality Assurance Manager. Some particular requirements for GE inspections have been identified.

6.3.2 PARTS PROGRAM

Several parts vendors with whom GE has placed orders were contacted concerning the quality requirements. A survey was conducted at National Semiconductor and several other vendor contacts are planned. Because of the HAC specification, GE cover sheets and the data requirements, an early evaluation of vendor capabilities will be made.

6.3.3 TV CAMERA SUBSYSTEM

Vendor quality requirements were incorporated into the Purchase Order for the TVCS and a visit was made to Lear-Siegler for a discussion of these requirements. Subsequent visits were made to Lear-Siegler to perform a quality capability survey, discuss the TV camera specification and work statement, and the vendor's quality control plan.

6.3.4 POWER CONTROL UNIT

Quality Control inspection planning was generated for the fabrication of modules within the PCU. QC requirements were placed on the Purchase Orders for parts and Receiving Inspections performed on the engineering parts that have been delivered.

Melpar was selected as the vendor for circuit boards based on their past quality performance. A quality representative visited this vendor to explain in detail GE's requirements for printed circuit boards.

6.3.5 COMBINATION PASSIVE DAMPER

Inspection planning has been provided on many of the detail parts of the CPD that have been released for the engineering units.

Vendor surveys were made in order to select the solenoid vendor. Koontz-Wagner was chosen based on a letter of justification prepared jointly by Engineering and Quality Control.

It was determined that vendor surveillance should be provided on a number of angle detector parts and Chicago Miniature Lamp Co. was visited.

A vendor survey was made at Holex, Inc. who will supply the explosive devices for the CPD. Holex meets the requirements of NPC 200-3.

The work statement and SI 217,260 were discussed with TRW Inc. during a vendor survey of their facilities. Proposed MRB delegation was also discussed. (See para. 6.1.4). TRW appeared to meet the quality requirements; they have assigned a QC Project Manager to the Passive Hysteresis Damper. Subsequent trips were made to review their QC activity and witness the final testing of Engineering Unit No. 1.

6.3.6 BOOM SUBSYSTEM

Vendor surveillance was provided at deHavilland during fabrication of the test track.

A trip was made to Conax with the deHavilland Quality Control Superintendent. Conax supplies the bolt cutter to deHavilland for which GE is responsible to qualify. Trip Report 4323-RM-018 details the findings that Conax meets the requirements of NPC 200-3. The bolt cutters will be manufactured concurrently for both GE and deHavilland.

During this period, there has been heavy vendor surveillance activity at deHavilland by the assigned GE representative. Discussions were held on the application of NPC 200-3 to deHavilland suppliers, the dynamic and thermal model configuration was reviewed, along with the basic specification and work statement. Environmental fixture

and test equipment requirements were reviewed. The deHavilland QC and Inspection/ Test Plans were discussed as well as the particular problems of the test dolly, which has been accepted by GE. The initial deployment testing was witnessed on Engineering Unit No. 1. Audits of the deHavilland quality system were performed in addition to specific drawing dimension verification by vendor surveillance personnel.

6.3.7 GENERAL

In addition to hardware inspection, the inspection planning and subsequent inspection of test equipment and fixturing was provided during fabrication.

6.4 MATERIALS AND PROCESSES

6.4.1 SOLAR ASPECT SENSOR

A possible materials problem was identified concerning the silver and fish glue spalling or cracking off of the slit on the reticle. This condition was evaluated by testing a reticle under the worst temperature conditions, conducting ultraviolet and thermal-vacuum tests. The coating appeared to be stable throughout the testing - PIR 4374-0029.

The Adcole bonding of solar cells and submodules was reviewed and their process adequately considers the problems of high coefficient of thermal expansion.

Zn O white paint, Vitavor PV-100 and Pyromark Standard white were considered for thermal control coatings for the SAS.

The approved materials list was updated as a result of the review of the Adcole materials.

6.4.2 BOOM SUBSYSTEM

Several small scale tests were conducted on samples of BeCu rod material to determine the feasibility of a thermal bending test to verify the math model. It was determined that a test must be performed in a vacuum and not in air. The major problem area with a test of this nature is instrumentation of the rod with thermocouples to adequately measure the temperature gradient. PIR 4375-043.

Four suggested motor lubricants were evaluated by testing in the laboratory.

A plan has been implemented for evaluating the silver tarnish on the gravity gradient rods by periodically measuring α over a span of several months.

Boom materials compatability was reviewed on a first-look basis via a deHavilland visit. PIR 4375-039 lists all of the materials presently utilized.

Micrometeorite simulation tests were started. Velocities varied and additional measurements of the setup are required prior to actual bombardment of the test specimen.

6.4.3 TV CAMERA SUBSYSTEM

A process specification was written for the materials and processes utilized in formulating the TV tip targets. The targets consist of vapor deposited aluminum plus a SiO_2 or Al_2O_3 overcoat on Lexan covered on the other side by quartz microspheres PIR 4375-031.

Resin Bonded Solid Film Lubricant MoS_2 per MIL-L-25504A was recommended by GE for the sun shutter mechanism.

6.4.4 COMBINATION PASSIVE DAMPER

PIR 4374-0039 gives recommended procedures for electro-depositing gold on type 304 stainless steel and aluminum alloys to increase reflectivity. PIR 4374-0042 describes a procedure for coating magnets with a flexible epoxy resin.

A sample of Buna S Rubber was machined to simulate the impact absorbers and tested to determine the load vs compression curve, impact damage after 300 impacts, and the dimensions of the deformed piece.

The thermal properties of aluminum alloys and surface coatings which can be applied on the alloys are discussed in PIR 4375-032.

The use of magnesium alloy is acceptable if the recommended service temperature is not exceeded per PIR 4375-031.

Belleville washers were heat treated and tensile tests were run. Suspension wire plugs were fabricated. TV targets were coated during the period to satisfy production requirements for the engineering units.

Galvanic corrosion tests are being performed on various combinations of CPD materials and dissimilar metals problem between 304 SS and 2024 Al hard anodized was evaluated.

A method was suggested for obtaining the torsional restraint via iron carbonyl.

SECTION 7

MANUFACTURING

During this period the full scale manufacturing cycle has been stated for the fabrication of the thermal, dynamic and engineering hardware. Work is also progressing on the component test equipment, component test fixtures and the system test equipment.

Although there has been a slight slip in schedule on the engineering units the thermal and dynamic units are progressing per schedule.

In the area of magnetic particle contamination control during the manufacturing cycle of the Combination Passive Damper, the detailed procedures are complete. These procedures have been documented in the Manufacturing Standing Instruction MSI-236924.

Tooling for control of the mechanical interface between the damper and damper boom is complete. Interface tooling requirements for the damper/satellite mechanical interface is presently in process.

8. RELIABILITY, AND PARTS & STANDARDS

8.1 RELIABILITY

Reliability activity during the quarter is summarized as follows:

1. Participated in design reviews for the Passive Hysteresis Damper, lamps for the Angle Indicator, Boom Subsystem, TV Camera System, and the Power Control Unit.
2. Reapportioned the reliability goals for components in the Gravity Gradient Stabilization System. This effort was based on a better definition of system configuration and duty cycle than existed at the time of the original apportionment, which was published in the First Quarterly Progress Report. The revised reliability goals for a one-year and three-year mission were published in Table 7-1 of the Eleventh Monthly Progress Report.
3. Definitions were established for the component review boards and their procedures (ITPB, FARB).
4. Redefined the Parts Qualification Program.
5. Prepared a formal Reliability Program Plan for ATS. The plan will be used as the controlling document to govern the execution of the reliability tasks. The plan also includes sections on Parts and Standards.

Analyses were completed for the Solar Aspect Sensor and the Passive Hysteresis Damper. The Solar Aspect Sensor is being fabricated by the Adcole Corporation and the Passive Hysteresis Damper is under subcontract to TRW Inc., formerly STL.

8.1.1 SOLAR ASPECT SENSOR

The basic analysis was performed by the vendor in accordance with provisions of GE TRA 873-74, and was reviewed by the Reliability Engineering operation of the GE Spacecraft Department. A summary of the Reliability Analysis is shown in Table 8-1.

$$\lambda = 4.5671 \times 10^{-5} \text{ failure/hour}$$

$$t = 27{,}000 \text{ hours} \times 50\% \text{ duty cycle} = 13{,}500 \text{ hours}$$

$$R = e^{-\lambda t} = e^{-4.5671 \times 10^{-5} \times 13{,}500} = e^{-.6166}$$

$$R = .5398$$

TABLE 8-1. SUMMARY OF SAS RELIABILITY ANALYSIS

Element	Number per System	Element Failure	Total Failure
Power Supply	1	0.1088	0.1088
Output Circuit	38	0.0017	redundant, insignificant
Parallel Output Register	1	0.1414	0.1414
Decode and Select	5	0.0248	0.1240
AGC	1	0.1225	0.1225
Bit Register	16	0.0299	0.4784
Switch Driver	5	0.0064	0.0320
Bit Switch	80	0.0037	0.2960
Solar Cell	80	0.0383	3.0640
Reticle	15	0.0200	0.2000
TOTAL FAILURE RATE			4.5671

This figure includes all failures, whether catastrophic or degrading. The reliability block diagram for the Solar Aspect Sensor is shown in Figure 8-1 together with a description of the effect of any element failure.

8.1.1.1 SAS Catastrophic and Degradation Failures

Table 8-2 lists the element groups, the effect of single part failure within the group, and the probabilities of occurrences of such failures for the Solar Aspect Sensor.

8.1.1.2 SAS Failure Modes

The following list and Table 8-3 include the possible modes in which the Solar Aspect Sensor could fail, and the effect on the component if a specific failure should occcur:

1. A failure in the power supply, parallel output register or the AGC circuits will cause catastrophic failure of the SAS function.
2. A failure in the decode and select, switch driver, or reticle circuits will disable one sensor and cause mission failure if that sensor is in or moves into the duty sector (i.e., toward the sun). Since (nominally) only one of the five sensors is used at one time, the average mission time of each sensor and its associated circuits is equal to one-fifth of the total mission time.

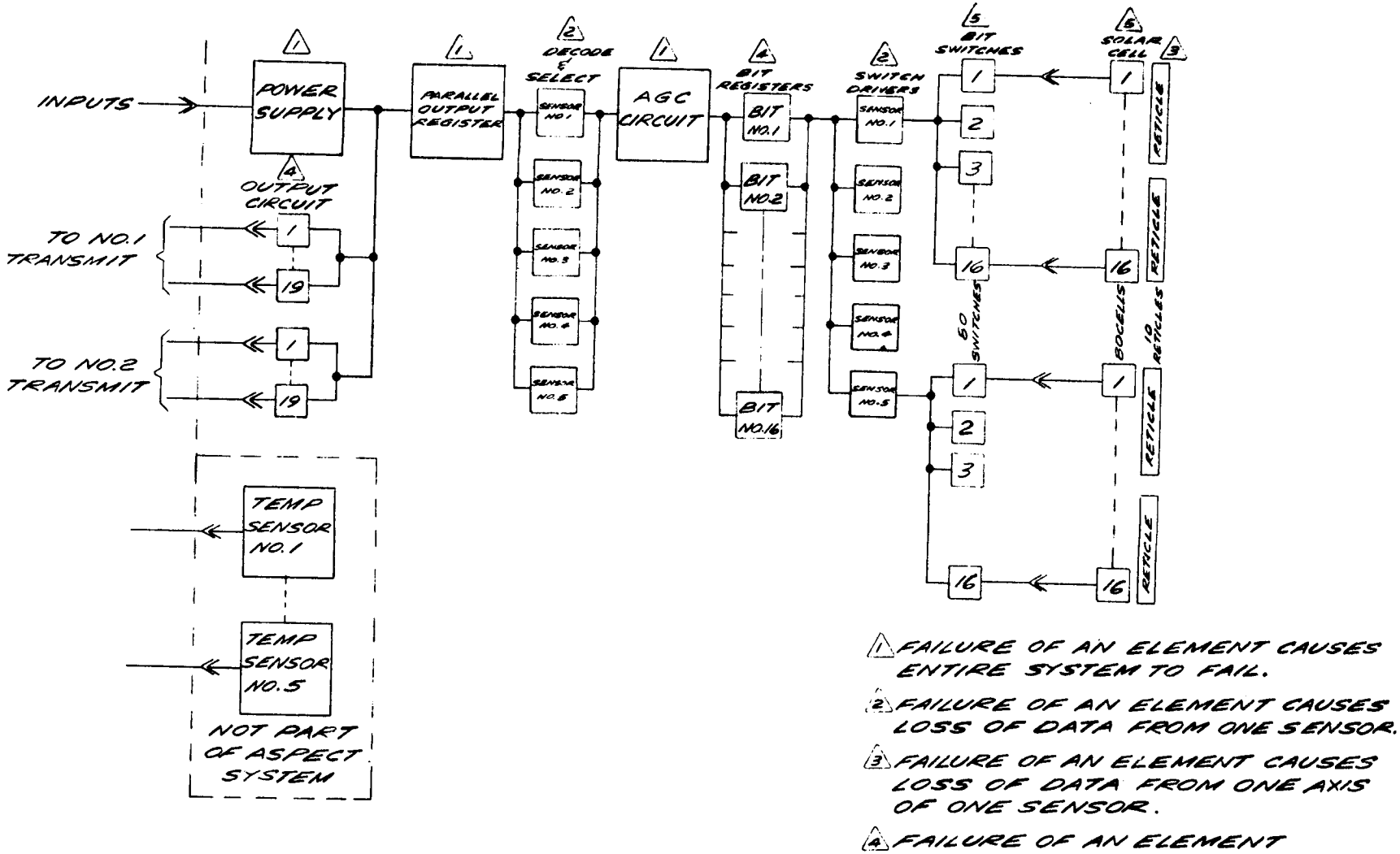

Figure 8-1. Solar Aspect Sensor Reliability Block Diagram

TABLE 8-2. FUNCTIONAL FAILURE EFFECTS ANALYSIS — SOLAR ASPECT SENSOR

Element Group (Single Failure)	Effects of Failure	Probability of Occurrence
Power Supply Parallel Output Register, or AGC	Complete failure of solar aspect sensor function.	.04906
Decode and Select, Switch Driver, or Reticle	Loss of both axes; one sensor. Degradation depends upon sun aspect with relation to sensor disabled.	.04696
Bit Registers	Loss of one bit of one axis of all five sensors. Degradation depends upon significance of bit lost: Dual ambiguity of 1/2° for loss of least significant bit, and 1/2° to 120° for loss of most significant bit.	.06256
Bit Switch or Solar Cell	Loss of one bit of one axis of one sensor. Degradation of the axis depends upon significance of bit lost (see above), and sun aspect with relation to sensor involved.	.36466
All Elements (Total Risk)	Any of the above effects, depending upon location of failure part.	.4602

TABLE 8-3. POSSIBLE FAILURE AND DEGRADATION EFFECTS FOR SAS

Effect	Cause*	Failure Probability	Reliability
Complete Failure	1	.04906	.95094
Loss of "Duty" Sensor	2	.00955	.99045
Loss of One Bit From All Sensors	3	.06256	.93744
Loss of One Bit From "Duty" Sensor	4	.08668	.91332
TOTAL PROBABILITY ANY FAILURE	ANY OF ABOVE	.19366	.80634

*Refer to Items 1 through 4 of the preceding list.

3. A failure in the bit register circuits would cause loss of a bit of information from all of the five sensors.

   The effect of a lost bit will result in a 50% chance of mis-reading the angle, since the lost bit will constantly read as either a "0" or a "1". No knowledge of the malfunction will exist, except as may be indicated by inconsistency of consecutive readings, especially when passing from the range of view of one sensor into another.

   Loss of the least significant bit will degrade the resolution in that plane to one degree. This failure may be noted after a few observations.

   Loss of the most significant bit will cause the "mirror image" of the angle to be read (in 50% of the cases).

4. A failure in the bit switches or solar cells will cause loss of one bit if the sensor is active. The average mission time for these circuits is equal to one-fifth of the mission time, as with the other sensor circuits cited in Item 2.

Table 8-3 lists the possible failure and degradation effects and their probabilities of occurrence. The reliabilities (probabilities of failures not occurring) are also listed.

8.1.2 PASSIVE HYSTERESIS DAMPER

The Preliminary Reliability Program Plan and the Preliminary Reliability Design Analysis were received from the subcontractor for the Passive Hysteresis Damper, TRW Inc. A review of these documents is presented in the following paragraphs. A more detailed discussion of the TRW method and the possible application to other ATS subassemblies will accompany the final analysis of the PHD, presently scheduled to be included in the Fifth Quarterly report.

The TRW analysis indicates that the PHD will be capable of meeting its apportioned reliability goal of 0.95 for a three-year mission. A preliminary prediction of 0.99 was obtained. A Failure Mode/Effects Analysis is also included (based for the most part of a previous analysis of a similar unit for COMSAT). Failure to uncage is shown to be the most likely mode, followed by failure of the end flexures. Reliability of the torsion wires is listed as quite high, but the method of calculation does not take fatigue into consideration.

8.1.2.1 Method of Reliability Prediction

The prediction method used by TRW is an adaptation of interference theory — briefly, the assumption is made that strengths and loads are normally distributed, the reliability of a structure is calculated as the probability that its strength will not be exceeded by a service load. Due to the use of expressions without derivation, and to some typographical errors, TRW's approach is not clear from a review of their analysis. A presentation of the method in general terms is therefore attached, along with a sample page of the TRW report. Several sources were consulted in the preparation of the attached presentation (see list of references, para. 8.1.3.1.5), none of which cover this method in its present form — it is hoped that consolidation of these various approaches under one system of nomenclature here will prove helpful.

8.1.2.2 Comments on Method of Reliability Prediction

The prediction method employed by TRW is mathematically valid, but has several drawbacks in its application. (1) No provision is presently included for time varying loads (leading to fatigue failure); (2) the method obviously requires a detailed knowledge of the structure and its service environment — more detailed than is probably presently available; and (3) as used by TRW, the method requires that terms such as Factor of Safety and Margin of Safety be employed with the same precise mathematical definition by all persons submitting inputs to the analysis.

8.1.2.3 Other Comments

It is anticipated that future revisions of TRW's analysis of the PHD will include some consideration of the following.

1. Fatigue or creep of torsion wire – possibility and effect of boost-induced null offset.
2. Effect of clutch induced shock.
3. Long term stability of magnetic properties.
4. Possibility and effect of magnetic particle contamination
5. Possibility and effect of gas/particle discharge from squib(s).

8.1.2.4 Structural Reliability Prediction

Structural reliability is defined here as the probability that service loads will not exceed the maximum stress that a material can withstand in a given structural configuration.

Let S be the structural strength and L the loading applied in service. The reliability R is then

$$R = P\ \{S > L\}$$

Assume that S and L are independent random variables with normal* probability density functions f(s) and $g(\ell)$, and with means μ_S, μ_L, and standard deviations δ_S, δ_L, respectively:

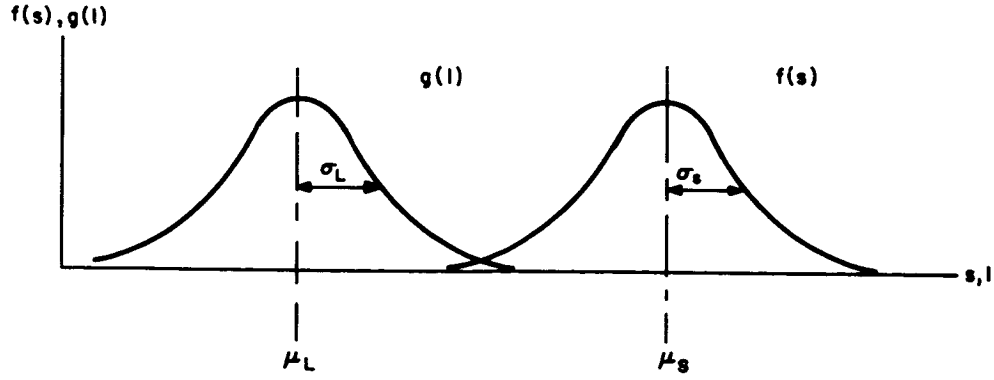

*This assumption theoretically allows negative values of S and L to occur; In the usual situation ($\mu_S \gg 0$), however, this may be ignored. >>

Now we can define the reserve strength, ρ :

$$\rho = S - L$$

And we can redefine the reliability

$$R = P\{\rho > 0\}$$

We know from Reference 1 (para. 8.1.2.5) that ρ also has a normal P.D.F., with mean

$$\mu_\rho = \mu_S - \mu_L$$

and with standard deviation

$$\delta_\rho = \sqrt{\delta_S^2 + \delta_L^2}$$

Hence

$$R = P\{\rho > 0\} = \frac{1}{\delta_\rho \sqrt{2\pi}} \int_0^\infty \epsilon^{-\frac{1}{2}\left(\frac{\rho - \mu_\rho}{\delta_\rho}\right)^2} \, d\rho \qquad (1)$$

From Equation 1 we have

$$R = \frac{1}{\delta_\rho \sqrt{2\pi}} \int_0^\infty \epsilon^{-\frac{1}{2}\left(\frac{\rho - \mu_\rho}{\delta_\rho}\right)^2} \, d\rho$$

Now let

$$z = \frac{\rho - \mu_\rho}{\delta_\rho} \qquad \text{and} \qquad dz = \frac{d\rho}{\delta_\rho}$$

Note that at $\rho = 0$ and at $\rho = \infty$

$$z = -\frac{\mu_\rho}{\delta_\rho} \qquad z = \infty$$

Substituting:

$$R = \frac{1}{\sqrt{2\pi}} \int_{-\frac{\mu\rho}{\delta\rho}}^{\infty} \epsilon^{-\frac{z^2}{2}} \, dz$$

and finally

$$R = \frac{1}{\sqrt{2\pi}} \int_{-\infty}^{z'} \epsilon^{-\frac{z^2}{2}} \, dz, \quad z' = \frac{\mu\rho}{\delta\rho} = \frac{\mu_S - \mu_L}{\sqrt{\delta_S^2 + \delta_L^2}} \qquad (2)$$

With z' known, the value of this integral may be obtained from published tables, Reference 2 of para. 8.1.2.5.

This method may be carried further, to enable prediction of structural reliability from a knowledge of the factor of safety F_S and the Margin of Safety M_S. These terms are related (Reference 3 of para. 8.1.2.5) as follows:

$$M_S = \frac{\text{Ultimate Strength of Member}}{\text{Applied (or max probable) Load x } F_S} - 1$$

Which may be written (Reference 4) as:

$$F_S \, (M_S + 1) = \frac{\text{Allowable Stress}}{\text{Applied Stress}}$$

In the expression

$$F_S \, (M_S + 1) = \frac{\text{Allowable Stress}}{\text{Applied Stress}} \, ,$$

"Allowable Stress" is normally taken as some value $n\,\delta_S$ below the useable strength of the material, and the "Applied Stress" is conservatively taken as some value $m\,\delta_L$ above the expected load. Thus we have

$$F_S \, (M_S + 1) = \frac{\mu_S - n\,\delta_S}{\mu_L + m\,\delta_L}$$

We will return to this expression.

From Equation 2 we have

$$z' = \frac{\mu_\rho}{\delta_\rho} = \frac{\mu_S - \mu_L}{\sqrt{\delta_S^2 + \delta_L^2}} .$$

Dividing numerator and denominator by μ_L

$$z' = \frac{\frac{\mu_S}{\mu_L} - 1}{\sqrt{\frac{\delta_S^2}{\mu_L^2} + \frac{\delta_L^2}{\mu_L^2}}} ,$$

and multiplying the first term in the denominator by $\left(\frac{\mu_S}{\mu_S}\right)^2 = 1$, we obtain

$$z' = \frac{\frac{\mu_L}{\mu_L} - 1}{\sqrt{\left(\frac{\delta_S}{\mu_S}\right)^2 \left(\frac{\mu_S}{\mu_L}\right)^2 + \left(\frac{\delta_L}{\mu_L}\right)^2}} .$$

Note that

$\frac{\delta_S}{\mu_S} = V_S$, the strength coefficient of variation

and $\frac{\delta_L}{\mu_L} = V_L$, the load coefficient of variation

Thus we now have

$$z' = \frac{\frac{\mu_S}{\mu_L} - 1}{\sqrt{\left(V_S\right)^2 \left(\frac{\mu_S}{\mu_L}\right)^2 + \left(V_L\right)^2}} \qquad (3)$$

To obtain the quantity $\frac{\mu_S}{\mu_L}$, we return to the expression on equation 3 relating F_S and M_S:

$$F_S\ (M_S + 1) = \frac{\mu_S - n\,\delta_S}{\mu_L + m\,\delta_L}$$

$$= \frac{\mu_S\ (1 - n\,\frac{\delta_S}{\mu_S})}{\mu_L\ (1 + m\,\frac{\delta_L}{\mu_L})} \qquad (4)$$

$$= \left(\frac{\mu_S}{\mu_L}\right)\left(\frac{1 - n\,V_S}{1 + m\,V_L}\right)$$

Whence

$$\frac{\mu_S}{\mu_L} = F_S\ (M_S + 1)\left(\frac{1 + m\,V_L}{1 - n\,V_S}\right)$$

Finally we have

$$R = \frac{1}{\sqrt{2\pi}} \int_{-\infty}^{z'} \epsilon^{-\frac{z^2}{2}}\, dz$$

where

$$z' = \frac{\frac{\mu_S}{\mu_L} - 1}{\sqrt{\left(V_S\right)^2 \left(\frac{\mu_S}{\mu_L}\right)^2 + \left(V_L\right)^2}} \qquad (5)$$

and

$$\frac{\mu_S}{\mu_L} = F_S\ (M_S + 1)\left(\frac{1 + m\,V_L}{1 - n\,V_S}\right)$$

with

F_s = Factor of Safety

M_s = Margin of Safety

V_L = Load Coefficient of Variation

V_s = Strength Coefficient of Variation

n, m = Multipliers of the Strength and Load Standard Deviations, respectively.

8.1.2.5 Numbered References:

1. Hoel: Introduction of Mathematical Statistics, Wiley 1962

2. Volk: Applied Statistics for Engineers, McGraw-Hill 1958

3. Roark: Formulas for Stress and Strain, McGraw-Hill 1954

4. TRW: Preliminary PHD Reliability Analysis

8.1.2.6 Additional References:

a) Lloyd and Lipow: Reliability: Management, Methods and Mathematics, Prentice-Hall 1962

b) Koelle: Handbook of Astronautical Engineering, McGraw-Hill 1961

c) Abraham: Structural Design of Missiles and Spacecraft, McGraw-Hill 1962

d) Lipson, et al: Engineering for Reliability, University of Michigan, 1962

e) Dick and Wilson: Structural Reliability - The General Engineering Design Approach, Proc 11th Nat. Symp. Rel. and QC 1965

8.1.2.7 Torsional Restraint Wire Test

Testing requirements have been defined for the wire lots to be used by TRW to meet torsional and flexure loads in the passive hysteresis damper suspension system. To have a reasonable confidence in the strength of the suspension/ torsional restraint wire, a sufficient sample size of wire should be tested. As a

minimum reliability requirement, at least 15 to 50 cumulative mission cycles should be demonstrated, with the oscillatory motion run between ±5° for 90% of the cycles and between ±45° for 10% of the cycles. Tension in the wire during tests must be essentially the same as in the worst case mission constraint. The damping oscillations of the PHD for one mission as defined in paragraph 3.3.6 of Specification SVS-7331 are 5000 cycles/3 years for the ATS-A and 1250 cycles/3 years for the ATS-D/E. Table 8-4 shows the demonstrated reliability at various confidence levels which can be achieved by testing from 1 to 50 missions with zero failures. TRW has been requested to demonstrate the capability of the suspension/torsional restraint wire to withstand the torsional end flexure which may occur in the ATS mission.

TABLE 8-4. DEMONSTRATED RELIABILITY AT VARIOUS CONFIDENCE LEVELS

Missions Demonstrated	Reliability Demonstrated at % Confidence Levels, "0" Failures, x^2 Distribution		
	50	90	95
1	0.50	0.10	0.05
2	0.70	0.31	0.22
3	0.79	0.46	0.36
4	0.84	0.56	0.47
5	0.87	0.63	0.54
6	0.89	0.68	0.60
7	0.90	0.72	0.65
8	0.91	0.75	0.68
9	0.92	0.77	0.71
10	0.93	0.79	0.74
* 15	0.95	0.85	0.81
20	0.96	0.89	0.86
25	0.97	0.91	0.88
50	0.98	0.95	0.94

*Minimum recommended for demonstrated tests

A second reliability analysis will be forthcoming from TRW incorporating the results of recent changes, including:

1. Change to 3.5 dynes/cm wire
2. Deletion of entire caging mechanism
3. Removal of connector and switches resulting from the deletion of the caging mechanism
4. Change in interface drawing 47-207083-1, which affected the clutch face mounting.

8.1.3 TV CAMERA SUBSYSTEM

At the design review on June 4, 1965, Lear Siegler representatives agreed to the following conditions for the conduct of the life test on the engineering model of the TV camera system:

1. The life test plan will be sent to GE in one month. Testing will begin within two weeks of issuance of test plan. The testing period will encompass 52 weeks.
2. The camera system will undergo launch environment tests prior to life tests; (shock, vibration).
3. Thermal vacuum testing will be conducted with the camera system operating and instrumented* to detect hot spots. The thermal vacuum tests will be run until the camera system temperatures stabilize at or about the specified mission temperature.
4. The camera system will be removed from the thermal-vacuum chamber and bench tested at ambient temperature under consecutive cyclic operating conditions of one hour operating and two hours off for the remainder of the 52 week period or until 2500 consecutive hours of failure-free operation has occurred.
5. GE shall be kept informed of the life test program through monthly reports and failure reports.

8.1.4 POWER CONTROL UNIT

The interface of the PCU with HAC equipment and other GE equipment is being analyzed to determine if any critical areas exist regarding power or signal requirements for all ATS mission functions. Dual Pin connections vs. Single pin connections

*Instrumentation will be placed at the locations determined to be most susceptible to hot spots by thermal analyses of the camera system.

in the interface connectors of the PCU and Boom Subsystem is being determined for its reliability gain vs. harness complexity, weight, and failure probability during the testing cycle.

8.2 PARTS AND STANDARDS

8.2.1 INTRODUCTION

A summary of activities by Engineering Standards during the quarter is listed below:

1. Parts selection.
2. Parts application analysis and review.
3. Generation of parts drawings.
4. Selection of sources.
5. Resolution of procurement problems.
6. Review of subcontractor's parts lists.
7. Updating approved Parts Lists.
8. Generation of individual qualification plans.
9. Ordering of parts for qualification.
10. Initiation of qualification testing.
11. Computer programming for degradation analysis.
12. Initiation of computer processing of parts data received.

These tasks are continuing, and the most significant items of progress are reported in the following paragraphs.

8.2.2 PARTS, DRAWINGS, AND PARTS LISTS

8.2.2.1 Discussion

Parts selection has been mostly completed, consistent with the status of the electrical and mechanical design of the various components. In isolated cases, additional parts will be introduced to meet design requirements. As each new part is identified, a procurement drawing is prepared and released, and is

entered on the approved Parts List, 490L106. Parts which have been added during the quarter are:

Drawing Number	Description
R2313	Relay, Latching
R4609	Transistor, High Frequency
R4610	Transformer, Inverter
R4611	Solar Cell Assembly
R4612	Two-way Solenoid
R4613	Transistor, Power
171A8324	Metal Film Resistor
47C207076	Sensor, Surface Temperature
47C207184	Thermistor Probe Assembly

The preparation of parts drawings has included a definition of the requirements of the parts, identification of the selected and approved part vendor, definition of the procedures for qualification testing and acceptance testing, and the assignment of burn-in and extended power aging procedures and requirements, as applicable. The appearance of new parts requires an examination of the qualification status, which is based on the established qualification criteria, and may result in revisions to the list of parts to be qualified. As parts are identified as "no longer used", they are deleted from the approved parts list and from the qualification plan.

8.2.2.2 Angle Indication Head Assembly

The assembly is made up of the following items:

1. One Lamp
2. One Fiber Optics Assembly
3. Twelve Lenses
4. Five Phototransistors
5. One Electronic Module - contains about 30 parts; attaches to the head assembly.

The lamp and the phototransistors represented the major part selection and specification effort by Engineering Standards in the Angle Indicator Head Assembly. Procurement documents for these parts are in process.

8.2.2.2.1 Lamp

A survey of sources for the lamp has resulted in the selection of the Chicago Miniature Lamp Company as the supplier. Each lamp contains two identical rhenium-tungsten filaments. One filament is to be used as back-up for the other. If the filament in use were to fail, power will be switched to the other filament. As specified by the procurement drawing, each lamp will be screened for visual and mechanical inspection, electrical performance measurements, vibration, and burn-in. At present, five lamps have been placed on life test by the vendor who is burning both filaments at the rated voltage and plans to continue until burn-out.

8.2.2.2.2 Phototransistor

The phototransistor used in the Angle Indicator Head Assembly is an NPN silicon surface passivated device which is processed in a manner similar to that used to fabricate conventional transistors that have a successful history of reliability and long-term stability. The principal difference between these devices and conventional transistors are: the package is a hard-glass, hermetically sealed case that is approximately 1/2 inch long by 0.082 inch in diameter, and the phototransistor is activated by light energy instead of electrical energy. The silicon wafer, which measures 0.25 inch by 0.30 inch, is placed directly under the lens in the end of the package for maximum use of the sensitive area.

A survey of the semiconductor industry for photoelectric devices resulted in the selection of Texas Instrument as the supplier. This device has been in continuous production for about the past three years. Available test data from the vendor and reports from users indicate that the device has the reliability and long-term stability that is required for the application. Parts supplied for the ATS program will be initially selected from manufactured lots by the vendors for specified output current levels. The procurement specification will include Group B Acceptance Inspection and the 1500-hour screening test followed by degradation analysis - consistent with Hughes Aircraft Company procedures for electronic parts.

8.2.2.3 Damper Clutch Solenoid (Two-Way Solenoid)

The solenoid for the Combination Passive Damper is specified by GE drawing R4612. Preliminary designs were submitted by two subcontractors, G. W. Lisk Co. and Koontz-Wagner. Vendor surveys were performed on both sources, and an order for qualification, engineering, prototype, and flight hardware was placed with Koontz-Wagner. A further order was placed with that vendor to perform the qualification testing per GE drawing R4612.

8.2.2.4 Solar Cell Assembly

GE, in conjunction with the subcontractor for the Solar Aspect Sensor (Adcole Corporation) has had difficulty in finding a suitable and capable source for the solar cell assembly. Two vendors who are presently building the assembly are Hoffman and Edgerton, Germeshausen, and Grier. The assembly is specified by GE drawing R4611 which incorporates the Adcole Specification 8182.

8.2.2.5 Component Parts Lists

Parts lists representing current designs have been received for the following components:

Component	Designer
Solar Aspect Sensor	Adcole Corp.
Power Control Unit	GE

These parts lists are being surveyed for conformance to proper part callout and use of approved parts. Non-approved parts are being identified and evaluated for acceptability, documentation, and qualification. When completely accepted and documented, the parts will be added to the approved Parts List, 490L106.

8.2.3 PARTS QUALIFICATION

8.2.3.1 Qualification Program

The Parts Qualification Program has been updated to include minor revisions. The present plan is outlined in Tables 8-5 and 8-6. Table 8-5 lists the parts assigned to Group A, which contain the parts and assemblies that are to be subjected to qualification testing per the applicable specifications. Table 8-6 lists the parts assigned to Group B, which contain the parts for which a favorable history of reliability already exists. The latter group is to be subjected to tear-down and analysis for evaluation of design features, workmanship, and identification of risk characteristics.

Changes that have been made in the program from that previously published are identified below.

TABLE 8-5. GROUP A - PARTS REQUIRING QUALIFICATION

Item	Part	Part No.	Vendor	Component	Quantity	Where Tested
1	Transformer, Inverter	R4610	Edgerton	SAS	5	GE-SD
2	Solar Cell Assembly	R4611	Hoffman Edgerton	SAS	5	Adcole
3	Damper Clutch (Two-Way) Solenoid	R4612	Koontz-Wagner	CPD	5	GE-SD
4	Angle Indicator Head Assembly	47E207350	GE-SD	CPD	5	GE-SD
5	Cable Cutter	(115C7516 895D724)	Holex	CPD	20	Holex
6	Bolt Cutter	5325-L4 (deHavilland)	Conax	Booms	18	—
7	Pressure Transducer	—	C.I.C.	Booms	5	—
8	Potentiometer, Scissoring	TSPR10K(2)L2	Helipot	Booms	5	—
9	Potentiometer, Extension	T223R10K(1)L2	Helipot	Booms	5	—
10	Limit, Switch, Extension	2HM1-3	Minn. Honey.	Booms	10	—
11	Limit Switch, Scissoring	6HM1-1	Minn. Honey.	Booms	10	—
12	Motor, Boom Drive	—	Globe Ind.	Booms	15	—
13	Motors, Scissoring	—	Globe Ind.	Booms	15	—
14	Sealed Drive Unit	—	deHavilland	Booms	2	GE-SD

TABLE 8-6. GROUP B - PARTS FOR TEAR-DOWN AND ANALYSIS

Item	Part	Vendor	Component	Number to Be Purchased
1	Transistor	TI 2N2432	SAS	5
2	Transformer	Tresco	PCU	5
3	Transformer	Raytheon	PCU	5
4	Relay	R2313	PCU	5
5	Temp. Sensors	—	All	5
6	Thermistor	Fenwal	Booms	5
7	Solenoid, Rotary	Ledex	Booms	5
8	Switch - 1HM1	M.H.	Booms	5
9	Switch - 12SM4T	M.H.	Booms	5
10	Bellows	—	Booms	5
11	Capacitor	Sprague	Booms	5
12	Connector	Cannon DEM	Booms	5
13	Connector	Cannon DCM	Booms	5
14	Connector	Cannon DBH	Booms	5

8.2.3.1.1 Additions to Group A.

1. The Holex Cable Cutter (Item 5 of Table 8-5) has been added to the qualification program. This part is now used in the Combination Passive Damper to release the damper boom shaft, the eddy-current damper, and the solenoid.
2. The Angle Indicator Head Assembly (Item 4 of Table 8-5) has been added to qualify the parts, the materials, and the structure of the assembly. See 8.2.3.2.2.

8.2.3.1.2 Changes in Group A.

1. The DBH Cannon connector has been removed from Group A and placed in Group B because of available data.
2. The solar cell and the lamp that are used in the Angle Indicator Head Assembly have been replaced by the complete assembly (Item 4 of Table 8-5). See paragraph 8.2.3.2.2.

3. A reduction in the number of specimens to be tested was implemented to conform with the changes in the Parts and Standards program as of April, 1965.

8.2.3.1.3 Deletions from Group A

1. The AMP connector for the Power Control Unit has been deleted from the qualification program because it is no longer used.
2. The dimple motors for the damper have been deleted from the qualification program because they are no longer used.
3. The transistor for the Angle Indicator has been deleted from the qualification program because it was replaced by a phototransistor.
4. The special transformer for the Angle Indicator has been deleted from the qualification program because it is no longer used.

8.2.3.2 Qualification Plans

In general, the qualification plans are as specified in the individual part specification/drawing. Applicable details, explanations, and exceptions to this are described below.

8.2.3.2.1 Items 1, 2, and 3 of Table 8-5

The qualification plans for the transformer, the solar cell assembly, and the damper clutch solenoid are as specified in the respective GE drawings: R4610, R4611, and R4612.

8.2.3.2.2 Item 4 of Table 8-5

The Angle Indicator Head Assembly will be tested as a complete assembly, in place of performing qualification testing on the parts contained therein. The elements making up the assembly were evaluated for relative risk and are considered to be the following in the order listed.

1. Lamp
2. Phototransistors
3. Retention and positioning of the optical pieces
4. Electronic parts and circuits.

The bases for the decision to test the assembly were as follows:

1. Equipment and specifications. A test of parts separately requires test fixtures and test equipment for each part to position it, to provide inputs, and to monitor outputs. This is true for the phototransistors, the lenses, and the fiber optic assembly. However, in the head assembly, all of these fixtures are automatically provided by the assembly. This results in a major simplification of the testing effort. Testing of each of the items separately would also require a larger number of test specifications than would be needed to test the assembly.
2. Materials. Of major concern to the design engineers is the effect of the vacuum environment on the epoxy (and/or the other materials) used to locate and to retain the parts of the assembly. A test of the head assembly will assure qualification of the materials and processes used therein.
3. Environmental Facilities. Test facility requirements would be greater to test the parts separately than to test the completed head assembly.

The proposed qualification plan is given in paragraph 8.2.3.2.2.1 below.

8.2.3.2.2.1 Proposed Qualification Test Plan — It is proposed that a quantity of three head assemblies, with associated electronics modules, be subjected to the following tests:

1. Vibration
2. Acceleration
3. Thermal-vacuum with cycling
4. Life test.

The input voltage and the output current of each head assembly should be monitored periodically during the life test. Inspection and measurements of performance parameters will be done initially and after each environmental test, and at discrete points in the life test. Part parameters, such as light output of the lamp and light current output of the phototransistors, should be measured and recorded prior to assembly. These parameters can be rechecked upon completion of the life test and after dissection of the assemblies.

8.2.3.2.3 Item 5 of Table 8-5

The Holex Cable Cutter was qualified earlier by Holex, Inc., for the U.S. Navy. The qualification to be performed for ATS applies only to the requirements which exceed the levels already qualified. The qualification plan is given in paragraph 8.2.3.2.3.1. In addition, a lot acceptance test, to verify compliance with drawing

and specification, and to provide explosive compound data and output pressure limit data, is required. The number of items to be tested is 24 cartridges and 12 guillotine body assemblies. Approval of the explosive parameters data by GE is required prior to loading of prime cartridges by Holex.

8.2.3.2.3.1 Qualification Plan for Holex Cable Cutters — Twenty pieces shall be selected at random from each lot and subjected to the following tests per the referenced paragraphs of GE Specification No. SVS5292, "Component Specification for Electroexplosive Pressure Cartridge and Cable Cutter."

1. Visual and mechanical inspection (para. 4.5.1)
2. Dielectric strength (para. 4.5.4)
3. Insulation resistance (para. 4.5.3)
4. Bridgewire resistance (para. 4.5.2)
5. Electrostatic sensitivity (para. 4.5.5)
6. Vibration (para. 4.7.1)
7. Thermal vacuum (para. 4.8.3)
8. Repeat (1), (3), and (4) above.
9. Cable cutter assembly functioning test (para. 4.8.4)

Cost of the testing of the Holex Cable Cutter is being shared with the GGTS Project on the basis of proportionate use.

8.2.3.2.4 Items 6 through 13 of Table 8-5.

These parts are all contained in the Boom Subsystems and are presently lacking full documentation. Final qualification plans are not completed.

8.2.3.2.5 Item 14 of Table 8-5

The Sealed Drive Unit will be functionally and environmentally tested as an assembly. This course has the advantage of evaluating not only the parts in the assembly which are considered most critical, but also all other parts, materials, and interfaces involved in the unit. The test will amount to a combined parts qualification test and a component life capability verification test.

The plan is to test two units by subjecting them to an accelerated functional program designated a Dynamic Mission Equivalent (DME). This consists of the series performance of the dynamic mission functions, with the long-time static portions of the mission profile omitted. A number of DME's will be performed.

Such a test will provide life and capability data at a point early in the program, while the performance of an actual mission profile test could not reasonably be completed within the scheduled life of the program.

8.2.4 DEGRADATION ANALYSIS

Initial computer programming is completed to receive and process parts test data. Power aging data are processed to calculate the average, standard deviation, and skewness of parameter distributions, and to rank them to facilitate selection of stable parts for flight. The first lot of measurements at time zero (when initial readings are made for the part being measured) has been received and processed. Each lot of data will be processed as noted from interim and final measurements during the power aging tests.

A plan was initiated to check out the computer program and to test the selection criteria for the ATS degradation analysis. This will be done using 15,000-hour life test data that have already been collected on other programs. The selection criteria will be applied to the measurements data taken early in life. The selection will be made as if choosing the superior parts for flight. The correctness of the choice will then be either confirmed or refuted by examining the condition of those parts after 15,000 hours of testing. If faults or shortcomings are identified in the selection criteria, they will then be modified, as necessary, and retested. Results of this experiment will be described in a later report.

SECTION 9

NEW TECHNOLOGIES

In compliance with the provisions of the New Technologies caluse in the applicable contract, GE has continued to maintain surveillance over the design and development of the Gravity Gradient Stabilization System for reportable items. One such new technologies is reported that involves the computer analysis of screening parts data.

The vendor data on parts screened will be processed in accordance with the Hughes Aircraft Company computer program, as outlined in their specifications. This program organizes and analyzes parts data that is derived from testing, and presents it in a way to facilitate selection of the most stable parts by visual scanning. Briefly, the program is as follows:

The data for all measured parameters for an individual part for as many as four measurement periods will be punched on an IBM card. As many as four parameters may be measured per part. Typical parameters include the resistance of a resistor; the capacitance, dissipation factor and leakage current of a capacitor; leakage current, forward voltage drop and Beta of a transistor. Data processing for a lot of parts for each of four time periods consists of calculating the average, standard deviation and skewness, and printing the parameter values (with part serial number) in order of magnitude for each of the parameters. Four typical time periods are:

- t_1 Initial Reading
- t_2 After 240 hours
- t_3 After 500 hours
- t_4 After 1500 hours

When the data for the first two time periods are received, the rate of change of each parameter for each part will be calculated and used to determine the time to reach an arbitrarily assigned end point. This is called a figure of merit. The same procedure will be followed for the data from the third and fourth time periods. The results are punched on IBM cards and tabulated by serial number.

The two figures of merit are combined into a quality factor by dividing the square of the second by the first. This weights the result in favor of the second slope. These results are also tabulated and put on cards.

The cards from both of the last two operations are then put through the first procedure to get the distribution parameters and print-out in order of magnitude.

The Hughes procedure consisted of to make the complete calculation for one parameter only, the one selected as most significant. The GE program will process all parameters (as many as four). If the parameters do not all show the same ranking, engineering decisions will be required at that time.

Hughes is in the process of changing their method of selection. Whether a different ranking results from the new procedure depends entirely on the end points selected and on whether there is a significant difference in magnitude of the measured parameter at time periods t_2 and t_4.

The fundamental question remains, do either of these selection procedures identify those parts which will fail first in servide. GE-SD has no data to substantiate the selection process; however, GE is in a position to do this since the Spacecraft Department has data from other programs on groups of parts operated at different stress levels for thousands of hours. The trend tests could be applied to the early data to determine whether the early failures could be predicted.

This check on the computer analysis is valid only if it can be assumed that the parts failing under high temperature conditions would be the same ones which would fail under service conditions. Also, the screening would be based on the changes during operation at the same stress levels as imposed during the life test. Obviously the assumption cannot be proved. However, it is an assumption that is made for most accelerated testing. Also, the fact that the screening stress is the same as the service stress in this case may affect the correlation.

A considerable number of computer runs would be necessary to check out a program of this complexity since there are several arbitrary parameters to be selected. If the first analysis procedure does not give the desired results, it would then be necessary to write a new program. This might have to be done a total of three times before a satisfactory program is developed.

The final program would not only rank a group of parts on the basis of each parameter but would also rank them on the basis of a combination of the measured parameters. One print-out would be made on gummed paper which could be attached to the part storage containers to identify the part and show its quality ranking in the lot.

In summary, the new technologies identified here are as follows:

1. Use of all parameters (up to four) instead of only one parameter for ranking and selection.
2. Trend calculations through the use of the equation

$$DM = \frac{U - x_4}{\left|\frac{S_2}{S_1}\right| S_2} .$$

DM = Quality Factor

U = Upper Specification Limit

x_4 = Parameter Measured

S_1 = Slope of Original Trend

S_2 = Slope of Final Trend

This equation states that the distance to the upper specification limit is divided by the modified slope, which is weighted in favor of the second slope. Most significant is the fact that the modified slope retains the sign of the second slope.

3. Combination of the individual trend rankings (properly weighted) into a single, overall quality ranking.

4. The use of 15,000-hour life test data that have been collected by GE on other programs to test the selection criteria and constants that have been chosen for the ATS degradation analysis.

5. Use of gummed labels, printed from the computer output, to record not only the part and serial numbers of the item, but also the combined quality ranking of the item within the lot.

SECTION 10

GLOSSARY

The following is a list of abbreviations and definitions for terms used throughout this report.

ADTF	Advanced Damping Test Fixture (used for CPD testing)
ATS-A	Medium Altitude Gravity Gradient Experiment (6000-nautical mile orbit flight)
ATS-D/E	Synchronous Altitude Gravity Gradient Experiment (24-hour orbit flight)
CPD	Combination Passive Damper
Crab Angle	Out-of-orbit angle flight caused by changes in X-rod angle
DME	Dynamic Mission Equivalent (Accelerated Functional Program)
GE-MSD	General Electric Company Missile and Space Division
G^2S/ATS	Gravity Gradient System/ATS
HAC	Hughes Aircraft Company
ITPB	Integrated Test Program Board
Local Vertical	Imaginary line extending from the satellite center of mass to the center of mass of the earth
LOFF	Low Order Force Fixture (used for CPD testing)
MTBF	Mean Time Before Failure
MTTF	Mean Time to Failure
PCU	Power Control Unit
PIR	Program Information Request/Release, GE documentation
SAS	Solar Aspect Sensor
Scissoring	Changing the angle included between the primary booms in a manner that maintains a symmetrical configuration about the satellite yaw axis
STEM	Storable Tubular Extendable Member
Stiction Torque	That amount of torque required to overcome the initial effects of friction
SVA Fixture	Shock and Vibration Attachment Fixture

Thermal Twang	Sudden thermal bending which the booms experience in passing from a region of total eclipse into a region of continuous sunlight or vice versa
TR	Torsional restraint
TVCS	TV Camera Subsystem

APPENDIX A

DIAMAGNETIC SHAFT SUPPORT - ANALYTICAL DESCRIPTION

I. ABSTRACT

An analytical description is given for a diamagnetic shaft support, for use in orbiting satellites. The shaft is provided with unlimited rotation about its axis, supported in stable equilibrium by frictionless diamagnetic forces. The mathematical model developed for the diamagnetic shaft support is applied to a complex shaft loading condition, and computer solutions are presented.

II. INTRODUCTION

This report is intended to provide a useful analytical description of the diamagnetic shaft support, to be used in the selection of design parameters, and to predict the behavior of the shaft under various conditions of loading. Figure 1/2 shows the basic elements and general principle of the diamagnetic shaft support, and defines the axes used in the analysis. An empirical expression for diamagnetic force is developed, and this is used in the derivation of an "exact" mathematical model for the suspension system. An approximation of this model is then developed, which sacrifices little in accuracy, and gains appreciably in usefulness. This approximate mathematical model is applied to the rather complex loading situation present in the ATS damper. Computer solutions of these equations were used to aid in the design of the diamagnetic shaft support. This report concludes with graphs of the computer solutions.

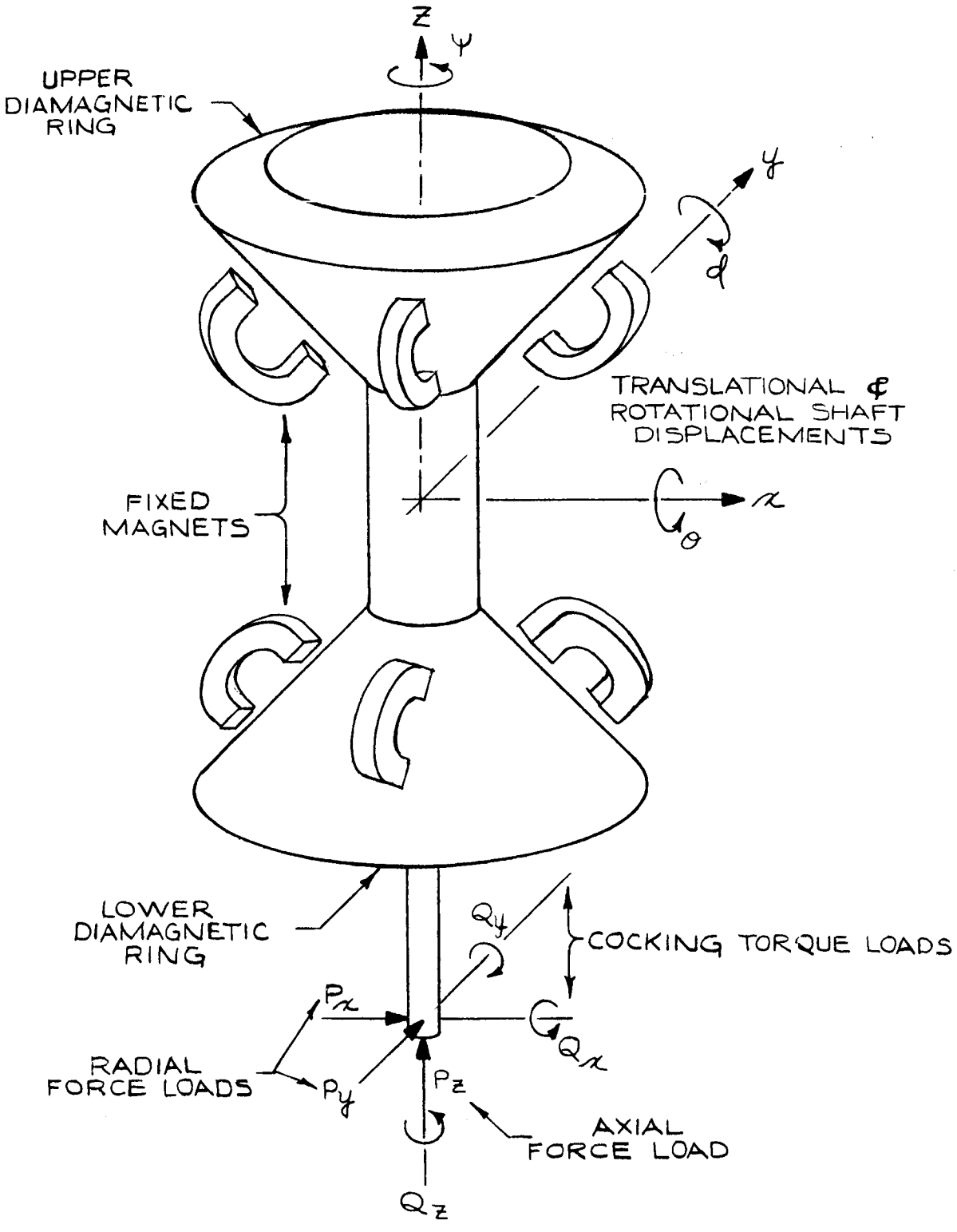

Figure 1/2. Diamagnetic Shaft Support

III. DIAMAGNETIC FORCES

A. THEORETICAL CONSIDERATIONS

It is not possible to suspend in stable equilibrium a body with a dielectric constant or a magnetic permeability greater than unity, in a static electric or magnetic field. For electrically charged bodies, this was shown by Earnshaw[1] in 1842 and is known as Earnshaw's Theorem. It has been extended by Maxwell[1] and Jeans[1] to the case of magnetic suspension.

The force experienced by a diamagnetic specimen, when immersed in a medium in a non-uniform magnetic field, has been shown by Trevena[2] to be the following:

$$dF_s = \frac{1}{2} (K_2 - K_1) \frac{dH^2}{ds} dv$$

where

dF_s = force on the specimen, in the s-direction

K_2 = volumetric magnetic susceptibility of specimen

K_1 = volumetric magnetic susceptibility of medium

$\frac{dH^2}{ds}$ = gradient of the square of the field intensity, in the s-direction

dv = the volume of the specimen

For a diamagnetic specimen (with negative susceptibility) immersed in a vacuum (with zero susceptibility) in the field of a permanent magnet, the force is seen to be in the direction

1. References are given in GE Report No. 63GL130 "Magnetic Bearings" by J.D. McHugh et al, dated September 27, 1963.
2. D. H. Trevena - "Static Fields in Electricity and Magnetism" - Butterworth & Co. Ltd. 1961, p. 232-233

opposite that of the field gradient. That is, the specimen is repelled by the magnet. To find the net force on a piece of diamagnetic material, the differential forces exerted on all the differential volumes must be integrated over the entire volume of the piece. Since the field gradient is difficult to define over the entire volume of the piece, the forces existing between magnet and specimen were determined experimentally, for several permanent magnets in combination with diamagnetic materials.

B. LABORATORY FORCE MEASUREMENTS

Diamagnetic specimens were prepared of bismuth and pyrolytic graphite, using flat plates of various thicknesses. Several commercially available types of permanent magnets were obtained, and the repulsion forces were measured as a function of the air gap between the magnet poles and the diamagnetic plate. Over 100 such tests were performed. Based on these tests the General Electric Type 5U41B magnet was selected for use in the diamagnetic shaft support. The results of three typical force measurements are shown in Figures 3/4, 5 and 6. These tests also show how the force magnitude is affected by the thickness of the diamagnetic plate, in this case pyrolytic graphite. A plate thickness of 1/4 inch was selected, based on these tests.

The diamagnetic forces are generally extremely weak, as shown by the test results. The diamagnetic shaft support will not operate in a 1-g gravitational field, because of the small support forces available. Special test equipment had to be developed to permit the measurement of these forces.

C. EMPIRICAL EXPRESSION FOR FORCE

For use in analytical design work, an empirical expression was found for the force between a single magnet and a diamagnetic plate. This expression has the form of a decaying exponential, and was found by a curve-fitting the following expression to the measured force (F) vs. air gap (s) characteristics:

$$F = a + F_o \, e^{-Ks}$$

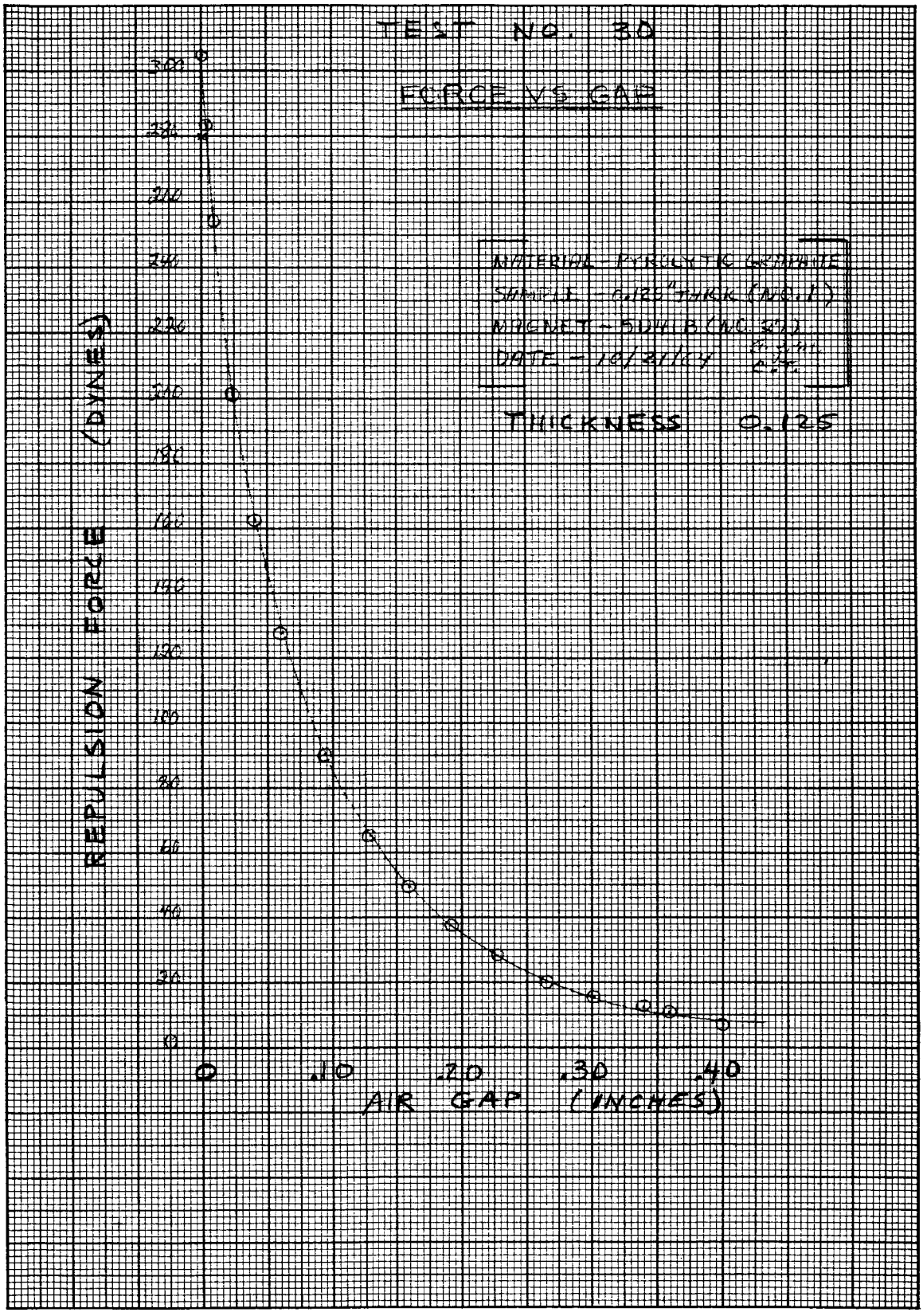

Figure 3/4. Force vs. Air Gap

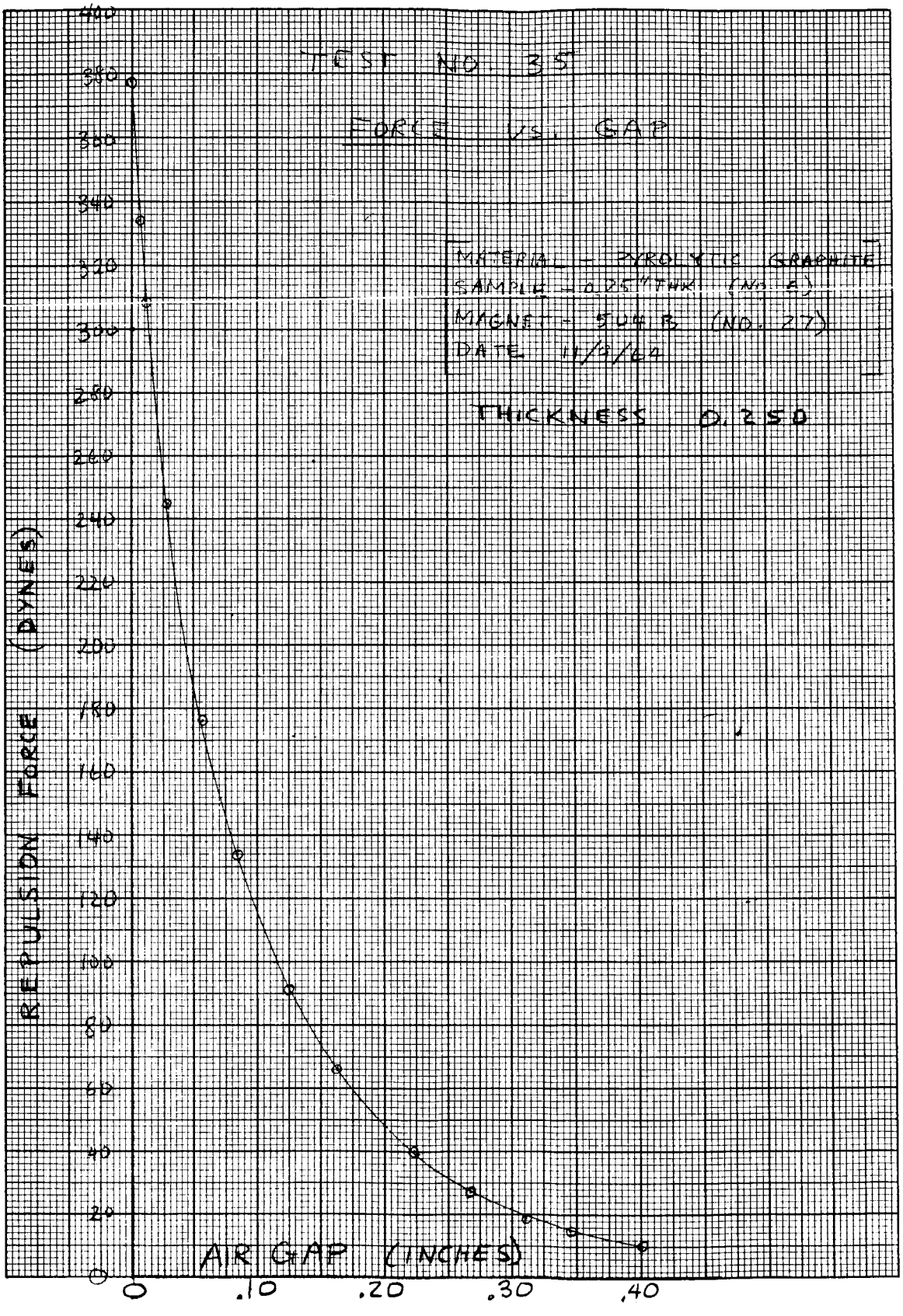

Figure 5. Force vs. Air Gap

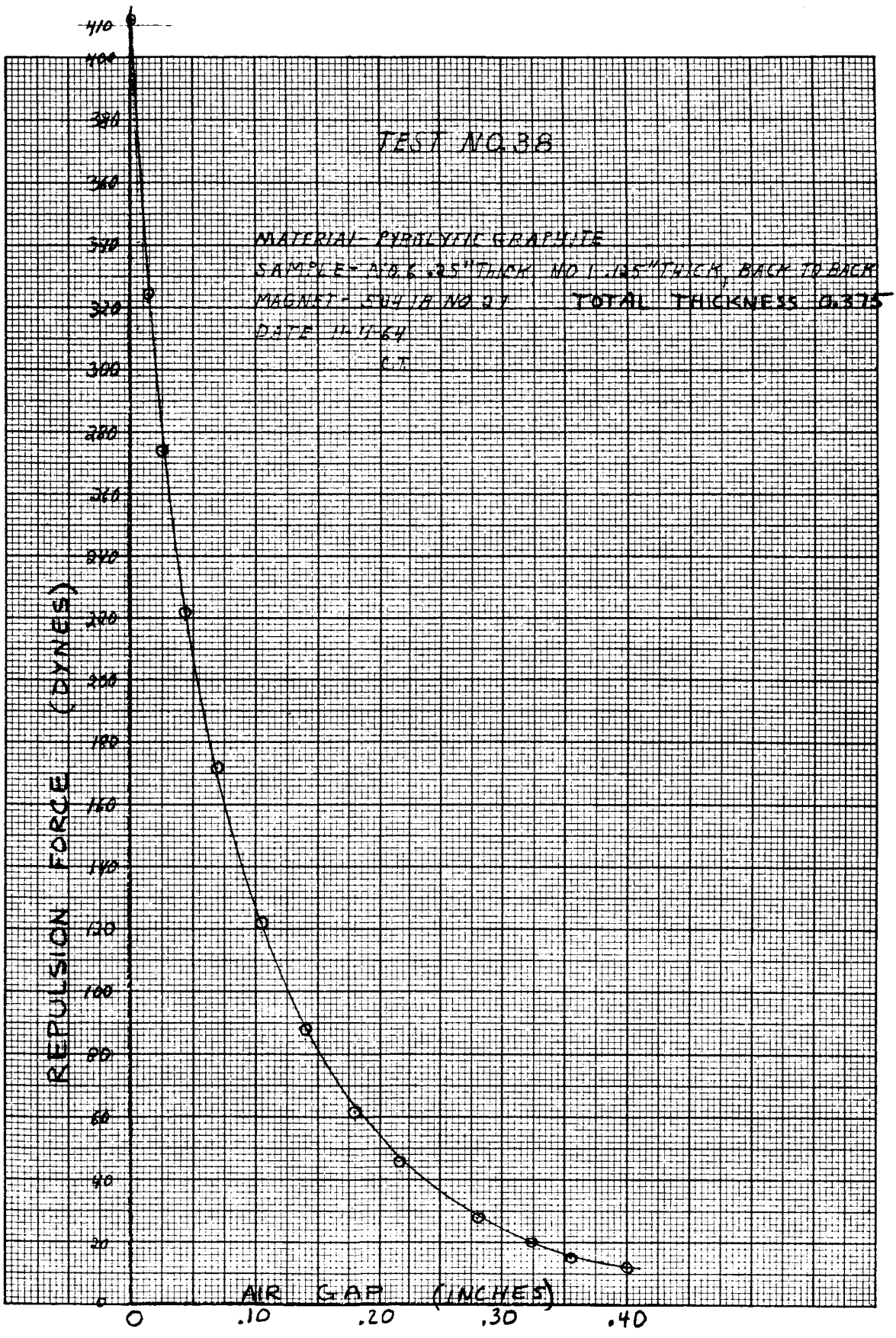

Figure 6. Force vs. Air Gap

For a GE 5U41B magnet in combination with pyrolytic graphite, 1/4 inch thick, the expression becomes

$$F = 30 + 270\, e^{-15s}$$

where

F = the repulsion force, dynes

s = air gap, inches

This empirical expression is plotted in Figure 7 and compared with typical test points. The fit is excellent in the range of air gaps of interest, from 0.01 inch to 0.12 inch.

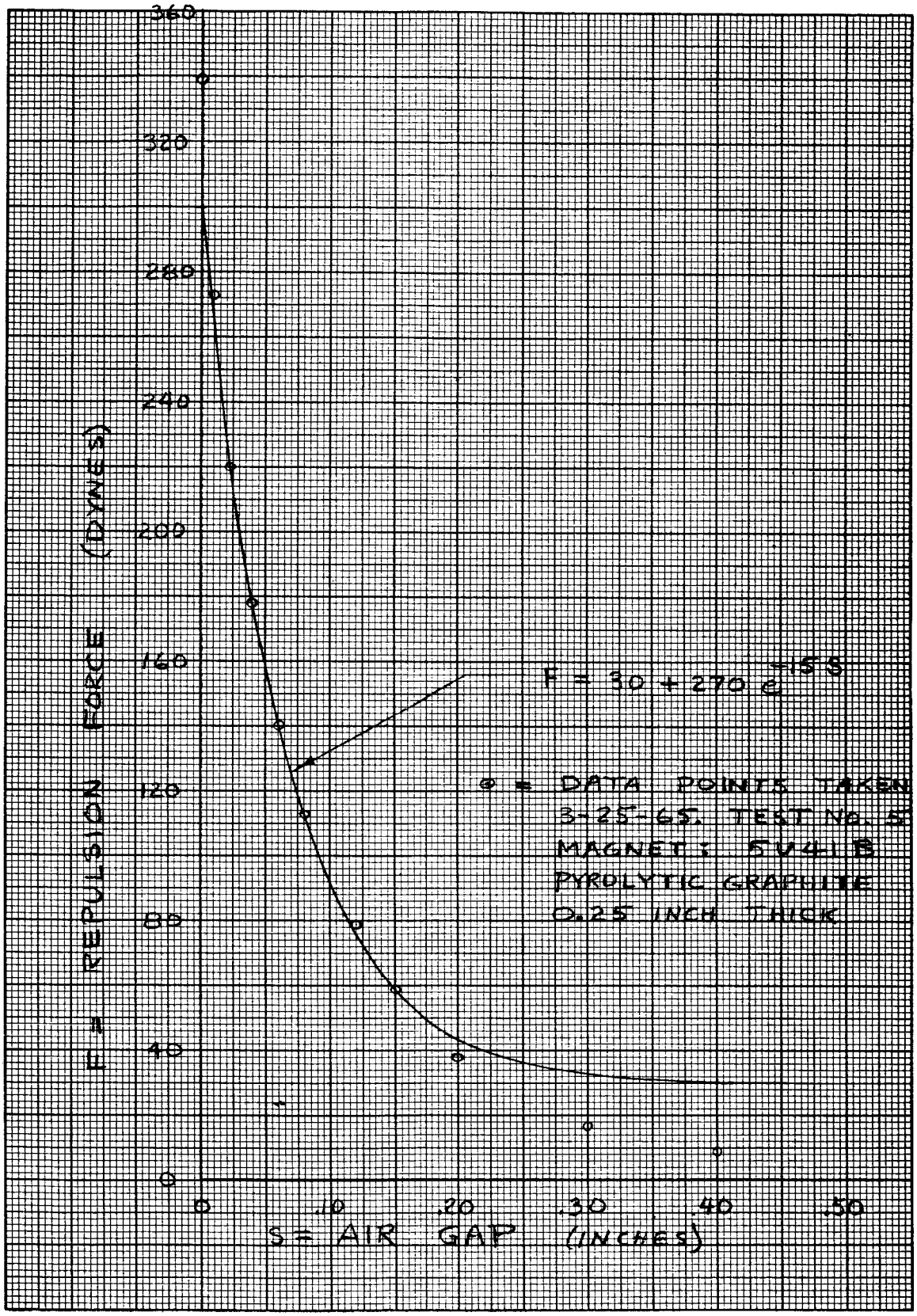

Figure 7. Force vs. Air Gap - Empirical Expression

IV EXPRESSION FOR MAGNET AIR GAPS

The diamagnetic rings are supported by forces which vary with air gap. A relationship is required which expresses the air gap at each of the support magnets as a function of the six degrees of freedom of the shaft. This relationship is derived below. The design parameters which describe the configuration are defined by Figure 8.

Let x, y, z = translational displacements of the rotor from the null position, parallel to the x, y, z axes, respectively, inches

θ, φ, ψ = rotational displacements of the rotor from the null position, about the x, y, z axes, respectively, radians

S_o = air gap for all magnets in the upper ring, with the rotor in the null position, inches.

U_o = air gap for all magnets in the lower ring, with the rotor in the null position, inches

S_i = air gap at the i^{th} magnet of the upper ring, inches.

U_j = air gap at the j^{th} magnet of the lower ring, inches.

If it is assumed that rotor displacements are small, then the air gap at any magnet may be expressed as follows:

$$\left.\begin{aligned} S_i &= S_o + x\frac{\partial S_i}{\partial x} + y\frac{\partial S_i}{\partial y} + z\frac{\partial S_i}{\partial z} + \theta\frac{\partial S_i}{\partial \theta} + \varphi\frac{\partial S_i}{\partial \varphi} + \psi\frac{\partial S_i}{\partial \psi} \\ U_j &= U_o + x\frac{\partial U_j}{\partial x} + y\frac{\partial U_j}{\partial y} + z\frac{\partial U_j}{\partial z} + \theta\frac{\partial U_j}{\partial \theta} + \varphi\frac{\partial U_j}{\partial \varphi} + \psi\frac{\partial U_j}{\partial \psi} \end{aligned}\right\} \quad (1)$$

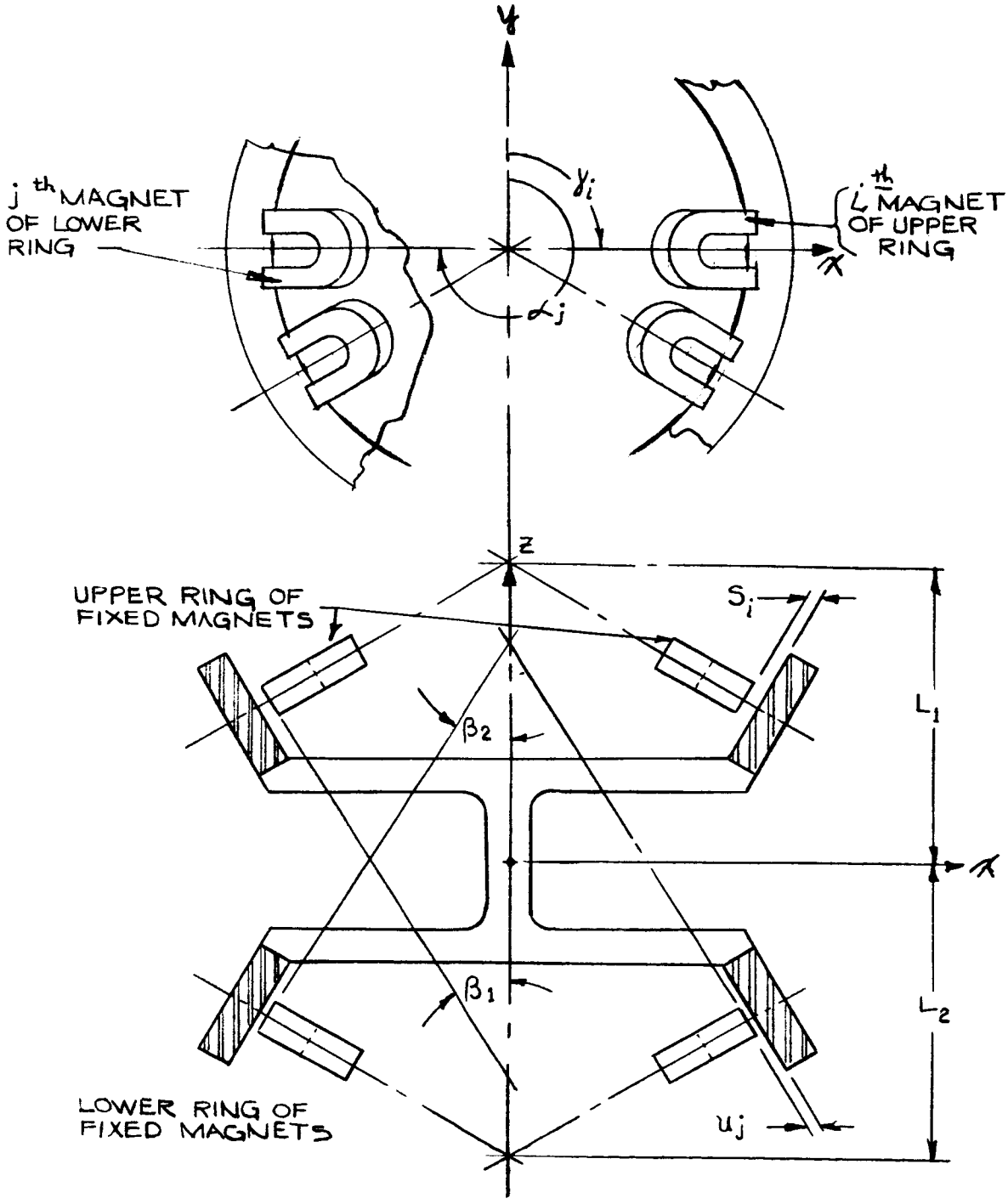

Figure 8. Design Parameter Definition

The partial derivatives for translational displacements may be obtained by inspection of Figure 8, and are indicated in Table 1. The effect of rotational displacements of the rotor will be derived with the aid of Figure 9, which shows the conditions at a magnet located on the x-axis of the upper ring ($\gamma_i = 90^o$), when the rotor is tilted about the y-axis through an angle φ.

As shown in Figure 9, the rotor has turned clockwise through an angle $+\varphi$, and point B on the rotor has moved to point C, through a distance

$$\overline{BC} = \sqrt{R_1^2 + L_7^2} \sin \varphi.$$

The change in air gap is

$$\Delta S_i = \overline{AB}.$$

Also, the angle $\angle ABC$ is

$$\angle ABC = (\arctan \frac{R_1}{L_7} - \beta_1).$$

Then, in the triangle ABC, the change in air gap may be expressed as follows:

$$\Delta S_i = \overline{AB} = \overline{BC} \cos (\angle ABC)$$

$$= \sqrt{R_1^2 + L_7^2} \sin \varphi \cos (\arctan \frac{R_1}{L_7} - \beta_1)$$

$$= \sqrt{R_1^2 + L_7^2} \sin \varphi \left[\frac{L_7 \cos \beta_1}{\sqrt{R_1^2 + L_7^2}} + \frac{R_1 \sin \beta_1}{\sqrt{R_1^2 + L_7^2}} \right]$$

$$= \left[L_7 + R_1 \tan \beta_1 \right] \cos \beta_1 \sin \varphi$$

$$= L_1 \cos \beta_1 \sin \varphi$$

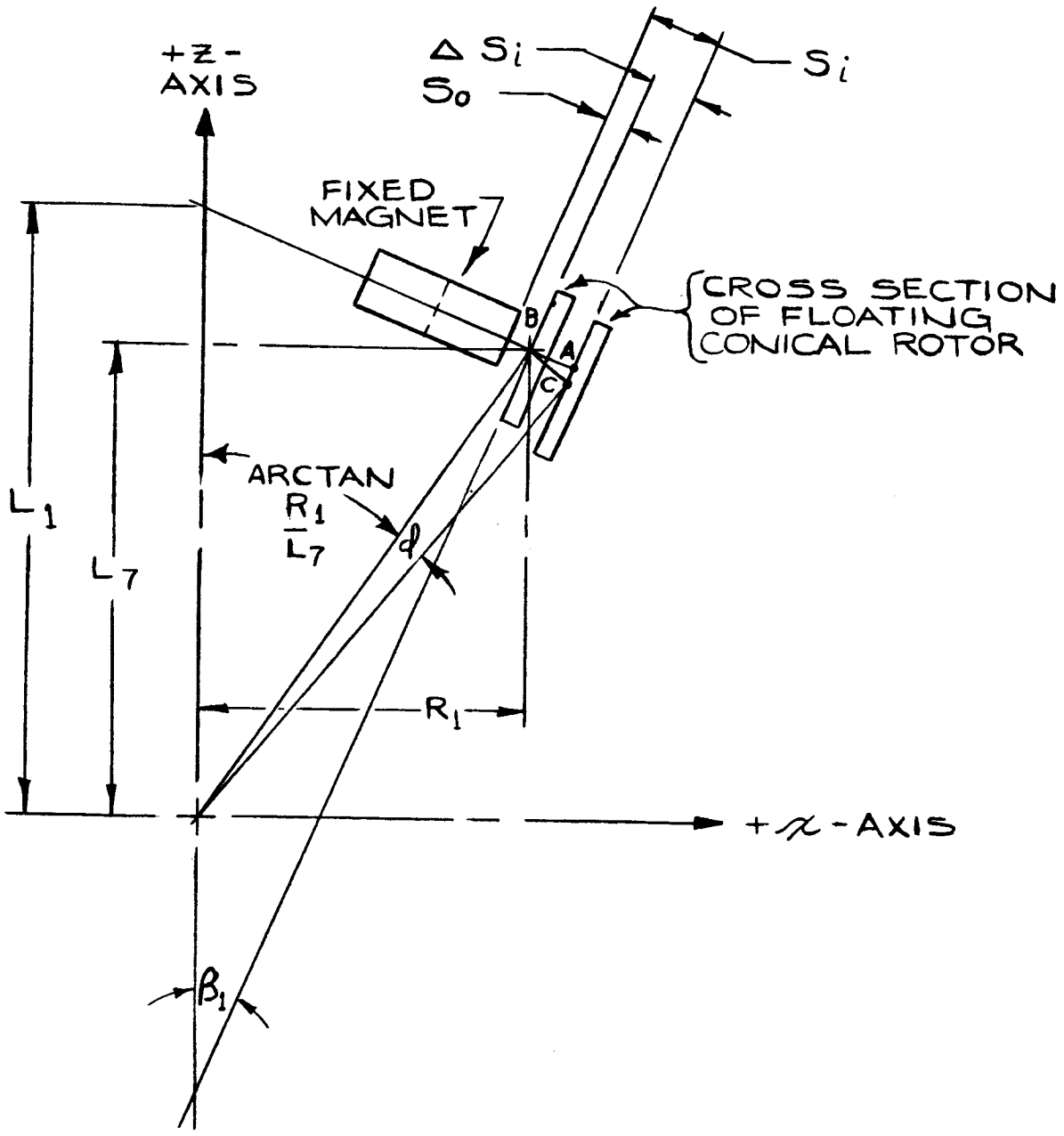

Figure 9. Effect of Rotational Displacement

Table 1. Air Gap Variations Due to Rotor Displacements

Rotor Displacement	Upper-Ring Air Gaps S_i	Lower-Ring Air Gaps U_j
x	$S_o + x \cos \beta_1 \sin \gamma_i$	$U_o + x \cos \beta_2 \sin \alpha_j$
y	$S_o + y \cos \beta_1 \cos \gamma_i$	$U_o + y \cos \beta_2 \cos \alpha_j$
z	$S_o - z \sin \beta_1$	$U_o + z \sin \beta_2$
θ	$S_o - \theta L_1 \cos \beta_1 \cos \gamma_i$	$U_o + \theta L_2 \cos \beta_2 \cos \alpha_j$
φ	$S_o + \varphi L_1 \cos \beta_1 \sin \gamma_i$	$U_o - \varphi L_2 \cos \beta_2 \sin \alpha_j$
ψ	$S_o + 0$	$U_o + 0$

For small displacements, sin φ may be replaced by φ, and the expression becomes

$$\Delta S_i = \varphi L_1 \cos \beta_1,$$

for a magnet originally assumed to be located on the x-axis of the upper ring ($\gamma_i = 90^o$). The expression may be generalized to apply to any magnet on the upper ring, as follows:

$$\Delta S_i = \varphi L_i \cos \beta_1 \sin \gamma_i$$

and the partial derivative of air gap with respect to rotational displacement is:

$$\frac{\partial S_i}{\partial \varphi} = L_1 \cos \beta_1 \sin \gamma_i$$

Similar expressions may be derived for rotations about the x-axis, and also for air gaps at the lower ring. The results are indicated in Table 1.

Substitution of these results into equations (1) yields the following expressions for the air gap at any magnet, under six degrees of freedom for rotor displacement:

$$\left.\begin{aligned} S_i &= S_o + x \cos\beta_1 \sin\gamma_i + y \cos\beta_1 \cos\gamma_i - z \sin\beta_1 - \theta L_1 \cos\beta_1 \cos\gamma_i \\ &\quad + \varphi L_1 \cos\beta_1 \sin\gamma_i \\ U_j &= U_o + x \cos\beta_2 \sin\alpha_j + y \cos\beta_2 \cos\alpha_j + z \sin\beta_2 + \theta L_2 \cos\beta_2 \cos\alpha_j \\ &\quad - \varphi L_2 \cos\beta_2 \sin\alpha_j \end{aligned}\right\} \quad (2)$$

It is noted that rotations about the z-axis (ψ) have no effect on the air gaps.

V. "EXACT" MATHEMATICAL MODEL OF DIAMAGNETIC SUSPENSION

A. DERIVATION

Let F_i = The repulsion force exerted on the diamagnetic rotor by the i^{th} magnet of the upper ring, normal to the conical surface, dynes.

G_j = The repulsion force exerted on the diamagnetic rotor by the j^{th} magnet of the lower ring, normal to the comical surface, dynes.

F_{x1}, F_{y1}, F_{z1} = Net force exerted on the diamagnetic rotor by the upper ring of magnets, parallel to the x, y, z axes, respectively, dynes.

M_{x1}, M_{y1}, M_{z1} = Net torque exerted on the diamagnetic rotor by the upper ring of magnets, about the x, y, z axes, respectively, dyne-inches.

F_{x2}, F_{y2}, F_{z2} = Net force exerted on the diamagnetic rotor by the lower ring of magnets, parallel to the x, y, z axes respectively, dynes.

M_{x2}, M_{y2}, M_{z2} = Net torque exerted on the diamagnetic rotor by the lower ring of magnets, about the x, y, z axes, respectively, dyne-inches.

m = number of magnets in upper ring

n = number of magnets in lower ring

Each magnet in the upper ring exerts a repulsion force F_i on the rotor, normal to the conical surface. These forces may be summed up to obtain the three components of net force, and the three components of net torque on the upper diamagnetic ring. By inspection of Figure 8, these net supports are as follows:

$$F_{x1} = \sum_{i=1}^{m} F_i \cos \beta_1 \sin \gamma_i$$

$$F_{y1} = \sum_{i=1}^{m} F_i \cos \beta_1 \cos \gamma_i$$

$$F_{z1} = \sum_{i=1}^{m} - F_i \sin \beta_1$$

$$M_{x1} = \sum_{i=1}^{m} - F_i L_7 \cos \beta_1 \cos \gamma_i + \sum_{i=1}^{m} - F_i R_1 \sin \beta_1 \cos \gamma_i$$

$$= \sum_{i=1}^{m} - F_i L_1 \cos \beta_1 \cos \gamma_i$$

$$M_{y1} = \sum_{i=1}^{m} F_i L_7 \cos \beta_1 \sin \gamma_i + \sum_{i=1}^{m} F_i R_1 \sin \beta_1 \sin \gamma_i$$

$$= \sum_{i=1}^{m} F_i L_1 \cos \beta_1 \sin \gamma_i$$

$$M_{z1} = 0 \qquad (3)$$

Similarly, the diamagnetic supports at the lower ring are expressed as follows:

$$F_{x2} = \sum_{j=1}^{n} G_j \cos \beta_2 \sin \alpha_j$$

$$F_{y2} = \sum_{j=1}^{n} G_j \cos \beta_2 \cos \alpha_j$$

$$F_{z2} = \sum_{j=1}^{n} G_j \sin \beta_2$$

$$M_{x2} = \sum_{j=1}^{n} G_j L_2 \cos \beta_2 \cos \alpha_j \qquad (4)$$

$$M_{y2} = \sum_{j=1}^{n} G_j L_2 \cos \beta_2 \sin \alpha_j$$

$$M_{z2} = 0$$

In each term of equations (3) and (4) appears the force F_i (or G_j), which has been shown earlier to depend on air gap in the following manner:

$$F_i = a + F_o e^{-k s_i}$$

$$G_j = a + F_o e^{-k u_j} \qquad (5)$$

where a, F_o, k are parameters determined experimentally.

The expressions for air gap in equations (2) may be substituted into the exponents of equations (5) to give the individual magnet forces. The resulting expressions may be substituted into equations (3) and (4) to give the diamagnetic supports as five simultaneous nonlinear equations in five variables, the variables being the five degrees of freedom which describe the rotor position. As an example of the complexity of these equations, one term of the F_{x1} equation will be written: the term corresponding to magnet number 3.

$$\ldots + \left[a + F_o e^{-k s_o} e^{-k x \cos \beta_1 \sin \gamma_3} e^{-k y \cos \beta_1 \cos \gamma_3} x \right.$$

$$\left. x e^{+ k z \sin \beta_1} e^{+ k \theta L_1 \cos \beta_1 \cos \gamma_3} e^{-k \varphi L_1 \cos \beta_1 \sin \gamma_3} \right]$$

$$x \cos \beta_1 \sin \gamma_3 + \ldots$$

A design which has, for example, 8 magnets in each ring would be described by five simultaneous equations, each containing 16 terms similar to the one written above, plus additional terms corresponding to external and internal force and torque loads on the rotor. As shown, the variables appear in the exponents of these terms.

The solution of these equations may be accomplished by a digital computer, using iterative computation techniques, but at great expense.

B. EXAMPLE OF "EXACT" MATHEMATICAL MODEL

In order to show the general shape of the support characteristics, a simple example will be used. In this example, it will be assumed for simplicity that the rotor has only one degree of freedom, namely, rotation (φ) about the y-axis. Further assumptions are as follows:

$m = n = 8$ magnets in each ring

All magnets equally spaced.

Cone half angle $\beta_1 = \beta_2 = 20^o$

$$L_1 = L_2 = 5 \text{ inches}$$

The force vs. air gap characteristic for a single magnet is

$$F_i = a + F_o e^{-k s_i}$$

$$F_i = 30 + 270\, e^{-15 s_i} \text{ dynes}$$

where

S_i = air gap, inches

All air gaps are initially set at $S_o = .050$ inches

Solution:

$$x = y = z = \theta = \psi = 0$$

First consider the upper ring:

Air gap $= S_i = S_o + \phi\, L_1 \cos\beta_1 \sin\gamma_i$

$$\text{Force} = F_i = a + F_o\, e^{-k\, s_i}$$

$$= 30 + 270\, e^{-15\, S_o}\, e^{-15\, L_1 \cos \beta_1 \sin \gamma_1 \phi}$$

$$= 30 + 270\, e^{-15(.050)}\, e^{-15(5) \cos 20^o \sin \gamma_i \phi}$$

$$= 30 + 128\, e^{-70.5 \sin \gamma_i \phi} \text{ dynes}$$

Also, the maximum rotation before closing the air gap is

$$\phi = \frac{0 - S_o}{L_1 \cos \beta_1 \sin \gamma_i} = \frac{-.050}{5\ (.94)\ (1)}$$

$$= -.01065 \text{ radians}$$

(= 0.61 degrees)

Calculations were made for ϕ in .002 radian increments.

It was calculated that $F_{x1} = F_{y1} = F_{z1} = M_{x1} = 0$

The results of calculations for M_{y1} are as follows:

$$M_y = M_{y1} + M_{y2}$$

$$M_{y1} = \sum_{i=1}^{m} F_i\, L_1 \cos \beta_1 \sin \gamma_i \text{ dyne-inches}$$

$$M_{y2} = \sum_{i=1}^{m} G_j\, L_2 \cos \beta_2 \sin \alpha_j = M_{y1}$$

The values for M_y have been calculated and converted to dyne-centimeters and plotted vs. angular displacement ϕ (Figure 10). The limiting values for angular displacement are shown, assuming stops are used to provide a magnet gap of at least .010 inches. The slope of the characteristic at the origin is plotted for later reference.

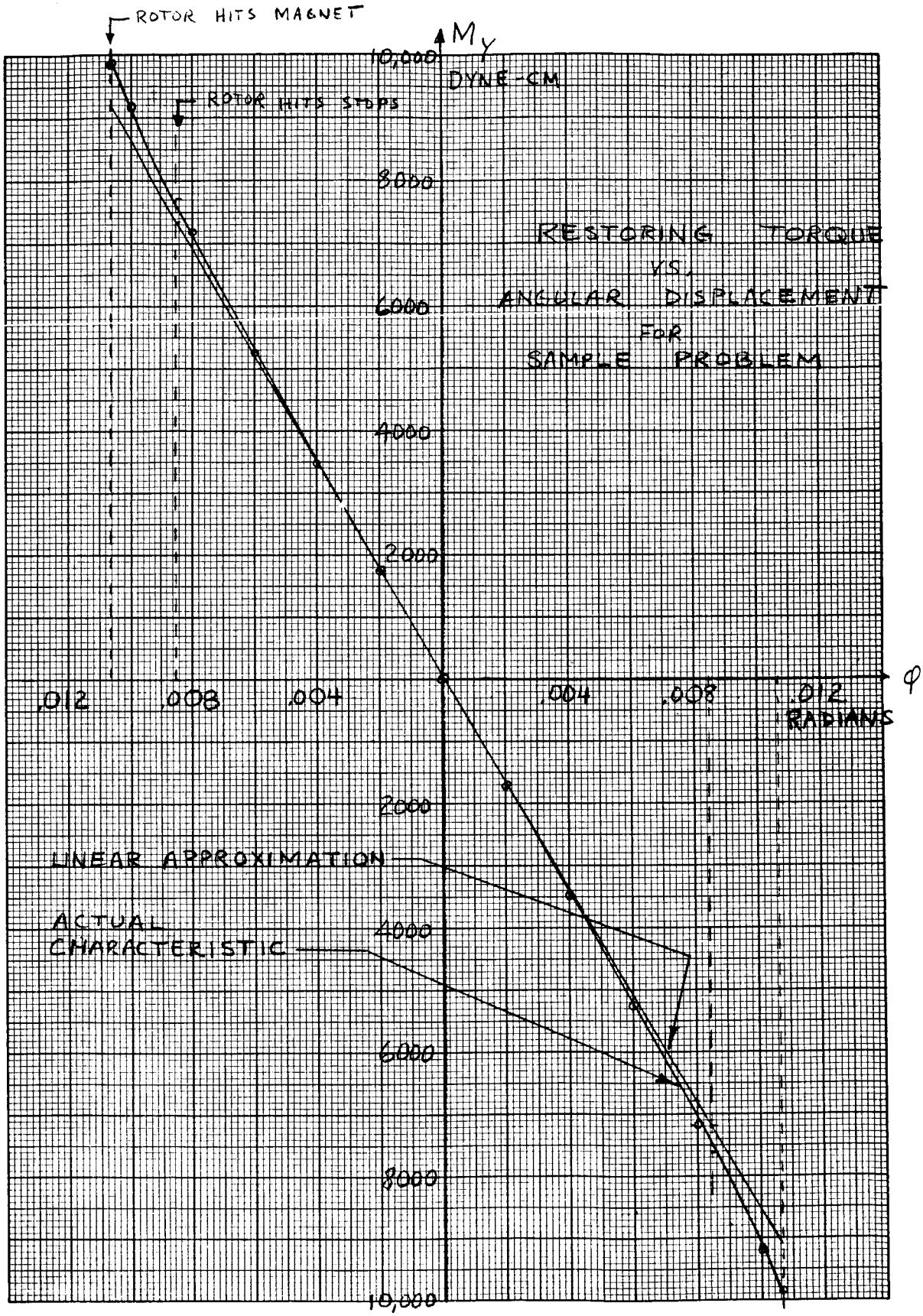

Figure 10. Support Characteristics -"Exact" Model

VI. "APPROXIMATE" MATHEMATICAL MODEL OF DIAMAGNETIC SUSPENSION

A. DERIVATION

The plotted results of the simplified example ("Exact" Mathematical Model) suggest that a linear approximation of the suspension characteristics would be very close to the exact characteristic. This linear approximation would be defined by the slope of the exact characteristic at the origin. In the example shown, the linear approximation would yield results about 5 percent more conservative than the "exact" analysis.

In the approximate mathematical model to be developed, it will be assumed that the rotor has only three degrees of freedom in addition to rotation about the z-axis, instead of five. These three displacements will be axial displacement (z), radial displacement (x), and an angular displacement (ϕ) about the y-axis. This constitutes the motion resulting from the most severe combination of loads applied to the rotor. Under these conditions, combinations of external cocking torques and radial and axial forces add together to increase the load to be supported by a given magnet. Hence, this selection of motions is the most conservative (and the necessary) approach to take for design of the suspension.

In the approximate mathematical model, we find the slopes of the diamagnetic characteristics at the origin, and assume that these slopes remain constant over the entire range of displacements. For the radial force exerted on the rotor in the x-direction by the upper ring of magnets, this is expressed as follows:

$$F_{x1} = F_{x1}\Big]_o + \frac{\partial F_{x1}}{\partial x}\Big]_o x + \frac{\partial F_{x1}}{\partial \varphi}\Big]_o \varphi + \frac{\partial F_{x1}}{\partial z}\Big]_o z \qquad (6)$$

From equation (3),

$$F_{x1} = \sum_{i=1}^{m} F_i \cos \beta_1 \sin \gamma_i$$

$$= \sum_{i=1}^{m} (a + F_o e^{-k s_i}) \cos \beta_1 \sin \gamma_i$$

$$= a \cos \beta_1 \left[\sin \gamma_1 + \ldots + \sin \gamma_m \right]$$

$$+ F_o e^{-k s_o} \cos \beta_1 \left[e^{-k\Delta s_1} \sin \gamma_1 + \ldots + e^{-k\Delta s_m} \sin \gamma_m \right]$$

At origin,

$$F_{x1}{}_o = 0$$

$$\frac{\partial F_{x1}}{\partial x} = F_o e^{-k s_o} \cos \beta_1 \left[-k e^{-k\Delta s_1} \sin \gamma_1 \frac{\partial s_1}{\partial x} - \ldots \right.$$

$$\left. - k e^{-k\Delta s_m} \sin \gamma_m \frac{\partial s_m}{\partial x} \right]$$

From Table 1, we have

$$\frac{\partial S_i}{\partial x} = \cos \beta_1 \sin \gamma_i$$

Therefore

$$\frac{\partial F_{x1}}{\partial x} = - F_o k e^{-k s_o} \cos^2 \beta_1 \left[e^{-k\Delta s_1} \sin^2 \gamma_1 + \ldots + e^{-k\Delta s_m} \sin^2 \gamma_m \right]$$

At the origin,

$$\Delta s_1 = \Delta s_2 = \ldots = \Delta s_m = 0$$

$$e^{-k\Delta s_1} = e^{-k\Delta s_2} = \ldots = e^{-k\Delta s_m} = 1$$

$$\left.\frac{\partial F_{x1}}{\partial x}\right]_o = -F_o\, k\, e^{-k\, s_o} \cos^2 \beta_1 \left[\sin^2 \gamma_1 + \ldots + \sin^2 \gamma_m\right]$$

Let it now be assumed that the m magnets are equally spaced. Under this assumption, as will be shown in Appendix A, the expression within the brackets reduces to 1/2 m. The summation of m terms may now be expressed more compactly as follows:

$$\left.\frac{\partial F_{x1}}{\partial x}\right]_o = -\frac{1}{2}\, m\, F_o\, k\, e^{-k\, s_o} \cos^2 \beta_1 \tag{7}$$

Next, we examine $\dfrac{\partial F_{x1}}{\partial \varphi}$

$$\frac{\partial F_{x1}}{\partial \varphi} = F_o\, e^{-k\, s_o} \cos \beta_1 \left[-k\, e^{-k\Delta s_1} \sin \gamma_1 \frac{\partial s_1}{\partial \varphi} - \ldots - k\, e^{-k\Delta s_m} \sin \gamma_m \frac{\partial s_m}{\partial \varphi}\right]$$

From Table 1,

$$\frac{\partial s_i}{\partial \varphi} = L_1 \cos \beta_1 \sin \gamma_i$$

Therefore,

$$\frac{\partial F_{x1}}{\partial \varphi} = -L_1\, F_o\, k\, e^{-k\, s_o} \cos^2 \beta_1 \left[e^{-k\Delta s_1} \sin^2 \gamma_1 + \ldots + e^{-k\Delta s_m} \sin^2 \gamma_m\right]$$

As before, at the origin, and for equally spaced magnets,

$$\left.\frac{\partial F_{x1}}{\partial \varphi}\right]_o = - L_1 \left[\frac{1}{2} m F_o k e^{-k s_o} \cos^2 \beta_1\right] \tag{8}$$

Next, we examine $\frac{\partial F_{x1}}{\partial z}$

$$\frac{\partial F_{x1}}{\partial z} = F_o e^{-k s_o} \cos \beta_1 \left[- k e^{-k\Delta s_1} \sin \gamma_1 \frac{\partial s_1}{\partial z} - \ldots - k e^{-\Delta s_m} \sin \gamma_m \frac{\partial s_m}{\partial z}\right]$$

From Table 1,

$$\frac{\partial s_i}{\partial z} = - \sin \beta_1$$

Therefore,

$$\frac{\partial F_{x1}}{\partial z} = + F_o k e^{-k s_o} \sin \beta_1 \cos \beta_1 \left[e^{-k\Delta s_1} \sin \gamma_1 + \ldots + e^{-k\Delta s_m} \sin \gamma_m\right]$$

At the origin,

$$\left.\frac{\partial F_{x1}}{\partial z}\right]_o = + F_o k e^{-k s_o} \sin \beta_1 \cos \beta_1 \left[\sin \gamma_1 + \ldots + \sin \gamma_m\right] \tag{9}$$

$$\left.\frac{\partial F_{x1}}{\partial z}\right]_o = 0, \text{ for equally spaced magnets.}$$

Equations (7), (8), and (9) may be substituted into equation (6) to obtain the following result:

$$F_{x1} = -\left[\frac{1}{2} m F_o k e^{-k s_o} \cos^2 \beta_1\right] x$$

$$- L_1 \left[\frac{1}{2} m F_o k e^{-k s_o} \cos^2 \beta_1\right] \varphi + \left[o\right] z$$

$$F_{x1} = - K_1 (x + L_1 \varphi) \tag{10}$$

where

$$K_1 = \frac{1}{2} m F_o k e^{-k s_o} \cos^2 \beta_1 \tag{11}$$

Equation (10) expresses the diamagnetic radial restoring force exerted on the rotor by the upper ring of magnets, for three degrees of rotor freedom (x, φ, z). Equation (11) represents the radial stiffness of the suspension, for the upper ring.

A similar derivation for the lower ring of magnets yields the following result:

$$F_{x2} = - K_2 (x - L_2 \varphi) \tag{12}$$

where

$$K_2 = \frac{1}{2} n F_o k e^{-k u_o} \cos^2 \beta_2 \tag{13}$$

Next, we derive the expression for the diamagnetic restoring torque exerted on the rotor by the upper ring.

$$M_{y1} = M_{y1}\Big]_o + \frac{\partial M_{y1}}{\partial x}\Big]_o x + \frac{\partial M_{y1}}{\partial \varphi}\Big]_o \varphi + \frac{\partial M_{y1}}{\partial z}\Big]_o z \qquad (14)$$

From equation (3),

$$M_{y1} = \sum_{i=1}^{m} F_i L_1 \cos \beta_1 \sin \gamma_i$$

$$= \sum_{i=1}^{m} (a + F_o e^{-k s_i}) L_1 \cos \beta_1 \sin \gamma_i$$

$$= a L_1 \cos \beta_1 \left[\sin \gamma_1 + \sin \gamma_2 + \ldots + \sin \gamma_m\right]$$

$$+ F_o L_1 e^{-k s_o} \cos \beta_1 \left[e^{-k\Delta s_1} \sin \gamma_1 + \ldots + e^{-k\Delta s_m} \sin \gamma_m\right]$$

At origin,

$$M_{y1}\Big]_o = 0$$

$$\frac{\partial M_{y1}}{\partial x} = 0 + F_o L_1 e^{-k s_o} \cos \beta_1 \left[-k e^{-k\Delta s_1} \sin \gamma_1 \frac{\partial s_1}{\partial x} - \ldots - k e^{-k\Delta s_m} \sin \gamma_m \frac{\partial s_m}{\partial x}\right]$$

From Table 1, we have

$$\frac{\partial S_i}{\partial x} = \cos \beta_1 \sin \gamma_i$$

Therefore,

$$\frac{\partial M_{y1}}{\partial x} = - L_1 F_o k e^{-k s_o} \cos^2 \beta_1 \left[e^{-k\Delta s_1} \sin^2 \gamma_1 + \ldots + e^{-k\Delta s_m} \sin^2 \gamma_m \right]$$

At the origin,

$$\Delta s_1 = \Delta s_2 = \ldots = \Delta s_m = 0$$

$$e^{-k\Delta s_1} = e^{-k\Delta s_2} = \ldots = e^{-k\Delta s_m} = 1$$

$$\left.\frac{\partial M_{y1}}{\partial x}\right]_o = - L_1 F_o k e^{-k s_o} \cos^2 \beta_1 \left[\sin^2 \gamma_1 + \ldots + \sin^2 \gamma_m \right]$$

Let it now be assumed that the m magnets are equally spaced. As before,

$$\left.\frac{\partial M_{y1}}{\partial x}\right]_o = - L_1 \frac{1}{2} m F_o k e^{-k s_o} \cos^2 \beta_1 \qquad (15)$$

Next we examine the variation of M_{y1} with respect to φ.

$$\frac{\partial M_{y1}}{\partial \varphi} = 0 + F_o L_1 e^{-k s_o} \cos \beta_1 \left[- k e^{-k\Delta s_1} \sin \gamma_1 \frac{\partial s_1}{\partial \varphi} \right.$$

$$\left. - \ldots - k e^{-k\Delta s_m} \sin \gamma_m \frac{\partial s_m}{\partial \varphi} \right]$$

From Table 1, we have

$$\frac{\partial s_i}{\partial \varphi} = L_1 \cos \beta_1 \sin \gamma_i$$

Therefore,

$$\frac{\partial M_{y1}}{\partial \varphi} = - L_1^2 F_o k e^{-k s_o} \cos^2 \beta_1 \left[e^{-k\Delta s_1} \sin^2 \gamma_1 + \ldots + e^{-k\Delta s_m} \sin^2 \gamma_m \right]$$

At the origin,

$$\left.\frac{\partial M_{y1}}{\partial \varphi}\right]_o = - L_1^2 F_o k e^{-k s_o} \cos^2 \beta_1 \left[\sin^2 \gamma_1 + \ldots + \sin^2 \gamma_m \right]$$

For equally spaced magnets,

$$\left.\frac{\partial M_{y1}}{\partial \varphi}\right]_o = - L_1^2 \frac{1}{2} m F_o k e^{-k s_o} \cos^2 \beta_1 \qquad (16)$$

With respect to axial displacement z, the diamagnetic moment varies as follows:

$$\frac{\partial M_{y1}}{\partial z} = F_o L_1 e^{-k s_o} \cos \beta_1 \left[- k e^{-k\Delta s_1} \sin \gamma_1 \frac{\partial s_1}{\partial z} - \ldots - k e^{-k\Delta s_m} \sin \gamma_m \frac{\partial s_m}{\partial z} \right]$$

By Table 1,

$$\frac{\partial M_{y1}}{\partial z} = - L_1 F_o k e^{-k s_o} \cos \beta_1 \left[e^{-k\Delta s_1} \sin \gamma_1 (-\sin \beta_1) + \ldots + e^{-k\Delta s_m} \sin \gamma_m (-\sin \beta_1) \right]$$

At origin,

$$\left.\frac{\partial M_{y1}}{\partial z}\right]_o = +L_1 F_o k e^{-k s_o} \sin \beta_1 \cos \beta_1 \left[\sin \gamma_1 + \ldots + \sin \gamma_m\right]$$

$$\left.\frac{\partial M_{y1}}{\partial z}\right]_o = 0 \text{ for equally spaced magnets.} \tag{17}$$

Equations (15), (16), and (17) may be substituted into equation (14) to give the following:

$$M_{y1} = -L_1\left[\frac{1}{2} m F_o k e^{-k s_o} \cos^2 \beta_1\right] x$$

$$-L_1^2\left[\frac{1}{2} m F_o k e^{-k s_o} \cos^2 \beta_1\right] \varphi + \left[0\right] z$$

$$M_{y1} = -L_1 K_1 (x + L_1 \varphi) \tag{18}$$

where

$$K_1 = \frac{1}{2} m F_o k e^{-k s_o} \cos^2 \beta_1 \tag{19}$$

Equation (18) expresses the diamagnetic restoring torque exerted on the rotor by the upper ring of magnets, for three degrees of rotor freedom (x, φ, z). A similar derivation for the lower ring of magnets yields the following result:

$$M_{y2} = -L_2 K_2 (-x + L_2 \varphi) \tag{20}$$

where

$$K_2 = \frac{1}{2} n F_o k e^{-k u_o} \cos^2 \beta_2 \tag{21}$$

The quantity $(x + L_1 \varphi)$ appears both in equation (10) and in equation (18). It represents the radial displacement of a point on the rotor axis, located at a distance L_1 above the origin. We define this displacement as follows:

$$x_1 = x + L_1 \varphi \tag{22}$$

Equations (10) and (18) may now be written:

$$F_{x1} = -K_1 x_1 \tag{23}$$

$$M_{y1} = L_1 F_{x1} \tag{24}$$

Corresponding relationships for the lower ring are:

$$x_2 = x - L_2 \varphi \tag{25}$$

$$F_{x2} = -K_2 x_2 \tag{26}$$

$$M_{y2} = - L_2 F_{x2} \tag{27}$$

As suggested by equations (22) through (27), the upper ring of magnets may be considered to be replaced by a single radial force (F_{x1}) acting at a distance L_1 above the origin. The lower ring of magnets may be replaced by a single radial force (F_{x2}) acting at a distance L_2 below the origin. This simple concept is the essence of the approximate mathematical model.

It now remains to derive the expression for the axial force exerted on the rotor by the upper and lower rings of magnets. For the upper ring, from equation (3)

$$F_{z1} = \sum_{i=1}^{m} - F_i \sin \beta_1$$

$$= \sum_{i=1}^{m} - (a + F_o e^{-k S_i}) \sin \beta_1$$

$$= - m a \sin \beta_1 - F_o e^{-k S_o} \sin \beta_1 \left[e^{- k\Delta S_1} + \ldots + e^{-k\Delta S_m} \right]$$

At the origin,

$$F_{z1}\Big]_o = - m \sin \beta_1 \left[a + F_o e^{-k S_o} \right]$$

$$F_{z1} = F_{z1}\Big]_o + \frac{\partial F_{z1}}{\partial x}\Big]_o x + \frac{\partial F_{z1}}{\partial \varphi}\Big]_o \varphi + \frac{\partial F_{z1}}{\partial z}\Big]_o \qquad (28)$$

$$\frac{\partial F_{z1}}{\partial x} = - F_o e^{- k S_o} \sin \beta_1 \left[- k e^{- k\Delta S_1} \frac{\partial S_1}{\partial x} - \ldots - k e^{-k\Delta S_m} \frac{\partial S_m}{\partial x} \right]$$

From Table 1,

$$\frac{\partial S_i}{\partial x} = \cos \beta_1 \sin \gamma_i$$

$$\frac{\partial F_{z1}}{\partial x} = + F_o k e^{-k S_o} \sin \beta_1 \cos \beta_1 \left[e^{-k\Delta S_1} \sin \gamma_1 + \ldots + e^{-k\Delta s_m} \sin \gamma_m \right]$$

At the origin,

$$\left.\frac{\partial F_{z1}}{\partial x}\right]_o = + F_o\, k\, e^{-k s_o} \sin \beta_1 \cos \beta_1 \left[\sin \gamma_1 + \ldots + \sin \gamma_m\right]$$

$$\left.\frac{\partial F_{z1}}{\partial x}\right]_o = 0, \text{ for equally spaced magnets} \tag{29}$$

$$\frac{\partial F_{z1}}{\partial \varphi} = + F_o\, k\, e^{-k s_o} \sin \beta_1 \left[e^{-k\Delta s_1} \frac{\partial s_1}{\partial \varphi} + \ldots + e^{-k\Delta S_m} \frac{\partial S_m}{\partial \varphi}\right]$$

From Table 1,

$$\frac{\partial S_i}{\partial \varphi} = L_1 \cos \beta_1 \sin \gamma_i$$

$$\frac{\partial F_{z1}}{\partial \varphi} = + L_1 F_o\, k\, e^{-k s_o} \sin \beta_1 \cos \beta_1 \left[e^{-k\Delta s_1} \sin \gamma_1 + \ldots + e^{-k\Delta s_m} \sin \gamma_m\right]$$

At origin,

$$\left.\frac{\partial F_{z1}}{\partial \varphi}\right]_o = + L_1 F_o\, k\, e^{-k s_o} \sin \beta_1 \cos \beta_1 \left[\sin \gamma_1 + \ldots + \sin \gamma_m\right]$$

$$\left.\frac{\partial F_{z1}}{\partial \varphi}\right]_o = 0, \text{ for equally spaced magnets} \tag{30}$$

$$\frac{\partial F_{z1}}{\partial z} = + F_o\, k\, e^{-k s_o} \sin \beta_1 \left[e^{-k\Delta S_1} \frac{\partial S_1}{\partial z} + \ldots + e^{-k\Delta s_m} \frac{\partial S_m}{\partial z}\right]$$

From Table 1,

$$\frac{\partial S_i}{\partial z} = -\sin \beta_1$$

$$\frac{\partial F_{z1}}{\partial z} = -F_o k e^{-k S_o \sin^2 \beta_1} \left[e^{-k\Delta S_1} + \ldots + e^{-k\Delta S_m} \right]$$

At the origin,

$$\left.\frac{\partial F_{z1}}{\partial z}\right]_o = -F_o k e^{-k S_o \sin^2 \beta_1} \left[1 + 1 + \ldots + 1\right] m$$

$$\left.\frac{\partial F_{z1}}{\partial z}\right]_o = -m F_o k e^{-k S_o \sin^2 \beta_1} \tag{31}$$

Equations (29), (30), and (31) may be substituted into equation (28) to obtain the axial force exerted on the rotor by the upper ring:

$$F_{z1} = -m \sin \beta_1 \left[a + F_o e^{-k S_o}\right] - \left[m F_o k e^{-k S_o \sin^2 \beta_1}\right] z \tag{32}$$

For the lower ring,

$$F_{z2} = +n \sin \beta_2 \left[a + F_o e^{-k u_o}\right] - \left[n F_o k e^{-k u_o \sin^2 \beta_2}\right] z \tag{33}$$

The total axial force (F_z) is

$$F_z = F_{z1} + F_{z2}$$

$$F_z = - m \sin \beta_1 \left[a + F_o e^{-k S_o} \right] + n \sin \beta_s \left[a + F_o e^{-k u_o} \right]$$

$$- \left[m F_o k e^{-k S_o} \sin^2 \beta_1 \right] z - \left[n F_o k e^{-k u_o} \sin^2 \beta_2 \right] z \qquad (34)$$

For the special case where

$$m = n$$

$$\beta_1 = \beta_2$$

$$S_o = u_o$$

Then

$$F_z = 0 - \left[2 m F_o k e^{-k S_o} \sin^2 \beta_1 \right] z$$

$$F_z = - K_z z \qquad (35)$$

where

$$K_z = 2 m F_o k e^{-k S_o} \sin^2 \beta_1 \qquad (36)$$

Equation (36) represents the axial stiffness of the diamagnetic suspension (both rings).

The result of an external axial force P_z is the axial displacement of the rotor in the direction of the applied force:

$$z = \frac{P_z}{K_z} \qquad (37)$$

This axial motion effectively changes the initial air gap settings for the upper and lower rings, thereby causing the radial stiffness to increase for one ring, and decrease for the other.

$$\Delta S_o = - z \sin \beta_1 = - \frac{P_z \sin \beta_1}{K_z}$$

$$\Delta u_o = + z \sin \beta_2 = + \frac{P_z \sin \beta_2}{K_z}$$

Equations (19) and (21), representing the radial stiffness at the upper and the lower rings should then be modified as follows:

$$K_1 = \frac{1}{2} m F_o k e^{-k (S_o - z \sin \beta_1)} \cos^2 \beta_1 \qquad (38)$$

$$K_2 = \frac{1}{2} n F_o k e^{-k (u_o + z \sin \beta_2)} \cos^2 \beta_2 \qquad (39)$$

B. SUMMARY OF "APPROXIMATE" MATHEMATICAL MODEL

The philosophy and equations describing the approximate mathematical model are summarized below. The general approximation is that the diamagnetic supports vary linearly with rotor displacement, at the same rate as at the origin. It is assumed throughout that the magnets of each ring are uniformly spaced. In addition, the expression for axial stiffness (equation 36) assumes identical designs for upper and lower rings. The equation numbers originally used are repeated in this section, for easier reference to the derivations.

The axial stiffness is:

$$K_z = 2 m F_o k e^{-k S_o} \sin^2 \beta_1 \qquad (36)$$

Axial rotor motion depends on external axial force P_z:

$$z = \frac{P_z}{K_z} \tag{37}$$

The radial stiffnesses at the upper and lower rings are then

$$K_1 = \frac{1}{2} m F_o k e^{-k (S_o - z \sin \beta_1)} \cos^2 \beta_1 \tag{38}$$

$$K_2 = \frac{1}{2} n F_o k e^{-k (u_o + z \sin \beta_2)} \cos^2 \beta_2 \tag{39}$$

The upper and lower rings may then be considered to be replaced by radial forces (F_{x1}, F_{x2}) acting at "effective" distances (L_1, L_2) above and below the origin, at which points the radial displacements of the rotor are:

$$x_1 = x + L_1 \varphi \tag{22}$$

$$x_2 = x - L_2 \varphi \tag{25}$$

The diamagnetic radial forces on the rotor are

$$F_{x1} = - K_1 x_1 \tag{23}$$

$$F_{x2} = - K_2 x_2 \tag{26}$$

The corresponding moments on the rotor are

$$M_{y1} = L_1 F_{x1} \tag{24}$$

$$M_{y2} = - L_2 F_{x2} \tag{27}$$

By these equations and the equilibrium equations of basic statics, the ability of the diamagnetic suspension to support external shaft loads may be readily determined. In the next section the equilibrium equations for the rotor will be derived for a more complex loading situation, involving a magnetic attraction force load which varies with rotor displacement.

VII. APPLICATION OF MATHEMATICAL MODEL TO DESIGN PROBLEM

In this section the approximate mathematical model will be used in the design of a diamagnetic suspension system which supports a shaft loaded by external constant torques and forces and by an internal magnetic attraction force which varies with rotor displacement. The directions and points of application of these loads are defined by Figure 11.

The equilibrium equations for this system, and the conditions under which this equilibrium is stable (or unstable) will be derived. Then, expressions will be written to show the amount of clearance existing at both the lower and upper magnet rings, for any combination of external load torques and forces.

For the system shown in Figure 11, the total potential energy, V, stored in the rotor is given by

$$V = -\int F_x \, dx - \int M_y \, d\varphi - \int F_z \, dz \tag{40}$$

where

$$F_x = F_{x1} + F_{x2} + F_L + P \tag{41}$$

$$M_y = L_1 F_{x1} - L_2 F_{x2} + L_3 F_L - Q - PL_4 \tag{42}$$

The lateral force load, F_L, is radial, and has been found experimentally to vary linearly with displacement from null:

$$F_L = +K_3 x_L, \text{ where } x_L = x + L_3 \varphi \tag{43}$$

By equations (23) and (26):

$$F_{x1} = -K_1 x_1, \text{ where } x_1 = x + L_1 \varphi \tag{23}$$

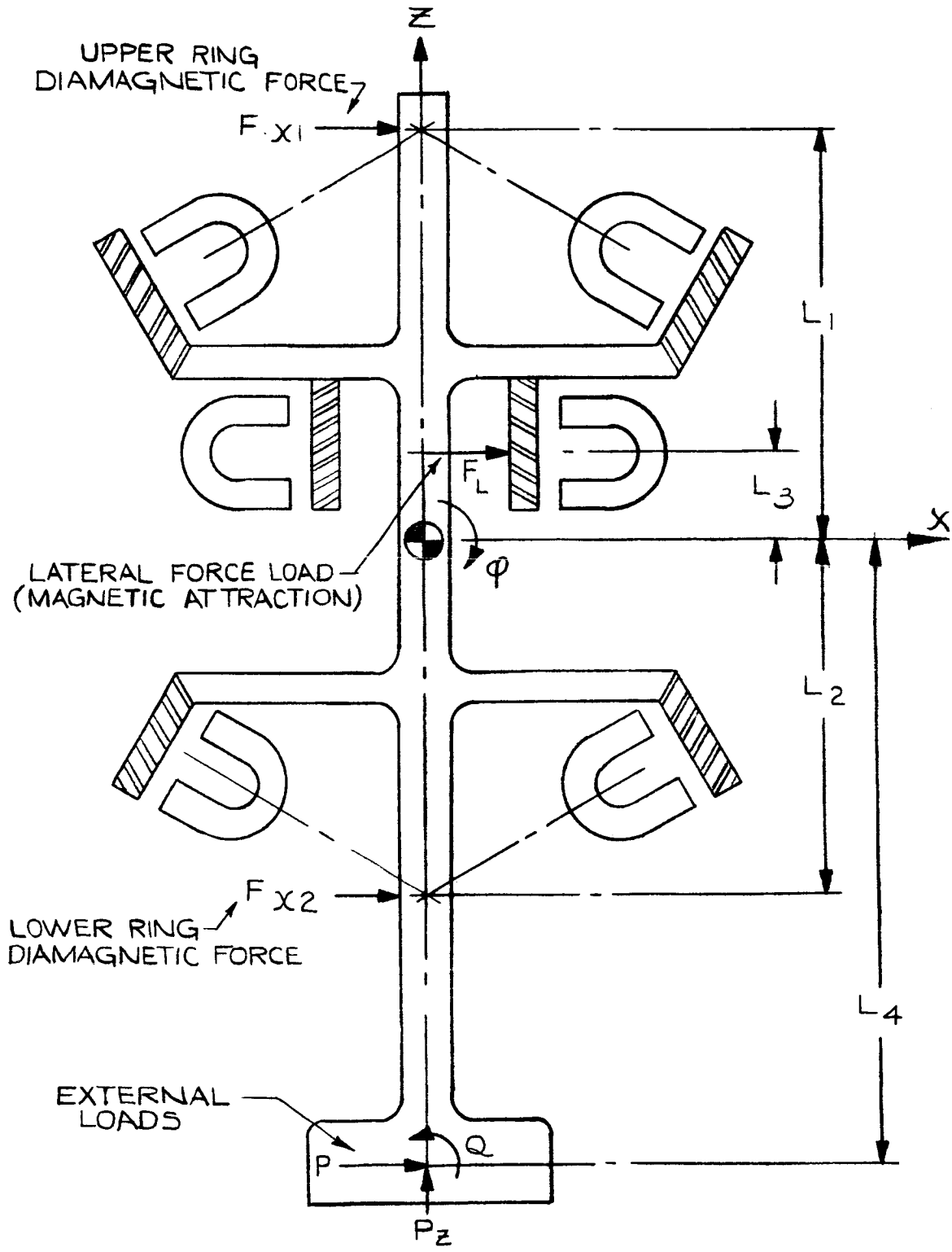

Figure 11. ATS Damper - Load Definition

$$F_{x2} = -K_2 x_2, \text{ where } x_2 = x - L_2 \varphi \tag{26}$$

By combining these relationships, the following results are obtained:

$$-F_x = (K_1 + K_2 - K_3)\, x + (K_1 L_1 - K_2 L_2 - K_3 L_3)\, \varphi - P \tag{44}$$

$$-M_y = (K_1 L_1 - K_2 L_2 - K_3 L_3)\, x + (K_1 L_1^2 + K_2 L_2^2 - K_3 L_3^2)\, \varphi + (Q + P L_4) \tag{45}$$

$$-F_z = K_z z - P_z \tag{46}$$

Equilibrium is established for the three degrees of freedom, if the potential energy gradients are zero.

$$\frac{\partial V}{\partial x} = 0 = -F_x \tag{47}$$

$$\frac{\partial V}{\partial \varphi} = 0 = -M_y \tag{48}$$

$$\frac{\partial V}{\partial z} = 0 = -F_z \tag{49}$$

Therefore, the equilibrium equations become:

$$(K_1 + K_2 - K_3)\, x + (K_1 L_1 - K_2 L_2 - K_3 L_3)\, \varphi = P \tag{50}$$

$$(K_1 L_1 - K_2 L_2 - K_3 L_3)\, x + (K_1 L_1^2 + K_2 L_2^2 - K_3 L_3^2)\, \varphi = -(Q + P L_4) \tag{51}$$

$$K_z z = P_z \tag{52}$$

Solution of these three simultaneous equations will yield the three components of rotor displacement (x, φ, z) for any combination of external loads (P, Q, P_z), and for any specified value for the lateral force load gradient K_3.

These components are

$$x = \frac{\begin{vmatrix} P & (K_1L_1 - K_2L_2 - K_3L_3) \\ -(Q + PL_4) & (K_1L_1^2 + K_2L_2^2 - K_3L_3^2) \end{vmatrix}}{\begin{vmatrix} (K_1 + K_2 - K_3) & (K_1L_1 - K_2L_2 - K_3L_3) \\ (K_1L_1 - K_2L_2 - K_3L_3) & (K_1L_1^2 + K_2L_2^2 - K_3L_3^2) \end{vmatrix}} \tag{53}$$

$$\phi = \frac{\begin{vmatrix} (K_1 + K_2 - K_3) & P \\ (K_1L_1 - K_2L_2 - K_3L_3) & -(Q + PL_4) \end{vmatrix}}{\begin{vmatrix} (K_1 + K_2 - K_3) & (K_1L_1 - K_2L_2 - K_3L_3) \\ (K_1L_1 - K_2L_2 - K_3L_3) & (K_1L_1^2 + K_2L_2^2 - K_3L_3^2) \end{vmatrix}} \tag{54}$$

$$z = \frac{P_z}{K_z} \tag{55}$$

For the equilibrium to be stable, the determinant of the equilibrium equations must be positive:

$$\begin{vmatrix} (K_1 + K_2 - K_3) & (K_1L_1 - K_2L_2 - K_3L_3) & 0 \\ (K_1L_1 - K_2L_2 - K_3L_3) & (K_1L_1^2 + K_2L_2^2 - K_3L_3^2) & 0 \\ 0 & 0 & K_z \end{vmatrix} > 0 \tag{56}$$

Since the axial stiffness, K_z, is positive, the stability criterion becomes

$$D = \begin{vmatrix} (K_1 + K_2 - K_3) & (K_1L_1 - K_2L_2 - K_3L_3) \\ (K_1L_1 - K_2L_2 - K_3L_3) & (K_1L_1^2 + K_2L_2^2 - K_3L_3^2). \end{vmatrix} > 0 \tag{57}$$

It is noted that equilibrium positions may be computed by equations (53) through (55), whether or not the stability criterion is satisfied. However, the results are meaningful only if the stability criterion is satisfied, because otherwise the solution represents a position of unstable equilibrium.

It now remains to examine the physical clearances existing between suspension magnets and diamagnetic rotors. Using equations (53) and (54), the deviations from initial air gaps are represented by x_1 and x_2 as follows:

$$x_1 = x + L_1 \phi$$

$$x_1 = \frac{1}{D} \left\{ Q \left[- K_2 (L_1 + L_2) + K_3 (L_1 - L_3) \right] + P \left[- K_2 (L_1 + L_2) (L_4 - L_2) + K_3 (L_3 + L_4) (L_1 - L_3) \right] \right\} \tag{58}$$

$$x_2 = x - L_2 \phi$$

$$x_2 = \frac{1}{D} \left\{ Q \left[K_1 (L_1 + L_2) - K_3 (L_2 + L_3) \right] + P \left[K_1 (L_1 + L_2) (L_4 + L_1) - K_3 (L_3 + L_4) (L_2 + L_3) \right] \right\} \tag{59}$$

where D is given by equation (57).

The clearance between the upper magnet ring and the rotor is

$$CL_1' = S_o - |x_1| \tag{60}$$

At the lower magnet ring,

$$CL_2' = u_o - |x_2| \tag{61}$$

It is customary to provide stops which prevent the rotor from approaching the magnet poles closer than some tolerable clearance. The remaining clearance between stops is then

$$CL_1 = S_o - TOL - |x_1| \tag{62}$$

$$CL_2 = u_o - TOL - |x_2| \tag{63}$$

at the upper and lower stops, respectively.

The magnitudes of CL_1 and CL_2 are a measure of the ability of the diamagnetic suspension to support the shaft under various loading conditions and for various values for the design parameters. A computer program was written to calculate CL_1 and CL_2 by the steps outlined above. In Figures 12 through 24 several curves are presented which show the minimum clearance existing for a particular combination of design parameters and loads.

In these plots, the minimum clearance is plotted vs. the lateral attraction force gradient load caused by the magnetic device. This parameter, K_3, is very critical; large values of K_3 cause the suspension to become unstable. The ability of the suspension system to support various load forces and torques is clearly shown by the curves. The curves indicate the number of magnets required and the proper location (L_3) for the lateral force load, for various specified values for the external loads.

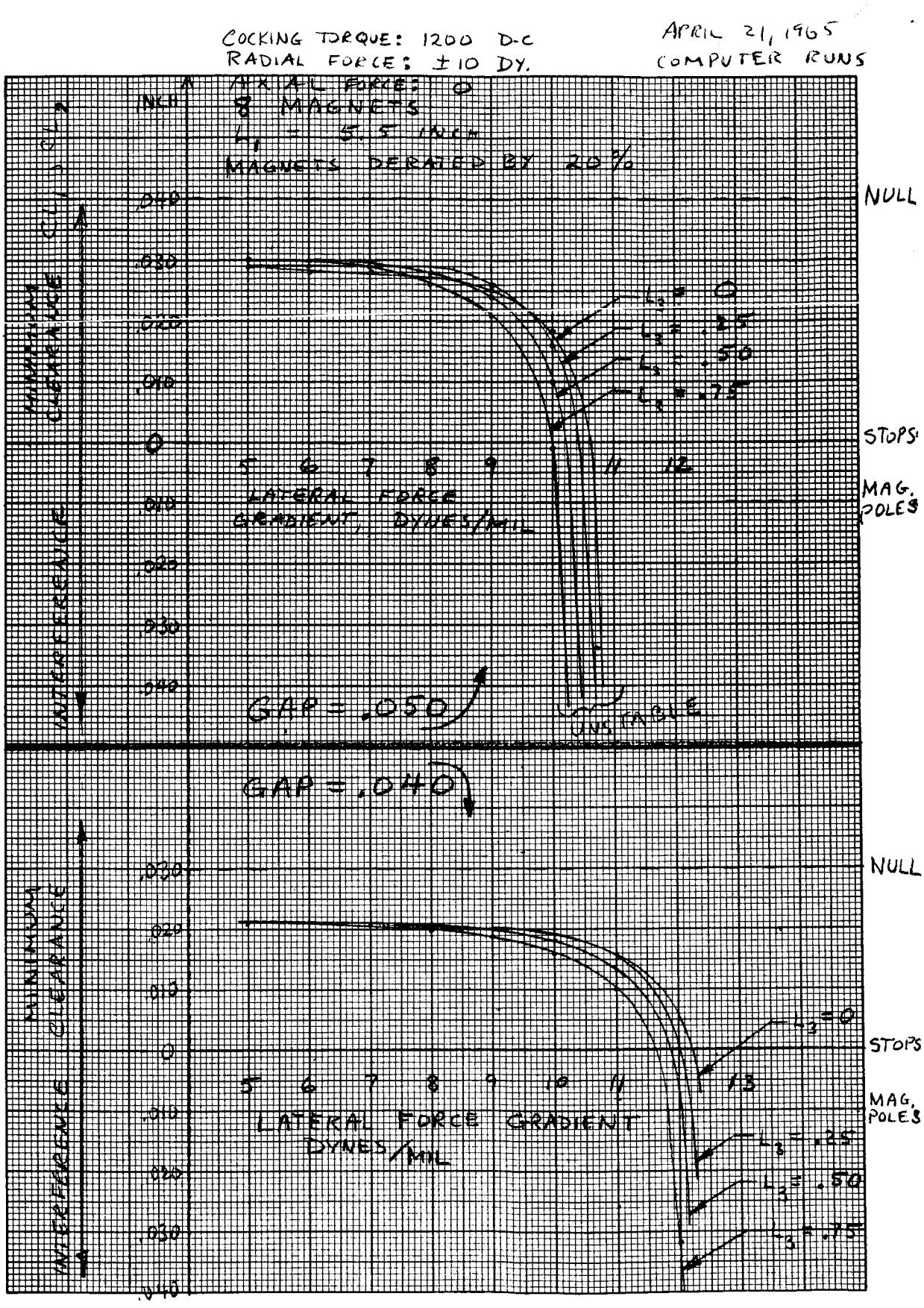

Figure 12. Rotor Clearance vs. Lateral Force Gradient - Computer Results

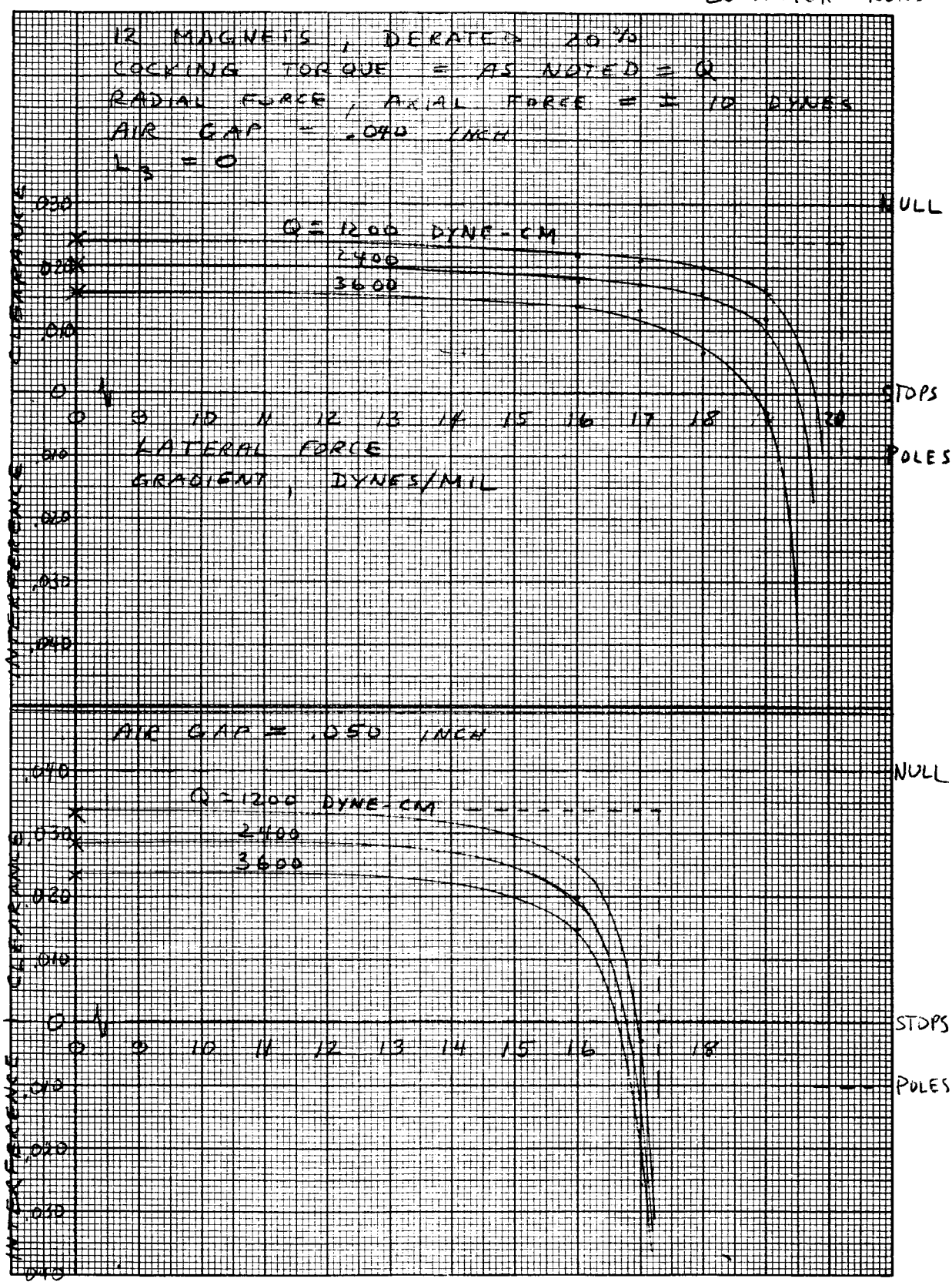

Figure 13. Rotor Clearance vs. Lateral Force Gradient - Computer Results

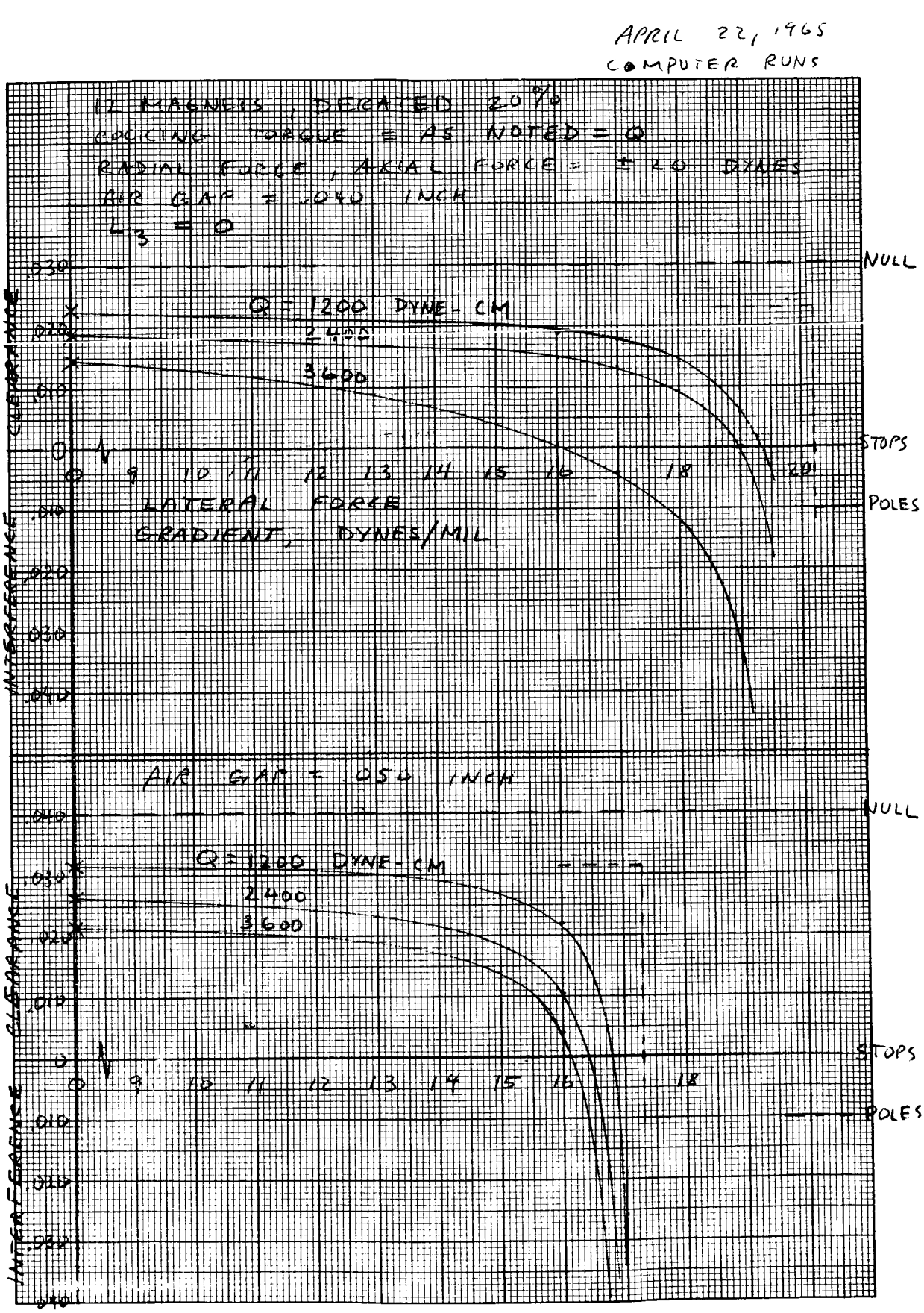

Figure 14. Rotor Clearance vs. Lateral Force Gradient - Computer Results

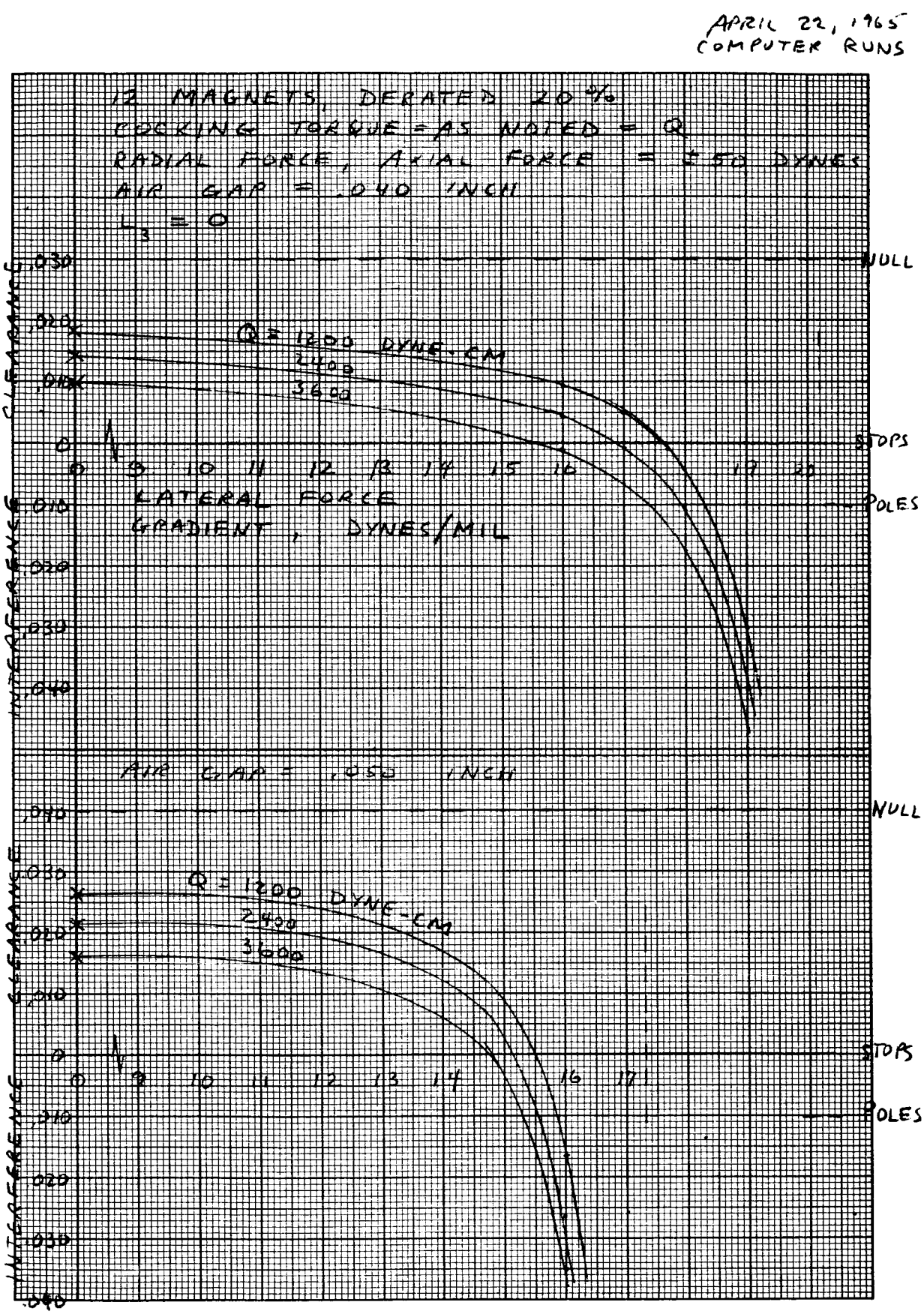

Figure 15. Rotor Clearance vs. Lateral Force Gradient - Computer Results

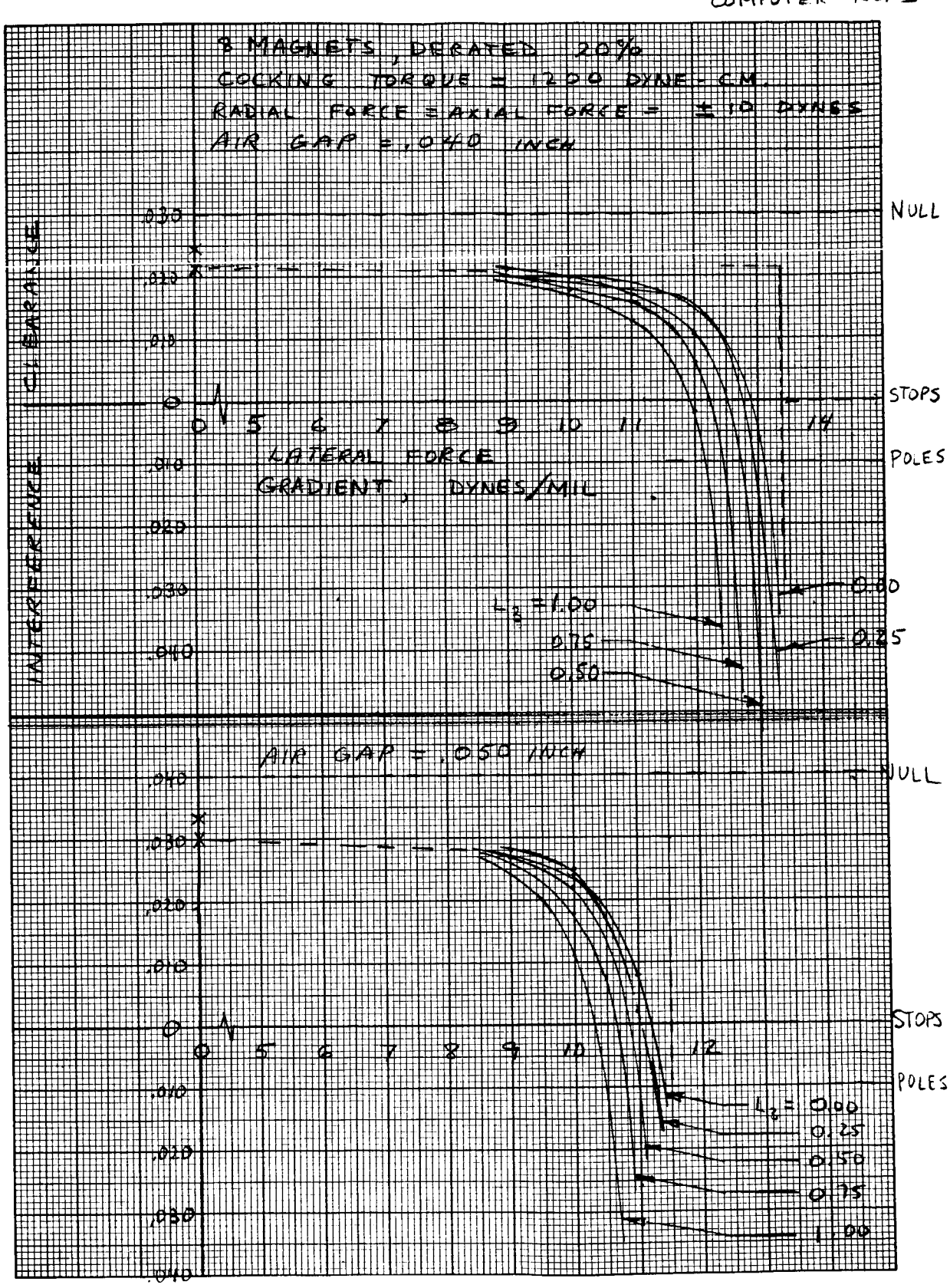

Figure 16. Rotor Clearance vs. Lateral Force Gradient - Computer Results

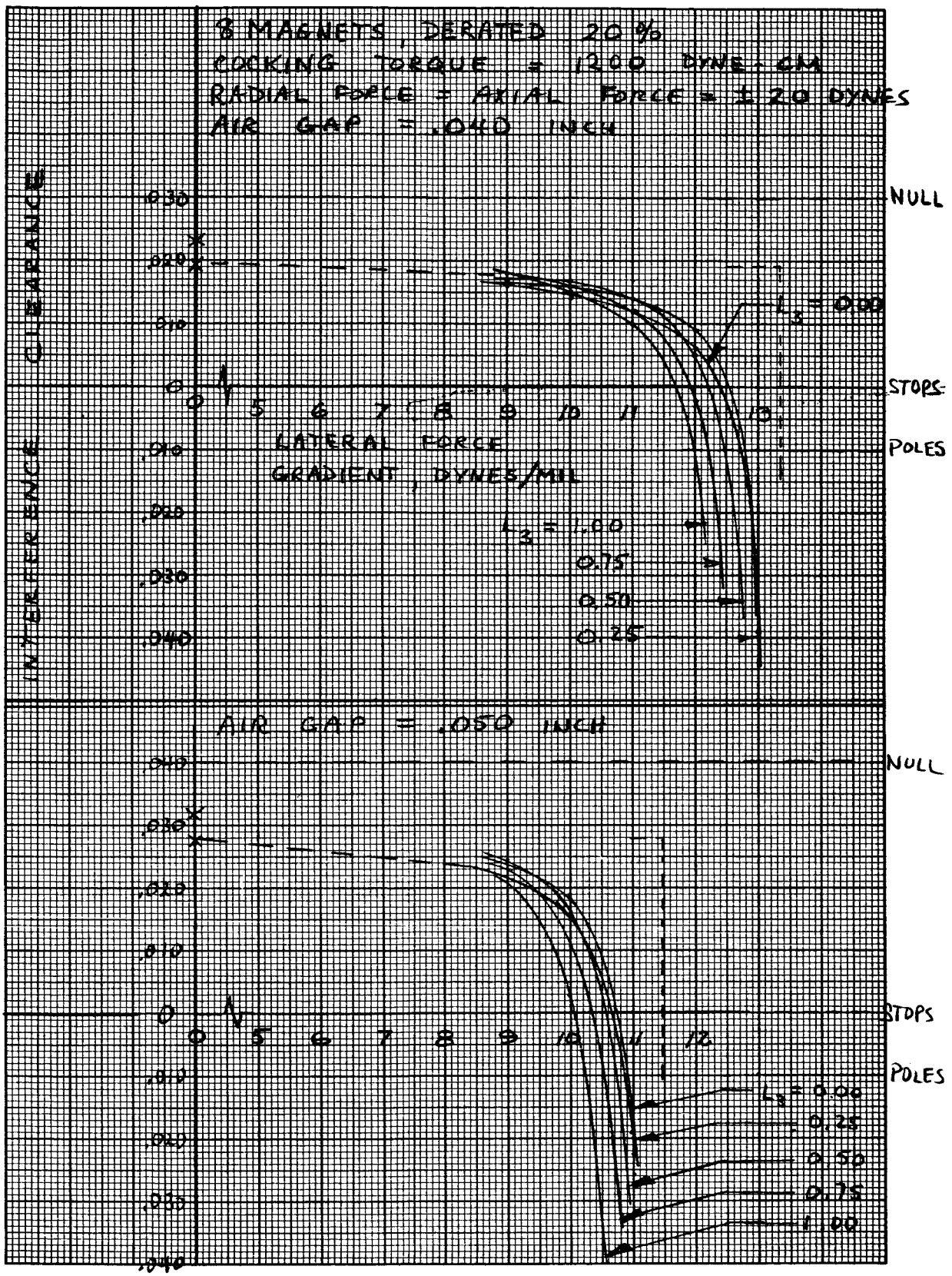

Figure 17. Rotor Clearance vs. Lateral Force Gradient - Computer Results

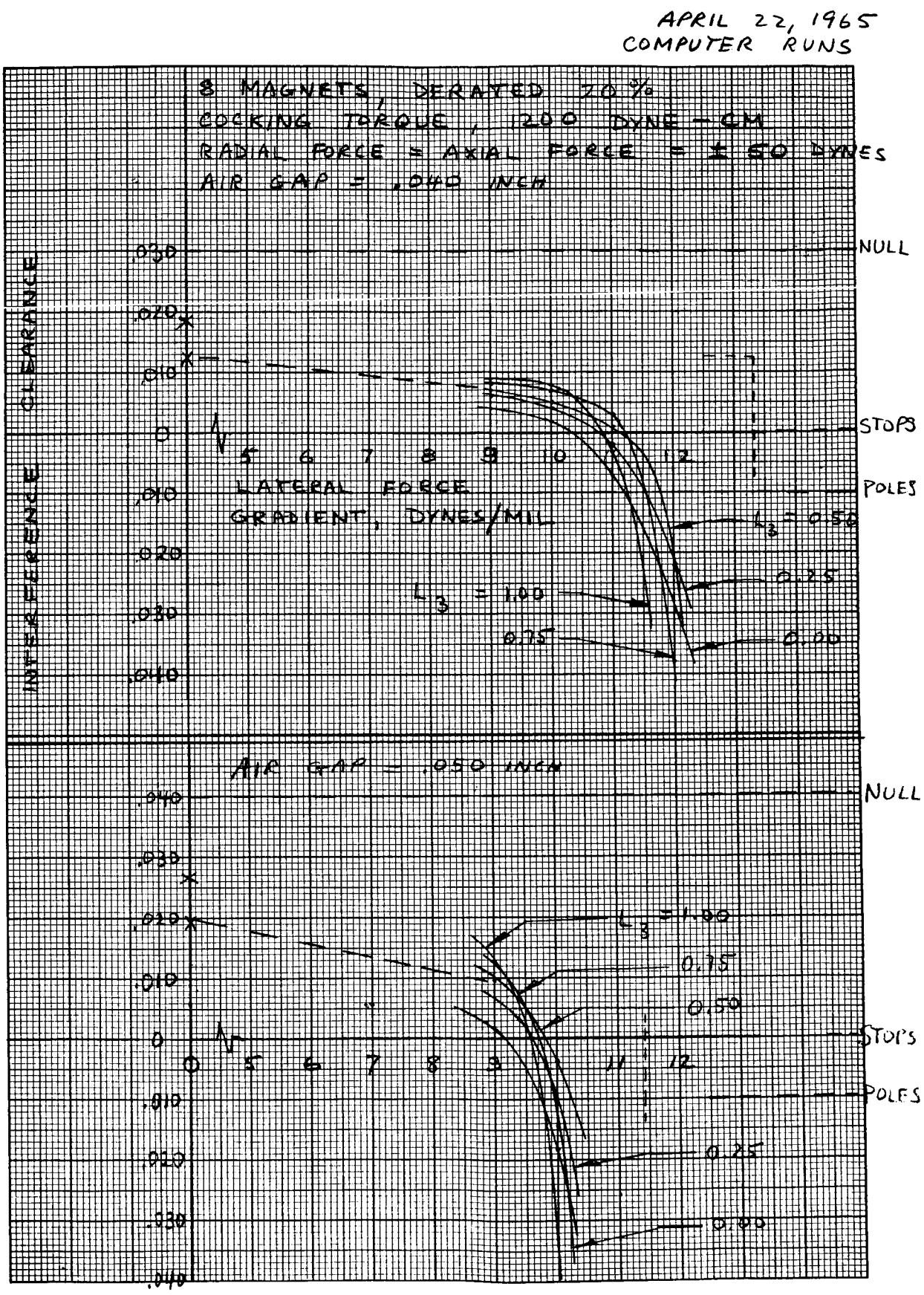

Figure 18. Rotor Clearance vs. Lateral Force Gradient - Computer Results

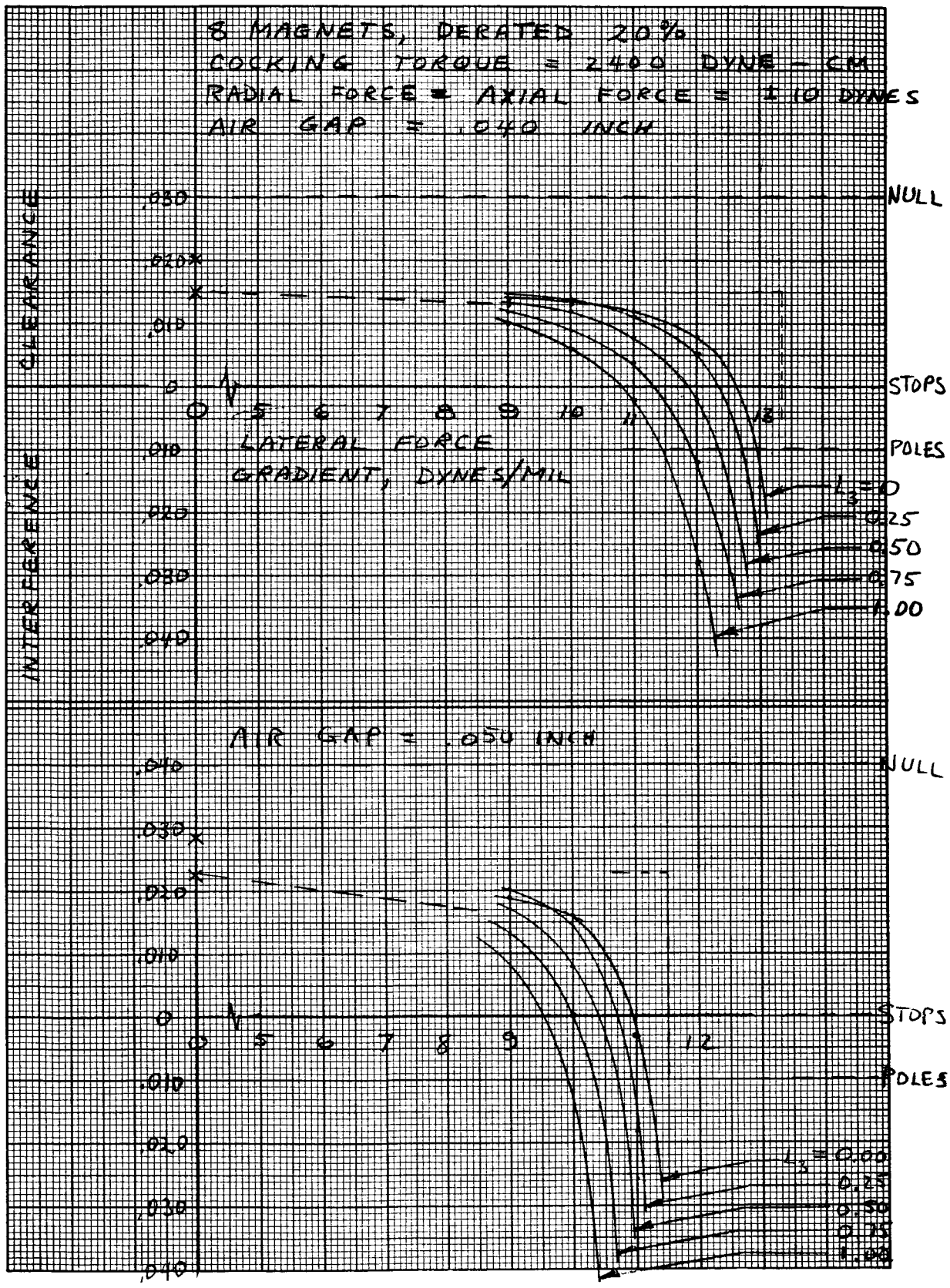

Figure 19. Rotor Clearance vs. Lateral Force Gradient - Computer Results

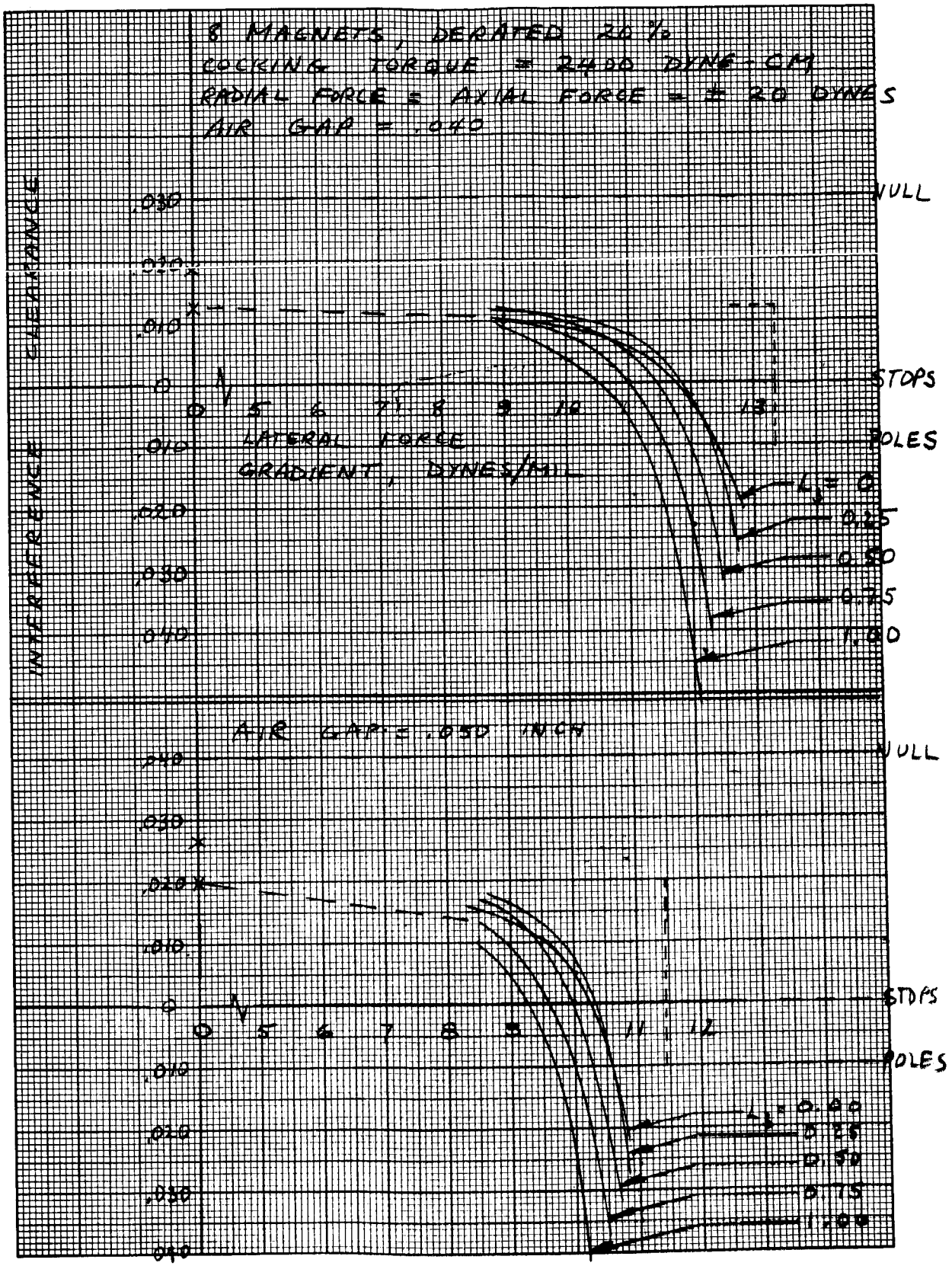

Figure 20. Rotor Clearance vs. Lateral Force Gradient - Computer Results

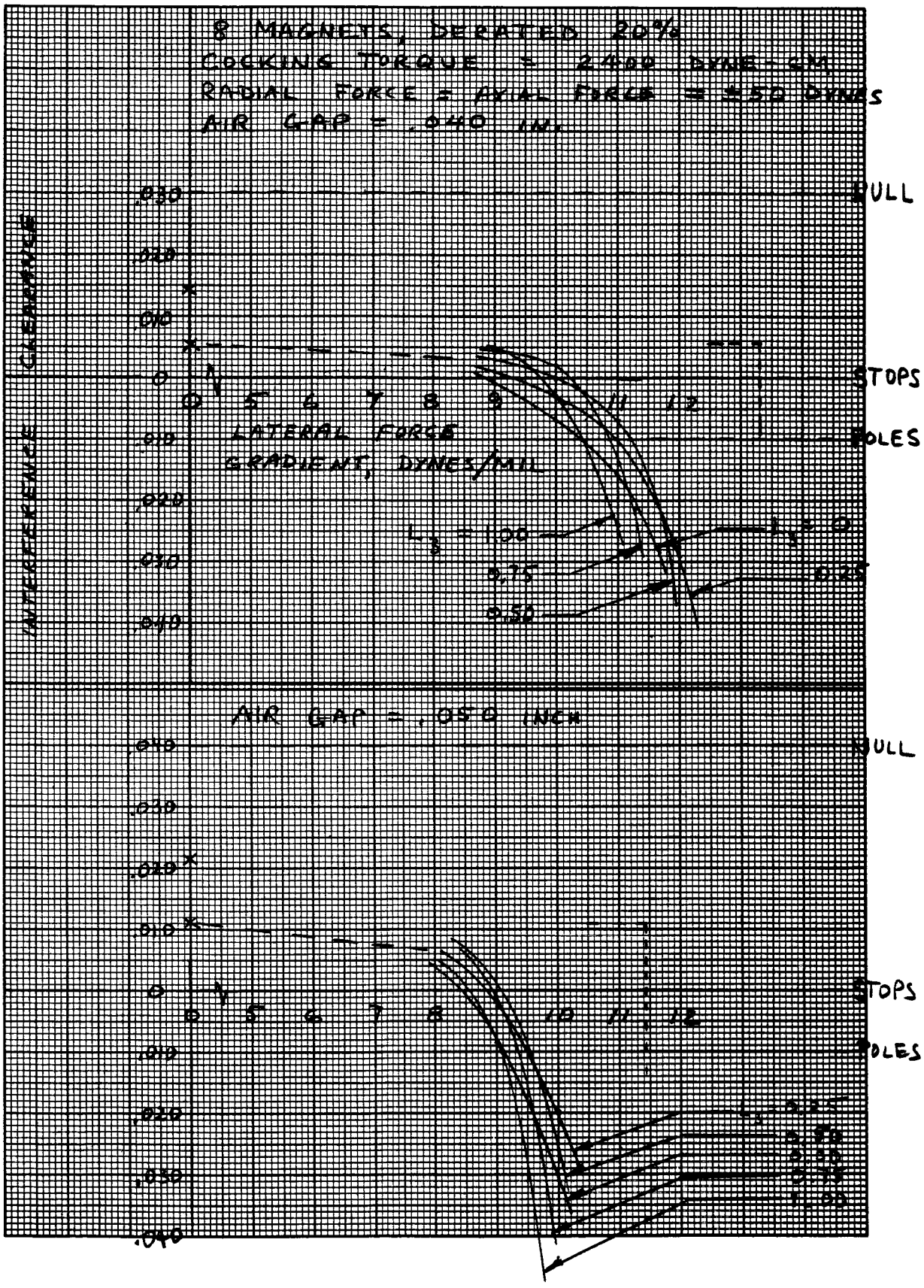

Figure 21. Rotor Clearance vs. Lateral Force Gradient - Computer Results

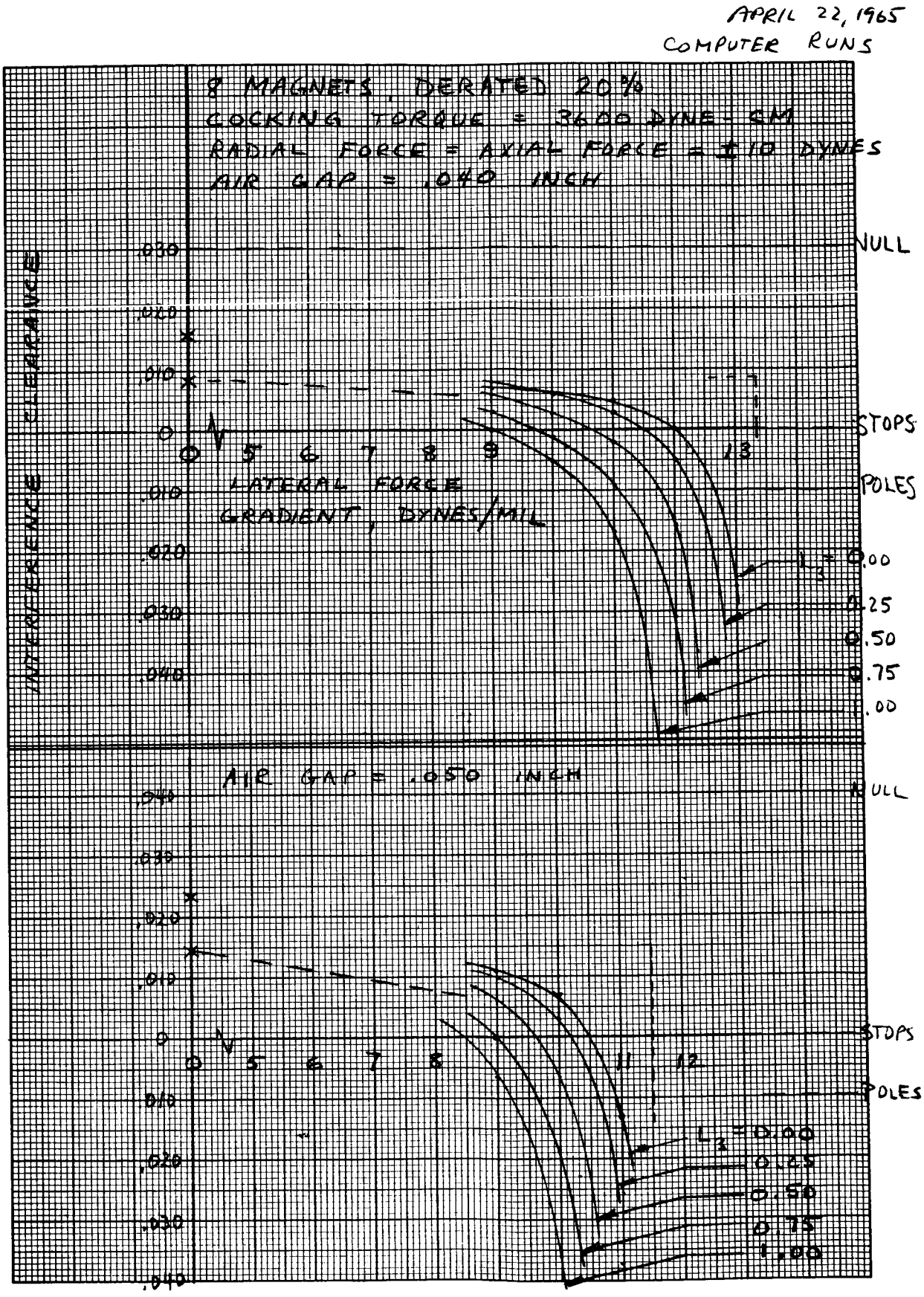

Figure 22. Rotor Clearance vs. Lateral Force Gradient - Computer Results

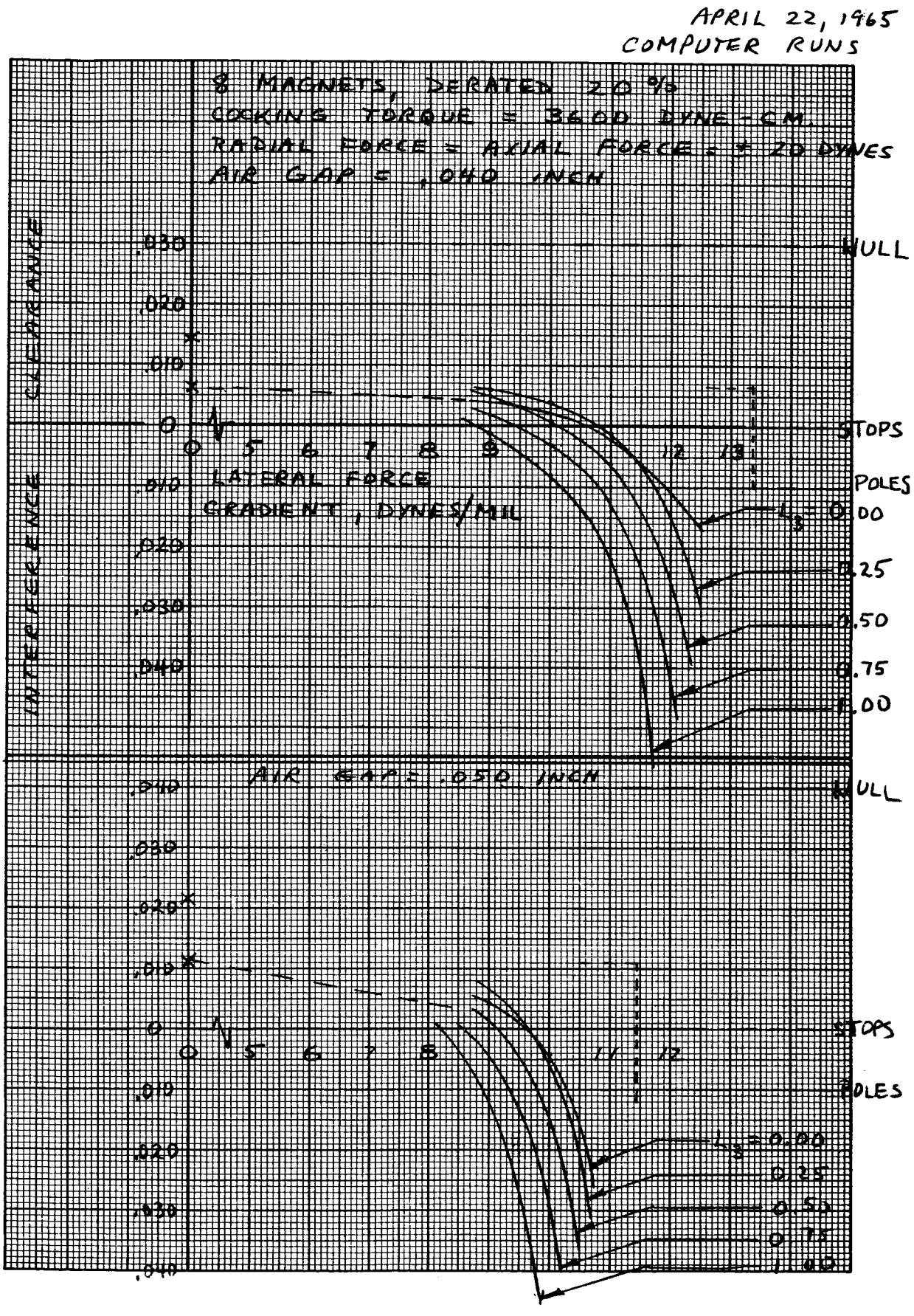

Figure 23. Rotor Clearance vs. Lateral Force Gradient - Computer Results

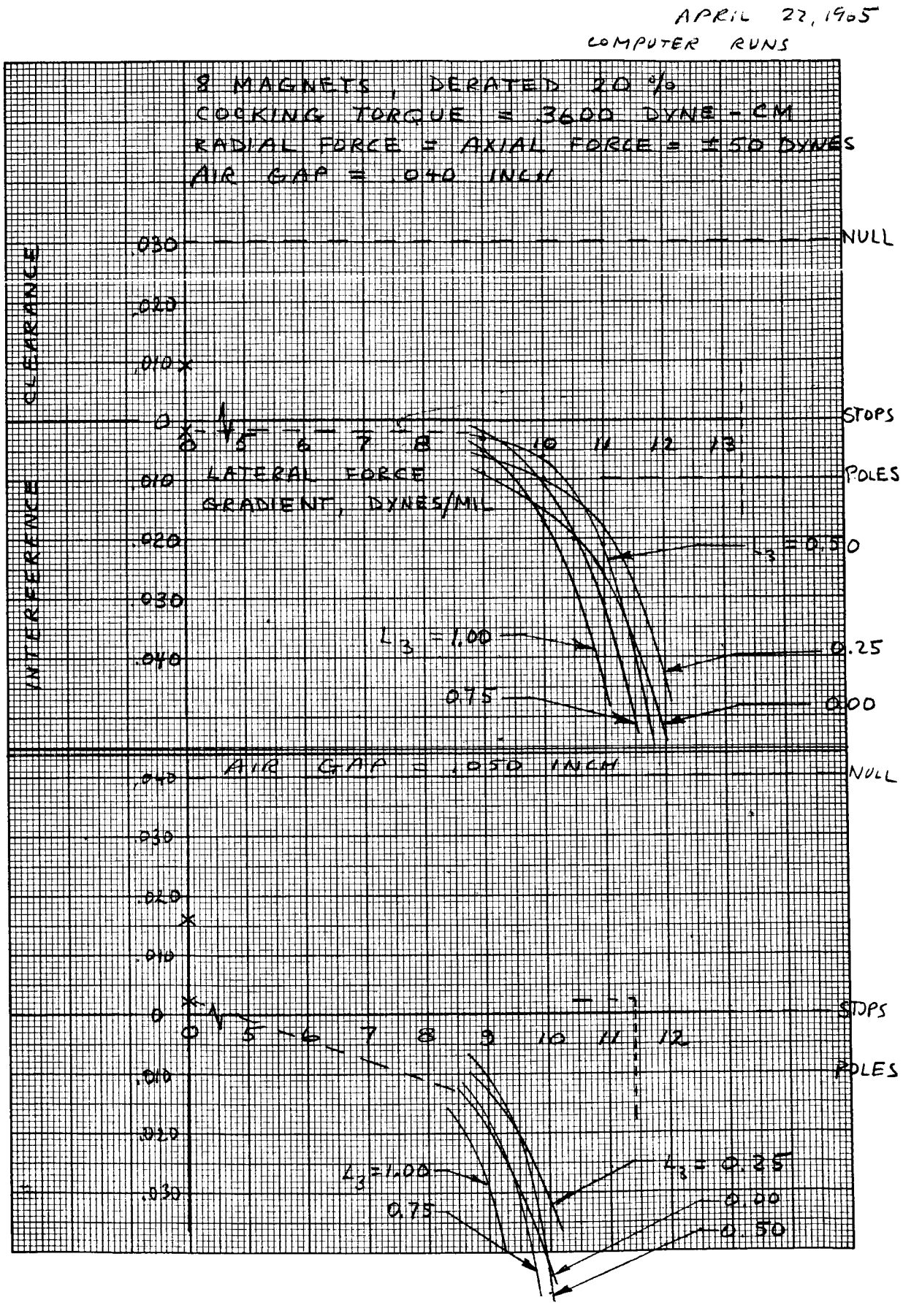

Figure 24. Rotor Clearance vs. Lateral Force Gradient - Computer Results

VIII. EVALUATION OF TRIG FUNCTION

It will be shown that

$$\sin^2 \gamma_1 + \sin^2 \gamma_2 + \ldots + \sin^2 \gamma_m = \frac{1}{2} m$$

for equally spaced magnets. Since the circle is thus divided into m equal parts, the function may be written

$$\sum_{k=1}^{m} \sin^2 \frac{k}{m} 2\pi = \sum_{k=1}^{m} \frac{1}{2} \left[1 - \cos 2 \frac{k}{m} 2\pi \right]$$

$$= \frac{1}{2} m - \frac{1}{2} \sum_{k=1}^{m} \cos \frac{k}{m} 4\pi$$

$$= \frac{1}{2} m - \frac{1}{2} C$$

where

$$C = \cos \frac{4\pi}{m} + \cos 2 \frac{4\pi}{m} + \ldots + \cos (m-1) \frac{4\pi}{m} + \cos m \frac{4\pi}{m}$$

$$C2 \sin \frac{2\pi}{m} = 2 \cos 2 \frac{2\pi}{m} \sin \frac{2\pi}{m}$$

$$+ 2 \cos 4 \frac{2\pi}{m} \sin \frac{2\pi}{m}$$

$$+ 2 \cos 6 \frac{2\pi}{m} \sin \frac{2\pi}{m}$$

$$+ \ldots$$

$$+ 2 \cos 2 (m-1) \frac{2\pi}{m} \sin \frac{2\pi}{m}$$

$$+ 2 \cos 2 m \frac{2\pi}{m} \sin \frac{2\pi}{m}$$

$$= \sin 3\,\frac{2\pi}{m} - \sin\frac{2\pi}{m}$$

$$+ \sin 5\,\frac{2\pi}{m} - \sin 3\,\frac{2\pi}{m}$$

$$+ \sin 7\,\frac{2\pi}{m} - \sin 5\,\frac{2\pi}{m}$$

$$+ \ldots - \ldots$$

$$+ \sin (2m-1)\,\frac{2\pi}{m} - \sin (2m-3)\,\frac{2\pi}{m}$$

$$+ \sin (2m+1)\,\frac{2\pi}{m} - \sin (2m-1)\,\frac{2\pi}{m}$$

$$= \sin (2m+1)\,\frac{2\pi}{m} - \sin\frac{2\pi}{m}$$

$$= 2\cos\frac{(2m+2)\,\frac{2\pi}{m}}{2}\,\sin\left(\frac{2m}{2}\,\frac{2\pi}{m}\right)$$

$$= 2\cos\frac{m+1}{m}\,2\pi\,\sin 2\pi$$

$$C = \frac{\sin 2\pi}{\sin\frac{2\pi}{m}}\,\cos\frac{m+1}{m}\,2\pi$$

$C = 0$ for $m \geq 3$ magnets

Therefore,

$$\sin^2\gamma_1 + \sin^2\gamma_2 + \ldots + \sin^2\gamma_m = \frac{1}{2}\,m$$

for $m \geq 3$ magnets